

AD- 320822

SECURITY REMARKING REQUIREMENTS

DOD 5200.1-R, DEC 78

REVIEW ON 28 OCT 80

## **DISCLAIMER NOTICE**

**THIS DOCUMENT IS BEST QUALITY  
PRACTICABLE. THE COPY FURNISHED  
TO DTIC CONTAINED A SIGNIFICANT  
NUMBER OF PAGES WHICH DO NOT  
REPRODUCE LEGIBLY.**

# **GENERAL DECLASSIFICATION SCHEDULE**

**IN ACCORDANCE WITH  
DOD 5200.1-R & EXECUTIVE ORDER 11652**

## **THIS DOCUMENT IS**

**CLASSIFIED BY \_\_\_\_\_**

**Subject to General Declassification Schedule of  
Executive Order 11652-Automatically Downgraded at  
2 Years Intervals- DECLASSIFIED ON DECEMBER 31, \_\_\_\_\_.**

**BY**

**Defense Documentation Center  
Defense Supply Agency  
Cameron Station  
Alexandria, Virginia 22314**

REPORT HAS BEEN DELIMITED  
AND CLEARED FOR PUBLIC RELEASE  
DER DOD DIRECTIVE 5200.20 AND  
RESTRICTIONS ARE IMPOSED UPON  
USE AND DISCLOSURE.

TRIBUTION STATEMENT A

PROVED FOR PUBLIC RELEASE;

TRIBUTION UNLIMITED.


UNCLASSIFIED

AD 320822

CLASSIFICATION CHANGED  
TO: UNCLASSIFIED  
FROM CONFIDENTIAL  
AUTHORITY: HDL DA  
17r, 9 Feb 81



UNCLASSIFIED

  
**AD 320 822**

*Reproduced  
by the*

**ARMED SERVICES TECHNICAL INFORMATION AGENCY  
ARLINGTON HALL STATION  
ARLINGTON 12, VIRGINIA**



NOTICE: When government or other drawings, specifications or other data are used for any purpose other than in connection with a definitely related government procurement operation, the U. S. Government thereby incurs no responsibility, nor any obligation whatsoever; and the fact that the Government may have formulated, furnished, or in any way supplied the said drawings, specifications, or other data is not to be regarded by implication or otherwise as in any manner licensing the holder or any other person or corporation, or conveying any rights or permission to manufacture, use or sell any patented invention that may in any way be related thereto.

**SECRET**

**TR-805**  
250 pages

Copy No. 19

**TERMINAL REPORT  
DEVELOPMENTAL SENSING COMPUTING SYSTEM  
FOR PROJECT DASH-DOT (U)**

10 October 1960

NOX



**DIAMOND ORDNANCE FUZE LABORATORIES  
ORDNANCE CORPS • DEPARTMENT OF THE ARMY**

258-26

**SECRET**

CATALOG BY ASTIA  
AS AD NO. 320 822

**ORDNANCE CORPS  
DIAMOND ORDNANCE FUZE LABORATORIES  
WASHINGTON 25, D. C.**

**Robert W. McEvoy, Lt Col  
COMMANDING**

**W. S. Hinman, Jr.  
TECHNICAL DIRECTOR**

The Diamond Ordnance Fuze Laboratories is a research, development, and engineering installation under the jurisdiction of the Chief of Ordnance.

The Diamond Ordnance Fuze Laboratories was established by the Ordnance Corps, Department of the Army, on 27 September 1953. The nucleus for these Laboratories was the personnel and facilities of the Ordnance Divisions of the National Bureau of Standards.

Typical fields of activity at the Diamond Ordnance Fuze Laboratories include electronics, physics, mechanics, chemistry, and applied mathematics. Examples of topics under these activities are radiation and field studies, circuit devices, chemical problems, and special electron tube design. The programs include all phases from basic research to product design.

The mission of the Laboratories is to:

1. Conduct research and development in the various physical science and engineering fields directed toward meeting the military characteristics for fuzes and related items.
2. Provide consulting and liaison services as required in connection with the development, production, and use of items developed in the laboratories, or of related items.
3. Fabricate models and prototypes of items under development at the laboratories.
4. Perform developmental testing, including destructive testing of prototypes.
5. Serve as principal Nuclear Radiation Effects Research Group to investigate and determine susceptibility of Ordnance electronic materiel to nuclear weapons radiation environment, mechanisms of those effects, and ways and means of developing less susceptible materiel.
6. Maintain and operate for OCO a special library of technical and progress reports, prepared by Army, Navy, Air Force, and their contractors.
7. Perform the Industrial Engineering Support Mission for all proximity fuze items.
8. Administer the Department of the Army Regional Training Center for the District of Columbia, Virginia, and Maryland region.

**SECRET**

**DIAMOND ORDNANCE FUZE LABORATORIES**  
**ORDNANCE CORPS**                      **WASHINGTON 25, D. C.**

DA-5W48-03-002  
ORD Proj. TW-410  
DOFL Proj. 21100

TR-805

10 October 1960

**TERMINAL REPORT**

**DEVELOPMENTAL SENSING COMPUTING SYSTEM**  
**FOR PROJECT DASH-DOT (U)**

H. W. Straub  
J. M. Arthaber  
A. L. Copeland  
L. Melamed  
J. E. Miller  
W. J. Moore  
R. J. Paradis  
R. R. Ulrich  
F. Vrataric, Jr.

FOR THE COMMANDER:  
Approved by

*B. M. Horton*  
B. M. Horton,  
Chief, Laboratory 200



Qualified requesters may obtain copies of this report from ASTIA.

**SECRET**

1

This document contains information affecting the national defense of the United States within the meaning of the espionage laws, title, 18 U. S. C., 793 and 794. Its transmission or the revelation of its contents in any manner to an unauthorized person is prohibited by law.

# CONTENTS

	Page
ABSTRACT . . . . .	9
1. INTRODUCTION . . . . .	11
2. GENERAL SYSTEMS ANALYSIS . . . . .	15
2.1 Limitations Imposed by Fragment Velocity . . . . .	15
2.2 Approaches Considered for the Timing Problem . . . . .	18
2.2.1 Front Overhang in Inclined-Beam Optical Approach . . . . .	23
2.2.2 End Overhang in Inclined-Beam Optical Approach . . . . .	26
2.2.3 Front Overhang in Vertical-Beam Optical Approach . . . . .	27
2.2.4 End Overhang in Vertical-Beam Optical Approach . . . . .	27
2.2.5 Overhang Reduction . . . . .	27
2.2.6 Effect of Restricting Overhang for Vertical Protected Area . . . . .	29
2.2.7 Flatness of Detection Fences . . . . .	38
2.3 Considerations of Defending-Charge Arrangement . . . . .	41
2.4 Optical Versus Microwave Approach . . . . .	46
3. OPTICAL APPROACH . . . . .	49
3.1 Specifications for Feasibility Test . . . . .	49
3.2 System Geometry . . . . .	49
3.2.1 Advantages of Geometry Chosen . . . . .	51
3.2.2 Fence Design . . . . .	51
3.2.3 Line-Charge Array . . . . .	52
3.3 Firing Time Equations . . . . .	53
3.4 Charge Selection Equation . . . . .	57
3.5 Error Analysis . . . . .	57
3.5.1 $V_m$ -Error Due to Random Fence Penetration . . . . .	58
3.5.2 $h$ -Error Due to Random Fence Penetration . . . . .	58
3.5.3 $T_0$ -Error due to Random Fence Penetration . . . . .	58
3.5.4 Error Analysis of Charge Selection . . . . .	60
3.5.5 Error Analysis of CG Firing Time Approximation . . . . .	69
4. OPTICAL DETECTION ELEMENTS . . . . .	75
4.1 Design of Reflector . . . . .	75
4.2 Selection of Photocell Type . . . . .	77
5. OPTICAL DETECTION EQUIPMENT . . . . .	81
5.1 Velocity-Only Detection Unit . . . . .	81
5.2 Subfence Unit . . . . .	81
5.2.1 Description . . . . .	81
5.2.2 Design Specifications . . . . .	83
5.2.3 Special Considerations . . . . .	83
5.2.4 Cell Mounting . . . . .	83
5.3 Mounting Structure . . . . .	88
5.3.1 System Layout . . . . .	88
5.3.2 Z-Shaped Structure . . . . .	88
5.4 Alignment Methods . . . . .	88
5.4.1 Picket Alignment . . . . .	88
5.4.2 Subfence Alignment . . . . .	90
5.5 Associated Equipment . . . . .	90

# CONTENTS (Continued)

	Page
6. PRELIMINARY SYSTEM . . . . .	93
6.1 Background . . . . .	93
6.2 Optical Equipment . . . . .	93
6.2.1 Detection Unit . . . . .	93
6.2.2 Performance of PbS Cells . . . . .	96
6.3 Rate-of-Rise Amplifier . . . . .	96
6.4 Velocity-Only Firing-Time Computer . . . . .	100
6.5 Field Tests on Preliminary System . . . . .	105
6.6 Test Results and Conclusions . . . . .	109
7. EQUIPMENT SUPPLIED TO PICATINNY ARSENAL AND BALLISTICS RESEARCH LABORATORIES . . . . .	113
7.1 Improvements over Preliminary System . . . . .	113
7.2 Firing Circuit . . . . .	114
7.3 Completed Equipment . . . . .	114
7.4 Results . . . . .	114
8. FUNCTION OF OVER-ALL ELECTRONIC CIRCUITRY . . . . .	121
9. SIGNAL PROCESSING AND SYSTEM LOGIC . . . . .	125
9.1 Analysis and Shaping of Signal Pulses . . . . .	125
9.1.1 Analysis of Signal Pulses . . . . .	125
9.1.2 Analysis of Signal-to-Noise Ratio . . . . .	129
9.2 Logic Gates . . . . .	138
9.2.1 Diode "OR" Circuit . . . . .	138
9.2.2 Height Fence "OR" Circuit . . . . .	138
9.2.3 Sequential Blocking Gates . . . . .	138
9.3 Size Discrimination . . . . .	142
9.3.1 Size Discrimination Analysis . . . . .	146
9.3.2 Size Discrimination Logic Circuitry . . . . .	149
10. FIRING-TIME COMPUTER . . . . .	163
10.1 General Considerations . . . . .	163
10.2 Transformation of Firing-Time Equation to Voltages . . . . .	163
10.3 Computer Operation . . . . .	165
10.4 Divider Operation . . . . .	171
10.5 $(K_1 \Delta T_1 + K_2 \Delta T_2 / \Delta T_1)$ Generator . . . . .	172
10.6 $(K_3 + \Delta T_2 + \Delta T_f)$ Function Generator . . . . .	172
10.7 Computer Design . . . . .	172
10.8 Divider Design . . . . .	174
10.9 Comparators . . . . .	180
10.10 Gates . . . . .	180
10.11 Computer Adjustment . . . . .	180
10.12 Field Test Results . . . . .	185
11. CHARGE-SELECTING COMPUTER . . . . .	189
11.1 Approach to Selection Problem . . . . .	189
11.2 Input Storage . . . . .	191
11.3 Center Resolution . . . . .	191
11.4 Resetting Input Cores and Readout to Selection Matrix . . . . .	198

# CONTENTS (Continued)

	Page
11.5 Charge-Selection Matrix . . . . .	200
11.6 Output Buffer Register and Output Gates . . . . .	200
11.7 Indicator Lamps . . . . .	201
11.8 Completed Charge-Selection Computer . . . . .	201
12. FIRING CIRCUIT . . . . .	207
13. FIELD TESTS WITH EXPERIMENTAL PROTOTYPE SYSTEM . . . . .	211
13.1 Test Objectives . . . . .	211
13.2 Firing Range . . . . .	211
13.3 Tests on Detection Unit Parameters . . . . .	211
13.4 Tests on Over-all System . . . . .	215
13.4.1 Test Layout . . . . .	215
13.4.2 Electronic Instrumentation and Test Method. . . . .	219
13.4.3 Determination of Microflash Delay . . . . .	223
13.5 Test Results . . . . .	224
13.5.1 Charge-Selection Computer . . . . .	224
13.5.2 Size Discrimination and K-Factor . . . . .	224
13.5.3 Over-all Experimental System . . . . .	224
13.6 Analysis of Results . . . . .	227
13.6.1 General Considerations . . . . .	227
13.6.2 Total Error . . . . .	227
13.6.3 Firing-Time Error . . . . .	233
14. MICROWAVE APPROACH . . . . .	239
14.1 Velocity Measurement. . . . .	239
14.2 Methods for Height Determination . . . . .	239
14.2.1 Multiple Bistatic System . . . . .	240
14.2.2 Three-Horn System for Height Determination. . . . .	240
14.3 FM Ranging Techniques . . . . .	243
14.4 Bibliography of Contractor's Reports . . . . .	243
15. CONCLUSION . . . . .	245
16. ACKNOWLEDGMENTS . . . . .	247

# ILLUSTRATIONS

	Page
Figure 2-1. Vertical fragment velocity versus round displacement . . .	16
2-2. Inclined fragment velocity versus round displacement . . .	16
2-3. Parallel sensing elements and defending charge . . . . .	17
2-4. Attacking round speed equals one-half fragment speed . . .	17
2-5. Intercept point for normal attack. . . . .	19
2-6. Intercept for nonnormal attack . . . . .	19
2-7. Inclined-beam geometry . . . . .	21
2-8. Vertical-beam geometry . . . . .	22
2-9. Minimum distance for defending charge . . . . .	25
2-10. Overhang for various degrees of armour protection . . . .	28
2-11. One method for reduction of overhang . . . . .	30
2-12. A second method for reduction of overhang . . . . .	31
2-13. Method for reduction of end overhang . . . . .	32
2-14. Effect of restricting overhang, case I . . . . .	33
2-15. Effect of restricting overhang, case II . . . . .	33
2-16. Effect of restricting overhang for case II with OTAC re- strictions. . . . .	37
2-17. Illustration of errors in fence flatness . . . . .	39
2-18. Top view of staggered defending-charge array . . . . .	42
2-19. Side view of line charge array . . . . .	43
2-20. Error versus velocity for alternate defending charge arrays. . . . .	44
Figure 3-1. System geometry . . . . .	50
3-2. Random fence penetration ambiguity for conical ogives . .	59
3-3. Typical picket array in a fence . . . . .	61
3-4. Ambiguity in attack angle . . . . .	62
3-5. Charge selection error . . . . .	63
3-6. Maximum charge coordinate error ( $\Delta Y_{max}$ ) versus attack angle $\theta$ (for calibers shown) . . . . .	68
3-7. Average charge coordinate error ( $\Delta Y$ ) versus attack angle $\theta$ (for all calibers) . . . . .	70
3-8. L (impact error in inches) . . . . .	72
Figure 4-1. Distribution of sensitivity, flash-light reflector . . .	76
4-3. Distribution of sensitivity, reflector of figure 4-2 . . .	76
4-2. Solid-glass, square cross-section reflector . . . . .	76
4-4. Unmodified square cell . . . . .	79
4-5. Grid or snake cell . . . . .	79
4-6. Average characteristics of lead sulphide cells tested . .	79
4-7. Relation between power dissipation in PbS photocell and signal voltage and signal-to-noise ratio obtained . . . .	80
4-8. Change of cell noise with illumination . . . . .	80
Figure 5-1. Velocity-only detection unit . . . . .	82
5-2. Arrangement of reflectors in subfence . . . . .	84
5-3. Subfence unit. . . . .	85
5-4. Design of baffles . . . . .	86
5-5. Subfence with baffle . . . . .	87
5-6. Z-frame on gun mount . . . . .	89
Figure 6-1. Preliminary detection layout . . . . .	94
6-2. Shell signature . . . . .	95
6-3. Pulse adding circuitry of preliminary system . . . . .	97
6-4. Equivalent circuit of rate-of-rise amplifier . . . . .	98

## ILLUSTRATIONS (Continued)

	Page
6-5. Schematic diagram of rate-of-rise amplifier . . . . .	101
6-6. Basic velocity-only layout . . . . .	102
6-7. Operation of velocity-only computer . . . . .	102
6-8. Chart for computer setting . . . . .	104
6-9. Special velocity-only layout . . . . .	104
6-10. Specialized computer-setting chart . . . . .	104
6-11. Block diagram of preliminary system . . . . .	106
6-12. Circuit diagram of preliminary system . . . . .	107
6-13. Range layout for preliminary system test . . . . .	108
6-14. Block diagram of electronic test instrumentation of preliminary system . . . . .	110
6-15. Recording of typical test firing . . . . .	111
Figure 7-1. Amplifier and anode follower . . . . .	115
7-2. Firing circuit . . . . .	116
7-3. Block diagram of equipment supplied to Picatinny and BRL . . . . .	117
7-4. Front view of preliminary computer rack . . . . .	118
7-5. Back view of preliminary computer rack . . . . .	119
Figure 8-1. Block diagram of complete system . . . . .	122
Figure 9-1. Signals from different time constant cells and different velocity shells . . . . .	126
9-2. Position of shell in relation to detection fence . . . . .	127
9-3. Tail reference system . . . . .	128
9-4. Nose reference system . . . . .	128
9-5. Equivalent circuit of amplifier . . . . .	130
9-6. Signal/noise function $y$ versus bandwidth factor $k$ . . . . .	132
9-7. Normalized signal/noise versus bandwidth factor $k$ . . . . .	134
9-8. Circuit diagram of sally amplifier . . . . .	135
9-9. Pulse delay in sally amplifier vs signal amplitude . . . . .	136
9-10. Views of sally amplifier . . . . .	137
9-11. Diode "OR" circuit . . . . .	139
9-12. Height fence "OR" circuit . . . . .	140
9-13. Block diagram of sequential blocking gates . . . . .	141
9-14. Sequential blocking gate circuitry . . . . .	143
9-15. Sequential blocking gate wave shapes . . . . .	145
9-16. Size discrimination circuitry . . . . .	147
9-17. Tail pulses and shell signatures . . . . .	151
9-18. Block diagram of size discrimination logic circuitry . . . . .	152
9-19. Logic circuitry for size discrimination . . . . .	153
9-20. Various shell height trajectories . . . . .	154
9-21. Shells specified for feasibility test . . . . .	155
9-22. Influence of shell length and orientation without $K$ factor. . . . .	156
9-23. Influence of shell length and orientation with $K$ factor . . . . .	157
9-24. Normal component $V_n$ of shell velocity $V_m$ . . . . .	159
9-25. Miller sweep voltages for $K$ -factor . . . . .	160
Figure 10-1. Time domain representation of pulses as used by firing-time computer . . . . .	164
10-2. Functions generated in firing-time computer . . . . .	166
10-3. Block diagram of firing-time computer . . . . .	167

# ILLUSTRATIONS (Continued)

	Page
Figure 10-4. Circuitry of firing-time computer. . . . .	169
10-5. Maximum permissible error in time versus missile velocity . . . . .	173
10-6. Miller sweep circuit with storage . . . . .	175
10-7. Waveform of function generated in divider . . . . .	176
10-8. Operational step generator . . . . .	177
10-9. Triangular-sweep generator . . . . .	179
10-10. Cathode-coupled comparator . . . . .	181
10-11. Amplified direct-coupled diode comparator (ADCDC) . . . . .	182
10-12. Waveforms of ADCDC of Figure 10-11 . . . . .	183
10-13. Monostable gate generator . . . . .	184
10-14. Front view of firing-time computer . . . . .	186
10-15. Top view of firing-time computer . . . . .	187
10-16. Bottom view of firing-time computer . . . . .	188
Figure 11-1. Charge-selection geometry . . . . .	190
11-2. Logic diagram of charge-selection computer . . . . .	192
11-3. Center-resolution circuitry . . . . .	193
11-4. Arrangement of magnet cores in center-resolution circuitry . . . . .	195
11-5. Center-resolution core matrix . . . . .	197
11-6. States of a center-resolution core . . . . .	199
11-7. States of a selection matrix core . . . . .	199
11-8. External view of charge-selection computer . . . . .	202
11-9. Front view of logic card side . . . . .	203
11-10. Back view of logic card side . . . . .	204
11-11. Logic cards and card extractor . . . . .	205
Figure 12-1. Firing circuit . . . . .	208
12-2. Wave form of firing pulse . . . . .	208
12-3. Switching array for 12 defending charges - FC = Firing circuit, LC = Defending charge . . . . .	209
Figure 13-1. Dash-dot range at DOFL Test Area; view toward detection station. . . . .	212
13-2. Dash-Dot range at DOFL Test Area; view toward instrumentation trailer . . . . .	213
13-3. Possible variations in shell penetration . . . . .	214
13-4. Layout for shell penetration test . . . . .	216
13-5. Typical picture pair from penetration tests; black dots are fiducial marks on screen . . . . .	217
13-6. Plotting board . . . . .	218
13-7. Layout for over-all system accuracy test . . . . .	220
13-8. Optical system in detection station . . . . .	221
13-9. Interior of electronic laboratory trailer . . . . .	222
13-10. Block diagram of field instrumentation . . . . .	225
13-11. Camera-triggering and velocity-measurement circuitry . . . . .	226
13-12. Penetration error . . . . .	235
13-13. Scatter diagram of penetration vs velocity . . . . .	236
13-14. Positional error vs shell velocity . . . . .	237
Figure 14-1. Multiple bistatic system . . . . .	241
14-2. Practical three-horn system . . . . .	242

# SECRET

## ABSTRACT

(S) An experimental sensing-computing system to protect tanks from anti-tank rounds has been developed. It locates an approaching round within a few feet from the tank, determines electronically its velocity and trajectory, and decides whether it is potentially dangerous. If found not dangerous, it is ignored. If it is found dangerous, the system then selects, out of a multitude of defending charges arrayed on the tank periphery, one which is in the right position, and transmits to the selected charge a firing pulse at the correctly computed time, so that the charge fragments intercept and defeat the attacking rounds.

(S) The optical approach followed is essentially passive, using sky light in daytime and invisible infrared light only at nighttime. In a preliminary system that computed the firing time for the defending charge as a function of the round velocity alone, with altitude and angle of attack preset, various types of HEAT and AP rounds were consistently destroyed regardless of their velocities. It is probably the first time in history that this has been accomplished.

(S) In a simplified version of the complete experimental setup which, however, contained the full assembly of the electronic computers, a Microflash unit was employed to simulate the defending charge. The rounds were "hit", that is, illuminated by the Microflash light pulse and photographed automatically in a camera that is sighted along the fragmentation plane of the hypothetical charge, with the timing of the Microflash computed in the same way as the timing of the defending charge firing pulse would have been computed. In field tests made with velocities from 1200 to 3300 ft/sec, altitudes from 0 to 5 ft, and angles of attack from 0 to 55 deg off-normal, the photographs showed the rounds "frozen" in the position in which they would have been impacted by the defending charge fragments.

(S) In an alternative, active X-band microwave approach, the problems of locating the approaching round and determining its height of attack have not yet been solved with sufficient accuracy. For the velocity determination, the radar-doppler method proved to be able to furnish the accuracy necessary. The firing-time computer has been completed, while the charge-selection computer has not yet been attacked.

# SECRET

# SECRET

## 1. INTRODUCTION

H. W. Straub

(C) With the advent of high-penetration projectiles of the shaped-charge, kinetic-energy, or high-explosive-plastic type, static armor as it has been used with increasing refinement throughout the millennia since the Stone Age has finally lost the race to the attack weapons. As these rounds are capable of defeating steel armor ten and more in. in thickness, a tank carrying sufficient armor to withstand them would no longer be acceptable in terms of weight (air-transportability) and maneuverability.

(S) The purpose of the Project Dash-Dot is to develop a system for the protection of tanks that defeats the approaching projectiles at a distance large enough to prevent damage to the vehicle. Credit for this basic concept is due to Picatinny Arsenal.

(S) The over-all system consists of:

(a) A sensing-computing system that locates an approaching round within a few feet from the tank, computes its trajectory, decides whether or not it is potentially dangerous (discrimination against small arms fire) and, if the round is found dangerous, selects the defending charge in the right place and transmits to it a firing pulse at the right time to defeat the attacking round.

(b) An array of defending charges located on the tank periphery and so oriented as to be capable of intercepting and defeating an approaching round, if the right charge is fired at the right time.

(C) Early in 1957 over-all responsibility for the project was officially assigned to OTAC, with the responsibility for the defending charges going to Picatinny Arsenal, the research and development work on defending charges to be carried by BRL/APG, and the responsibility for the sensing-computing system going to DOFL. A test of the feasibility of the system was scheduled for June 1960.

(U) The history of the project since 1957 as well as a summary of the achievements made under it until mid 1959 have been set forth in a report by OTAC.\*

(S) However, prior to the official assignment of responsibilities, Picatinny Arsenal had already been doing work on Project Dash-Dot. A contract concerning development of a sensing-computing system using

\* "Summary Report on Project Dash-Dot," by M. Michaelson: Report No. RRD 3, Ordnance Tank Automotive Command, Detroit Arsenal, Centerline, Michigan, September 1959, SECRET.

# SECRET

11

## SECRET

X-band microwaves for sensing had been let to United Shoe Machinery Company, Beverly, Massachusetts. In April 1956, technical supervision of the contract was assigned to, and assumed by, DOFL. Work done under it is described in section 14 of this report.

(S) Also prior to the official assignment of responsibilities, in December 1955, Mr. Wilbur S. Hinman, Jr., Technical Director of Diamond Ordnance Fuze Laboratories, suggested another approach which would use optical, preferably infrared techniques, for detecting an oncoming round and supplying the information for the computation of its trajectory. Work on an optical-electronic sensing and computing system was immediately initiated at the Diamond Ordnance Fuze Laboratories and carried on with DOFL R&D funds until the official assignment of responsibility under OTAC's cognizance with OTAC funds.

(S) The work has been subdivided into the following phases:

- (a) Detection of the approach of an attacking round,
- (b) Computation of the velocity and the trajectory,
- (c) Decision on potential danger of the round (rejection of small-arms fire),
- (d) Selection of the defending charge to be fired,
- (e) Transmission of a firing pulse to the selected charge at the time computed to produce interception of attacking round by defending charge fragments.

(S) Only horizontal, that is, point-blank attack has been considered at this stage because this is the expected direction of attack and because deviations within plus/minus 15 deg off the horizontal cause errors that are small compared with the maximum acceptable error of the over-all system.

(C) It has been assumed that the vehicle to be protected has some residual armor on it to defeat small-arms fire.

(U) The initial equipment, which used rather crude optics, and the tests that proved that it is indeed possible to obtain from fast-moving shells signals of sufficient magnitude as to be usable in a computer, have been described in previous reports.\*

\* DOFL Report TR-470, "A Sensing System for Dash-Dot," (U) by L. Melamed, H. W. Straub, R. R. Ulrich, 1 September 1957 (SECRET)

"A Sensing System for Dynamic Armor," (U) by H. W. Straub, Report of Army Science Conference, United States Military Academy, West Point, New York, 26-28 June 1957, Volume 4, pp 256-263 (SECRET)

**SECRET**

(U) The experimental equipment designed and constructed to solve the successive phases of the project and to meet the specifications for the June 1960 feasibility test, and the results of the laboratory and field tests made with it, are described in the following sections. The description is encyclopedic in most places because it is expected that many of the items developed can be of use elsewhere for applications other than the immediate one.

(U) Noteworthy among them is an electronic dividing computer (section 10.8) in which the dividing process is initiated before the total dividend has been entered and in which there is no delay in obtaining the result.

(S) Anticipating the field test results described in section 13, it may be pointed out that kinetic energy as well as HEAT rounds have consistently been defeated. This is probably the first time that shells have been intercepted and defeated intentionally in flight.

(U) The project was placed on the deferred list in September 1959 before the optical detection hardware intended for the June 1960 test had been designed. However, since an experimental prototype of the sensing system and all the electronic computers had been nearly completed at the cutoff date, it was decided at DOFL to complete the equipment and, to make a field test evaluation of the practicability of the basic concept with DOFL R&D funds.

**SECRET**

13

This document contains information affecting the national defense of the United States within the meaning of the espionage laws, title, 18 U. S. C., 793 and 794. Its transmission or the revelation of its contents in any manner to an unauthorized person is prohibited by law.

# SECRET

## 2. GENERAL SYSTEMS ANALYSIS

W. Moore, A. Copeland, R. J. Paradis

(C) In order to evaluate various sensing-computer schemes to solve the Dash-Dot problem, it is advantageous to examine certain phases of the state of the art and their effect on the type of sensing-computer systems that may be employed to meet the basic system requirements. Among the most easily analyzed is the effect of defending charge fragment velocity.

### 2.1 Limitations Imposed by Fragment Velocity

(S) As stated previously, the defending charge is to be initiated at some point on the periphery of the tank, such that the fragments intercept and destroy the attacking round. These fragments travel in essentially straight lines to form a jet or sheet of lethal particles traveling at a high rate of speed. Figure 2-1 illustrates these points for the case where the fragment trajectory and attacking round trajectory are normal to each other.

(S) If the fragments travel at a speed greatly in excess of that of the attacking round speed, say, at 100 times that speed, the attacking round travels only a small distance,  $h/100$  (figure 2-1) in the time required for the fragments to travel the distance,  $h$ . From figure 2-1, it follows that, if the attacking round passes over the defending charge at a height,  $h$ , which is 5 ft = 60 in., the attacking round can only travel 0.6 in. in the time the fragments travel 60 in. When the two trajectories are inclined to each other, as in figure 2-2, the movement of the attacking round is greater for a given height of trajectory. If the angle  $\beta_1$  shown is 30 deg, the fragments must travel the distance  $h/\cos 30 \text{ deg}$ . The time required for the fragments to travel this distance is  $h/(100 V_m \cos 30 \text{ deg})$ , where  $V_m$  is the speed of the attacking round. Thus, the attacking round will move a distance  $h/100 \cos 30 \text{ deg}$  in this same time. For the case where  $h$  equals 60 in., the round will travel 0.693 in. In most cases this movement of the attacking round could be tolerated.

(S) Thus, when the fragment velocity greatly exceeds that of the attacking round, the sensing beam of the optical-sensing device may coincide, as nearly as may be practicable (figure 2-3) with the path of the fragments, and no offset between sensing beam and fragment path and no computing equipment is needed to compensate for variations in the speed of the attacking round and the height and orientation of its trajectory.

(S) In the present state of the art, however, the fragment velocity does not greatly exceed that of the attacking round, the presently attainable maximum values being about 12,000 and 5000 fps, respectively. The simple system described above is, therefore, not practicable. Figure 2-4 illustrates this fact for the case of the fragment velocity normal to the

# SECRET

15

SECRET

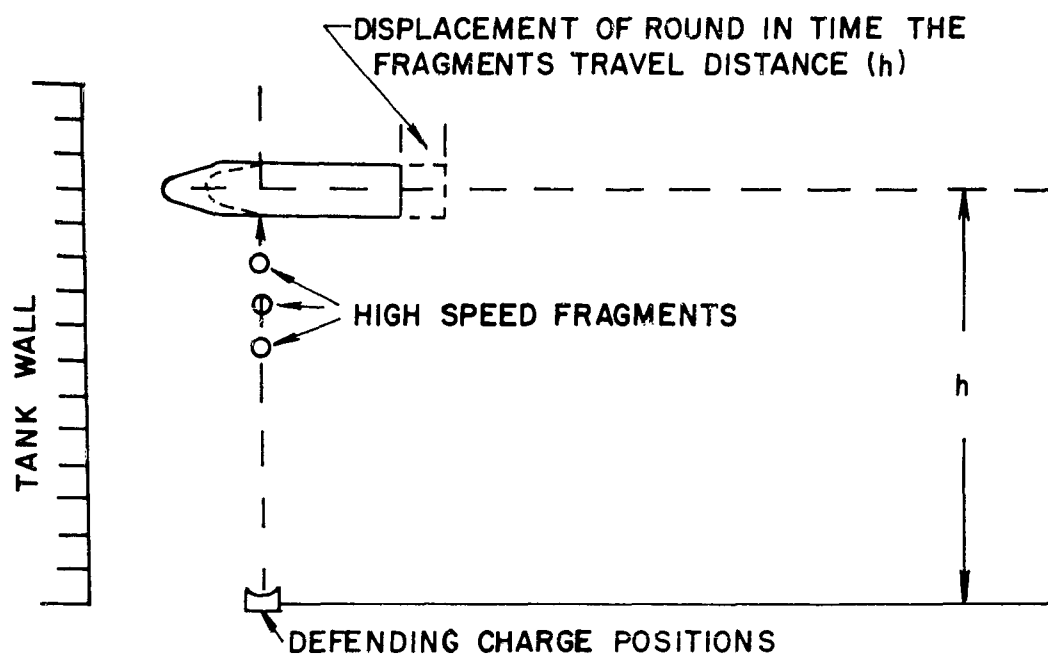


Figure 2-1. Vertical fragment velocity versus round displacement

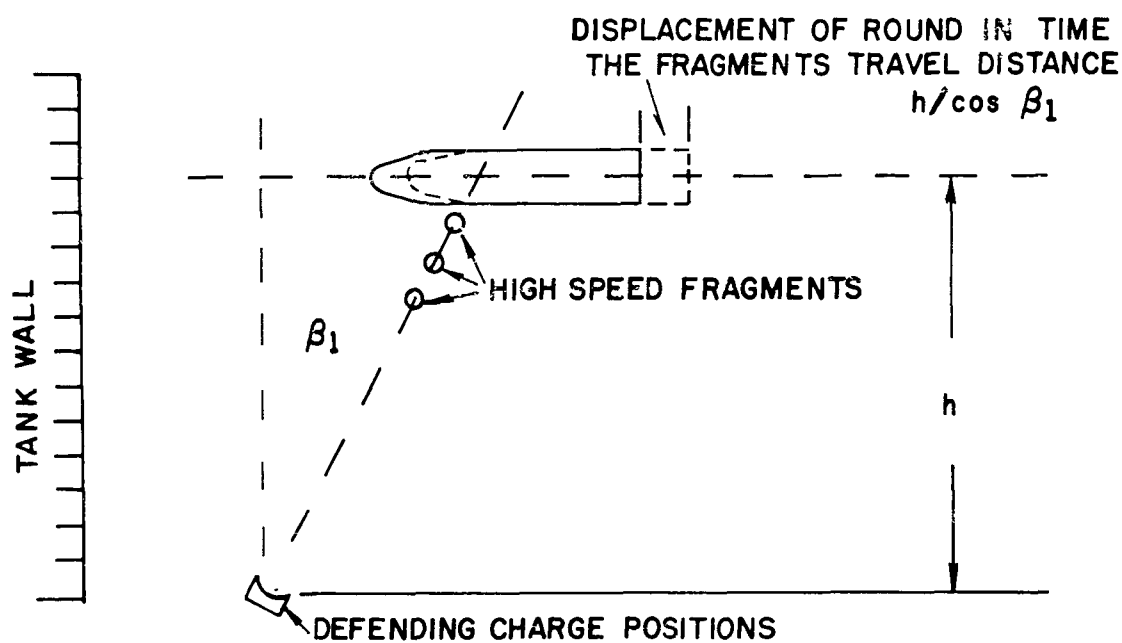


Figure 2-2. Inclined fragment velocity versus round displacement

SECRET

**SECRET**

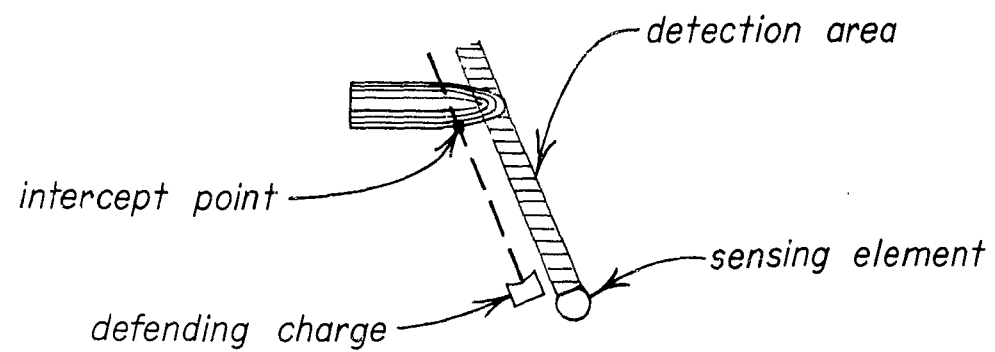


Figure 2-3. Parallel sensing elements and defending charge

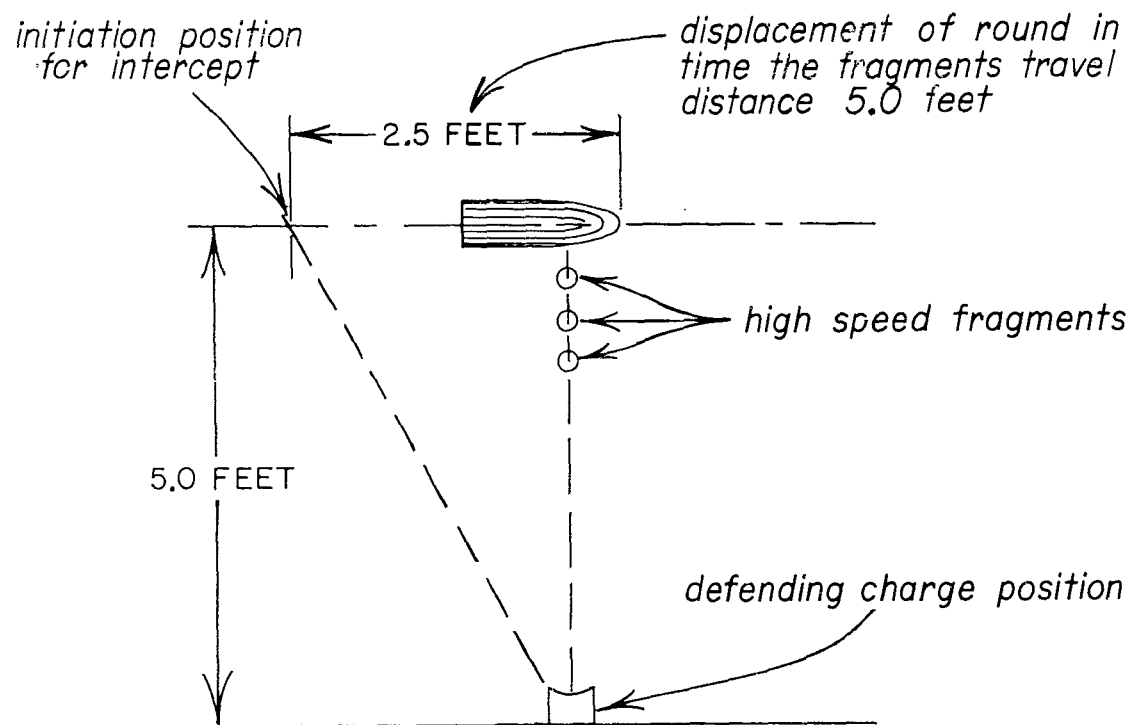


Figure 2-4. Attacking round speed equals one-half fragment speed

**SECRET**

## SECRET

round trajectory. When the attacking round speed is one-half the fragment speed, the charge must be initiated when the round is 2.5 ft in front of the fragment trajectory for a height of 5 ft.

(S) This may be developed for the general case using figure 2-5. The quantity to be determined is the distance in front of the intercept point at which the attacking round must be, when the defending charge is initiated, in order to accomplish an intercept. The conditions to be satisfied for normal attack are that the time required for the attacking round to go from E to D is equal to the time for the fragments to travel from A to D, or

$$\frac{\overline{DE}}{V_m} = \frac{\overline{AD}}{V_c},$$

where

$V_m$  = the attacking round speed, and

$V_c$  = the fragment speed.

Then

$$\overline{DE} = (V_m/V_c) h/\cos \beta_1,$$

where

$\beta_1$  = angle of fragment trajectory with the vertical.

(S) It is obvious that the maximum value of  $\overline{DE}$  occurs for the maximum speed and trajectory height of the attacking round. It will be noticed that the distance  $\overline{DE}$  is independent of the attack angle of the round, but the actual spatial position varies as the attack angle changes. Thus, for a round with a nonnormal attack angle  $\beta_2$ , figure 2-6, and the same speed, the charge must be initiated when the round is at point E' where  $\overline{DE'} = \overline{DE}$ .

(S) From this, it is apparent that any sensing-computer system used must be capable of determining the attacking round speed, trajectory height, and spatial position before the attacking round is within the distance  $\overline{DE}$  of the fragment trajectory.

### 2.2 Approaches Considered for the Timing Problem

(S) Two approaches were considered for solving the Dash-Dot problem: (a) optical and (b) microwave. The microwave approach is discussed in section 14 of this report.

SECRET

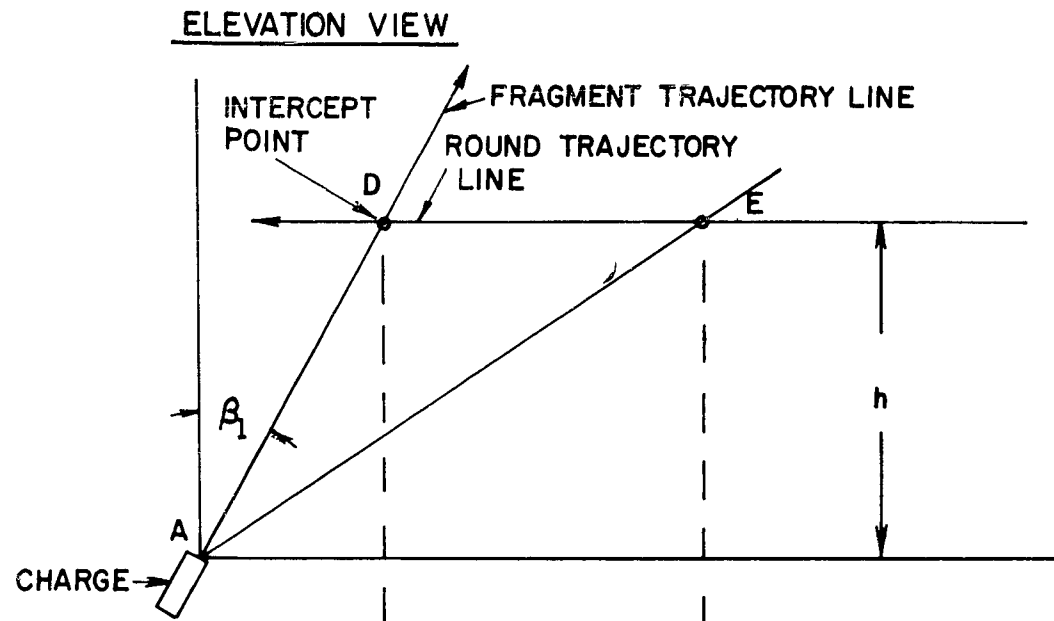


Figure 2-5. Intercept point for normal attack

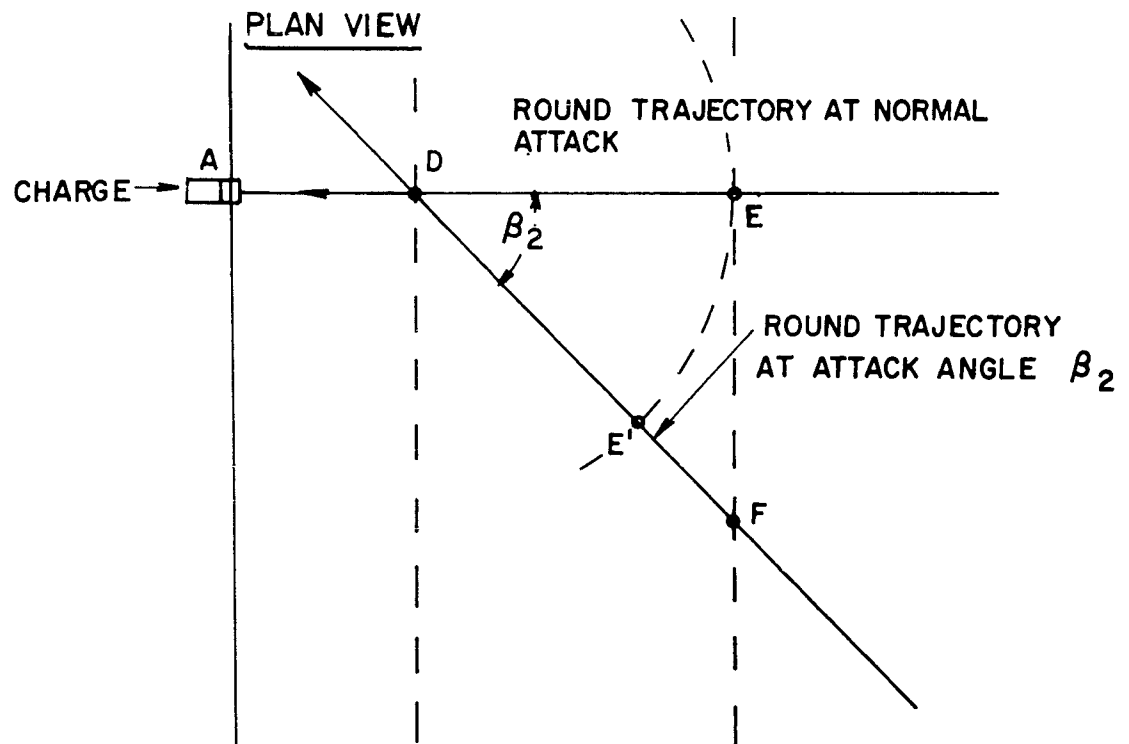


Figure 2-6. Intercept for nonnormal attack

SECRET

## SECRET

(S) The optical approach employs optical techniques to establish a set of detection areas in space; these areas are so arranged that the necessary information regarding velocity and trajectory of the approaching round can be obtained.

(S) The information is derived from the electrical output of photo-cells associated with the optical elements (section 4). When the projectile passes through the field of view of an optical detecting beam, the photocell and associated circuitry produce an electrical output pulse.

(C) The manner in which the detecting beams are arranged is referred to as the geometry of a particular system. There are many geometries that may be employed to give the same basic information regarding velocity and trajectory.

(S) Although many geometries were surveyed for the optical approach, only two received serious consideration. Each of these two geometries is based on the following assumptions:

- (a) Speed of attacking round is essentially constant.
- (b) Trajectories are straight line paths parallel to the ground.

Figures 2-7 and 2-8 show the basic arrangements of the two geometries. For purposes of convenience they are referred to as inclined-beam and vertical-beam geometries.

(S) In various applications the space required for mounting the defending charges and sensing elements is very important. Two quantities of primary interest are the distance that the defending charges and sensing elements extend in front of the protected area (front overhang) and the distance these elements must extend beyond the corner of the defended area (end overhang) to provide full protection for oblique attack. Some of the parameters that influence the overhangs are:

- (a) Type of detection pattern employed,
- (b) Ratio of maximum attacking round speed to defending charge fragment speed,
- (c) Physical protection for sensing units from defending charge blast and attacking round blast,
- (d) Methods employed for measuring the velocity, and trajectory, e.g., microwave Doppler or spaced detection areas for obtaining velocity,
- (e) Protection for defended area from defending charge blast,
- (f) Type of area to be defended (vertical or sloping plate) and size of defended area,

## SECRET

SECRET

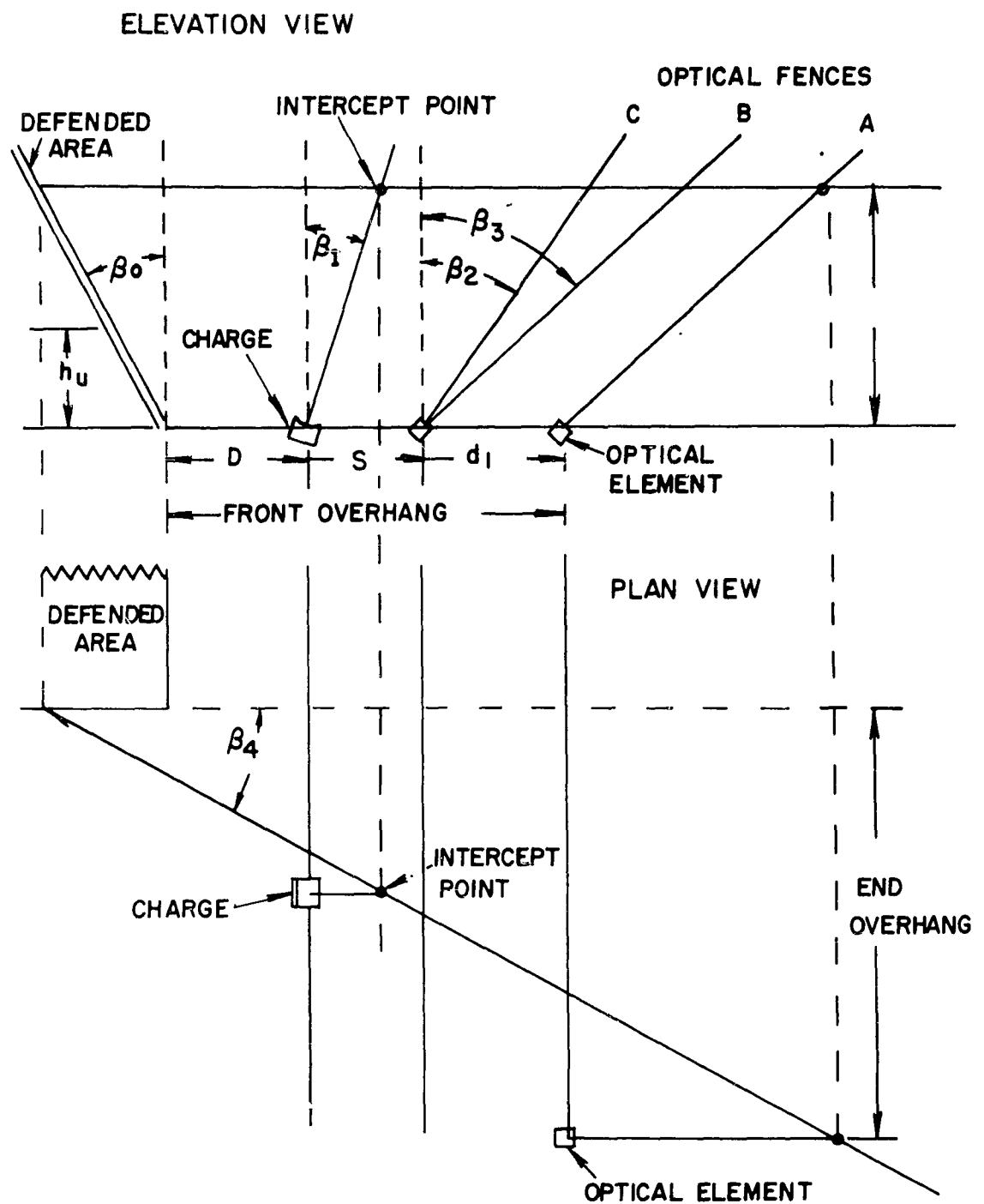


Figure 2-7. Inclined-beam geometry

SECRET

SECRET

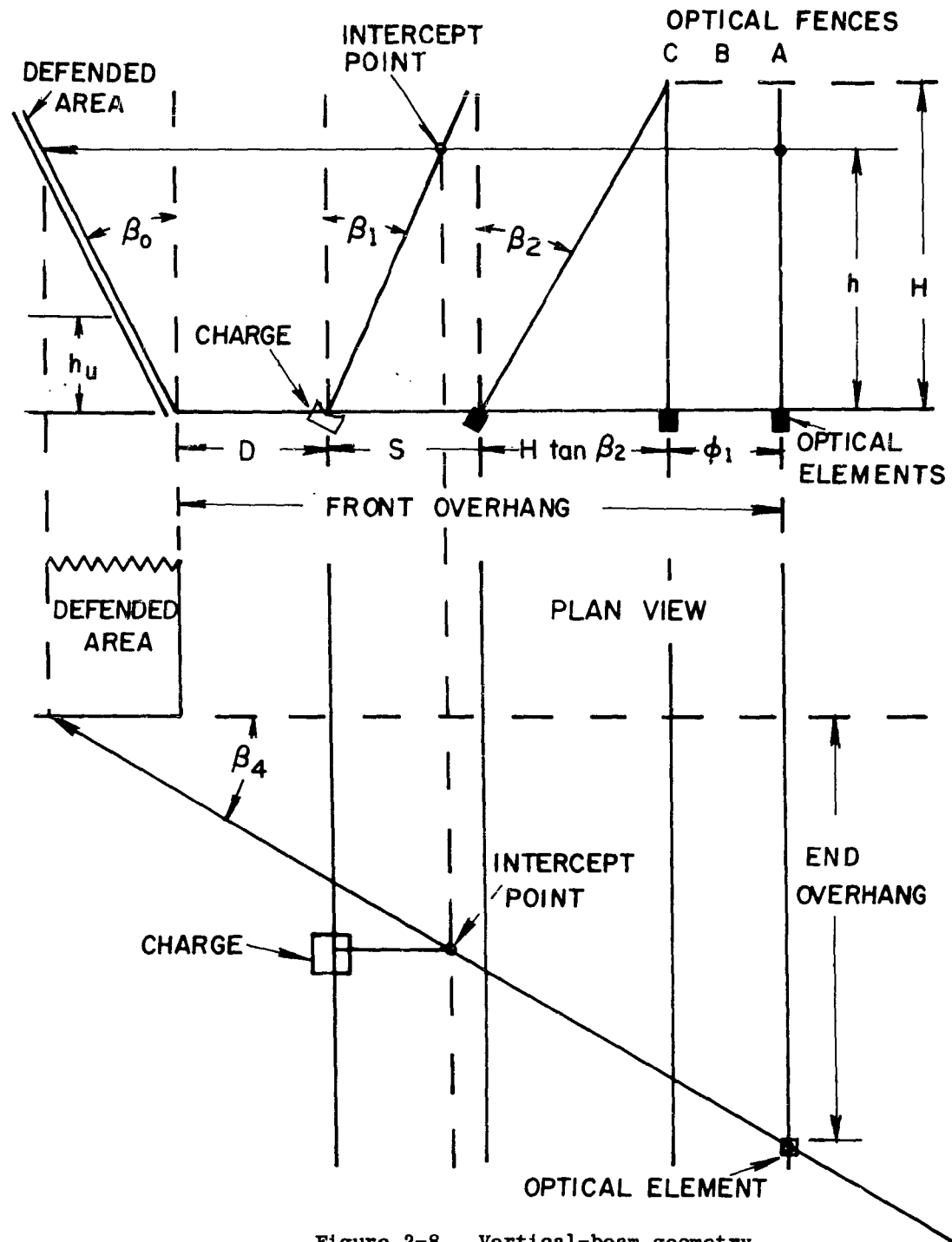


Figure 2-8. Vertical-beam geometry

SECRET

# SECRET

- (g) Time required for computation and defending charge initiation,
- (h) Maximum speed, height, and attack angles to be protected against.

## 2.2.1 Front Overhang in Inclined-Beam Optical Approach

(S) In the geometries considered, the detecting beams are arranged in three straight fences. All beams in any one fence are parallel to each other and their spatial position is known from the design data. Also, the photocells in the detection elements are individually connected with the computer.

(S) The inclined-beam geometry has the fences so arranged that they and the defending charge fragment paths are inclined with respect to the vertical by angles  $\beta_1$ ,  $\beta_2$ , and  $\beta_3$  (figure 2-7). The fences A and B are parallel and are used to obtain velocity information. Fences B and C make an angle  $\beta_3 - \beta_2$  with respect to each other and provide the means for obtaining height-of-attack information once the velocity is known.

(S) It can be seen that the front overhang for this geometry is equal to the distance S plus  $d_y$  plus the distance D that the defending charges may be placed in front of the protected area. The distance s is determined by certain restrictions of physical protection for the optical elements and the maximum velocities of the defending charge fragments and the attacking round.

(S) Only after the attacking round has passed all optical fences, A, B, and C, and generated an electric pulse in the photocell of each, is there sufficient information to determine the time when the defending charge should be initiated. This places the restriction upon the geometry that the time required for the attacking round to pass from the fence C to the fragment trajectory must be greater than the time required for the fragments to travel to the particular height of the attacking round trajectory. From the geometry this is seen to be:

$$\frac{h}{v_c \cos \beta_1} < \frac{S + h (\tan \beta_2 - \tan \beta_1)}{v_m} - I_t, \quad (2.1)$$

or

$$S > v_m h \left[ \frac{1}{v_c \cos \beta_1} - \frac{(\tan \beta_2 - \tan \beta_1)}{v_m} \right] + I_t v_m, \quad (2.2)$$

# SECRET

This document contains information affecting the national defense of the United States within the meaning of the espionage laws, title, 18 U. S. C., 793 and 794. Its transmission or the revelation of its contents in any manner to an unauthorized person is prohibited by law.

# SECRET

where

$h$  = height of attacking round trajectory above zero level,  
 $V_c$  = velocity of defending charge fragments,  
 $V_m$  = velocity of attacking round,  
 $\beta_1$  = angle between fragment trajectory and vertical,  
 $\beta_2$  = angle between C-fence and vertical, and  
 $I_t$  = time required to initiate the defending charge.

(S) The angle  $\beta_1$  depends a great deal upon the type of area to be protected, i.e., whether it is a vertical plate or slopes back from the vertical and whether the area to be defended can have an unprotected region for some height  $h_u$  above the defending charges. It may also depend upon the allowable distance  $D$  that the defending charge may be placed in front of the protected area and the type of attacking round. To illustrate this relationship, assume that for a particular attacking round the charge fragments must intercept the round at some distance  $D_1$  back of the nose (figure 2-9). Then the distance from the intercept point to the defended area must be greater than  $D_1$  or the shell will strike the defended area before the fragments destroy the attacking round. This condition may be stated as:

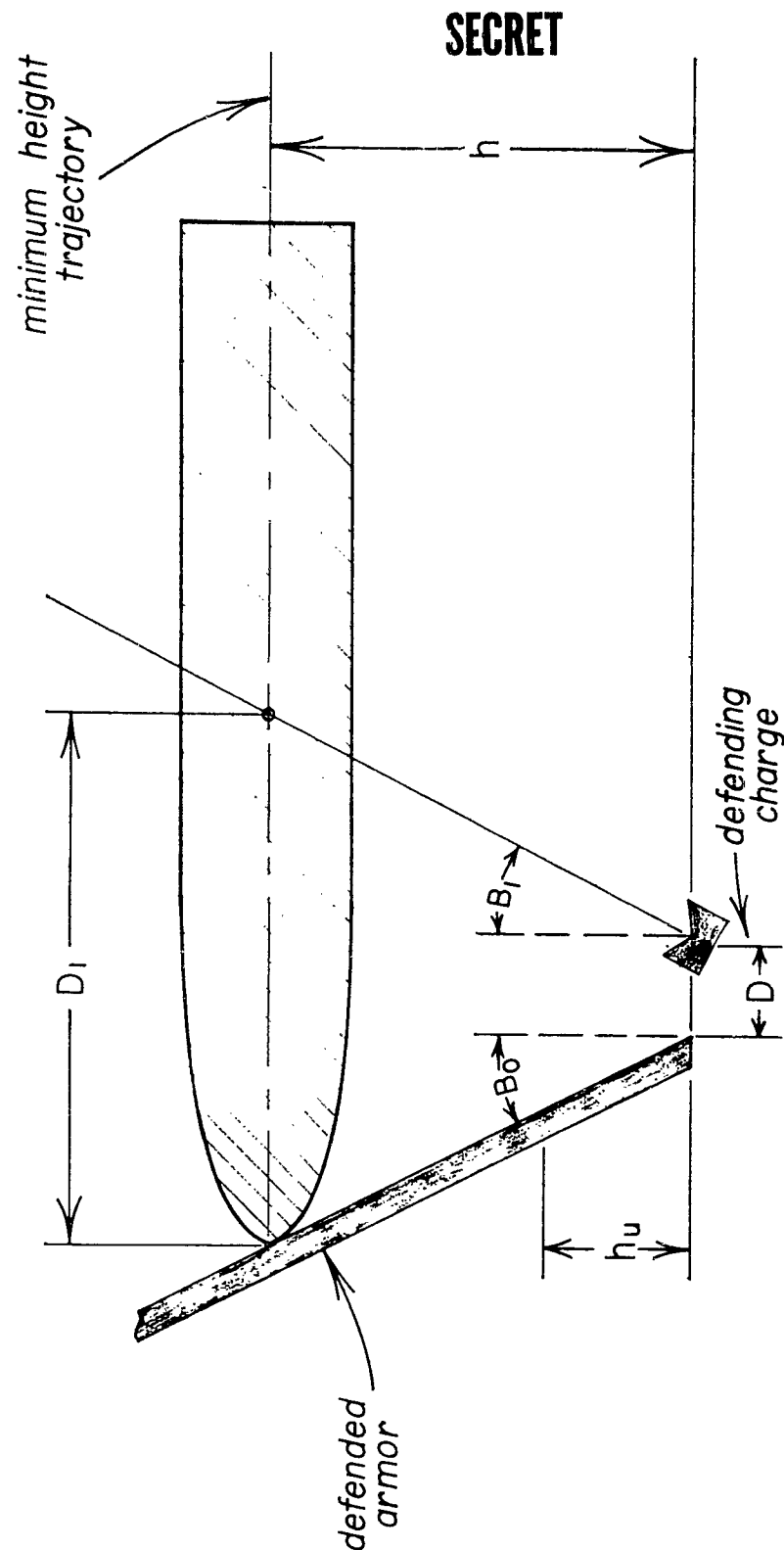
$$D > D_1 - h_u (\tan \beta_0 + \tan \beta_1) . \quad (2.3)$$

(S) It is known that for some shell  $D_1$  will be as great as 14 in. The unprotected height, defending charge placement, and the angle  $\beta_0$  will probably be specified by the particular application; if so, the minimum  $\beta_1$  will be determined.

(S) The distance  $d_1$  between the fences A and B is determined on the basis of the minimum distance required to give accurate velocity measurements consistent with the practical mounting of the optical elements. If  $d_1$  is made too small, slight errors in displacement cause large percentage errors in the velocity determination. A distance of one foot for  $d_1$  was found to be compatible with the accuracies required.

(S) The final result is that the front overhang for the inclined-beam geometry can be found with reasonable accuracy from:

$$D + S + d_1 > D_1 - h_u (\tan \beta_1 + \tan \beta_0) + \frac{V_m \max h \max}{V_c \cos \beta_1} \left[ \frac{1}{V_c \cos \beta_1} - \frac{(\tan \beta_2 - \tan \beta_1)}{V_m} \right] + I_t V_m \max + d_1 , \quad (2.4)$$



**SECRET**

Figure 2-9. Minimum distance for defending charge

# SECRET

where the individual conditions to be satisfied are:

$$(a) \quad D > D_i - h_u (\tan \beta_1 + \tan \beta_o),$$

$$(b) \quad S > V_{m|max} h_{max} \left[ \frac{1}{V_c \cos \beta_1} - \frac{(\tan \beta_2 - \tan \beta_1)}{V_m} \right] + I_t V_{m|max}, \text{ and}$$

$$(c) \quad d_1 \text{ is great enough to assure accurate velocity determination.}$$

The maximum attacking round speed and height are used in order to meet the worst conditions to be encountered.

## 2.2.2 End Overhang in Inclined-Beam Optical Approach

(S) The end overhang for a system may or may not be a real physical extension beyond the edge of the protected area. For the inclined-beam geometry, the extension will be real if the sensing elements define cylindrical detection regions of one form or another. The optical elements considered for this approach had such cylindrical detection regions.\*

(S) The end overhang for this system (figure 2-7) can be expressed by

$$L_{eo} = \left\{ D + S + d_1 + h [\tan \beta_o + \tan \beta_3] \right\} \tan \beta_4, \quad (2.5)$$

where all parameters are the same as used for the front overhang and  $\beta_4$  is the attack angle of the attacking round. When the parameters  $h$ ,  $\beta_o$ ,  $\beta_3$ , and  $\beta_4$  are fairly large, the end overhang may become intolerable. For example: let  $h = 5$  ft,  $\beta_o = 45$  deg,  $\beta_3 = 45$  deg, and  $\beta_4 = 60$  deg, then

$$L_{eo} = 1.73 (D + s + d_1) + 5.0 (1 + 1) 1.73, \text{ or}$$

$$= 1.73 (D + s + d_1) + 17.3 \text{ ft.}$$

Thus, even if there were no front overhang, the end overhang would be 17.3 ft.

\* Sensing elements having flat, fan-shaped detection regions, which render unnecessary any physical extension, were developed near the conclusion of this work. They could not be incorporated in the system because of lack of time.

# SECRET

# SECRET

## 2.2.3 Front Overhang in Vertical-Beam Optical Approach

(S) The vertical-beam geometry is shown in figure 2-8. Detection fences A and B are vertical and parallel and are used to obtain velocity information. Fence C is inclined at an angle  $\beta_2$  and the defending charge fragment path is inclined at an angle  $\beta_1$ .

(S) The front overhang for this geometry is equal to the distance S plus the distance  $d_1$  plus  $H \tan \beta_2$  plus the distance, D, at which the defending charges may be placed in front of the protected area. The distance S is determined by the maximum attacking round speed expected as well as the minimum height of the round. As in the inclined-beam geometry, the vertical geometry restrictions are such that the fragment time  $(h/V_c \cos \beta_1)$  must satisfy the relation

$$\frac{h}{V_c \cos \beta_1} < \frac{S + h (\tan \beta_2 - \tan \beta_1)}{V_m} - I_t, \quad (2.6)$$

where the parameters are the same as the inclined geometry. The maximum front overhang can be determined in the same manner as the inclined-beam geometry.

## 2.2.4 End Overhang in Vertical-Beam Optical Approach

(S) The optical elements used in this approach are again assumed to define a cylindrical detection region. The end overhang can be expressed as:

$$L_{eo} = (D + S + d_1 + h \tan \beta_0 + H \tan \beta_2) \tan \beta_4 \quad (2.7)$$

where again the parameters are the same as for the inclined-beam geometry.

(S) A typical example of overhang for full protection of the tank armor versus a 60-deg attacking round is shown in figure 2-10. It will be noted that for full protection, an overhang of 25 ft is required. Examples of overhang for less than full protection are also shown in figure 2-10.

## 2.2.5 Overhang Reduction

(S) It is obvious from the foregoing discussion that some overhang, both front and side, will be required for both the inclined and vertical approaches. Other methods were analyzed in an attempt to reduce front

SECRET

SECRET

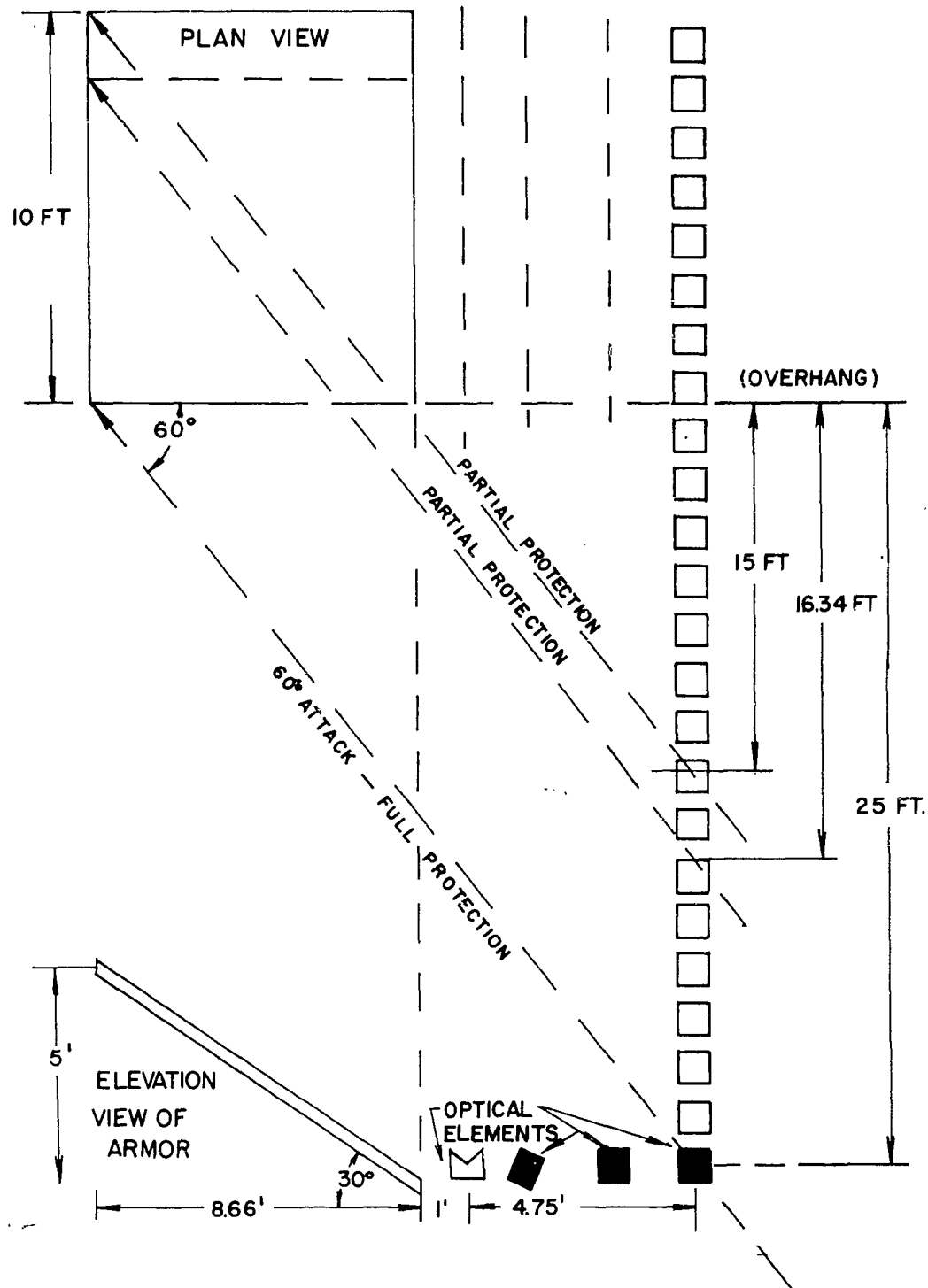


Figure 2-10. Overhang for various degrees of armour protection

SECRET

# SECRET

overhang. Two such methods are shown in figures 2-11 and 2-12. Each of these would reduce front overhang and their parameters can be derived in the same manner as they were for the inclined-beam geometry.

(S) A method for reducing end overhang is shown in figure 2-13. In this figure it is assumed that the front and sides of the tank armor are protected. A 45-deg array is attached to the corner of the tank. The array is an independent system, that is, it would contain its own computer and defending charges. It is readily apparent that this method would reduce the end overhang considerably. Other methods of reducing end overhang may be employed; however, lack of time precluded investigation of this phase of the project.

## 2.2.6 Effect of Restricting Overhang for Vertical Protected Area

(C) It was stated (oral communication) by OTAC in June 1959 that in any system used on a vehicle, the front overhang should not exceed 6 in. and that the maximum allowable space in the vertical for mounting the system would be 1 ft. As a consequence of these restrictions, the following analysis was made:

(S) Assuming that in some cases a shell must be hit 14 in. back of its nose, e.g., as in the 106-mm HEAT round, then the intersection of the minimum height trajectory line (figure 2-14) and the fragment trajectory line must occur at a distance of 14 in. or more from the plate to be protected (point P in figure 2-14.)

### CASE I

(S) If the line charge lies at the intersection of the fragment trajectory and the plate line, then the unprotected height  $h_u$  above the line charge is determined by:

$$h_u = 14 \text{ in.} / \tan x, \quad (2.8)$$

where  $x$  is the angle between the fragment trajectory and the plate line. The distance that the line charge fragments have to travel to the minimum trajectory line is given by:

$$L = 14 \text{ in.} / \sin x. \quad (2.9)$$

(S) If  $L_{\max}$  is the greatest lethal range of the line charge fragments, then the protected height  $h_u$  is seen to be:

# SECRET

SECRET

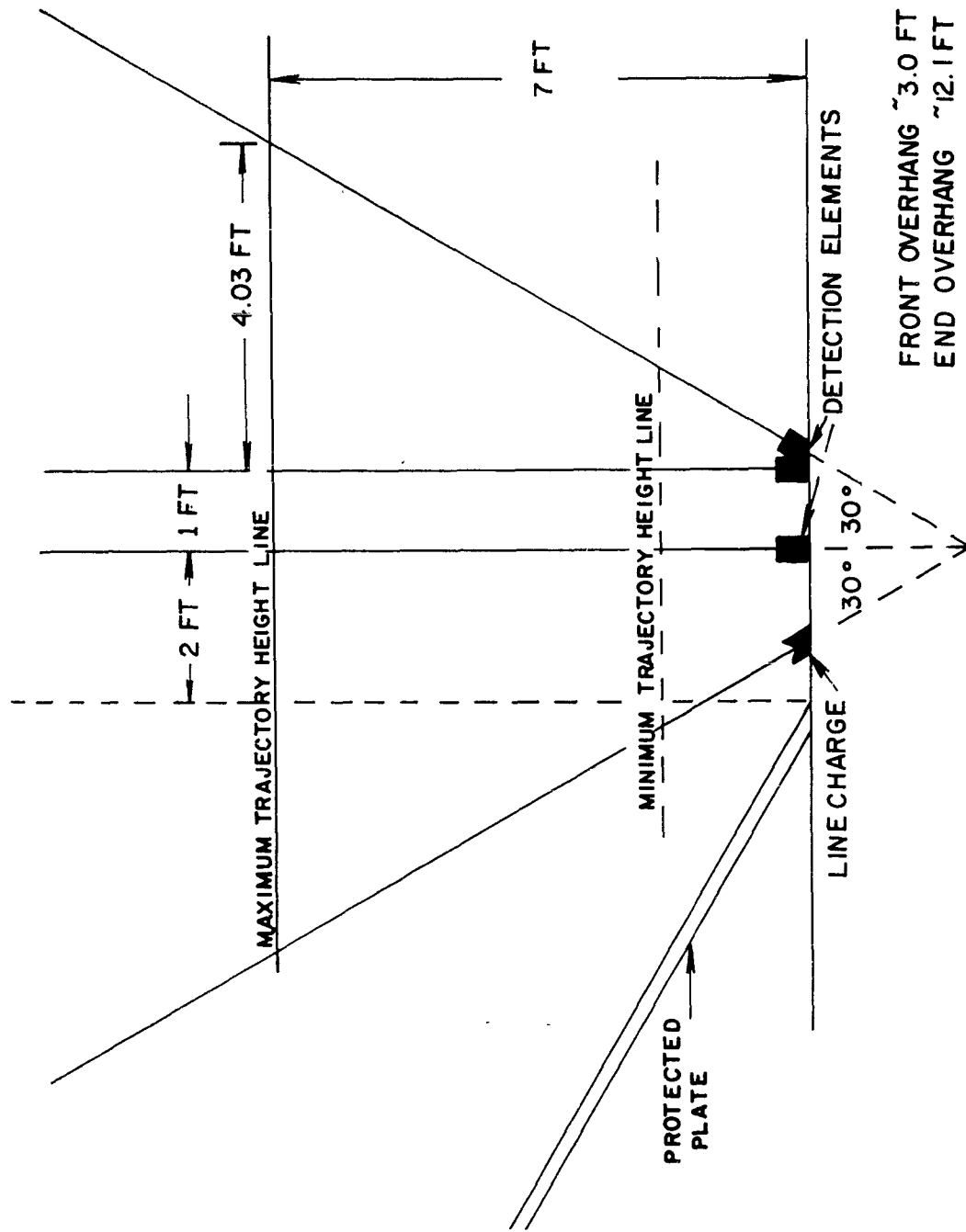


Figure 2-11. One method for reduction of overhang

SECRET

SECRET

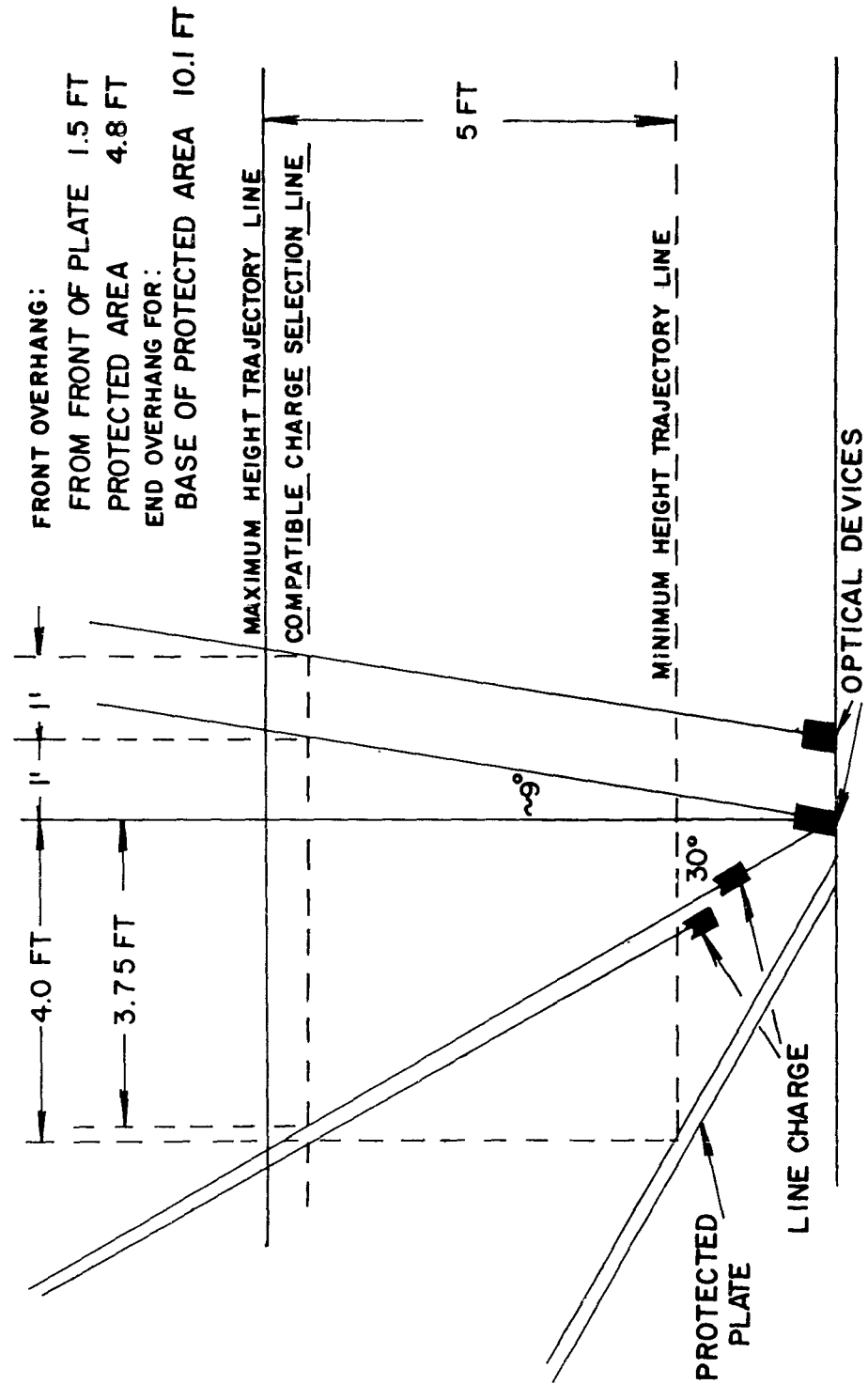


Figure 2-12. A second method for reduction of overhang

SECRET

SECRET

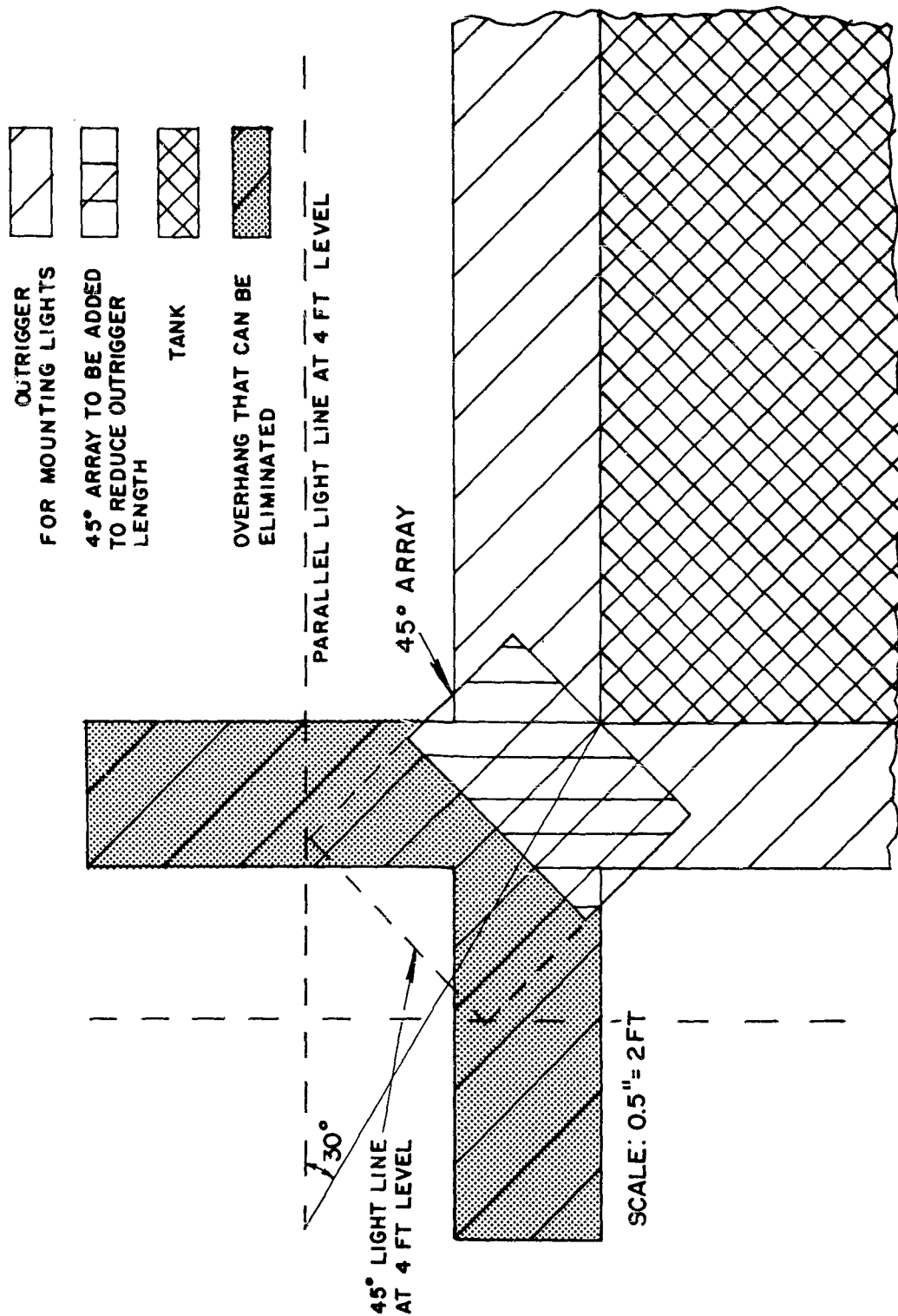
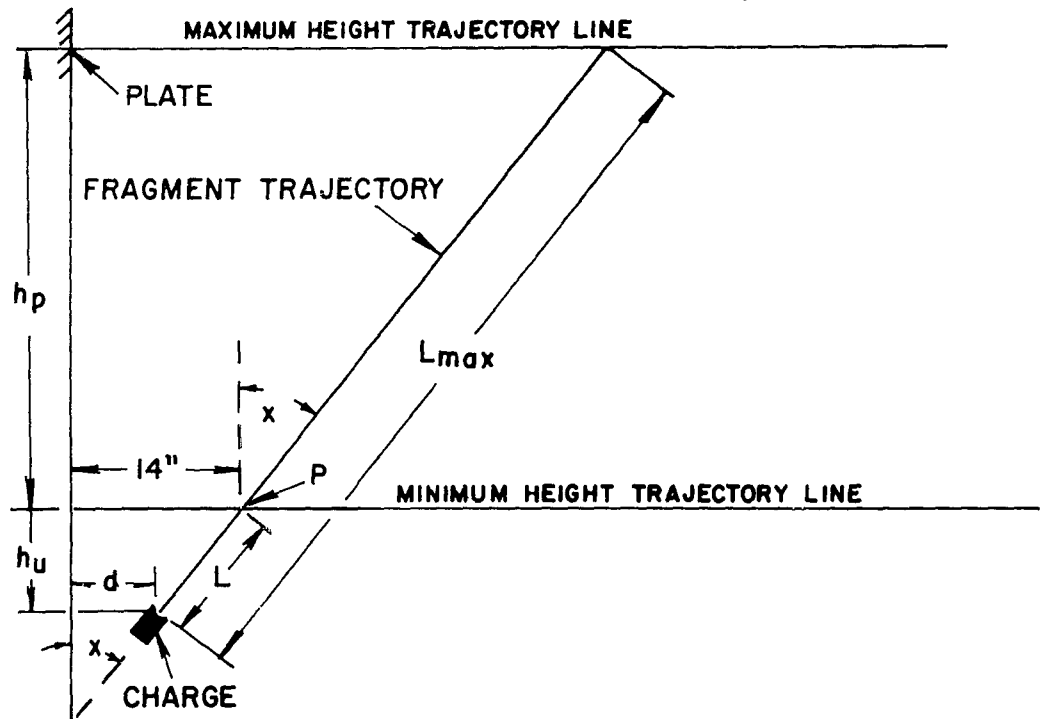
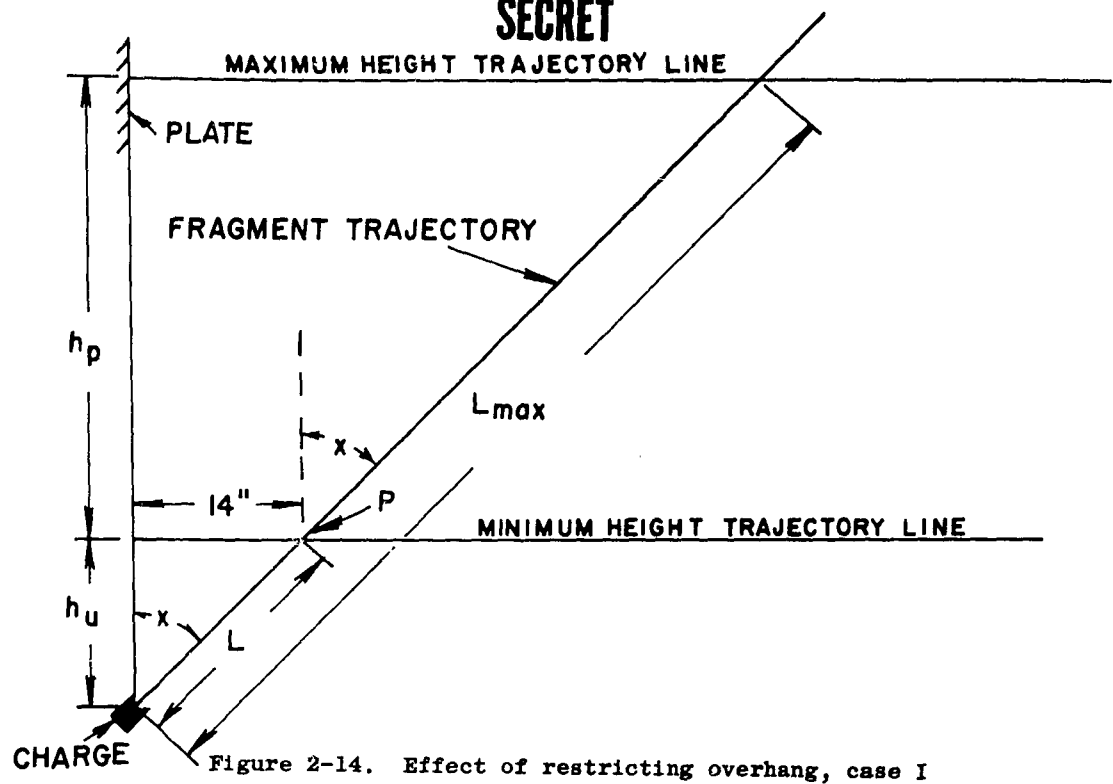


Figure 2-13. Method for reduction of end overhang

SECRET

**SECRET**



**SECRET**

# SECRET

$$h_p = (L_{\max} - L) \cos x, \text{ or} \quad (2.10)$$

$$\begin{aligned} h_p &= (L_{\max} - 14/\sin x) \cos x \\ &= (L_{\max} \cos x - 14 \cot x). \end{aligned}$$

To find the maximum ( $h_p$ ) for a given  $L_{\max}$ , we differentiate ( $h_p$ ) with respect to ( $x$ ),

$$\frac{dh_p}{dx} = -L_{\max} \sin x + 14 \csc^2 x.$$

For maximum and minimum, equate to zero,

$$\frac{dh_p}{dx} = 0 = -L_{\max} \sin x + 14 \csc^2 x.$$

Therefore,

$$\sin^3 x = 14/L_{\max}, \text{ or}$$

$$\sin x = (14/L_{\max})^{1/3}, \text{ for maximum protected height.} \quad (2.11)$$

## CASE II

(S) If the line charge can be mounted at some distance ( $d$ ) from the protected plate as shown (figure 2-15) then the following conditions hold:

$$h_u = (14 - d)/\tan x; \text{ or} \quad (2.12)$$

$$= 14/\tan x - d/\tan x; \quad (2.12a)$$

$$L = (14 - d)/\sin x; \quad (2.13)$$

$$h_p = (L_{\max} - L) \cos x; \text{ or} \quad (2.14)$$

$$= (L_{\max} - 14/\sin x + d/\sin x) \cos x. \quad (2.14a)$$

# SECRET

# SECRET

It is seen from equations (2.12) and (2.14a) that for the same  $x$ , case II differs from case I by decreasing the unprotected height  $h_u$  by  $d/\tan x$ , while increasing the protected height by the same amount.

(U) The maximum  $h_p$ , given  $L_{\max}$ , for case II, however, differs from case I, since  $h_p$  depends upon both  $x$  and  $d$ .

(U) From inspection of equations (2.12) and (2.14), it can be seen that  $h_p$  will equal  $L_{\max}$  if  $d = 14$  in. and  $x$  is zero. However, the restriction that  $d$  must be 6 in. or less prohibits  $h_p$  from equaling  $L_{\max}$ .

(C) Equation (2.14a) also shows that for a given  $x$  the value of  $h_p$  increases as the distance  $d$  increases from zero toward 6 in. Therefore, if  $d$  is made 6 in. and then the maximum value of  $h_p$  is determined as a function of  $x$ , the protected height will be as large as possible under the specified restrictions.

(U) By a process similar to that used in case I, the value of  $x$  needed for this maximum  $h_p$  is shown to be:

$$\begin{aligned}\sin x &= (14 - d)/L_{\max}^{1/3} \text{ with } d \text{ equal to } 6.0 \text{ in., or} \\ &= (8/L_{\max})^{1/3}.\end{aligned}\quad (2.15)$$

## CASE II with OTAC Requirements

(U) Requirements:  $d = 6$  in. and  
 $h_u = 12$  in. (figure 2-16).

(U) It can be seen that  $h_p$  in equation (2.14a) will be as great as possible if  $d$  is as large as possible in the range from zero to 14 in. -- 6 in. in this case -- and  $x$  is as small as possible.

(C) From equation (2.12).

$$\tan x = (14 - 6)/h_u.$$

Therefore,  $x$  will be as small as allowable when  $h_u$  is as large as possible, i.e., 12 in., so that

$$\begin{aligned}\tan x &= (14 - 6)/12 = 2/3 \text{ or} \\ x &= 33.7 \text{ deg.}\end{aligned}$$

(C) It also follows under these conditions, that since

$$h_p = (L_{\max} \cos x - h_u),$$

the protected height will be:

$$h_p = 0.832 L_{\max} - 12 \text{ in.}$$

SECRET

# SECRET

(S) The next quantity to determine would be the charge initiation line for maximum velocity shell (locus of points where maximum velocity shell must be when the charge is initiated to accomplish interception).

(S) The conditions to be satisfied are (figure 2-16) that the time required for the attacking round to go from E to D is equal to the time for the charge fragments to travel from A to D, or  $\overline{DE}/V_{\max} = \overline{AD}/V_c$ . From the geometry, however,

$$\overline{DE}/\sin x_2 = \overline{AD}/\sin x_3, \quad (2.16)$$

$$90^\circ + x_1 + x_2 + x_3 = 180^\circ, \text{ and}$$

$$x_3 = 90^\circ - (x_1 + x_2). \quad (2.17)$$

Therefore,

$$\begin{aligned} \sin x_2/\sin x_3 &= \overline{DE}/\overline{AD} = V_{\max}/V_c, \\ \sin x_2/\sin (90^\circ - x_1 - x_2) &= V_{\max}/V_c, \\ \sin x_2/\cos (x_1 + x_2) &= V_{\max}/V_c, \text{ and} \\ \sin x_2/(\cos x_1 \cos x_2 - \sin x_1 \sin x_2) &= V_{\max}/V_c. \end{aligned} \quad (2.18)$$

If reciprocals are taken and simplified, the result is

$$\begin{aligned} \cot x_2 \cos x_1 - \sin x_1 &= V_c/V_{\max}, \text{ and} \\ \cot x_2 &= (V_c/V_{\max} + \sin x_1)/\cos x_1. \end{aligned} \quad (2.19)$$

Using the values,

$$V_c = 8500 \text{ ft/sec}, V_{\max} = 5000 \text{ ft/sec}, \text{ and } x_1 = 33.7^\circ, \text{ yield}$$

$$\begin{aligned} \cot x_2 &= (8500/5000 + \sin 33.7^\circ)/\cos 33.7^\circ \text{ or} \\ &= (1.7 + 0.555)/0.832 = 2.7, \text{ and} \\ x_2 &= 20.3^\circ. \end{aligned}$$

**SECRET**

CONDITIONS FOR INTERCEPT:

$$\overline{DE}/V_{\max} = \overline{AD}/V_c$$

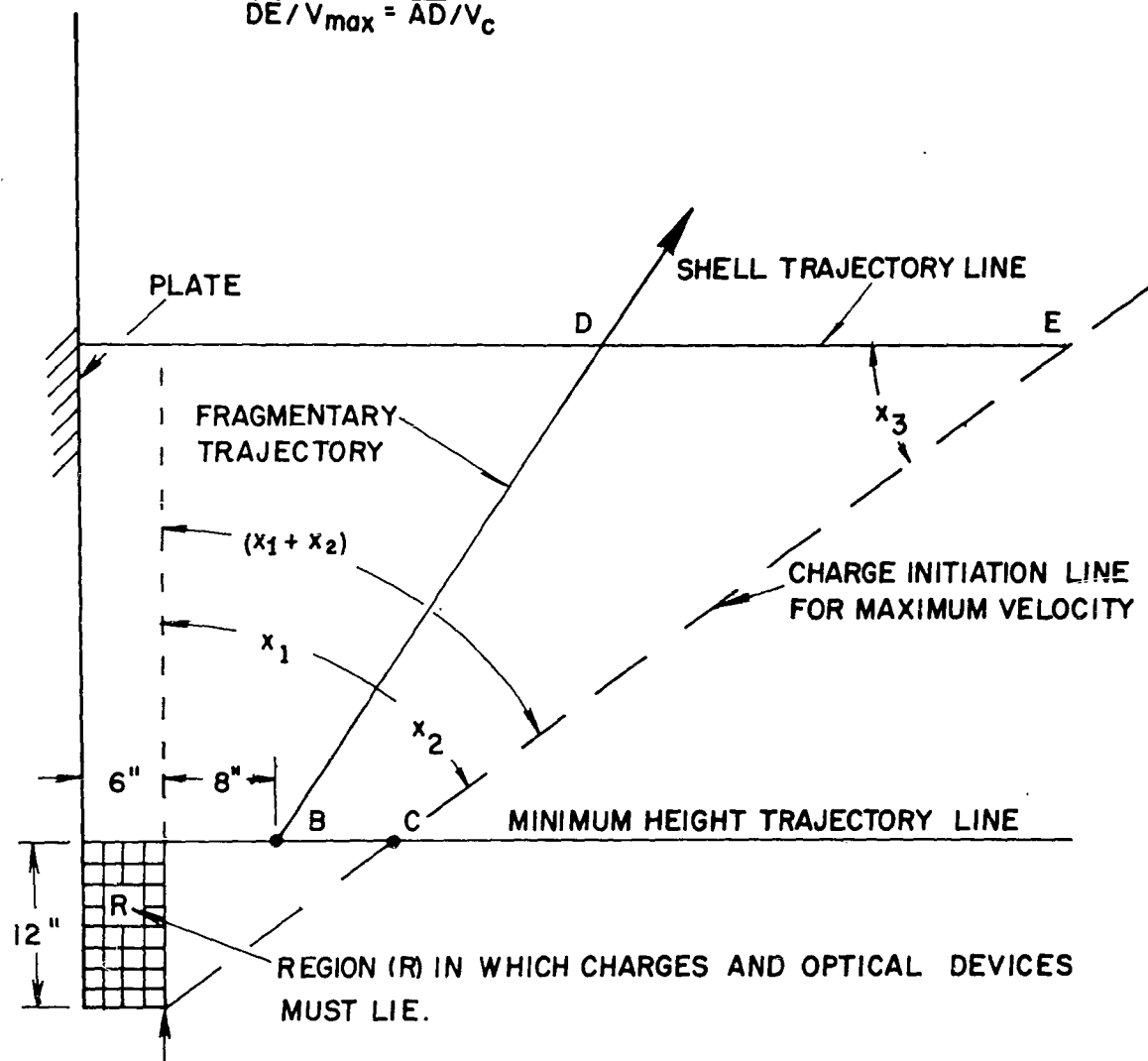


Figure 2-16. Effect of restricting overhang for case II with OTAC restrictions

**SECRET**

## SECRET

(S) It can be seen from this that the angle the charge initiation line makes with the defended plate ( $x_1 + x_2$ ) is equal to 54.0 deg.

(S) Since all sensing beams must lie outside the charge initiation line, while originating within the specified region (R) of figure 2-16, the angles between the sensing beams and the protected plate become intolerably large.

### 2.2.7 Flatness of Detection Fences

(S) It has been found necessary that the rounds be hit at a particular point, that is, their most vulnerable point; with an accuracy of  $\pm 1$  in. Evidently, the hitting accuracy depends critically on the accuracy of the determination of the firing time of the defending charge, which in turn, depends on the accuracy of the flatness of the detecting fences.

(S) Figure 2-17 illustrates the geometric configuration in its most simple form.  $P_1$  and  $P_2$  are the edges of the ideal plane fences (solid lines). The dotted lines represent the actual edge of any two particular actual fences. It is assumed that the error  $\Delta d$  is symmetrical about the ideal plane.

(S) The two ideal planes,  $P_1$  and  $P_2$ , are separated by distance  $d_1$ ;  $d_2$  is the distance from the ideal plane  $P_2$  to a point in the desired line charge impact plane;  $d_1'$  is the actual distance between the two actual fences at the points corresponding to interceptions for any particular shell;  $d_2'$  is the distance from the ideal  $P_2$  plane and the particular shell's nose position at the time a firing pulse is generated.

(S) The line charge in figure 2-17 has to be initiated a certain time  $T_{f2}$  after the shell has traversed fence  $P_2$ , which, for the moment, is assumed ideal. It can be derived that this time  $T_{f2}$  equals  $(T_{p2} - T_{p1}) (d_2/d_1)$  where  $T_{p2}$  and  $T_{p1}$  are the times of traversal of fences  $P_1$  and  $P_2$ . It thus follows that the time differential  $(T_{p2} - T_{p1})$  is magnified by the leverage factor  $d_2/d_1$ , which also applies to any error in the time differential. Since this error is solely due to deviations of the fences  $P_1$  and  $P_2$  from flatness, the maximum tolerable deviation must be determined.\*

(C) The greatest errors will occur under the two following conditions: (a) Fence  $P_1$  triggered at the latest possible time and  $P_2$  triggered at the earliest possible time, that is, at points  $P_1'$  and  $P_2'$  or

\* In the calculation, the characteristics of the other system components, such as photocells, computers, defending charges, are assumed to have no errors. A more detailed analysis of the influence of some component characteristic errors on the over-all system accuracy follows in section 3.5.

SECRET

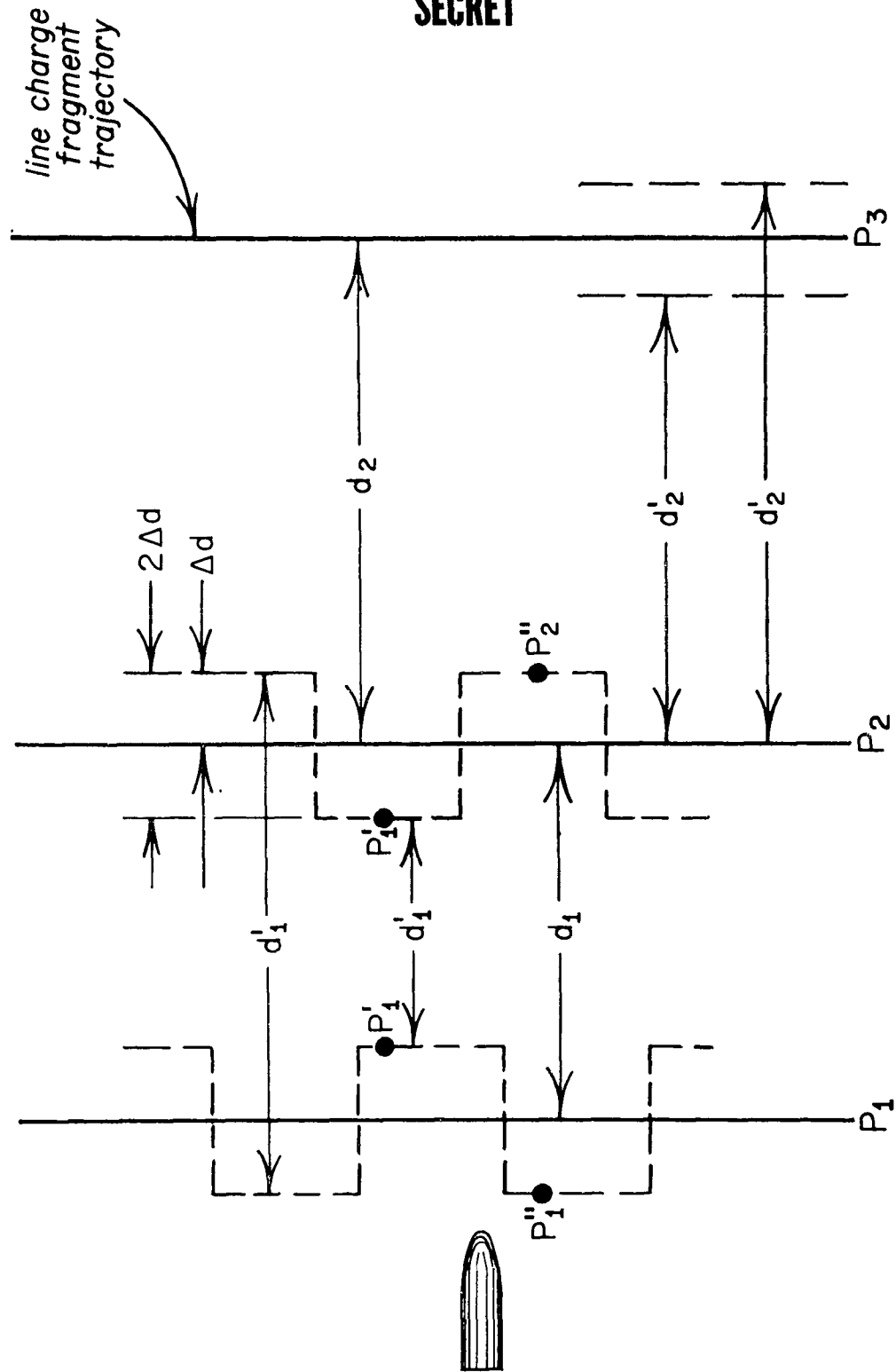


Figure 2-17. Illustration of errors in fence layout

SECRET

# CONFIDENTIAL

(b) fence  $P_1$  triggered at the earliest possible time and fence  $P_2$  triggered at the latest possible time, that is, at points  $P_1''$  and  $P_2''$ .

(C) It can be seen by referring to figure 2-17 that the true distance between the two actual screens will be shorter than the ideal for case a, and longer than the ideal for case b. The time required for the shell to pass through this actual distance will be multiplied by the factor  $\frac{d_2}{d_1}$  and a firing pulse will be supplied at that time.

(U) By setting up the equations to solve for a  $\Delta d$  max on a  $\pm 1$ -in. tolerance in a shell position at the firing plane, and by assuming all other errors to be zero, from figure 2-17

$$\frac{d_2}{d_1} = R_1 \text{ a dimensionless ratio and} \quad (2.20)$$

$$d_1' = (d_1 \pm 2\Delta d_1) \text{ for the extremes.} \quad (2.21)$$

From equation (2.20)

$$d_2 = R d_1; \quad (2.22)$$

and from figure 2-17

$$d_2' = R d_1' \pm \Delta d \quad (2.23)$$

(U) By substituting for  $d_1'$  and imposing the limits on  $d_2'$  which are

$$d_2' \leq d_2 + 1 \text{ in. and} \quad (2.24)$$

$$d_2' \geq d_2 - 1 \text{ in.} \quad (2.25)$$

from equation (2.23) the two limiting cases are obtained:

$$d_2' = d_2 + 1 \text{ in.} = R(d_1 + 2\Delta d) + \Delta d, \text{ and} \quad (2.26)$$

$$d_2' = d_2 - 1 \text{ in.} = R(d_1 - 2\Delta d) - \Delta d. \quad (2.27)$$

**SECRET**

Transposing equation (2.27) results in

$$d_2(\pm) = R d_1 \pm \Delta d (2R \pm 1) \pm 1 \text{ in.} \quad (2.28)$$

Division by  $d_1$  gives

$$\frac{d_2}{d_1} = R \pm \frac{\Delta d}{d_1} (2R \pm 1) \pm \frac{1 \text{ in.}}{d_1}, \text{ but}$$

$$\frac{d_2}{d_1} = R, \text{ (eq 2.20), therefore} \quad (2.29)$$

$$0 = \pm \frac{\Delta d}{d_1} (2R \pm 1) \pm \frac{1 \text{ in.}}{d_1}, \text{ or} \quad (2.30)$$

$$0 = \Delta d (2R \pm 1) \pm 1 \text{ in., and} \quad (2.31)$$

$$\Delta d \pm \Delta d = \pm \frac{1 \text{ in.}}{2R \pm 1} \text{ (eq 2.22)} \quad (2.32)$$

If  $R = 5$ , as is likely in the present case, equation (2.32) gives

$$\Delta d \leq \pm \frac{1}{11} \text{ in.} = 0.091 \text{ in.}$$

(S) It is obvious that, with a maximum tolerable deviation of less than 0.09 in. from ideal flatness of the detection fences, circular cross-section detection beams making up the fences were not acceptable. In order to insure the required degree of flatness, the square cross-sectional detection elements described in section 4 were developed. When properly aligned side by side with the unavoidable minimum of spacing between them, their detection patterns form fences that are flat within the tolerance limit.

### 2.3 Considerations of Defending-Charge Arrangement

(S) It has been found necessary by Picatinny Arsenal to arrange the line charges into two rows at different heights and in a staggered array, as shown in figure 2-18, and in the two possible alternatives (figures 2-19 and 2-20).

(S) In order to maintain the best possible firing time accuracy for a system that includes the aforementioned line-charge array, two separate

**SECRET**

41

SECRET

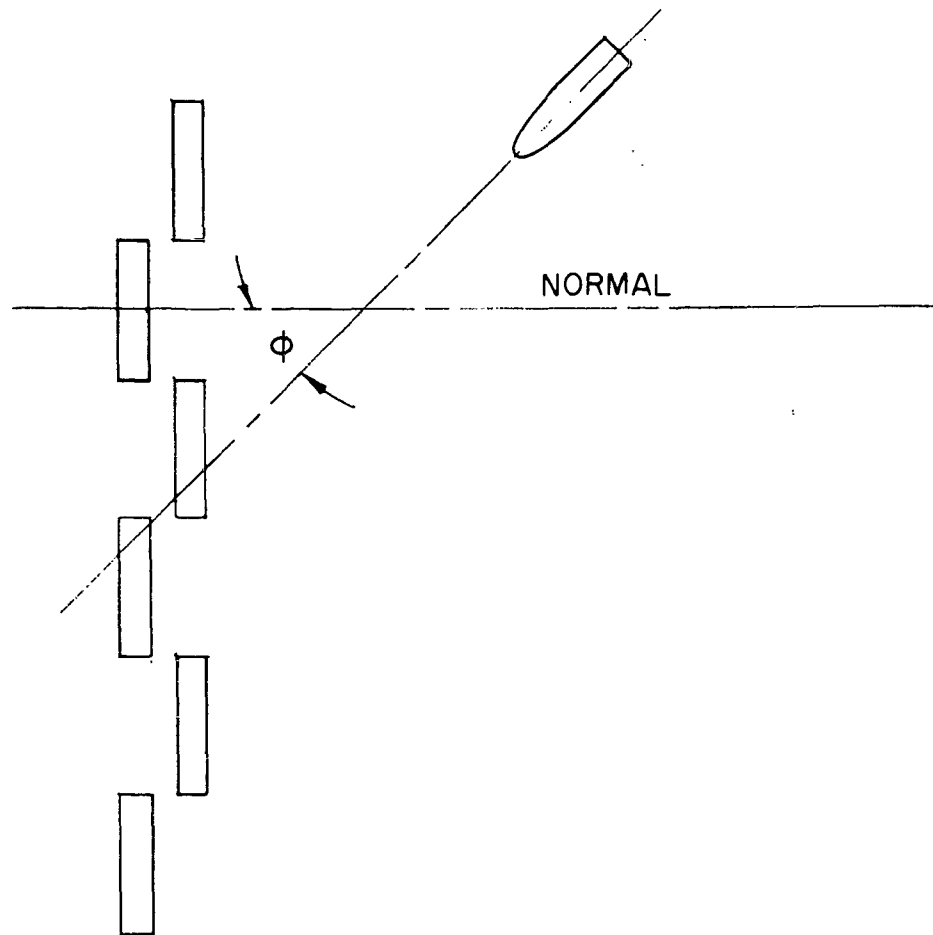
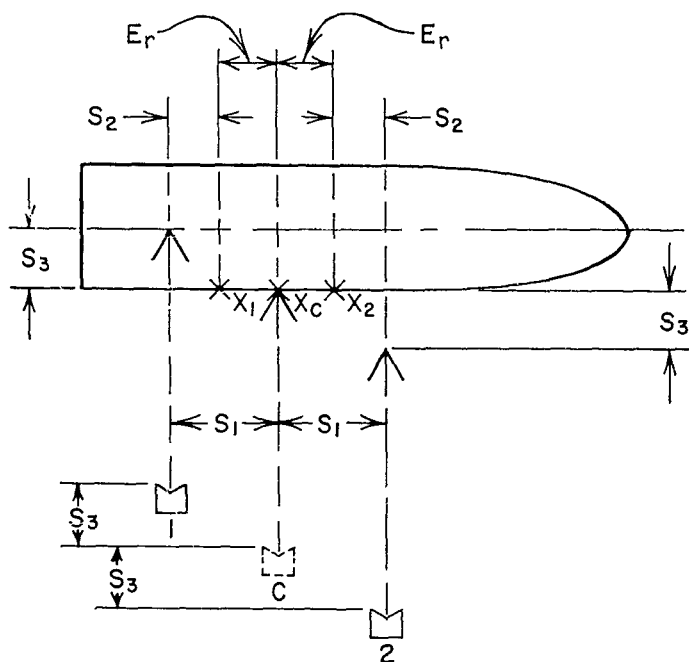


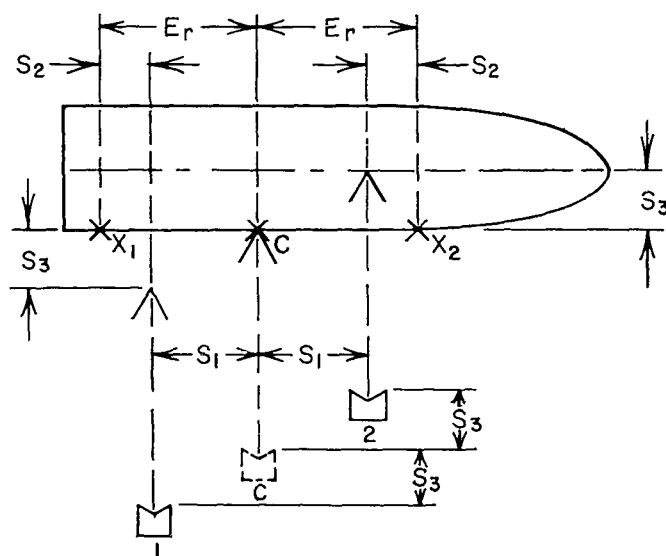
Figure 2-18. Top view of staggered defending-charge array.

SECRET

**SECRET**



(a) REAR LINE LOWER



(b) FRONT LINE LOWER

Figure 2-19. Side view of line-charge array

**SECRET**

CONFIDENTIAL

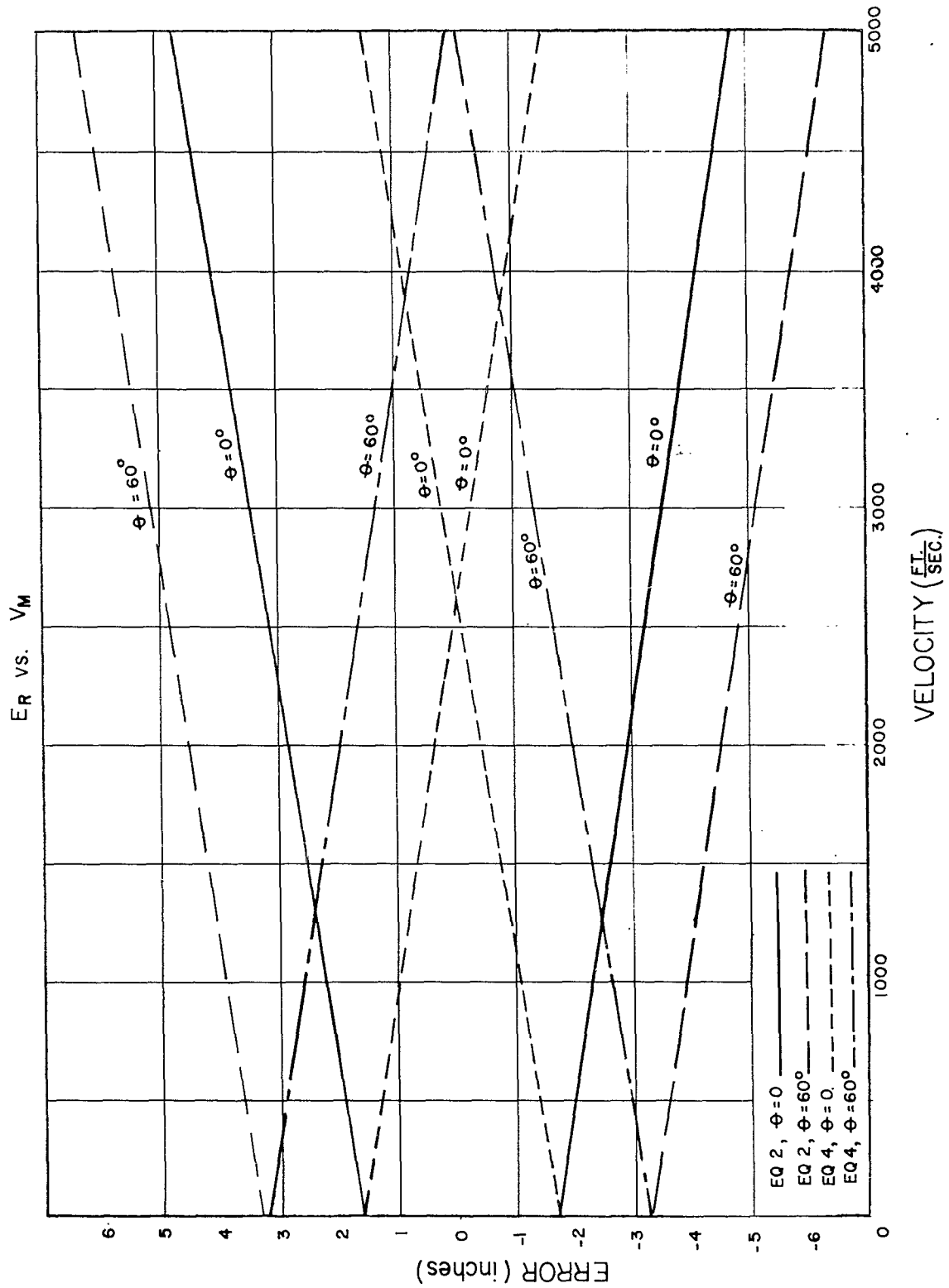


Figure 2-20. Error versus velocity for alternate defending-charge arrays

CONFIDENTIAL

# SECRET

computers are necessary, one for each row of line charges. However, if the charges can be considered to detonate at a position  $c$  that is midway between the two existing rows of charges, a single computer may be used provided that the resulting error can be accepted (section 3.5.5).

(S) The staggered array may assume one of either configuration shown (a) and (b) of figure 2-19. In both cases, the original firing time equation still applies, with the line-charge distance being that from the second optical fence to the hypothetical charge  $c$ . The errors that develop are due to the differences between the location of the hypothetical charge and the actual ones.

(S) The computer will behave as though it is delivering a firing pulse to a charge in the hypothetical row of line charges  $c$  which, if it were at the position indicated in figure 2-19, would hit the attacking round at precisely the proper point  $x_c$ . However, points  $x_1$  or  $x_2$  would be the actual points hit depending upon whether the line charge that would actually be fired would lie in row 1 or 2. The resulting error for the configuration (b) of figure (2-19) is

$$E_r = \pm S_1 \pm S_2 = S_1 \pm \frac{S_3}{V_c} V_m \quad (2.33)$$

where  $S_1$ ,  $S_2$ , and  $S_3$  are the distances indicated,  $V_c$  is line charge velocity of 8000 ft/sec, and  $V_m$  is the attacking round velocity. For angular approaches, equation (2.33) becomes

$$E_r = \pm \frac{S_1}{\cos \theta} \pm \frac{S_3}{V_c} V_m. \quad (2.34)$$

For the configuration (a) of figure 2-19 the equation is

$$E_r = \pm S_1 \pm \frac{S_3}{V_c} V_m, \quad (2.35)$$

or for angular approaches

$$E_r = \pm \frac{S_1}{\cos \theta} \pm \frac{S_3}{V_c} V_m, \quad (2.36)$$

where the values  $S_1$ , and  $S_3$ ,  $V_c$ , and  $V_m$  are as defined for equation (2.33).

(U) The error equations (2) and (4) are plotted on the graph (figure 2-20) for the following values of the parameters:

# SECRET

# SECRET

$$S_1 = 1.625 \text{ ft}, \quad S_3 = 5 \text{ ft}, \quad V_c = 8000 \text{ ft/sec},$$

and for two values of  $\theta$ ,

$$\theta = 0 \text{ (normal attack) and}$$

$$\theta = 60 \text{ deg (oblique attack).}$$

(S) It can be seen from the graph that configuration (b) of figure 2-19 (equation (2.36)) produces smaller errors than does configuration (a) of figure 2-19 (equation (2.34)) and that the error may be zero for some attacking round velocities. For this reason, the decision was made in favor of configuration (b) of figure 2-19.

## 2.4 Optical Versus Microwave Approach

(S) Both systems under investigation, i.e., infrared and microwave systems, are based upon the establishment of a reference geometry in space whereby the trajectory and velocity of the attacking rounds can be determined. The only essential differences between the microwave and infrared systems are the types of detectors and radiators and the method of measuring the shell velocity. The following table is a comparison of the two approaches on a very broad basis.

(S) The space requirements of either system depend greatly upon the over-all requirements for a particular application.

Parameters	Microwave System	Optical system
Velocity determination	Doppler frequency	Spaced parallel fences
Height determination	2-divergent fences	2-divergent fences
Charge selection	3-divergent fences	Numerous pickets*; 3-divergent pickets*
Type of computer	Analog*; digital**	Analog*; digital***
Equation to solve	Same as optical system	Same as microwave system
Capable of:		
Daylight operation	Yes	Passive; using reflected daylight
Night operation	Yes	Active; using artificial infrared light
Minimum overhang:		
Front	Depends on over-all system	
End	Potentially zero	

Note: \*Completed; \*\* Proposed methods no tests made to date;  
\*\*\* Some work done on velocity computer

**SECRET**

(S) It has been stated erroneously that a microwave sensing system for Project Dash-Dot would be highly preferable to an optical system because of its inherently negligible space requirements. The fact is that, since both systems use the same geometry, their space requirements are also essentially the same.

**SECRET**

This document contains information affecting the national defense of the United States within the meaning of the espionage laws, title, 18 U. S. C., 793 and 794. Its transmission or the revelation of its contents in any manner to an unauthorized person is prohibited by law.

# SECRET

## 3. OPTICAL APPROACH

L. Melamed

### 3.1 Specifications for Feasibility Test

(U) The following specifications for the feasibility test, which had been scheduled for June 1960, were agreed to by the cooperating installations, OTAC, PA, BRL/APG, and DOFL.

(S) A piece of armorplate 10 ft x 10 ft in size, 2 in. in thickness, and inclined at 30 deg to the ground, thus presenting a projected area of 10 ft wide and 5 ft high, was to be defended against HEAT and AP rounds varying from 37 mm to 106 mm in caliber. The plate would also be fired at with machine gun bullets, which would have to be ignored by the system (size discrimination). Attack would be point-blank, including oblique firings at azimuth angles from 0 deg to 60 deg off normal and height of attack between 17 in. and 5 ft. The plate described would simulate the so-called glaxis of a present-day tank.

(S) In order to reduce the number of components in the computer and save funds, without sacrificing any of the test objectives or obscuring the system capabilities, it was also agreed that only the right-hand 3-ft portion of the armorplate, as seen from the gun position, would be fired at, leaving a 7-ft end overhang on the left-hand side. Furthermore, angle shots would only be fired from the left-hand side.

### 3.2 System Geometry

(S) Figure 3-1 shows the geometry as actually employed. A double array of line charges is arranged in staggered brickwork fashion along the lines  $x_3$  and  $x_4$  (plan view), which are set 0.25 ft apart. The separation in elevation is 1.0 ft. The charge fragments are expelled perpendicular to the ground along the lines labeled  $P_{c3}$  and  $P_{c4}$ . Three optical detection planes (fences) are employed. Their cross section (in elevation view) is represented by the fences labeled A, B, and C. Fences A and B are parallel to each other and lie perpendicular to the ground. Fence C is inclined at an angle  $\phi = 20$  deg to the other two fences and intersects fence B at a distance of 6.5 ft from ground level. The points 0, 1, and 2 (plan and elevation) represent the intersection points of the missile path with the three fences. In the plan view, these intersection points are labeled  $X_0$ ,  $Y_0$ , etc. Each fence in turn consists of a parallel uniform spacing of square independent distinguishable detection pickets. The pickets are spaced 1.43 in. apart, resulting in seven pickets per running foot. The maximum attack altitude is 5 ft from ground level; the minimum altitude is 17 in. = 1.42 ft. A target missile approaches along the line  $P_m$  at an attack angle  $\theta$  deg measured from the normal to the line of charges and at an altitude of (6.5-h) ft. Points 3 and 4 represent the intersection

# SECRET

49

SECRET

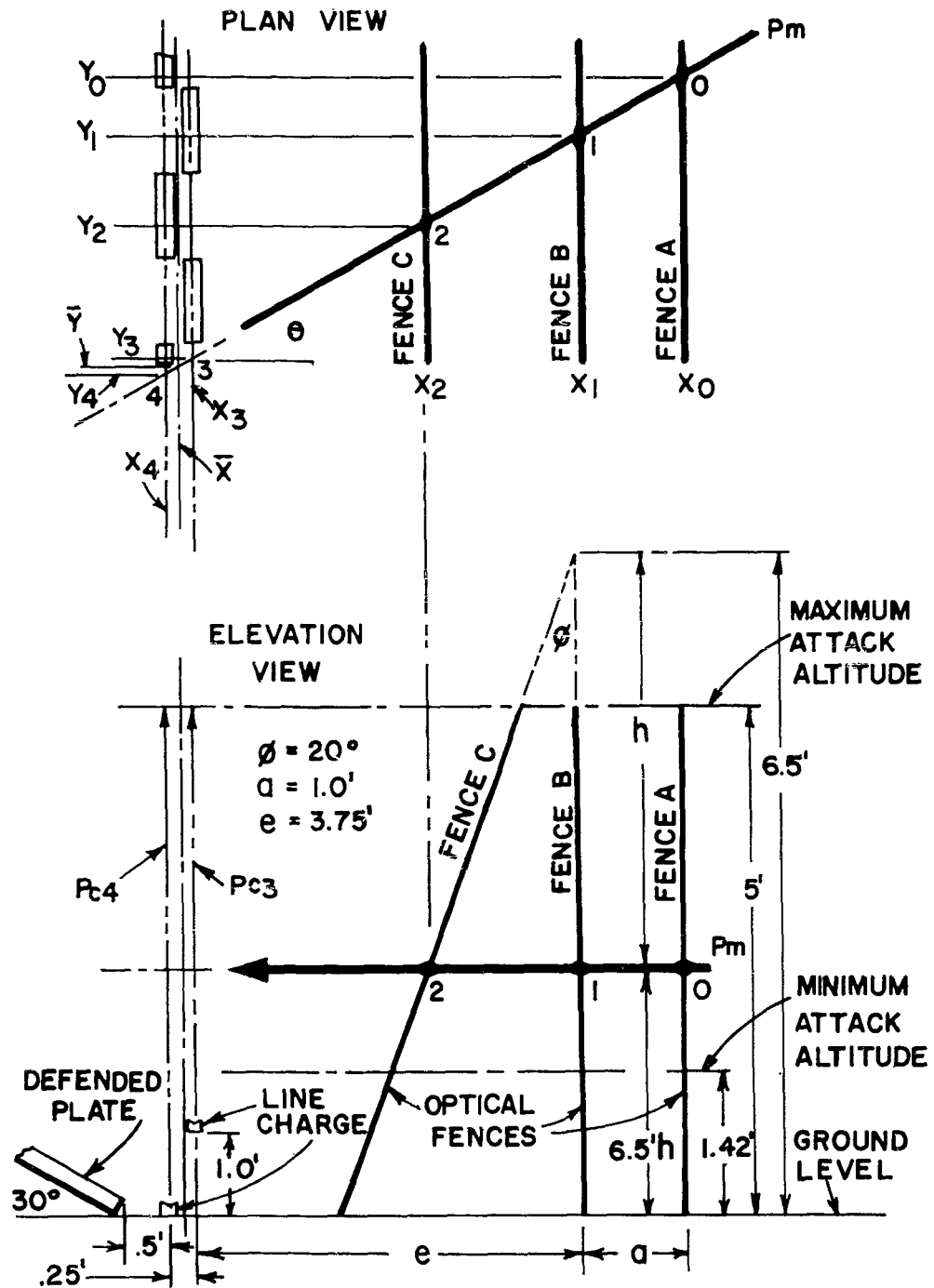


Figure 3-1. System geometry

SECRET

# SECRET

of the missile path with lines  $X_3$  and  $X_4$ . The point  $\bar{X}, \bar{Y}$  is the intersection of the missile path with an imaginary line lying midway between the 2 lines of charge (plan and elevation). This line shall be referred to as the center-of-gravity (cg) line in the sequel. The plate to be defended is inclined at 30 deg to the horizontal as stated in the test specification (section 3.1).

## 3.2.1 Advantages of Geometry Chosen

(S) A number of other configurations would have been possible for successful function. The particular one chosen has several advantages over all others considered but is not the most economical solution in regard to system size. Specifically bulk (overhang) was accepted for simplicity to facilitate demonstration of the Dash-Dot concept. For incorporation in a tank, considerable size reduction should be possible.

## 3.2.2 Fence Design

(S) The optical elements were chosen to look upward (rather than downward), not only to simplify mounting the system, but also to eliminate ground reflection noise and the disturbing effect of shell shadows on the ground. Satisfactory performance is possible for either case. This feature had to be weighed against factors such as the increased IR jamming, susceptibility to the sun, flares, and gun flashes. This susceptibility arises merely from an abnormally increased background level that has the effect of temporarily lowering over-all detector sensitivity; malfunction as such will not occur because of the requirement of the sequential alert of fences A, B, and C. Thus an external flare will excite all 3 fences simultaneously and will automatically be ignored.

(S) A saving in overhang is realized if the velocity-measuring fences (A and B) are inclined to the vertical and brought closer to the defended plate. However, the advantages of the configuration of figure 3-1 are:

- (a) Charge selection is made independent of the attack altitude  $h$ .
- (b) Increased velocity-measuring precision.

(S) Fence C intersects fence B above  $P$  (rather than below), thereby matching the longer fragmentation flight<sup>m</sup> time required at large attack altitudes to an earlier computer decision (earlier intercept of fence C).

(S) Altitude measuring precision increases with increasing angle  $\phi$ . Twenty degrees is a working compromise between a moderate amount of overhang and system accuracy. Velocity measuring precision increases with

SECRET

51

## SECRET

increasing  $a$ . At  $a = 1$  ft, velocity errors are about 0.8 percent. Distance  $e$  ( $= 3.75$  ft) is dictated by the firing delay time, the fragmentation flight time (at a minimum attack altitude), and a minimum overhang.

(C) It is necessary to make the velocity measuring fences (A and B) the first two intercepted fences since

- (a) The altitude computation requires previous knowledge of the velocity,
- (b) The charge selection computer functions from information from the velocity-measuring fences only.

### 3.2.3 Line-Charge Array

(S) The ideal line-charge array would be a single line charge equal in length to the defended structure. There would then be no need for a charge selection computer and no potential target could get past such a wall of fire unscathed. Such a proposal is infeasible for several fairly obvious reasons. (a) Such a single wall of fragmentation would require about 100 lb of high explosive (for, say, a tank wall 20 ft long); the resultant blast and shock wave would destroy the system, the defended-vehicle personnel, or both, and (b) even if no damage resulted, the tank would be left completely undefended until another such (unwieldy and heavy) charge could be repositioned.

(S) Since the maximum anticipated caliber of attacking artillery is about 4 in., a more workable solution is to construct the line charge in segments and detonate (per decision of the charge selection computer) the appropriate segment. The segments chosen are about 10 in. long, have an effective lateral\* coverage of about 12 in. and contain about 6 lb of high explosive. It should be further noted that with a segmentation design, the tank is not left completely undefended immediately after system function, indeed, the tank remains defended except for a small length representing the recently detonated charge. The likelihood of a second missile directed to the same vertical strip on the tank within, say, 2 sec,\*\* is statistically small.

(S) With the choice of a segmented line-charge defense\*\*\* two new problems arise: (a) adjacent line charges must not detonate sympathetically and (b) no holes should exist in the array of line charges for any angle of attack and any caliber. To satisfy these conflicting requirements, the staggered brickwork array of charges was adopted

\* i.e., along the major axis of the charge.

\*\* Assuming an automatic device reloads the blank station in this arbitrary interval.

\*\*\* To be simply called line charge in sequel.

## SECRET

# SECRET

(figure 3-1). Not shown in the figure are steel deflector plates surrounding each charge; these allow closest packing of the charges without sufficient blast to cause nearest-neighbor detonation.

(S) From a measurement of the transit times of an attacking round between fence A and fence B and between fence B and fence C, it is apparent that it is possible to directly measure the normal component of velocity and height of attack. From a knowledge of which particular pickets in fences A and B are triggered, it is possible to measure  $\theta$ . It is thus possible to completely specify the three-dimensional trajectory in the horizontal plane of any missile approaching the system. Provided with this information, a firing time may be computed (for the appropriate line charge) to effect a collision between any selected point on the missile axis and the line of charge fragments.

## 3.3 Firing Time Equations\*

(S) Define,

$T_{f3}$  = firing time\*\* for an  $X_3$  selected charge,

$T_{f4}$  = firing time for an  $X_4$  selected charge,

$\bar{T}_f$  = firing time for an  $\bar{X}$  selected charge,

$T_3$  = collision time\*\*\* for an  $X_3$  selected charge,

$T_4$  = collision time for an  $X_4$  selected charge,

$\bar{T}$  = collision time for an  $\bar{X}$  selected charge,

$T_{c3}$  = fragmentation flight time\*\*\*\* for an  $X_3$  selected charge,

$T_{c4}$  = fragmentation flight time for an  $X_4$  selected charge,

$\bar{T}_c$  = fragmentation flight time for an  $\bar{X}$  selected charge,

$V_c$  = line charge fragment velocity (8000 fps),

\* The early work on the geometrical analysis is contained in DOFL Report TR-433, "Theoretical Analysis of a Dash-Dot Sensing System," by Orval R. Cruzan, December 1957, (Secret).

\*\* i.e., time at which the firing pulse is delivered to a charge lying on  $X_3$ .

\*\*\* i.e., time at which a collision occurs between line charge fragments and missile.

\*\*\*\* i.e., elapsed time interval (sec) between firing command and missile intercept.

# SECRET

# SECRET

$V_m$  = true missile velocity (fps),  
 $a$  = fixed distance between fence A and fence B (1 ft),  
 $e$  = fixed distance from fence B to  $X_3$  line (3.75 ft),  
 $\phi$  = fixed angle between fences B and C (20 deg),  
 $T_0$  = time of missile interception of fence A,  
 $T_1$  = time of missile interception of fence B,  
 $T_2$  = time of missile interception of fence C, and  
 $h$  = distance from  $P_m$  to intersection of fence B with fence C.

For a collision, there must be

$$T_{f3} + T_{c3} = T_3, \quad (3.1a)$$

$$T_{f4} + T_{c4} = T_4, \quad (3.1b)$$

$$\bar{T}_f + \bar{T}_c = \bar{T}. \quad (3.1c)$$

From figure 3-1,

$$T_{c3} = \frac{6.5 - h - 1.0}{8000} = \frac{5.50 - h}{8000}, \quad (3.2a)$$

$$T_{c4} = \frac{6.5 - h}{8000}, \text{ and} \quad (3.2b)$$

$$\bar{T}_c = \frac{6.5 - h - 1.0/2}{8000} = \frac{6.00 - h}{8000}. \quad (3.2c)$$

To express  $h$  write

$$\tan \phi = \frac{X_2 - X_1}{h}, \text{ but} \quad (3.3)$$

$$X_2 - X_1 = V_m \cos \theta (T_2 - T_1); \quad (3.4)$$

also

$$\frac{a}{T_1 - T_0} = V_m \cos \theta. \quad (3.5)$$

# SECRET

# SECRET

By eliminating  $V_m \cos \theta$  from equations (3.4) and (3.5), the result is

$$X_2 - X_1 = a \left( \frac{T_2 - T_1}{T_1 - T_o} \right). \quad (3.6)$$

Inserting equation (3.6) in equation (3.4) gives the height

$$h = \frac{a}{\tan \phi} \left( \frac{T_2 - T_1}{T_1 - T_o} \right). \quad (3.7)$$

To determine the collision time  $T_3$  for a charge located on the  $X_3$ -line, write

$$\frac{T_3 - T_1}{T_1 - T_o} - \frac{e}{a} = \text{constant or}$$

$$T_3 = T_1 + \frac{e}{a} (T_1 - T_o). \quad (3.8)$$

From equation (3.1a),

$$T_{f3} = T_3 - T_{c3}.$$

From combining equations (3.1a), (3.2a), and (3.7) with (3.8), the firing-time  $T_{f3}$  results for a charge located on the  $X_3$ -line:

$$T_{f3} = T_1 + \frac{e}{a} (T_1 - T_o) + \frac{a}{8000 \tan \phi} \left( \frac{T_2 - T_1}{T_1 - T_o} \right) - \frac{5.50}{8000} \quad (3.9)$$

which is the first firing time equation sought. Inspection of figure 3-1 gives

$$T_{f4} = T_{f3} + \frac{.25}{V_m \cos \theta} - \frac{1.0}{8000} \quad (3.10)$$

From using equations (3.5) and (3.9) to eliminate  $V_m \cos \theta$  and  $T_{f3}$  in equation (3.10) the result is

$$T_{f4} = T_1 + \frac{e + .25}{a} (T_1 - T_o) + \frac{a}{8000 \tan \phi} \left( \frac{T_2 - T_1}{T_1 - T_o} \right) - \frac{6.5}{8000} \quad (3.11)$$

which is the second kind of firing time equation. Finally  $T_f$  is

# SECRET

# SECRET

determined from either of the pair of equations,

$$\bar{T}_f = T_{f3} + \frac{.125}{V_m \cos \theta} - \frac{1.0/2}{8000} \quad \text{and} \quad (3.12a)$$

$$\bar{T}_f = T_{f4} - \frac{.125}{V_m \cos \theta} + \frac{1.0/2}{8000} . \quad (3.12b)$$

Substituting equations (3.9) and (3.5) into, say, equation (3.12a) yields

$$\bar{T}_f = T_1 + \frac{e + .125}{a} (T_1 - T_o) + \frac{a}{8000 \tan \phi} \left( \frac{T_2 - T_1}{T_1 - T_o} \right) - \frac{6.0}{8000} \quad (3.13)$$

To simplify equation (3.13) set

$$T_2 - T_1 \equiv \Delta T_2 ,$$

$$T_1 - T_o \equiv \Delta T_1 , \quad \text{and}$$

$$\bar{T}_f - T_2 \equiv \Delta T_f .$$

To get that

$$\Delta T_f = \frac{e + .125}{a} \Delta T_1 + \frac{a}{8000 \tan \theta} \frac{\Delta T_2}{\Delta T_1} - \Delta T_2 - \frac{6.0}{8000} . \quad (3.14)$$

On substituting in equation (3.14) the actually used values for e, a, and  $\theta$ , equation (3.14) becomes

$$\Delta T_f = 3.89 \Delta T_1 + 3.43 \times 10^{-4} \left( \frac{\Delta T_2}{\Delta T_1} \right) - \Delta T_2 - 7.50 \times 10^{-4} . \quad (3.15)$$

Equation (3.15) is the third kind of firing time equation that holds exactly for a hypothetical cg line charge that hits the ogive of an attacking round.

(S) If it is desired that the line charge fragments intercept the attacking missile at, say 10 in. (0.83 ft) back of the ogive, an additional time delay must be added to  $\Delta T_f$  in equation (3.15). This additional time delay will be

$$\frac{0.8333}{V_m} = 0.833 \cos \theta \Delta T_1 \text{ sec.} \quad (3.16)$$

# SECRET

## SECRET

(S) For the special case of  $\theta = 0$ , equation (3.16) combines with equation (3.15) to yield

$$\Delta T_f = 4.71 \Delta T_1 + 3.43 \times 10^{-4} \frac{\Delta T_2}{\Delta T_1} - \Delta T_2 - 7.50 \times 10^{-4} \text{ sec} \quad (3.17)$$

It is this firing time equation that has actually been employed in the working system.

### 3.4 Charge Selection Equation

(C) Since the two lines of charges are only 0.25 ft apart, it is permissible to set up the charge selection equation for  $\bar{X}$  (rather than separately for the  $X_3$  line and the  $X_4$  line). It is therefore required to determine the point  $\bar{X}$ ,  $\bar{Y}$ . The actual charge whose center lies nearest this point will be selected by the computer. Thus,

$$\frac{\bar{Y} - Y_0}{Y_1 - Y_0} = \frac{\bar{X} - X_0}{X_1 - X_0} = \frac{e + 0.125 + a}{a}$$

The coordinate  $\bar{Y}$  of the charge to be fired is obtained by solving for  $\bar{Y}$ :

$$\bar{Y} = Y_0 + \left( \frac{e + 0.125 + a}{a} \right) (Y_1 - Y_0) \quad (3.18)$$

(C) The equation given above, which is based on the analytical method, has not been used for the design of the charge-selecting computer; it has only been introduced for the sake of completeness, that is, full utilization of the previous equations. In the experimental system actually built, a geographic approach has been employed (section 9).

### 3.5 Error Analysis

(S) The successful defeat of an attacking missile will depend on the correct computation of two distinct quantities. These are:

- (a) Selecting the proper defending charge, and
- (b) Computing the required firing time of that charge.

Objective (a) is accomplished by measuring (figure 3-1)  $Y_0$  etc., and  $\theta$ ; for objective (b) we require to know the velocity  $V$ , height  $h$ , time  $t_0$ , etc. The inherent errors in measuring  $Y_0$  and  $\theta$  are due to the quantized nature of the detection fence. As each fence approaches the ideal case of a continuum of infinitesimally narrow quasi-parallel pickets very close together, these errors approach zero. The quantities  $V_m$ ,  $h$ , and

## SECRET

## CONFIDENTIAL

$t_o$  are all subject to a random but small geometrical error that arises from the non-continuum nature of each fence. Representing the worst ogive by a simple 30-deg cone with rounded point, (figure 3.2), the instant of fence intercept will be different for the case of the line of attack,  $P_m$ , directed in the space between adjacent pickets and the case of head-on intercept. The principal ogive shapes likely to occur are flat (blunt) nose, pointed nose, or spherical. The penetration error is zero for all of these except the rounded-point 30-deg cone as shown in figure 3-2. This case is discussed below.

### 3.5.1 $V_m$ -Error Due to Random Fence Penetration

(C)  $V_m$  is measured by the time interval  $t_1 - t_o$ . An error in  $V_m$  will arise only when fences A and B are penetrated differently. Thus when both fences are penetrated between centers, say, the error in  $V_m$  cancels out. The maximum error otherwise in  $V_m$  is  $\frac{0.2}{12} \times 100$  percent = 1.7 percent for the worst possible case.

### 3.5.2 h-Error Due to Random Fence Penetration

(C) The argument is identical to the one for  $V_m$  except that fences B and C are employed. The percent error, however, is different varying in this case from a maximum of 3.4 percent ( $h = 1.5$  ft) to a minimum of 0.9 percent ( $h = 5.08$  ft).

### 3.5.3 $T_o$ -Error due to Random Fence Penetration

(C) From figure 3-2 this error in  $t_o = \Delta t_o = \frac{0.2/12}{V_m}$  sec =  $\frac{0.017}{V_m}$  sec (max). The other, more important error under objective (b) is self-imposed. This occurs when, in the interest of simplification, we imagine that the 2 rows of charges,  $X_3$  and  $X_4$  in figure 3-1, are replaced by a center-of-gravity line of charges,  $\bar{X}$  in figure 3-1, and when the firing time is computed on the assumption that the computer-selected charge lies along  $\bar{X}$ . In the sequel, this will be referred to as the cg error.

(C) The concept of required firing time needs some additional discussion. In general, it is insufficient merely to hit an incoming missile any where along its length. Each potential target will have a different caliber, length, and area of maximum vulnerability. A successful system should be capable of making additional decisions on which portion of a given target is probably most vulnerable to line-charge attack. A study made of likely antitank missiles suggests that the incoming target be hit at a given (compromised) percentage of its own length back of the nose. This adds, in addition to the stated detection parameters, a length and cosine measurement of the attacking object. This may be readily accomplished by measuring the duration of signal T in any one fence, as shown in section 9.4.

## CONFIDENTIAL

CONFIDENTIAL

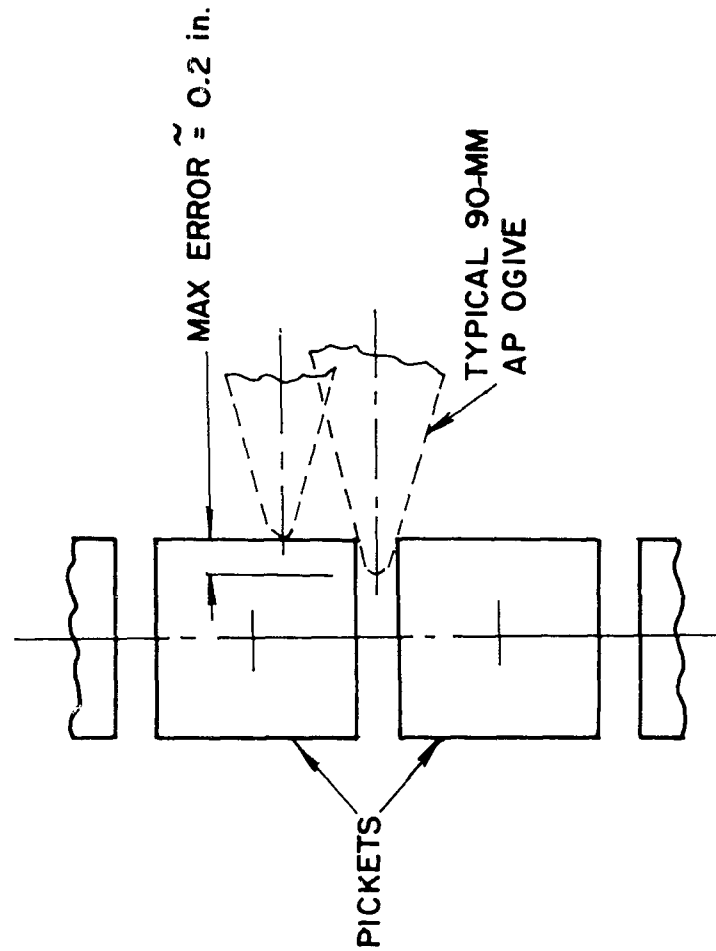


Figure 3-2. Random fence penetration ambiguity for conical ogives

CONFIDENTIAL

## CONFIDENTIAL

(U) Thus length =  $L = V_m T_{d_0}$ . In addition to a knowledge of  $V_m$ ,  $h$ , and  $t_0$  under objective b, there should, therefore, be added a knowledge of  $T$ .

### 3.5.4 Error Analysis of Charge Selection

(C) From figure 3-1, it is noted that the error in the appropriate charge selection may be defined in terms of the additive errors in either the set  $Y_0$  and  $\theta$  or in the set of  $Y_0$  and  $Y_1$ . The latter method is chosen for convenience.

(C) Figure 3-3 indicates a short cross section of fence A (or fence B) as it appears to an approaching missile. Figure 3-4 is an enlarged section of a missile intercept with fences A and B. The true and apparent attack paths are, in general, different because of the quantized nature of each fence. Figure 3-5 (to a reduced size) indicates the resultant error in charge selection. It is assumed that each square detection picket has uniform sensitivity over its cross section and zero sensitivity anywhere else.

Let

$\theta$  = Attack angle (angle between attack path and normal to the fence),

$b$  = Pickets center-to-center spacing,

$r$  = Effective picket radius,

$c$  = Caliber (diameter) of attacking round,

$n$  = The number of alerted pickets in a fence (tangential or grazing attack is considered a full intercept),

$Q$  = Total ambiguity in attack attitude (i.e. ambiguity in  $Y_0$  and  $Y_1$ ) given  $n$ ,  $b$ ,  $c$ ,  $r$ ,  $\theta$ ,

$b' = b \cos \theta$  = effective picket spacing at an attack angle  $\theta$ ,

$Y$  = correct charge coordinate,

$\Delta Y$  = error in charge coordinate.

For an attack angle of  $\theta$  (figure 3-2), the picket radius  $DE$  is

$$DE = DF \cos (45^\circ - \theta),$$

$$\text{or } DE = .8351 \cos (45^\circ - \theta). \quad (3.19)$$

If the pickets were round (dotted circle) in figure 3-3 the attack cross-section radius = 0.5906 in. always. However, the corners of the square pickets are relatively ineffective in producing a missile intercept. The

## CONFIDENTIAL

CONFIDENTIAL

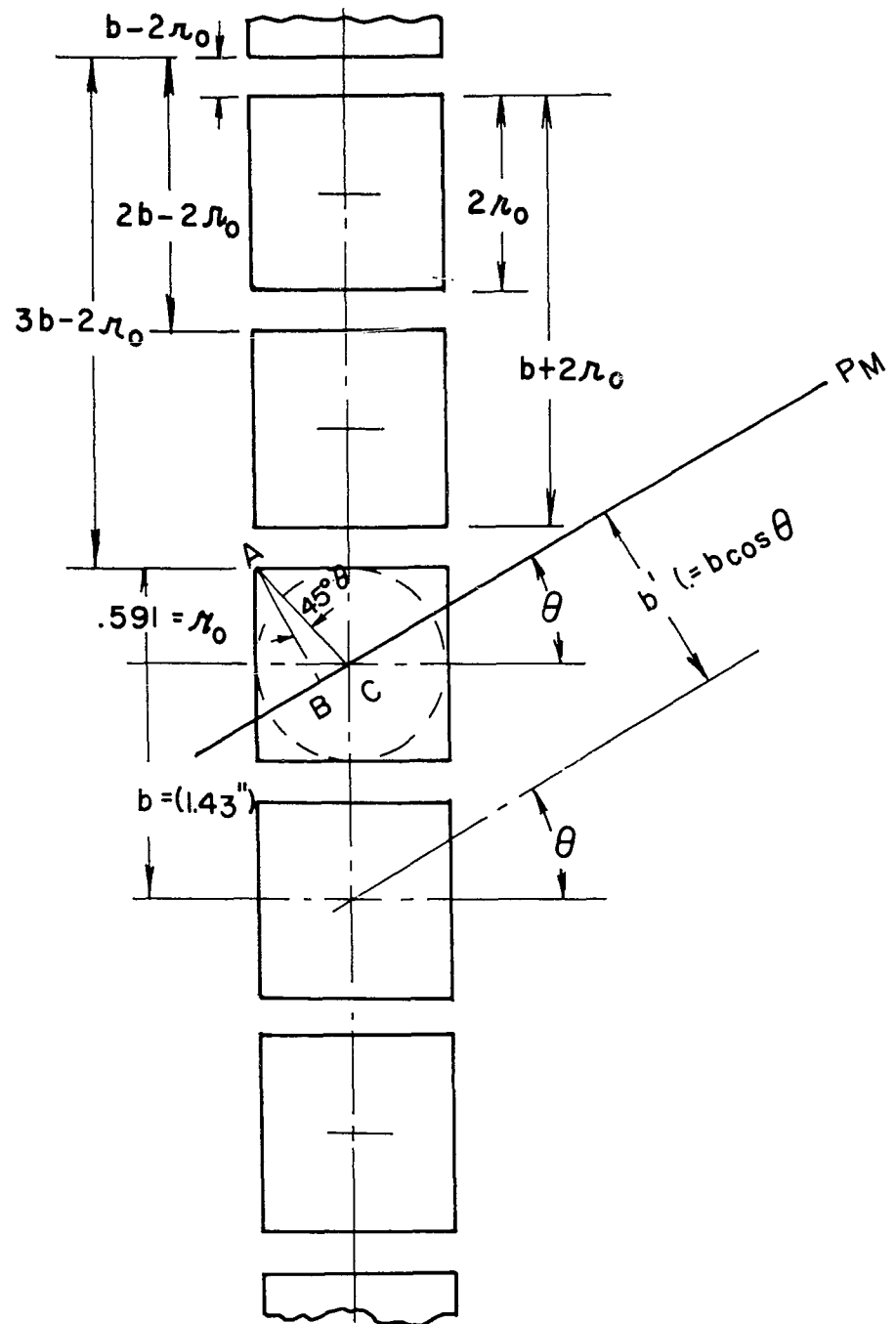


Figure 3.3 Typical picket array in a fence

CONFIDENTIAL

SECRET

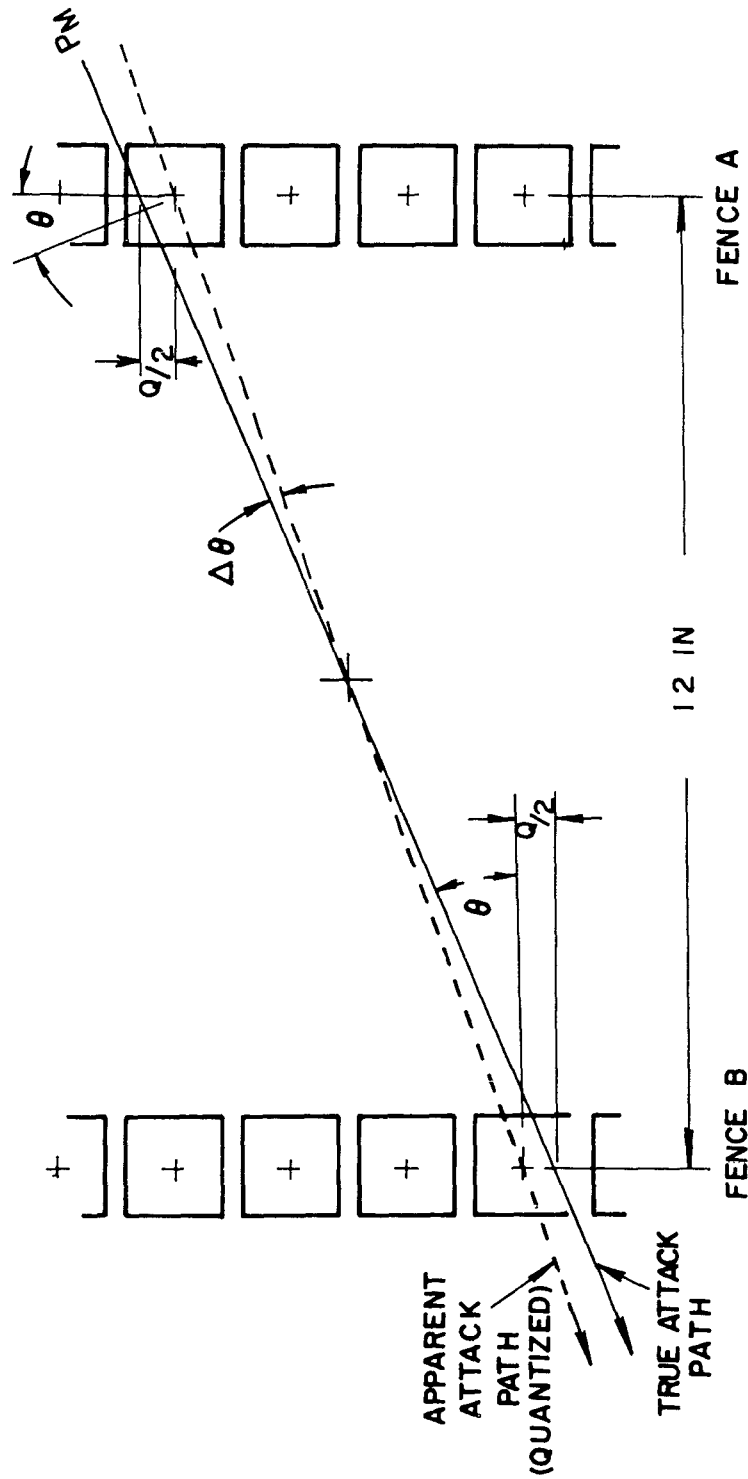
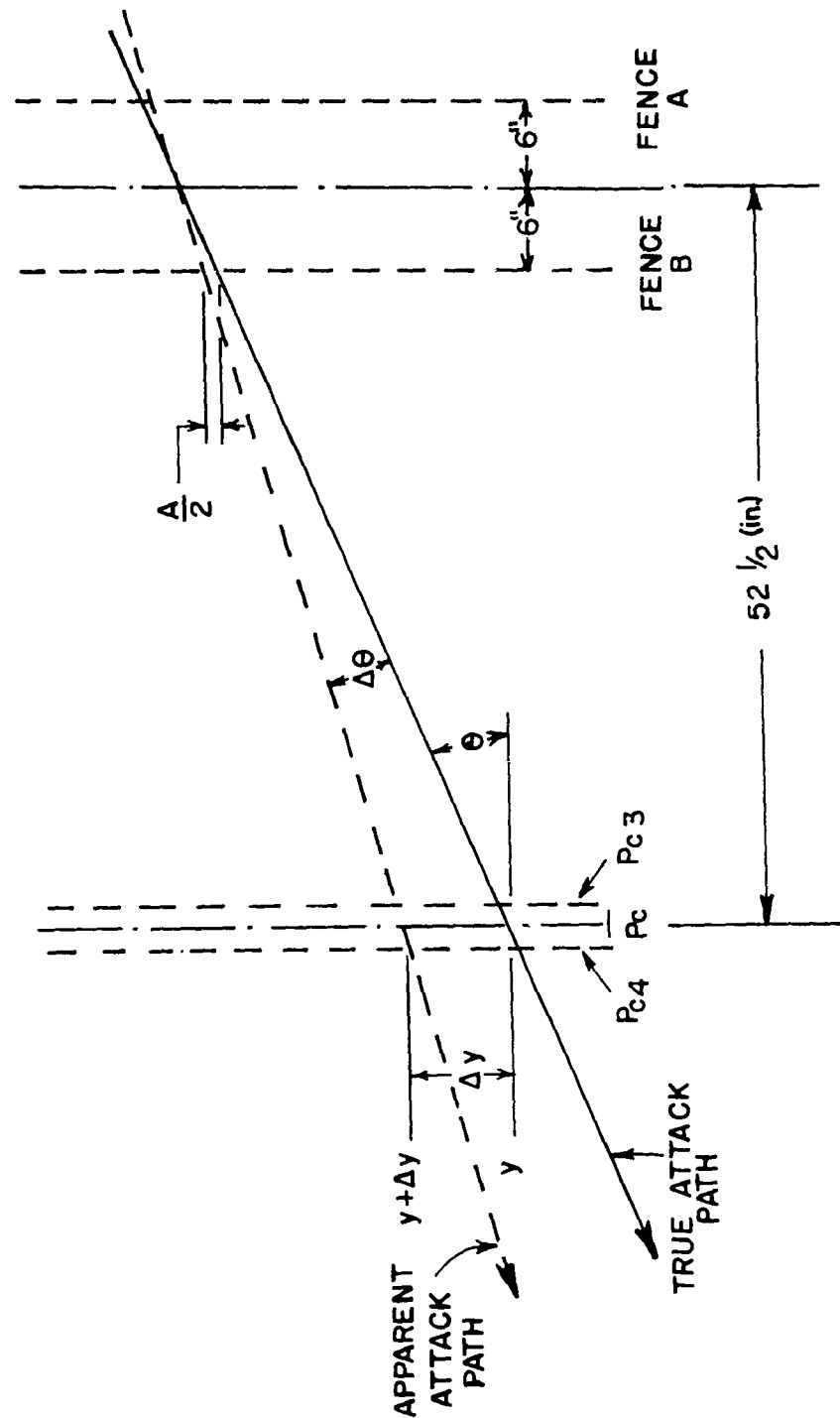


Figure 3-4. Ambiguity in attack angle

SECRET

SECRET



SECRET

Figure 3-5. Charge selection error

# CONFIDENTIAL

quantity 'effective picket radius',  $r$ , will be defined by

$$r = \frac{DF + .5906}{2}, \quad (3.20)$$

as a working compromise.

(C) The attack attitude shall be defined as the relative displacement of the attack path along the line joining picket centers in any one fence. It may be measured as the distance between  $Y_0$  and the nearest picket center in fence A, or as the distance between  $Y_1$  and the nearest picket center in fence B. Considering any particular picket in figure 3-3, the attack attitude (at  $\theta = 0$ ) ranges from a maximum of  $+\frac{b}{2}$  to a minimum of  $-\frac{b}{2}$ .

(C) Hence  $Q(\max) = 2(\frac{b}{2}) = b$ ; at any other  $\theta$ ,  $Q \max = b'$ . To determine  $\Delta Y$ , it is first necessary to define the function  $Q$  in terms of  $n$ ,  $C$ ,  $b$ , and  $r$ . From figure 3-5, it is evident that

$$\frac{\Delta Y_{\max}}{52.5} = \frac{Q/2}{6}, \text{ or } \Delta Y_{\max} = 4.38 Q. \quad (3.21)$$

Simple trigonometry yields  $\Delta\theta$  in terms of  $Q$ , viz,

$$\Delta\theta_{\max} = \arctan \frac{Q \cos \theta/2}{6/\cos \theta} = \arctan \frac{Q \cos^2 \theta}{12}. \quad (3.22)$$

Figure 3-4 shows an enlarged portion of figure 3-5 for greater clarity.

## 3.5.4.1 Special Case of Normal Attack ( $\theta = 0^\circ$ )

(U) Zero pickets alerted is operationally uninteresting since this implies a caliber less than  $b-2r$ . A minimum requirement is, therefore,

$$c > (b - 2r) \text{ for } n \geq 1. \quad (3.23)$$

To determine  $Q$  under all operational conditions, it is necessary to fix  $n^*$  and examine what conditions must then be imposed on  $c$ ,  $b$ , and  $r$ . Upon examination of figure 3-3, the tabulation given below results.

\* i.e., a particular subset  $n$  out of the entire array of pickets is chosen, e.g., if  $n = 3$ , the 6th, 7th, and 8th pickets might have been selected. Since the computing system can distinguish, say, picket 4 from picket 5 (for  $n = 1$ ) there is no loss in generality in selecting a particular subset.

# CONFIDENTIAL

C		n	Applicable constraint	Q
mm	In.			
37	1.46	1	$b - 2r < C < 2b - 2r$	$(2b - 2r) - C$
57	2.24	1	Impossible; since $C > 2b - 2r$	
75	2.96	1	Impossible	
90	3.54	1	Impossible	
105	4.13	1	Impossible	
37	1.46	2	$b - 2r < C < 2b - 2r$	$C - (b - 2r)$
57	2.24	2	$2b - 2r < C < 3b - 2r$	$(3b - 2r) - C$
75	2.96	2	$2b - 2r < C < 3b - 2r$	$(3b - 2r) - C$
90	3.54	2	Impossible	
105	4.13	2	Impossible	
37	1.46	3	Impossible	
57	2.24	3	$2b - 2r < C < 3b - 2r$	$C - (2b - 2r)$
75	2.96	3	$2b - 2r < C < 3b - 2r$	$C - (2b - 2r)$
90	3.54	3	$3b - 2r < C < 4b - 2r$	$(4b - 2r) - C$
105	4.13	3	$3b - 2r < C < 4b - 2r$	$(4b - 2r) - C$
37	1.46	4	Impossible	
57	2.24	4	Impossible	
75	2.96	4	Impossible	
90	3.54	4	$3b - 2r < C < 4b - 2r$	$C - (3b - 2r)$
105	4.13	4	$3b - 2r < C < 4b - 2r$	$C - (3b - 2r)$
	1.46 through 4.13	5	Impossible	
		.		
		n	$[(n-1)b-2r] < C < [nb - 2r]$	$C - [(n-1)b-2r] \quad (3.24)$
		n	$[nb - 2r] < C < [(n+1)b-2r]$	$[(n+1)b-2r] - C$

# CONFIDENTIAL

From the preceding discussion, it is evident that for any prescribed number of pickets alerted a maximum and a minimum caliber exist. To alert 3 and only 3 pickets requires at least that

$$[2b - 2r] < C < [4b - 2r] \quad (3.25)$$

Although equation (3.25) is a necessary condition, it is not a sufficient one since, for this caliber range, it is apparent that a 4-picket intercept may occur for certain attack attitudes. This arises from the overlapping requirements for adjacent values of  $n$  which again depend on the particular values assigned to  $r$  and  $b$ , i.e., on the quantized nature of the fence. For any specific value of  $n$  chosen, there will exist two attack ambiguity equations (expression for  $Q$ ) and two corresponding conditions on the caliber as given by equation (3.24). The tabulation provides a value for the function  $Q$  (case of  $\theta = \theta^0$ ) for all enumerable cases for the 5 typical antitank missile calibers chosen. Applying equation (3.21) (section 3.54) yields the final maximum error in charge selection  $\Delta Y$ .

#### 3.5.4.2 Case for $\theta \neq 0^\circ$

(U) Equation (3.24) is still valid if  $b$  is replaced by  $b'$  in the general case. As  $\theta$  increases from  $0^\circ$ , the pickets crowd together more and then overlap. The results of the detailed calculations that follow have assumed the worst possible conditions; that is, where the errors in attack attitude in fence A and fence B are additive, as seen in figure 3-4. Table 3-1 gives numerical values for  $\Delta Y_{\max}$  for the 5 arbitrarily chosen calibers over  $10^\circ$  steps in  $\theta$  (from  $\theta = 0^\circ$  to  $\theta = 60^\circ$ ) and covering all allowable values of  $n$ . All missing values of  $n$  are physically unrealizable. The data in table 3-1 may be plotted in several ways since the error value  $\Delta Y_{\max}$  is given as a function of  $c$ ,  $n$ , and  $\theta$ . In figure 3-5 the greatest value of  $\Delta Y_{\max}$  is plotted versus  $\theta$  for various calibers, where for each plotted point that particular value of  $n$  is chosen that yields the largest  $\Delta Y_{\max}$ . It must be understood that the  $\Delta Y_{\max}$  values listed in table 3-1 assume all allowable values of  $c$ ,  $n$ , and  $\theta$ . Thus for 37-mm caliber at  $\theta = 0^\circ$ , a 2-picket intercept ( $n = 2$ ) yields a larger value ( $\Delta Y_{\max} = 5.3$  in.) than for a 1-picket intercept ( $\Delta Y_{\max} = 0.96$  in.). Figure 3-6 shows what absolute maximum errors may be expected without regard to statistical probability. The computed points (every  $10^\circ$ ) have been arbitrarily connected in a smooth curve. Another more useful function to plot is  $\bar{\Delta Y}_{\max}$ , which is defined as the error averaged over all  $n$  when both  $C$  and  $\theta$  are specified. From table 3-1, at  $\theta = 30^\circ$ ,  $C = 57$  mm (for example) there are 2 distinct values for  $\Delta Y$ ; a 2-picket alert yields  $\Delta Y = 0.31$  in.; a 3-picket alert yields  $\Delta Y = 5.07$  in. In the absence of any a priori knowledge as to whether a 2-picket intercept may be more or less probable than a 3-picket intercept set

$$\Delta Y = \frac{0.31 + 5.07}{2} = 2.69 \text{ in.} \quad (3.26)$$

# SECRET

Table 3.1 Computed Maximum Errors in Charge Selection ( $\Delta Y$ )\*

Caliber (mm)	n	$\theta$ deg	$\Delta\theta_{(max)}$ deg	$\Delta Y_{(max)}$ in.	Caliber (mm)	n	$\theta$ deg	$\Delta\theta_{(max)}$ deg	$\Delta Y_{(max)}$ in.
37	1	0	1.05	0.96	75	4	30	2.33	2.84
37	2	0	5.7	5.30	90	4	30	4.41	5.38
57	2	0	4.1	3.76	105	4	30	2.37	2.89
75	2	0	0.67	0.61	105	5	30	2.08	2.54
57	3	0	2.67	2.45					
75	3	0	6.08	5.60	37	2	40	1.12	1.75
90	3	0	4.73	4.33	37	3	40	1.93	3.02
105	3	0	1.91	1.75	57	3	40	1.99	3.10
90	4	0	2.10	1.92	57	4	40	1.07	1.66
105	4	0	4.92	4.51	75	4	40	3.06	4.77
					90	4	40	1.43	2.23
37	1	10	0.29	0.35	75	5	40	0.29	0.04
37	2	10	1.53	6.04	90	5	40	1.65	2.58
57	2	10	3.25	3.06	105	5	40	2.83	4.42
57	3	10	3.25	3.06	105	6	40	0.22	0.31
75	3	10	6.40	6.08					
90	3	10	3.76	3.54	37	3	50	1.56	3.46
105	3	10	1.02	0.96	57	3	50	0.02	0.04
75	4	10	0.09	0.09	37	4	50	0.26	0.57
90	4	10	2.78	2.62	57	4	50	1.79	3.98
105	4	10	5.50	5.20	75	4	50	0.41	0.92
					75	5	50	1.40	3.11
37	2	20	5.16	5.33	90	5	50	1.08	2.41
57	2	20	1.85	1.92	90	6	50	0.73	1.62
37	3	20	0.51	0.53	105	6	50	1.71	3.81
57	3	20	3.8	3.93	105	7	50	0.08	0.18
75	3	20	4.47	4.63					
90	3	20	2.02	2.10	37	3	60	~0	~0
75	4	20	1.18	1.22	37	4	60	~0	~0
90	4	20	3.63	3.76	37	5	60	~0	~0
105	4	20	5.19	5.38	57	5	60	0.77	2.84
105	5	20	0.46	0.48	57	6	60	0.09	0.31
					75	6	60	0.76	2.80
37	2	30	3.05	3.72	90	6	60	0.07	0.26
57	2	30	0.25	0.31	75	7	60	0.09	0.31
37	3	30	1.36	1.66	90	7	60	0.77	2.84
57	3	30	4.16	5.07	105	7	60	0.21	0.79
75	3	30	2.12	2.58	105	8	60	0.63	2.32
90	3	30	0.03	0.04					

\* Assuming, (a) the lethally acceptable calibers are arbitrarily chosen to be 37, 57, 75, 90, and 105 mm, and (b) the attack angle  $\theta$  ranges from 0 deg to 60 deg in 10-deg steps. All unlisted combinations of caliber,  $\theta$ , and n are physically unrealizable.

# SECRET

This document contains information affecting the national defense of the United States within the meaning of the espionage laws, title, 18 U. S. C., 793 and 794. Its transmission or the revelation of its contents in any manner to an unauthorized person is prohibited by law.

SECRET

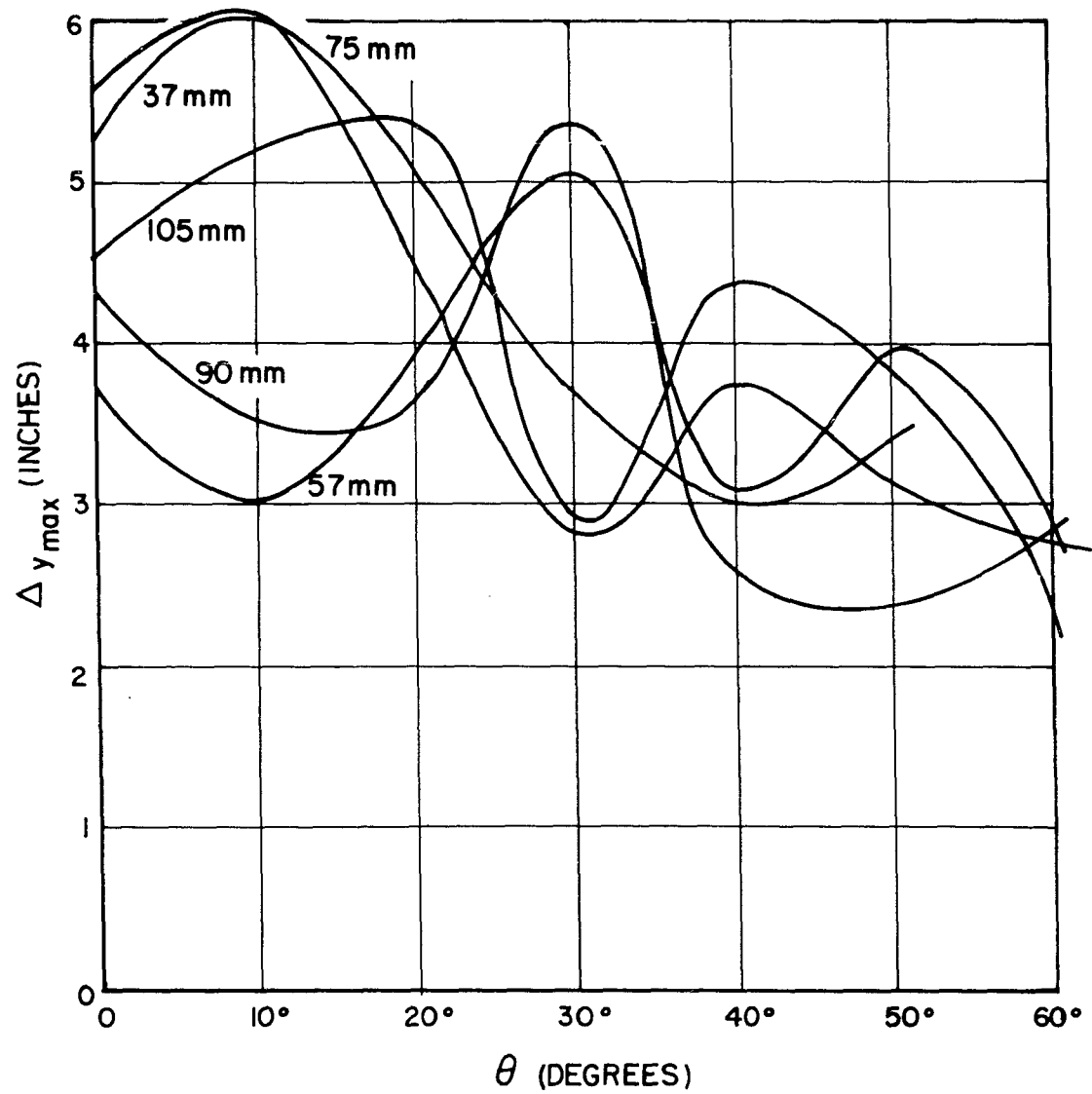


Figure 3-6. Maximum charge coordinate error ( $\Delta y_{\max}$  versus attack angle  $\theta$  (for calibers shown)).

SECRET

## SECRET

(U) Figure 3-7 has been constructed in this manner and yields the interesting result that  $\overline{\Delta Y}$  is independent of caliber; i.e., the family of curves of figure 3-6 shrinks into a single curve. Another interesting result is that only 2 different values for  $n$  exist for any given  $C$  and  $\theta$  combination. This result was predictable from the double set of equations (3.24). Inspection of the computed points in figure 3-7 shows that  $\overline{\Delta Y}$  varies as  $\cos \theta$ . In fact,

$$\overline{\Delta Y} = 3.12 \cos \theta . \quad (3.27)$$

This is consistent with the requirement that when the pickets move infinitely close together (effective picket separation = 0 at  $\theta = 90^\circ$ ),  $\overline{\Delta Y}$  approaches zero.

(S) From the data of figure 3-7, it is reasonable to require that on the average each individual line charge of 10 in. nominal length should have additional end coverages of about 3 in., making for an effective length of 16 in. If this additional coverage is achieved by shaping the fragmentation pattern into a fan-shaped beam (along the direction of a fence), the effective length of coverage will now be a function of  $h$ , the height of the attack. Hence the only reliable solution would be an array of 16 in. long line charges with 3 in. overlap and with a parallel fragmentation pattern. If the requirement is for 100 percent reliability under the worst possible conditions, it is apparent (from figure 3-6) that the overlap of adjacent charges should equal 6.1 in. (case of 75-mm caliber at 10 deg).

(S) The significant factor in the foregoing discussion is not the length of the charge but the overlapping lethal coverage of adjacent charges. If, however, a physical overlap arrangement is unfeasible (due to sympathetic detonation) and 100 percent reliability is required, it may be achieved by directing the system to detonate the computed charge in addition to its nearest-neighbor charges. In this case it is only necessary that the length of the individual line charge be at least as great as the maximum charge coordinate error. In conclusion, if this average error  $\overline{\Delta Y} \cong 3.12$  in., each line charge should  $\cong 3.3$  in. in length retaining the net explosive length of 10 in. Highly important as this consideration is, lack of time and funds has prevented its incorporation in the experimental system.

### 3.5.5 Error Analysis of CG Firing Time Approximation

(C) Equations (3.9), (3.11), and (3.13) of section 3.3 give the exact required firing times in terms of known constants and computer-measured time intervals. An analysis is now presented of the expected firing time errors if only equation (3.13) for  $T_f$  is used\* without regard as to

\*i.e., one averaged firing-time computer is needed instead of two exact firing-time computers.

## SECRET

69

SECRET

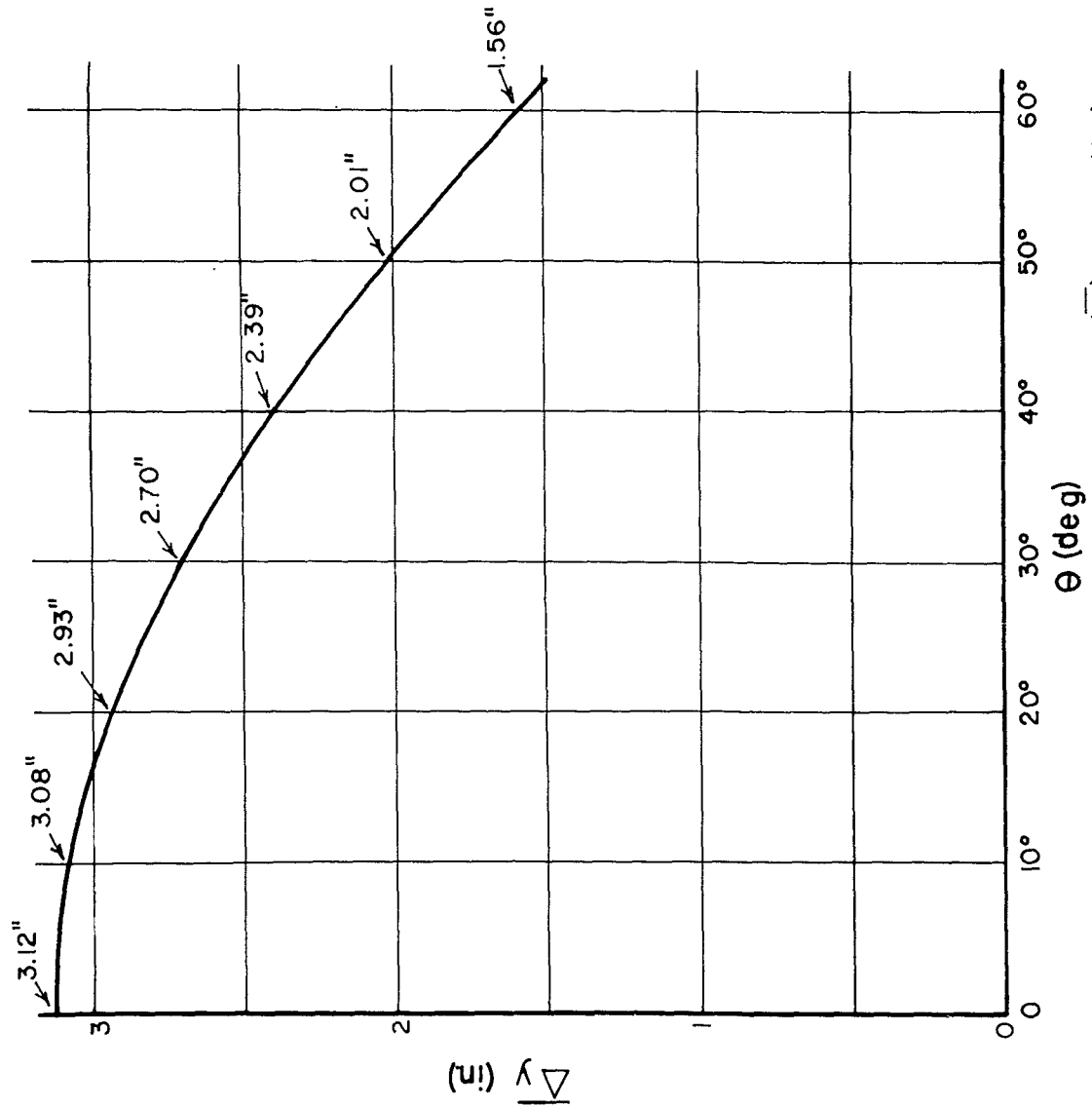


Figure 3-7. Average charge coordinate error ( $\Delta y$ ) versus attack angle  $\theta$  (for all calibers)

SECRET

# CONFIDENTIAL

whether the correctly chosen charge be of the  $X_3$  type or the  $X_4$  type. The resultant array of firing time errors will then be expressed in terms of an array of impact point errors subject to the parameters of missile velocity,  $V_m$ , and attack angle  $\theta$  in 10-deg steps from  $\theta = 0$  to  $\theta = 60^\circ$ .

Define,

$K_3$  = timing error incurred when an  $X_3$  charge is fired,

$K_4$  = timing error incurred when an  $X_4$  charge is fired,

$L_3$  = missile impact point error associated with  $K_3$ , and

$L_4$  = missile impact point error associated with  $K_4$ .

Thus,

$$K_3 = \bar{T}_f - T_{f3} \quad (3.28)$$

$$K_4 = \bar{T}_f - T_{f4} \quad (3.29)$$

From equations (12a) (section 3.3)

$$K_3 = \frac{+.125}{V_m \cos \theta} - \frac{.417}{8000} \quad \text{and} \quad (3.30)$$

$$K_4 = \frac{-.125}{V_m \cos \theta} + \frac{.417}{8000} \quad (3.31)$$

From the definition of  $L_3$  and  $L_4$ ,

$$L_3 = 12 K_3 V_m \text{ (in.)} = \frac{+1.5}{\cos \theta} - 5.95 \times 10^{-4} V_m \quad (3.32)$$

$$L_4 = 12 K_4 V_m \text{ (in.)} = \frac{-1.5}{\cos \theta} + 5.95 \times 10^{-4} V_m \quad (3.33)$$

(U) The factor of 12 gives the resultant error in inches. Table 3-2 gives the results of a numerical calculation of  $K_3$  ( $\mu\text{sec}$ ) and  $L_3$  (in.) for missile velocities ( $V$ ) from 200 to 4000 fps in about 500 fps steps and for  $\theta$  from 0 deg to  $60^\circ$  in 10-deg steps. Since  $K_3 = -K_4$ ,  $L_3 = -L_4$ , only  $K_3$  and  $L_3$  have been computed (for a  $T_{f3}$  'correct' firing time). Figure 3-8 is a plot of the numbers in table 3-2.

# CONFIDENTIAL

SECRET

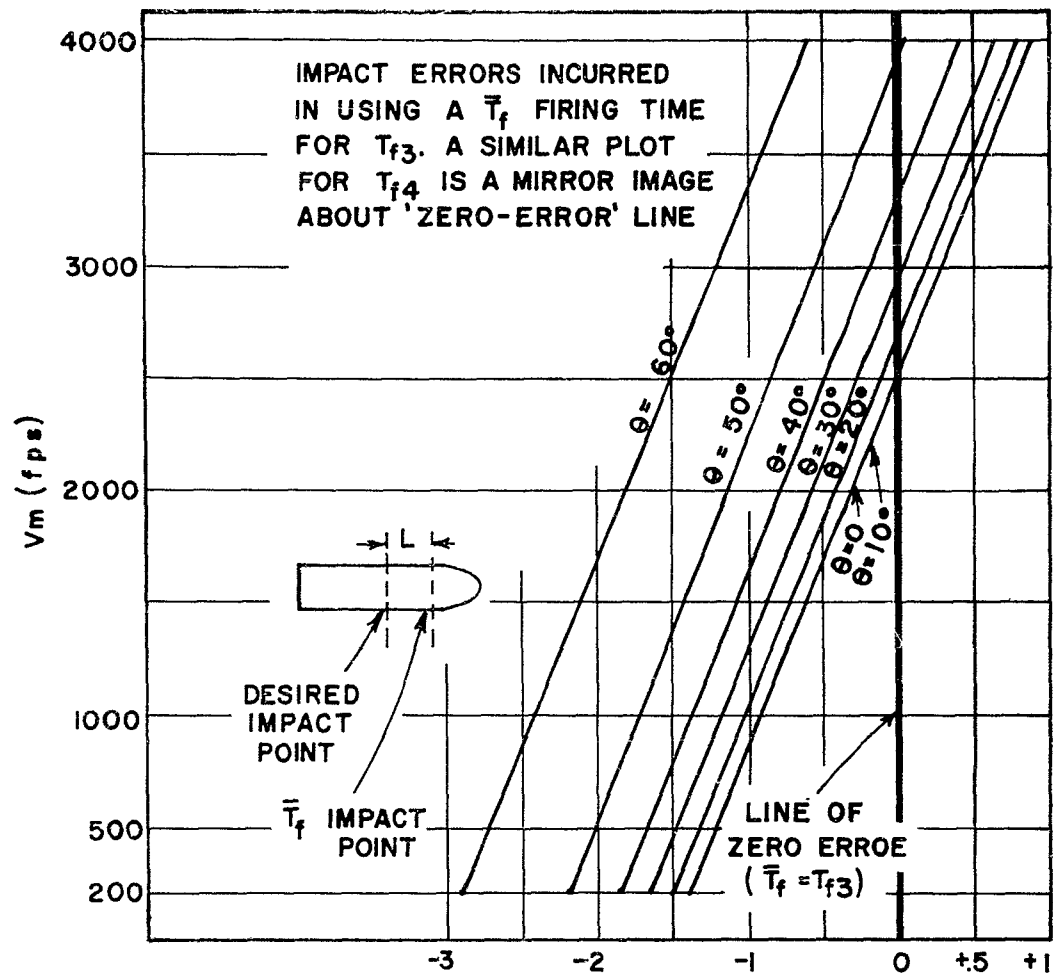


Figure 3-8.  $L$  (impact error in inches)

SECRET

**SECRET**

Table 3.2. Impact Error B as a Function of  $V_m$  and  $\theta$

$\theta$ deg	$V_m$ fps	$K_3$ $\mu$ sec	$L_3$ in.	$\theta$ deg	$V_m$ fps	$K_3$ $\mu$ sec	$L_3$ in.	$\theta$ deg	$V_m$ fps	$K_3$ $\mu$ sec	$L_3$ in.
0	4000	+18.3	+ .9	20	2500	- 4	- .1	40	1000	-113	-1.4
	3500	+13.8	+ .6		2000	-17	- .4		750	-168	-1.5
	3000	+ 8	+ .3		1500	-39	- .7		500	-277	-1.7
	2500	0	0		1000	-83	-1.0		200	-766	-1.8
	2000	-13	- .3		750	-128	-1.15	50	4000	+ 1	+ .05
	1500	-34	- .6		500	-217	-1.3		3500	- 6	- .25
	1000	-75	- .9		200	-616	-1.5		3000	-1.6	- .55
	750	-117	-1.05		4000	+13.5	+ .65		2500	- 28	- .8
	500	-200	-1.2	30	3500	+ 8	+ .35		2000	-48	-1.1
	200	-575	-1.4		3000	+ 2	+ .06		1500	-80	-1.4
10	4000	+18	+ .9		2500	- 8	- .2		1000	-144	-1.7
	3500	+13	+ .6		2000	-23	- .5	60	750	-209	-1.9
	3000	+7.5	+ .3		1500	-47	- .8		500	-338	-2.0
	2500	0	0		1000	-94	-1.1		200	-920	-2.2
	2000	-14	- .3		750	-142	-1.3		4000	-13	- .6
	1500	-35	- .6		500	-238	-1.4		3500	-22	- .9
	1000	-77	- .9		200	-670	-1.6		3000	-34	-1.2
	750	-119	-1.1	40	4000	+ 9	+ .4		2500	-50	-1.5
	500	-204	-1.2		3500	+ 3	+ .1		2000	-75	-1.8
20	200	-583	-1.4		3000	- 5	- .2		1500	-117	-2.1
	4000	+16	+ .8		2500	-16	- .5		1000	-200	-2.4
	3500	+11	+ .5		2000	-32	- .8		750	-283	-2.6
	3000	+ 5	+ .2		1500	-59	-1.1		500	-450	-2.7
									200	-1200	-2.9

**SECRET**

# SECRET

## 4. OPTICAL DETECTION ELEMENTS

H. W. Straub, J. Arthaber

### 4.1 Design of Reflector

(S) The first experiments that proved that it was indeed possible to obtain from fast-moving shell signals of sufficient strength to operate a computer were made with 50-mm diameter parabolic reflectors taken from commercial flashlights. The distribution of sensitivity across the beam at a 7-ft range, as measured by a recording method specially developed for this purpose,\* is shown in figure 4-1. This type reflector was still used in the first two-fence, velocity-only equipment (section 5.1) which was built to test the computer for determining the firing time of the defending charge as a function of the shell velocity alone (section 6). It was also used in two identical equipments constructed for the same purpose and supplied to Feltman Research and Engineering Laboratory, Picatinny Arsenal, and to Ballistics Research Laboratories, Aberdeen Proving Ground, to serve as timing tools for the defending-charge work done at these installations.

(U) However, it was realized in the very earliest stages that both definition and parallelism of beams from flashlight-type reflectors were entirely inadequate for the system accuracy required (section 3.2). In the process of designing an improved reflector, a novel optical concept has evolved. It has been termed the quasi-parallel light principle because it shows a way of producing beams only the boundary lines of which are parallel and only out to a given distance.\*\*

(U) Three sets of three reflectors, each set employing a different design detail, but having the same diameter, 50 mm, as the flashlight reflectors initially used, and a 7-ft length of the quasi-parallel detection pattern, were obtained from three contractors\*\*\* Laboratory measurements and actual firings verified the computed sharpness of the pattern. However, it also turned out that the sensitivity was higher than necessary for daytime use, meaning that the cross section could be reduced, which, in turn, improved the sensing accuracy.

(C) Further field tests and the system analysis (section 2.2.6) resulted in the additional requirement that, in the detection subfences (section 5.2), the leading, as well as the trailing, edge of the over-all sensitivity pattern should be straight lines rather than portions of circles and that the individual elements forming a fence should be packed as closely as possible.

\* DOFL Report TR-641, "Electronic Focus and Detection Pattern Indicator," by J. M. Arthaber, 30 September 1958

\*\* DOFL Report TR754, "The Quasi-Parallel Light Principle; Hollow-Conical, Flat or Tubular Radiation or Detection Patterns," by H. W. Straub, J. M. Arthaber, W. J. Moore, 13 January 1960.

\*\*\*American Optical Co., Bausch & Lomb Optical Co., Eastman Kodak Co.

# SECRET

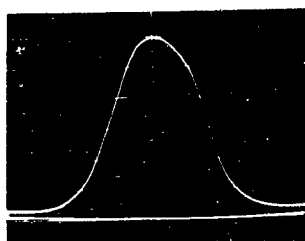
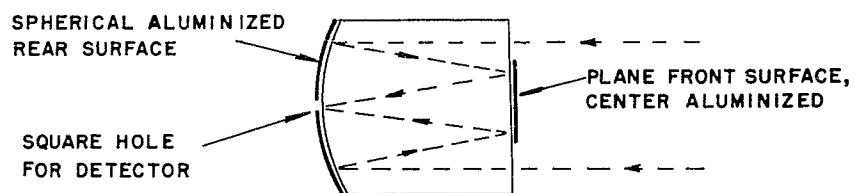


Figure 4-1. Distribution of sensitivity flash-light reflector



Figure 4-3. Distribution of sensitivity reflector of figure 4-2.

Distribution of sensitivity at 7 ft  
1 horizontal division = 2.5 cm  
Vertical deflections normalized



BACK VIEW

FRONT VIEW

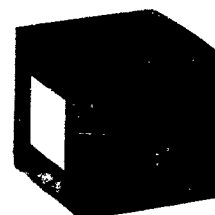
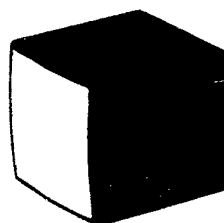


Figure 4-2. Solid-glass, square cross-section reflector

## CONFIDENTIAL

(C) In consequence, a square cross-section reflector\* of solid glass with sides 30 mm in length, employing the folded-beam technique, and maintaining quasi-parallelism out to a distance of 7 ft, was designed and manufactured.\*\* Figure 4-2 shows the design. Because of the design parameters, the dimensions of the hole in the mirror surface over which the photodetector was cemented had to be 0.6 x 0.6 mm.

(U) In figure 4-3 the distribution of sensitivity across the beam at the 7-ft range is shown. The improvement in sharpness over that in figure 4-1 is obvious.\*\*\*

(U) This type of reflector was intended for use in the hardware that was to be constructed for the feasibility test. It has been used successfully in the 3-fence experimental equipment described in section 5.

(C) It should be kept in mind that the 30-mm square cross section is a compromise between two conflicting requirements, namely, that of high sensitivity, calling for a large-area reflector, and that of high system accuracy, calling for as many as possible small reflectors packed as closely as possible.

### 4.2 Selection of Photocell Type

(U) Lead sulphide (PbS) photocells suggested themselves as detectors for application in the detection units of the Dash-Dot system because of the following properties. They have a responsivity that is high in the near infrared and fair in the visible region of the optical spectrum. They lend themselves to manufacture in small sizes, as required in this project, and their geometrical efficiency (ratio of sensitive area to front surface of cell assembly) recommends their incorporation into the present optical system. Also, they are rugged, nonmicrophonic, insensitive to vibration and mechanical shock, and can stand temperatures up to 100 deg C.

(U) In order to cover the hole for the detector in the reflector shown in figure 4-2, the dimensions of the PbS cells used were chosen to be 0.8 x 0.8 mm.

(U) The small time constant of the more expensive lead selenide photocells did not offer an effective advantage because of their lower responsivity. Lead telluride photodetectors were not readily available. Phototubes and photomultipliers were rejected because of their relatively large size and their comparatively poor response in the near infrared region.

\* The necessity of the square cross section was first pointed out by co-author R. J. Paradis

\*\* Bausch & Lomb Optical Co.

\*\*\* The structure of the peak of the trace is attributed to the sensitivity contour of the detector used.

CONFIDENTIAL

77

(U) It was evident that the output impedance of unmodified PbS cells (figure 4-4) was too high to permit matching it with the input impedance of the transistor circuitry connected with it. The difficulty was resolved by the so-called grid design of the cell electrodes or snake design of the sensitive area (figure 4-5). The expansion of the two electrodes into two interleaving comblike patterns results in a snake-like arrangement of the sensitive area, which, although remaining square in its over-all shape, now represents a long and narrow strip of photo-sensitive material with the electrodes connected to its long sides. In this manner, a reduction of cell resistance from about 0.8 megohms to 15 k ohms was achieved.

(U) To determine the usability of different photocells, the signal-to-noise ratio of their response to 20-kc square-wave light pulses from a neon lamp was measured and their short-circuit signal current computed (figure 4-6). These average data are given for sensitive areas of 1 x 1 mm, cell power dissipation of 1 mw and total radiation intensity of 1  $\mu\text{W}/\text{mm}^2$ .

(U) The effect of changing the voltage across the photocell and load resistor was investigated. The diagram in figure 4-7 shows the results of such a test.

(U) During field testing, the suspicion arose that the steady light input from the background tended to severely increase the photocell noise. No significant effect of that kind, however, was observed in laboratory tests in the range between 80 cps and 40 kc. The results for several samples are represented in the diagram in figure 4-8. The illumination of the photocells is indicated by the decrease in cell resistance. The load resistance was equal to the cell dark resistance. In the optical systems used, this resistance drop remained below 30 percent, depending upon the illumination.



Figure 4-4. Unmodified square cell

Figure 4-5. Grid or snake cell

	KODAK	INFRARED INDUSTRIES	KODAK	INFRARED INDUSTRIES
	GEOMETRY LIKE FIG. 4-4	GEOMETRY LIKE FIG. 4-4	GEOMETRY LIKE FIG. 4-5	GEOMETRY LIKE FIG. 4-5
DARK RESISTANCE	800 K OHMS	890 K OHMS	18 K OHMS	14.5 K OHMS
$\frac{S}{N}$ FOR 20 KC	3.7	2.0	6.0	7.7
SHORT CIRCUIT CURRENT IN nA	10.4	3.8	120	148

Figure 4-6. Average characteristics of lead sulphide cells tested

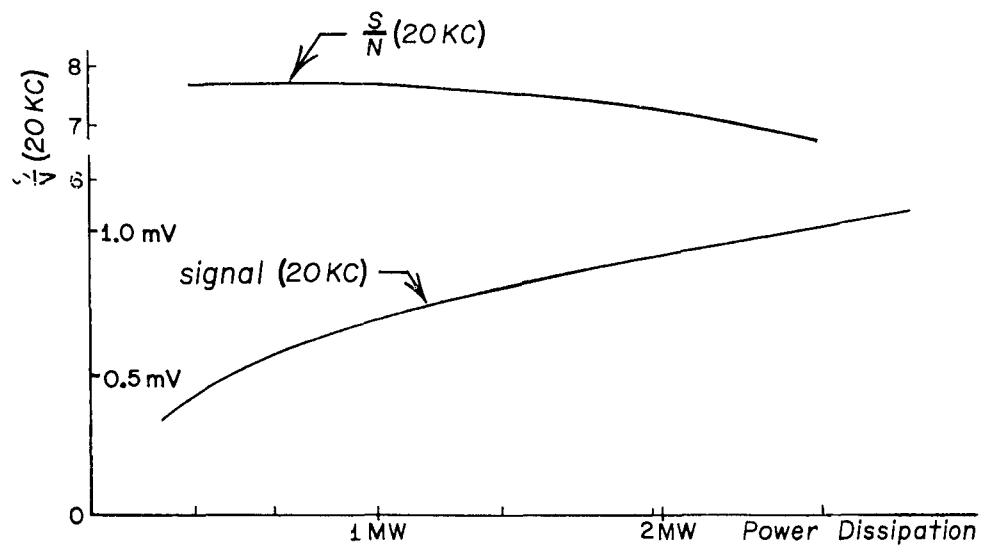


Figure 4-7. Relation between power dissipation in PbS photocell and Signal voltage and signal-to-noise ratio obtained

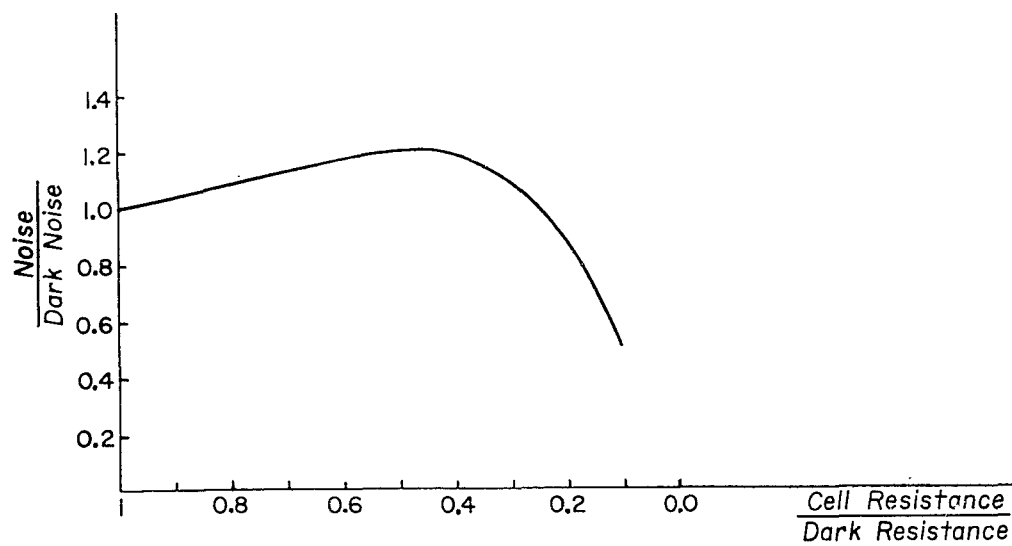


Figure 4-8. Change of cell noise with illumination

# SECRET

## 5. OPTICAL DETECTION EQUIPMENT

R. R. Ulrich, R. J. Paradis, L. Melamed

### 5.1 Velocity-Only Detection Unit

(C) Most of the earlier field testing of the computer system was done with a computer that determined the firing time as a function of velocity only. In these measurements the height of the projectile and the angle of approach were preset. Since a great deal of useful data were collected from these field tests, it is worthwhile to give some attention to the detecting unit involved. The velocity-only detection unit is shown in figure 5-1. It consists of two detection regions spaced exactly 1 ft apart. Each detection region originates from a series of four parabolic flashlight reflectors with a PbS cell mounted at the focal point of each reflector. Two aluminum baffle boxes with a 1-in. wide slot are located over the reflectors. The baffles prevent sunlight from striking the detectors, and they also sharpen the boundaries of the detection region. The unit shown is hermetically sealed and pressurized to prevent atmospheric humidity from affecting the PbS cells and is equipped with safety glass windows.

(S) Two units of the described type were supplied to Picatinny Arsenal and Ballistics Research Laboratory, Aberdeen Proving Grounds, as timing tools for their work on the defending charges. It was with these units that shells were consistently destroyed in flight.

### 5.2 Subfence Unit

#### 5.2.1 Description

(C) The basic optical element that forms the detection region for the investigations described in this report is the square reflector described in section 4.1 and shown in figure 4-2. A series of 84 pickets arranged in a line, each originating in one of these reflectors, forms a complete detection fence. The construction of the fence is greatly simplified by mounting the reflectors in units comprising only a small portion of the fence. These subfence units, when placed end to end, form a complete fence, each subfence unit serving as a building block module. This arrangement has the following advantages:

- (a) Defective portions of the fence are easily replaced.
- (b) The optical fence structure is transportable.
- (c) Closer tolerances can be held in the construction of the fence,
- (d) Alignment procedures are simplified.

SECRET

61

CONFIDENTIAL

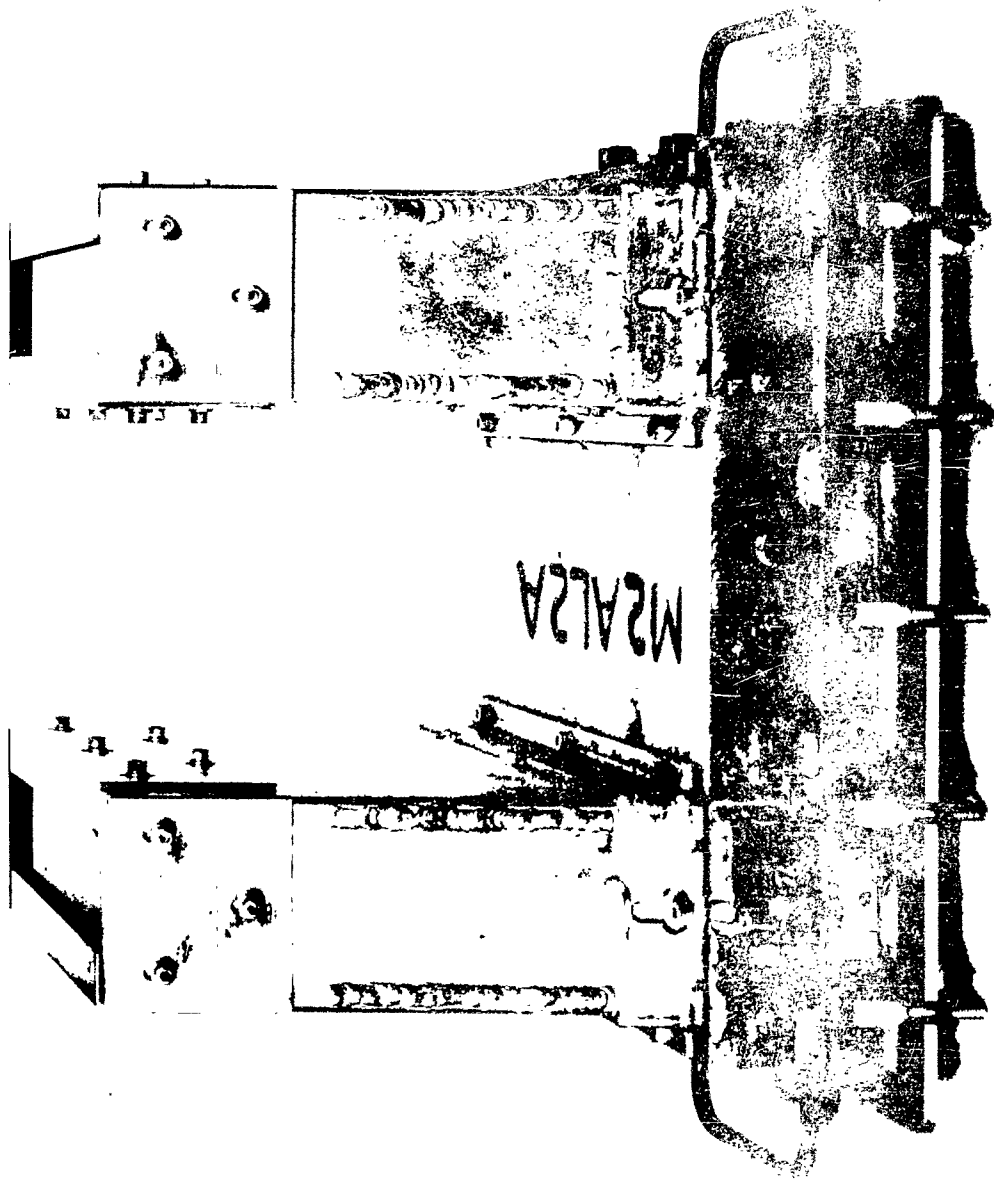


Figure 5-1. Velocity-only detection unit

CONFIDENTIAL

# CONFIDENTIAL

(C) The design of the subfence units used in the field tests was based mainly on the following considerations:

- (a) Positional accuracy of the detection region,
- (b) Ease of replacement of components.

Little or no regard was given to the following:

- (a) Cost of units,
- (b) Compactness of units,
- (c) Methods for mass-producing units.

Figure 5-2 shows an optical subfence.

## 5.2.2 Design Specifications

(U) The square reflectors are spaced so that the distance between the centers of every eighth reflector is 10 in. (254 mm). This results in a spacing of 36.28 mm from the center of one reflector to the center of the adjacent one and a separation of 6.28 mm between the edges of two adjacent detection beams. The subfence unit, which is also 10 in. long, holds seven reflectors (figure 5-2 and 5-3).

(C) The maximum tolerable deviation in detection picket alignment was set at  $\pm 1/8$  in. at 7 ft in accordance with the maximum acceptable time error that can be tolerated in the computer for proper functioning (section 2.2.6).

## 5.2.3 Special Considerations

(U) The square reflector consists of a folded optics system behind which the detector is located. Figure 5-4 illustrates the reflector optics and also shows a region in front of the reflector through which light can directly strike the detector. A baffle plate as shown in position A will prevent direct light from striking the detector. However, light could reflect off the baffle wall and on to the detector. Actually, spurious signals were obtained on sunny days as the shadow of a projectile fired over the subfence units crossed the baffle walls. This effect could be greatly reduced and often eliminated by using a specially designed baffle. A cross-sectional view of such a baffle is shown in position B, and it can be seen that the only light that could be reflected on to the detector must come from the baffle edges. Each subfence unit has its own light baffle structure between each reflector as shown in figure 5-5.

## 5.2.4 Cell Mounting

(U) An important but tedious task in the assembly of a subfence unit is the mounting of the detector on to the reflector. A low impedance

**CONFIDENTIAL**

83

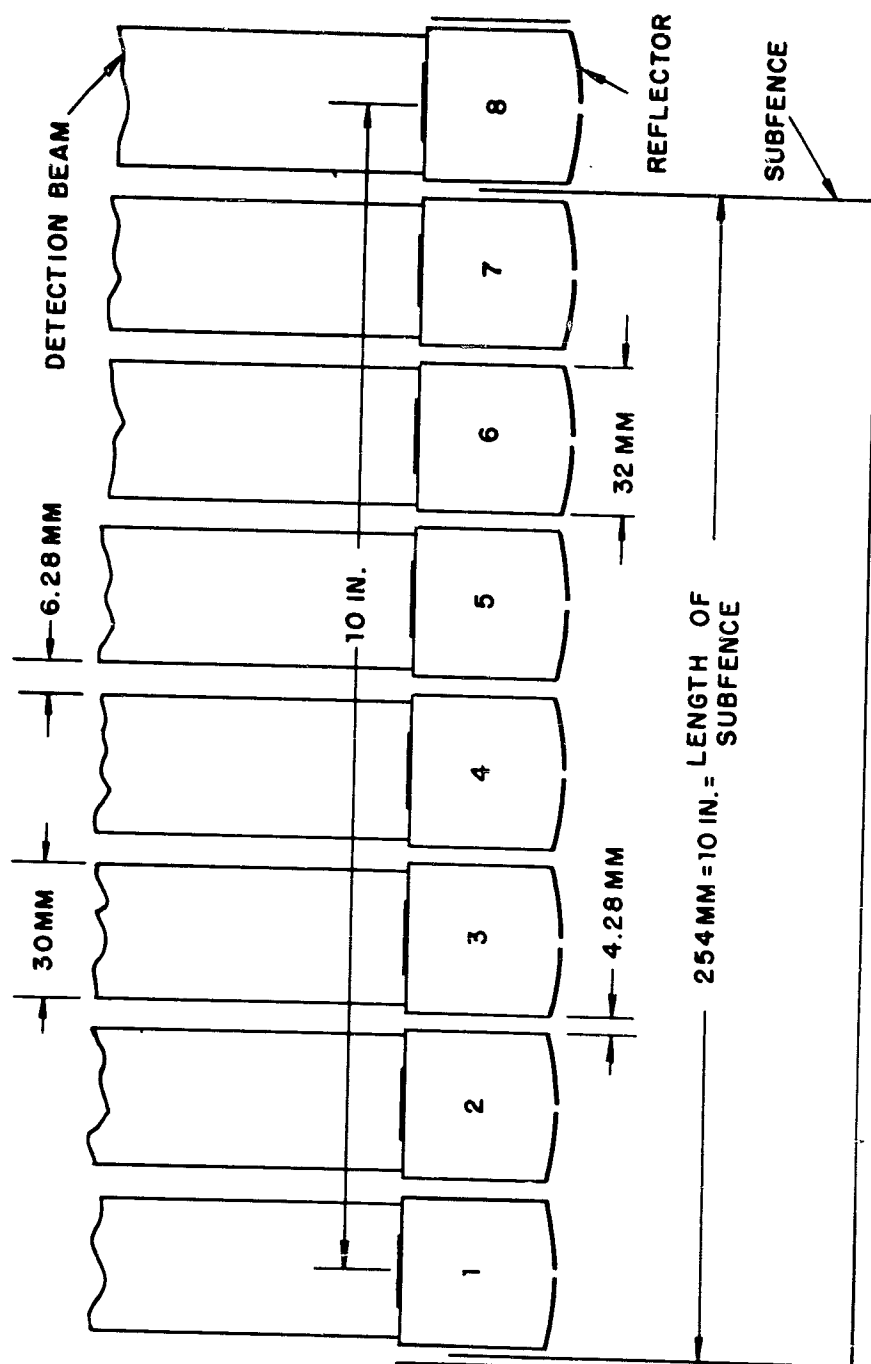


Figure 5-2. Arrangement of reflectors in subfence

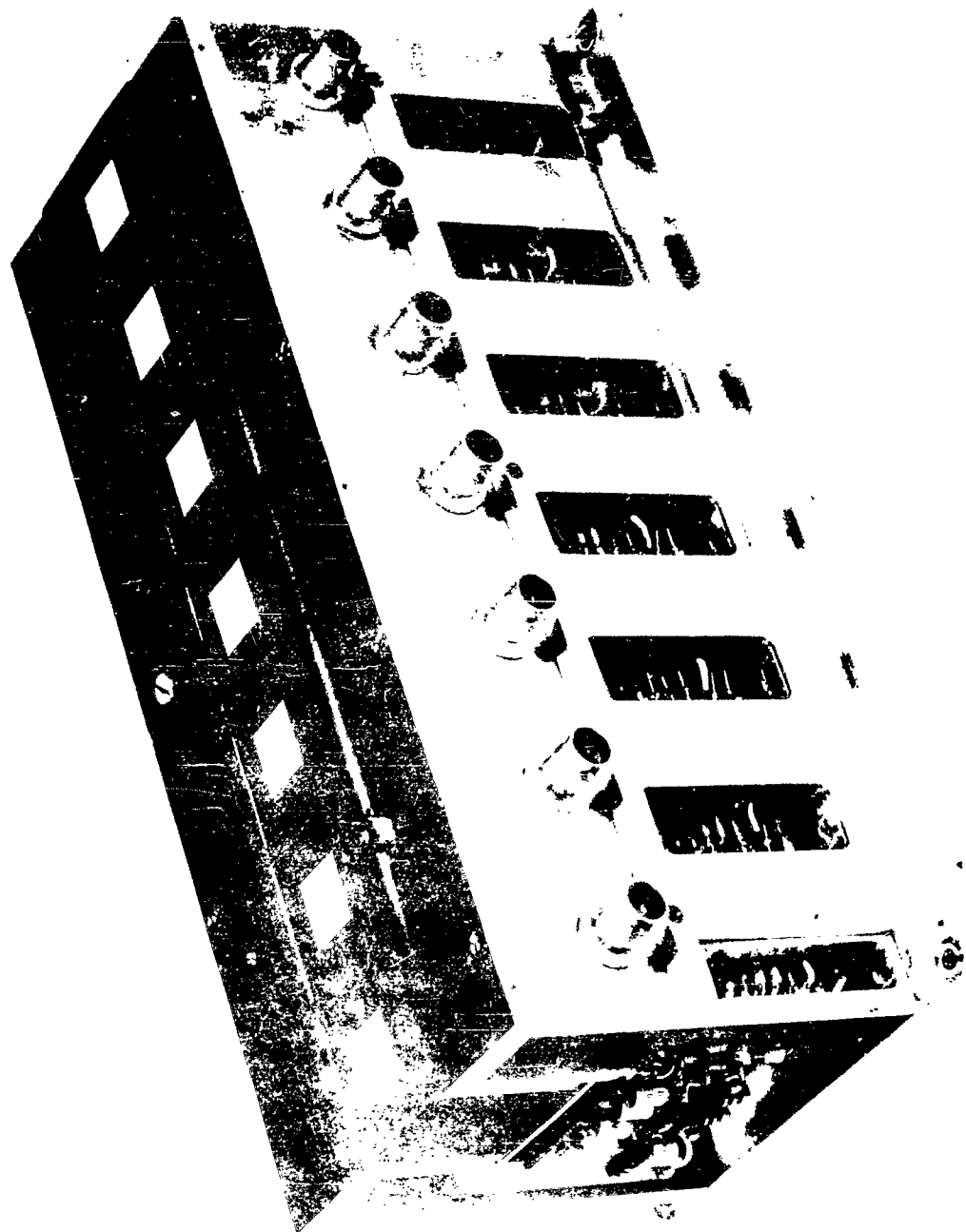


Figure 5-3. Subfence unit

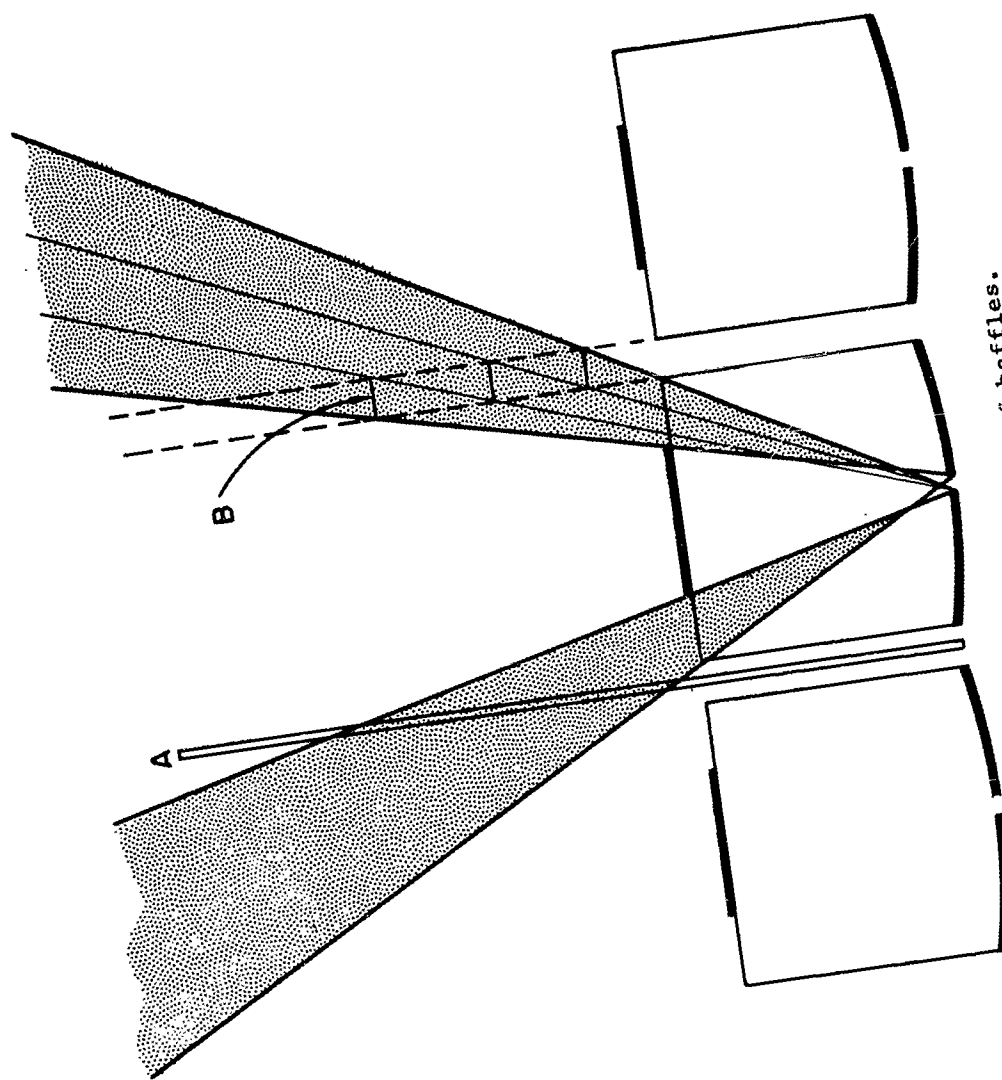


Figure 5-4. Design of baffles.

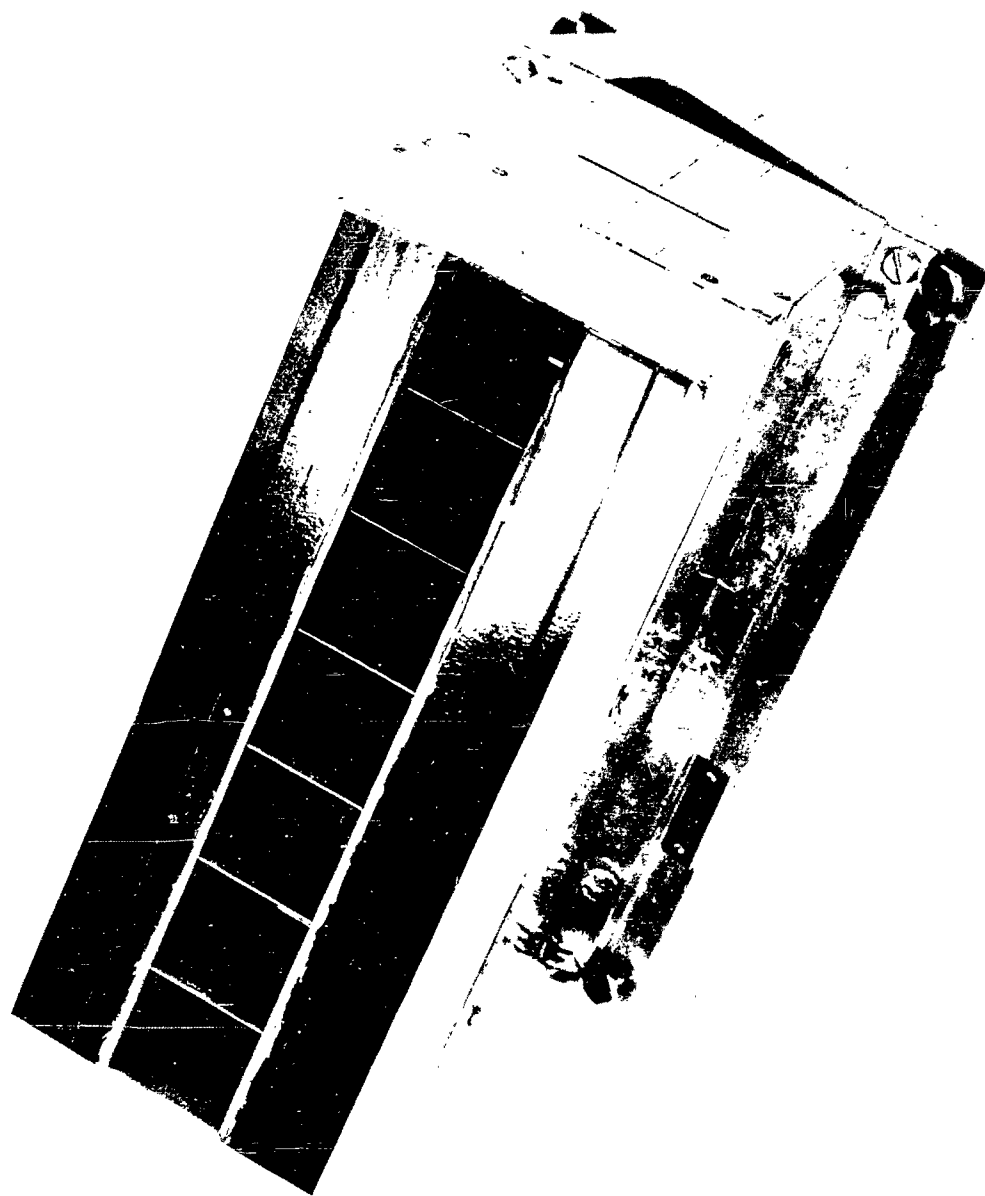


Figure 5-5. Subfence with baffle

# SECRET

0.8-mm square, lead sulfide cell (section 4.2) is mounted over the 0.6-mm square pinhole in the back of the reflector. To insure correct mounting of the cells, the picket detection beams were investigated by a method that displays the detection pattern on an oscilloscope.\*

## 5.3 Mounting Structure

### 5.3.1 System Layout

(C) The optical detection layout for the proposed test consists of three detection fences spaced as shown in figure 3-1 and described in section 3.2. Each fence is 10 ft long and consists of 12 subfence units placed end to end. There are 84 pickets in each fence.

### 5.3.2 Z-Shaped Structure

(C) A simplified, experimental mounting structure was designed and constructed specifically for field testing the computers. The structure consists of a Z-shaped platform secured on a rotatable gun mount as shown in figure 5-6. The platform supports three subfence units, each representing a portion of a different detection fence. Subfence units A and C can be moved to various positions along the arms of the Z. Unit B is in a fixed position with its center located directly over the center of rotation of the gun mount. By rotating the gun mount and displacing units A and C in the appropriate positions on the arms, all angles of approach of a projectile from 0 deg to 55 deg can be covered.

(S) For a 0 deg approach of a projectile, the three units are located directly behind each other along the central member of the Z-frame, and unit C can be located at various positions along this member. By changing the position of unit C, which is inclined at 20 deg with unit B, various approach altitudes can be simulated.

(U) To maintain flatness and levelness of the aluminum alloy mounting surface, elaborate heat treatment and machining procedures were employed. Three months after final machining, the surface had not shown any noticeable distortion.

## 5.4 Alignment Methods

### 5.4.1 Picket Alignment

(U) The alignment of the individual reflectors in a subfence was performed to an accuracy of  $\pm 1/8$  in. at 7 ft from the reflectors by using the following method. An extended, radiating area was formed by

\* DOFL Report TR-641, "Electronic Focus and Detection Pattern Indicator," by Joseph M. Arthaber, 30 September 1958.

# SECRET

CONFIDENTIAL

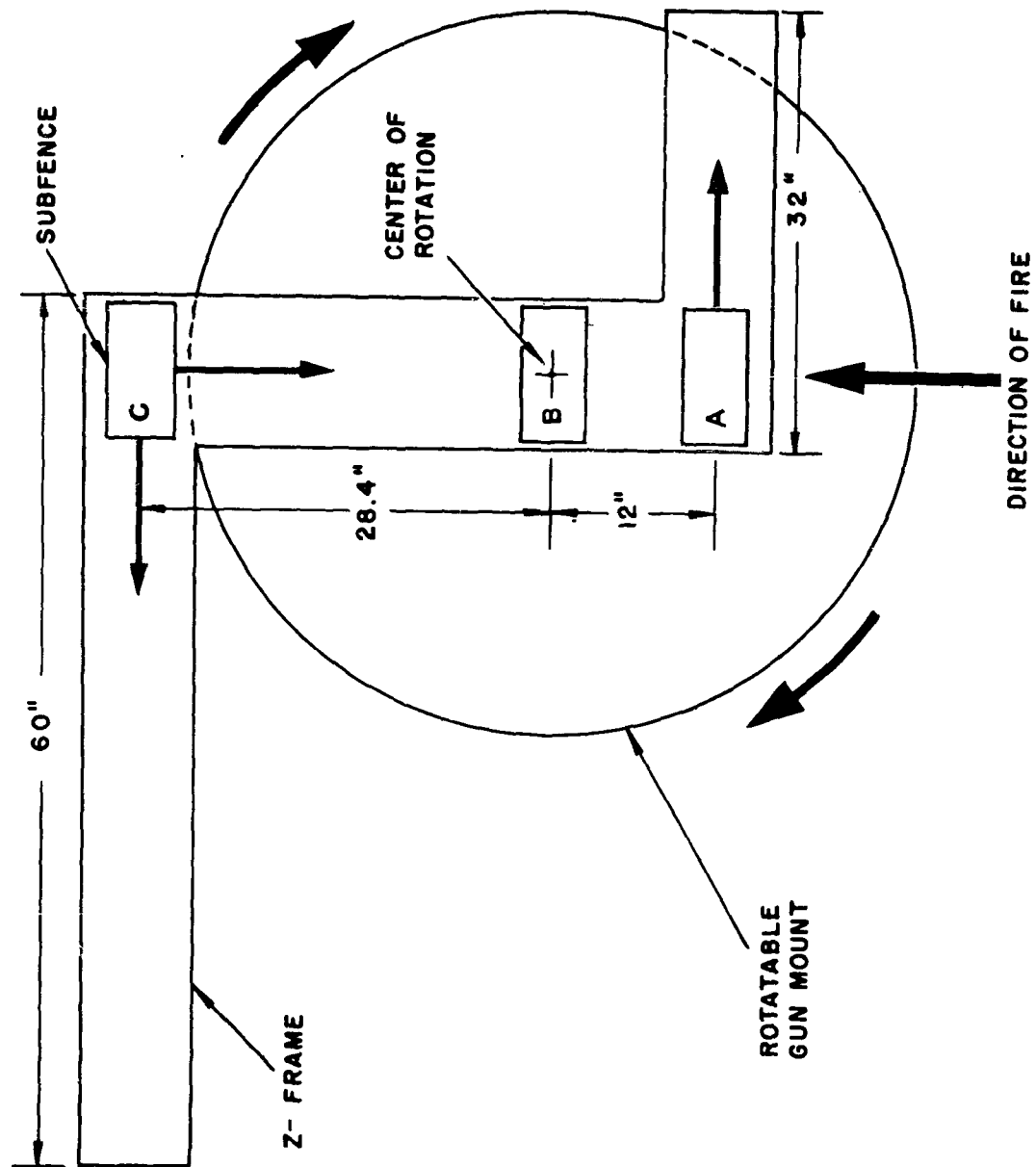


Figure 5-6. Z-frame on gun mount

CONFIDENTIAL

placing a group of fluorescent lamps behind a diffuse glass plate covered by translucent paper. The subfence was placed 7 ft above this light source. Perpendicularity of the reflector axes with the glass plate was maintained. A plumb line suspended from the corners of the subfence unit was used to project the subfence outlines onto the translucent paper, and lines that were now parallel with the edges of the square detection patterns were drawn on the paper. The straight edge of a large piece of opaque black paper was moved first parallel, then normal to these lines, and the position marked on the translucent paper where the 120-cps light signal first appeared in the detector. In this way, a square detection area was marked out for each detection element in the subfence unit. The general pattern of the optical fence and any misaligned elements can readily be discovered. A misalignment of a detection element may be due to either a machining inaccuracy in the subfence unit or an inaccuracy in the reflector itself. A reflector may be aligned by (a) replacing, (b) rotating, or (c) shimming.

#### 5.4.2 Subfence Alignment

(U) Once the detection elements within a subfence are aligned, it is then necessary to check the alignment of the various subfences with respect to each other on the Z-structure. In doing this, the levelness and uniformity of the mounting surface may be checked at the same time. The method of subfence alignment used is as follows: A sheet of dull white background material (painted Masonite) suspended at a known height above the mounting platform is maintained parallel with the Z-mounting surface. The image of a linear light source modulated at 10 cps is then swept across the Masonite in such a way that the image is parallel with the edges of the subfence unit. The image position at which the 10 cps signal was first detected by each subfence was then marked on a Masonite. The detection pattern of each fence is thus located at the known height and any deviation in the alignment becomes apparent.

#### 5.5 Associated Equipment

(U) Several items of associated equipment have been developed in connection with the field testing of the detection system and in the investigations of the detection patterns.

(U) In the field tests, triggering screens having a very precise accuracy were needed and this resulted in the development of the optical cavity triggering screen.\* In the laboratory, a method for determining the sensitivity patterns of the detection units was needed. This resulted in the development of the electronic focus and detection pattern indicator.\*\* To interpret and monitor the response of the

\* DOFL Report TR-654, An Optical Cavity Triggering Screen by R. R. Ulrich, 23 Dec. 1959.

\*\* DOFL Report TR-641, "Electronic Focus and Detection Pattern Indicator," by Joseph M. Arthaber, 30 September 1958.

optical system in the field, an infrared photometer was developed that measured the ambient infrared sky radiation.\*

---

\* DOFL Report TR-759, "A Near Infrared Photometer," by Louis Melamed, 20 November 1959.

# SECRET

## 6. PRELIMINARY SYSTEM

A. L. Copeland, R. J. Paradis

### 6.1 Background

(S) Before starting the design of the experimental system for the June 1960 feasibility test, which is described in sections 8 through 13, a preliminary system was built that contained only two vertical, parallel detection fences and a computer\* for determining the firing time and supplying a firing pulse as a function of the shell velocity alone. The normal angle of attack and the height of the shell trajectory were held constant. Since the velocity is the only variable, it is also called the velocity-only system.

(U) The purpose of the system was to provide experience in "wedding" the optical detection system to the following electronic evaluating system. One difficulty became apparent almost immediately. It was that of obtaining sharp trigger pulses from the output of the long time constant lead sulfide cell in a poorly defined detection pattern at the instant when the shell crossed the fence boundary.\*\*

### 6.2 Optical Equipment

#### 6.2.1 Detection Unit

(U) The optical detection unit was the one described in section 5.1 and shown in figure 5.1.

(C) The standard flashlight reflectors used in the two 4-reflector detection fences resulted in too broad a detection pattern (figure 6-1) and consequently produced a detection fence that departed by an unacceptably wide margin, E, in figure 6-1, from a true plane. Conditions were considerably improved by the installation in each fence of a baffle 1 ft in length with a collimating slit 1 in. in width 1 ft above the reflectors. The leading edge of each slit was set at a position where the detection sensitivity was adequate along its entire length to produce a pulse at the instant when the fence was pierced by a shell.

(U) But even after the baffles had been installed, the pulses were still too long under conditions of high signal level. They then appeared as shown in figure 6-2. When a brute-force amplifier was used to amplify the signal in order to produce a trigger pulse, the pulse occurred

\* DOFL Report TM-57-7, "A Simplified Computer for the Dash-Dot System," (U) by R. J. Paradis, A. L. Copeland, E. Ramos, 20 March 1958.

\*\*The improved reflectors (section 4.1) were not available at that time.

SECRET

93

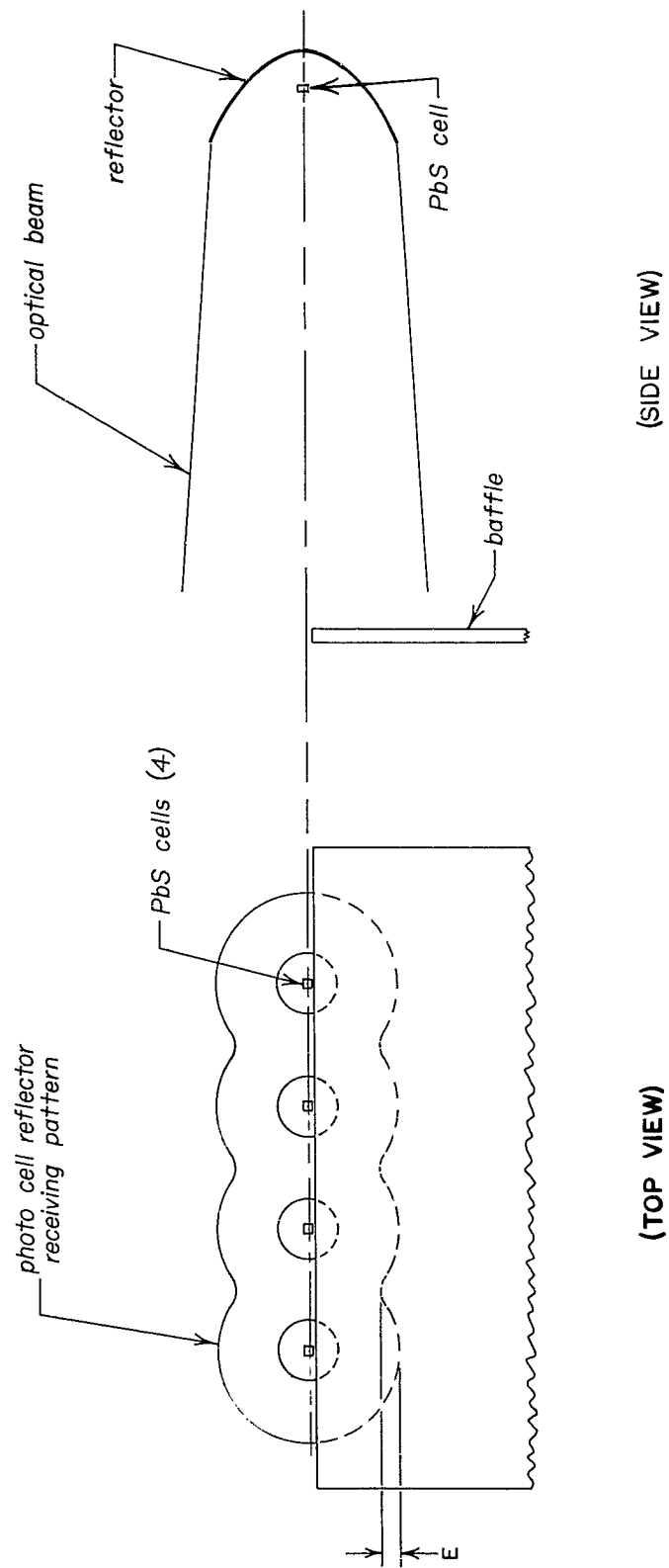


Figure 6-1. Preliminary detection layout

CONFIDENTIAL

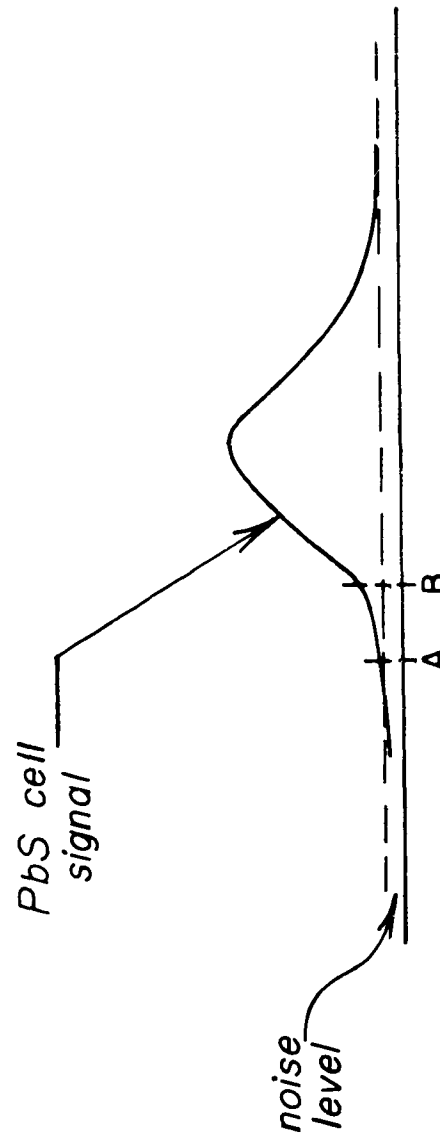


Figure 6-2. Shell signature

CONFIDENTIAL

## CONFIDENTIAL

somewhere in the shallow portion between points A and B, although the shell did not cross the slit edge until point B was reached. The difficulty was overcome by abandoning the brute-force amplifier in favor of a rate-of-rise amplifier, section 6.3.

(U) The baffle method, although rather crude optically speaking, served its purpose in the particular application. It could not have been applied in the full experimental system where the accuracy requirements were much higher.

### 6.2.2 Performance of PbS Cells

(C) It was found that the sensitivity of the Eastman Kodak PbS cells was sufficient under a bright, cloudy sky. It was found insufficient in the late afternoon under a heavy overcast, and under a clear-blue sky. The blue sky obviously lacks emission in the infrared region of the spectrum, while late afternoon overcast sky lacks over-all light emission. This limitation would not restrict the use of the system under operational conditions since artificial infrared floodlighting has been envisioned for use at night time.

(U) In field test practice, the Eastman Kodak PbS cells, when used in unsealed equipment, had a strong tendency to develop noise levels high enough to make them useless for the present application. This seemed to be especially so during prolonged periods of high relative humidity, and it was concluded that the noise was due to the absorption of moisture by the cells. The condition was remedied at various times by drying out the units. It was for this reason that in the last design the detection unit was hermetically sealed and pressurized, and contained a dessicant.

(U) The detection units also contained two pulse-adding circuits (figure 6-3), which added the pulse voltages generated in the four PbS cells of each fence. When more than one cell was observed by the traversing shell, and fed their sum to the following rate-of-rise amplifier. This method was chosen because of its advantage over its alternative of simply paralleling the cell outputs.

### 6.3 Rate-of-Rise Amplifier

(U) The rate-of-rise amplifier was designed to fulfill the following requirements:

- (a) High-impedance PbS cells working into a vacuum tube amplifier.
- (b) Minimum output signal required to trigger the computer gates to be 10 v.
- (c) Minimum initial signal rate-of-rise of lead sulfide cell output to be 50 mv in 500  $\mu$ sec.
- (d) Time lag between crossing of slit edge by shell and delivery of trigger pulse to be 20  $\mu$ sec.

CONFIDENTIAL

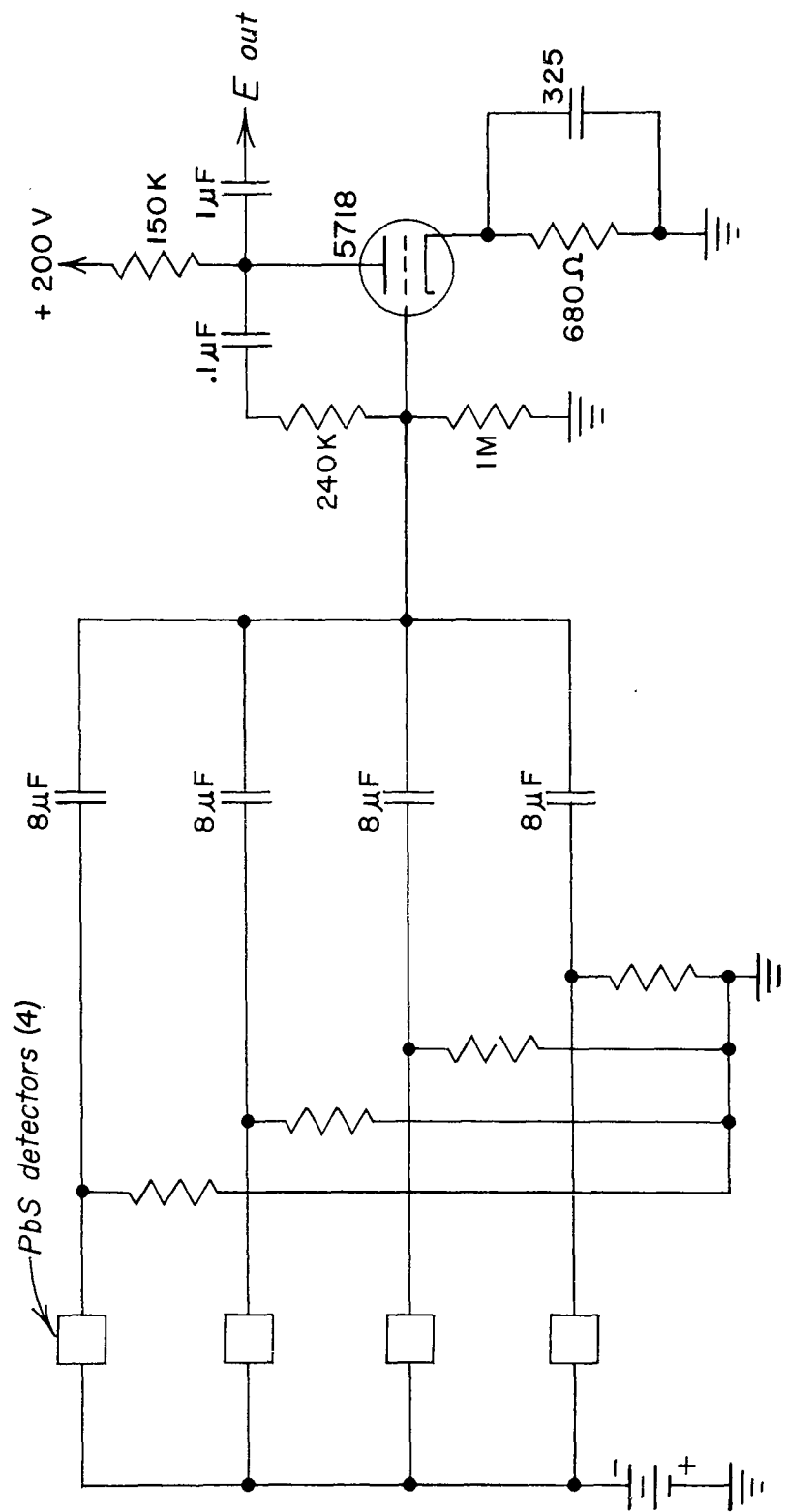


Figure 6-3. Pulse adding circuitry of preliminary system

(U) The equation for the rate of rise amplifier (figure 6.4), assuming a ramp input, is

$$e_o = -A\alpha T x e^{-x} \quad (6.1)$$

where

$A$  = gain of the amplifier,

$\alpha$  = rate of rise of the ramp input,

$T = R_1 C_1 = R_2 C_2$ , and

$x = \frac{t}{T}$ .

The value of  $T$  that will supply a 10-v pulse at 20  $\mu$ sec for the smallest value of  $\alpha$  that is practicable must then be found. To do so, the time at which the peak occurs in equation (6.1) must be determined.

(U) Differentiating equation (6.1) with respect to  $x$  gives

$$\frac{de_o}{dx} = -A\alpha T (-xe^{-x} + e^{-x}).$$

The right-hand side is now set to zero and solved for  $x$ :

$$-A\alpha T (-xe^{-x} + e^{-x}) = 0, \text{ therefore,}$$

$$x = 1 = \frac{t}{T}. \quad (6.2)$$

In order to determine the value of  $T$  required for the occurrence of the peak at 20  $\mu$ sec,  $t$  in equation (6.2) is set to 20  $\mu$ sec:

$$\frac{2 \times 10^{-5}}{T} = 1; \quad T = 2 \times 10^{-5} = 20 \mu\text{sec}.$$

(U) Substituting equation (6.2) into equation (6.1) gives

$$(e_o)_{\text{peak}} = -A\alpha T e^{-1} = -3.68 \times 10^{-1} A\alpha T. \quad (6.3)$$

(U) Since the computer requires a 10-v pulse, equation (6.3) must be solved for the amplifier gain  $A$ :

$$A = \frac{(e_o)_{\text{peak}}}{\alpha T (3.68 \times 10^{-1})} \quad (6.4)$$

\* "Pulse & Digital Circuits," by McGraw-Hill Book Co., New York, Toronto, London, 1956, p 40.

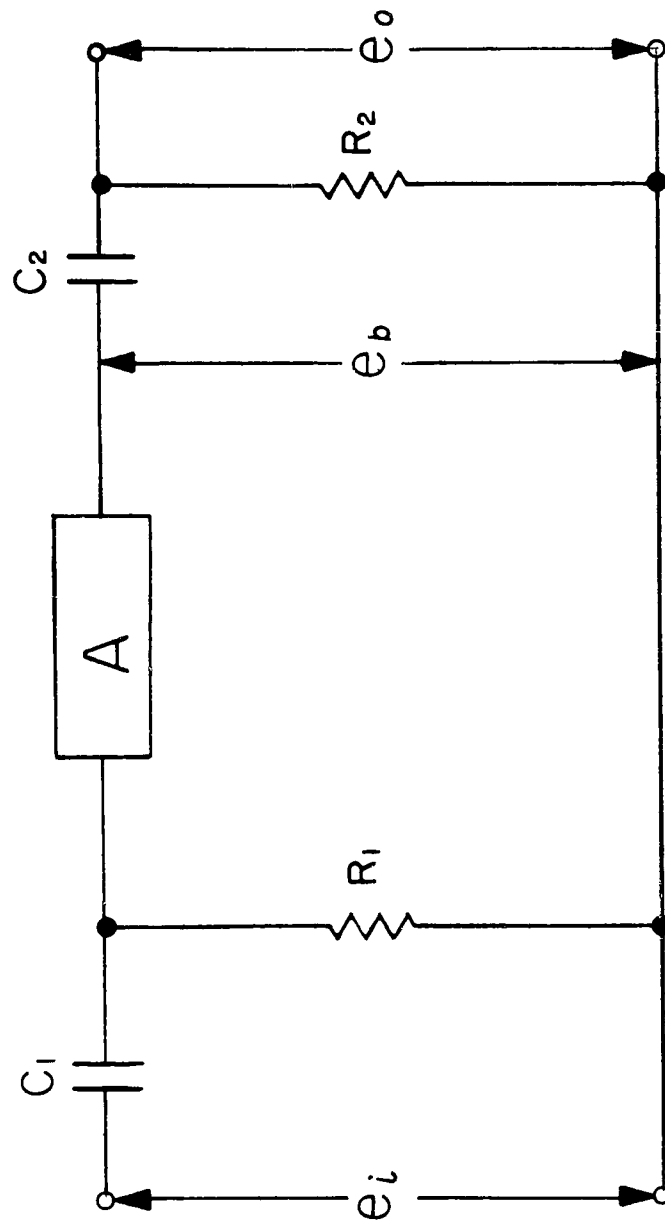


Figure 6-4. Equivalent circuit of rate-of-rise amplifier

# SECRET

Substituting the appropriate values for  $(e_o)_{\text{peak}}$ ,  $\alpha$ , and  $T$  gives

$$A = - \frac{1 \times 10^1 \text{ V}}{(1 \times 10^2 \text{ V/s})(2 \times 10^{-5}) (3.68 \times 10^{-1})}$$

$$A = - 1.358 \times 10^4.$$

(U) The amplifier must then have a minimum gain of about 14,000 in order to properly operate the computer within the requirements listed above.

(U) The rate-of-rise amplifier, as actually constructed (figure 6-5), also includes a noise-clipping level as well as an amplifier gain control in order to improve flexibility and to take advantage of future improvements in PbS cell noise.

(U) In the experimental system built for the proposed June 1960 feasibility test, the rate-of-rise amplifier, as described, has been superseded by the rally amplifier described in section 7.1.3.

## 6.4 Velocity-Only Firing-Time Computer

(S) In the geometry shown in figure 6-6,  $\Delta T_1$  is the interval between the times  $T_0$  and  $T_1$  when the projectile enters the first and the second fence, respectively, and  $\Delta T_2$  is the time interval between the time  $T_2$  when the projectile traverses the second fence and the time  $T_F$  when the defending charge has to be fired.

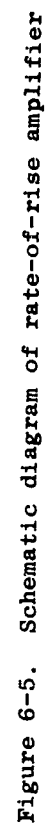
(U)  $\Delta T_F$  in terms of  $\Delta T_1$  and the other parameters in figure 6-6 is

$$\Delta T_F = \Delta T_1 \frac{d_2}{d_1} - d_3/V_c. \quad (6-5)$$

The height of attack  $d_3$  is known or preset;  $V_c$  is the known defending-charge velocity; therefore,  $d_3/V_c$  is the time of flight of the charge fragments.

(U) These parameters are set in the computer by the operator.

(U) Electronically, the operation of the computer is as follows (figure 6-7). At  $T_0$ , a Miller sweep is started at a run-down rate of  $C \frac{d_2}{d_1}$ ; at  $T_1$ , the voltage is held and a second Miller sweep is started and its run-down rate is  $C$ .



SECRET

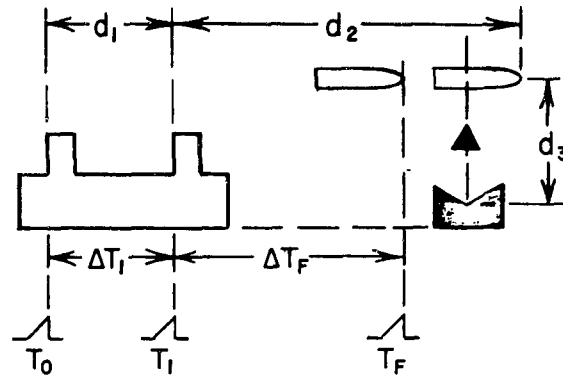


Figure 6-6. Basic velocity-only layout

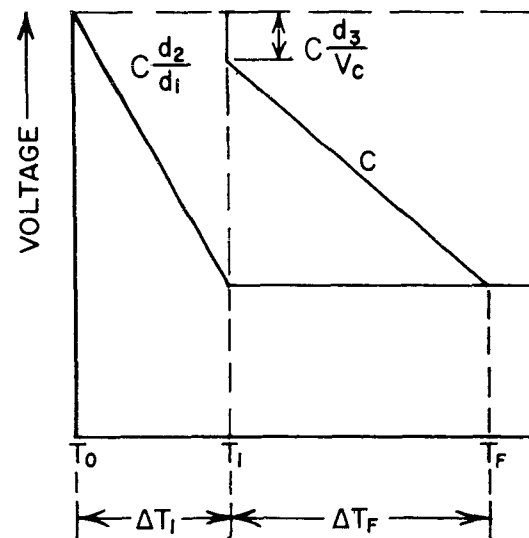


Figure 6-7. Operation of velocity-only computer

SECRET

# SECRET

Multiplying both sides of equation (6-5) by C, gives

$$C\Delta T_F = CK_1 \Delta T_1 - CK_2, \quad (6.6)$$

where

$$K_1 = \frac{d_2}{d_1}; \quad K_2 = \frac{d_3}{V_c}.$$

Notice that the parameters are not completely independent. For example, if a different point is required to be hit on the oncoming projectile,  $d_2$  is changed and this requires a change of C since the product  $C d_2/d_1$  is a constant of the computer. It is seen, then, that in order to hit a certain point on the projectile, C is adjusted or, in other words, the slope of the second Miller sweep is adjusted. Also the voltage step  $C d_3/V_c$  is clearly a function of C. In the rest of the derivation,  $C d_2/d_1$  and  $C d_3/V_c$ , will be called  $CK_1$  and  $CK_2$  respectively.

Now, since  $CK_1$  is a fixed constant of the computer, we let  $CK_1 = D$ .  $CK_2$  is a voltage parameter that has to be set in, so we will let  $CK_2 = \Delta V$ . Then

$$\Delta V = CK_2 = \frac{DK_2}{K_1}; \quad \Delta V = \frac{D}{K_1} K_2. \quad (6.7)$$

For ease in setting up and introducing the parameters into the language of the computer, charts have been prepared (figure 6-8). Notice that equation (6.7) is an equation for a straight line with slope  $D/K_1$ .

(S) Let an assumed case be set up using the dimensions in figure 6-9, where the missile is to be hit 10 in. behind the nose. Assuming

$$C\Delta T_F = CK_1 \Delta T_1 - CK_2,$$

$$K_1 = \frac{d_2}{d_1} = \frac{40}{12} = 3.34, \text{ and}$$

$$K_2 = \frac{2 \text{ ft}}{10^4 \frac{\text{ft}}{\text{sec}}} = 2 \times 10^{-4} \text{ sec.}$$

Defending charge velocity = 10,000 ft/sec and

$$CK_1 = 5.66 \times 10^4 \text{ v/sec.}$$

# SECRET

103

SECRET

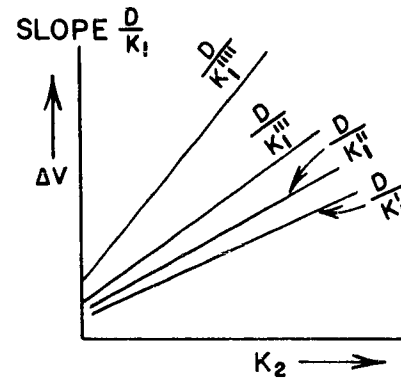


Figure 6-8. Chart for computer setting

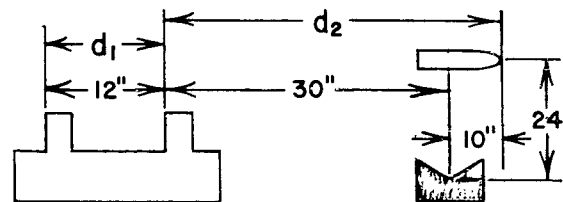


Figure 6-9. Special velocity-only layout

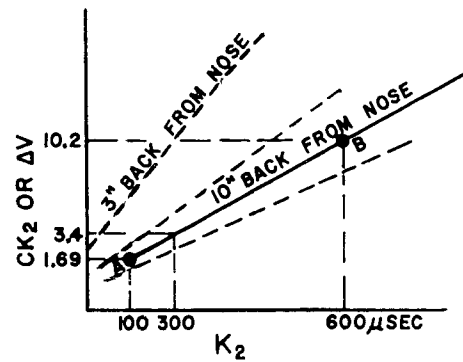


Figure 6-10. Specialized computer-setting chart

SECRET

## SECRET

CK<sub>2</sub> can be found from the above information for this one particular case, but to save arithmetic calculations, curves may be used. Redrawing figure 6-8 using the assumed parameters results in figure 6-10. Assuming that the line-charge flight time will be between 100 and 600 μsec gives, for point A,

$$\Delta V = \frac{5.66 \times 10^4}{3.44} \times 10^{-4} = 1.69 \text{ v, and}$$

for point B,

$$\Delta V = \frac{5.66 \times 10^4}{3.44} \times 6 \times 10^{-4} = 10.2 \text{ v.}$$

A line is drawn connecting these points, now for any K<sub>2</sub> between 100 and 600 μsec, ΔV can be read off. Once the proper parameters have been set into the computer, the oncoming projectile, regardless of its velocity, will be hit 10 in. back of its nose.

For the present case, the values of K<sub>2</sub> = 200 μsec and ΔV = 3.4 v were chosen. This voltage is set in, using a calibration curve. Similar curves are drawn for 3, 5, 7, 9, and 11 in. back-of-the-nose encounters.

(C) Figure 6-11 is the block diagram and figure 6-12 the diagram of the complete circuitry, including velocity-only computer, firing circuit, and power supplies. Figure 6-11 is so arranged that, if superimposed on figure 6-12, every block in figure 6-11 indicates the function of the circuitry underneath it in figure 6-12.

### 6.5 Field Tests on Preliminary System

(C) The field tests were conducted at the FOFL test area at Blossom Point, Maryland. A 75-mm and a 20-mm gun were used to shoot projectiles on a flat trajectory over the 2-fence detection unit. With the 75-mm ammunition, the velocity could be varied between 1400 and 2400 ft/sec, the 20-mm slugs moved at 3300 ft/sec. A camera, figure 6-13, was positioned at a point on the fragmentation plane of the hypothetical defending charge, looking at a shadow box that consisted of an enclosure faced with a translucent, calibrated screen and was backlighted by a Type 1530 General Radio Microflash. This lamp produced a high-intensity, 2 μsec light pulse that is adequate to stop the shells on film in the considered velocity range. As an example, a shell travelling at 4000 ft/sec would move approximately 0.1 in. in the duration of the flash.

(U) The camera shutter was actuated by a solenoid, which was excited by a capacitor discharging through it, at the instant a shell shorted the camera trigger screens. The shutter speed was so set that the shutter would be open when the shell arrived in the vicinity of the intercepting plane. Another set of screens was installed a short distance in front of the first optical fence and was used to trigger the oscilloscopes.

## SECRET

105

CONFIDENTIAL

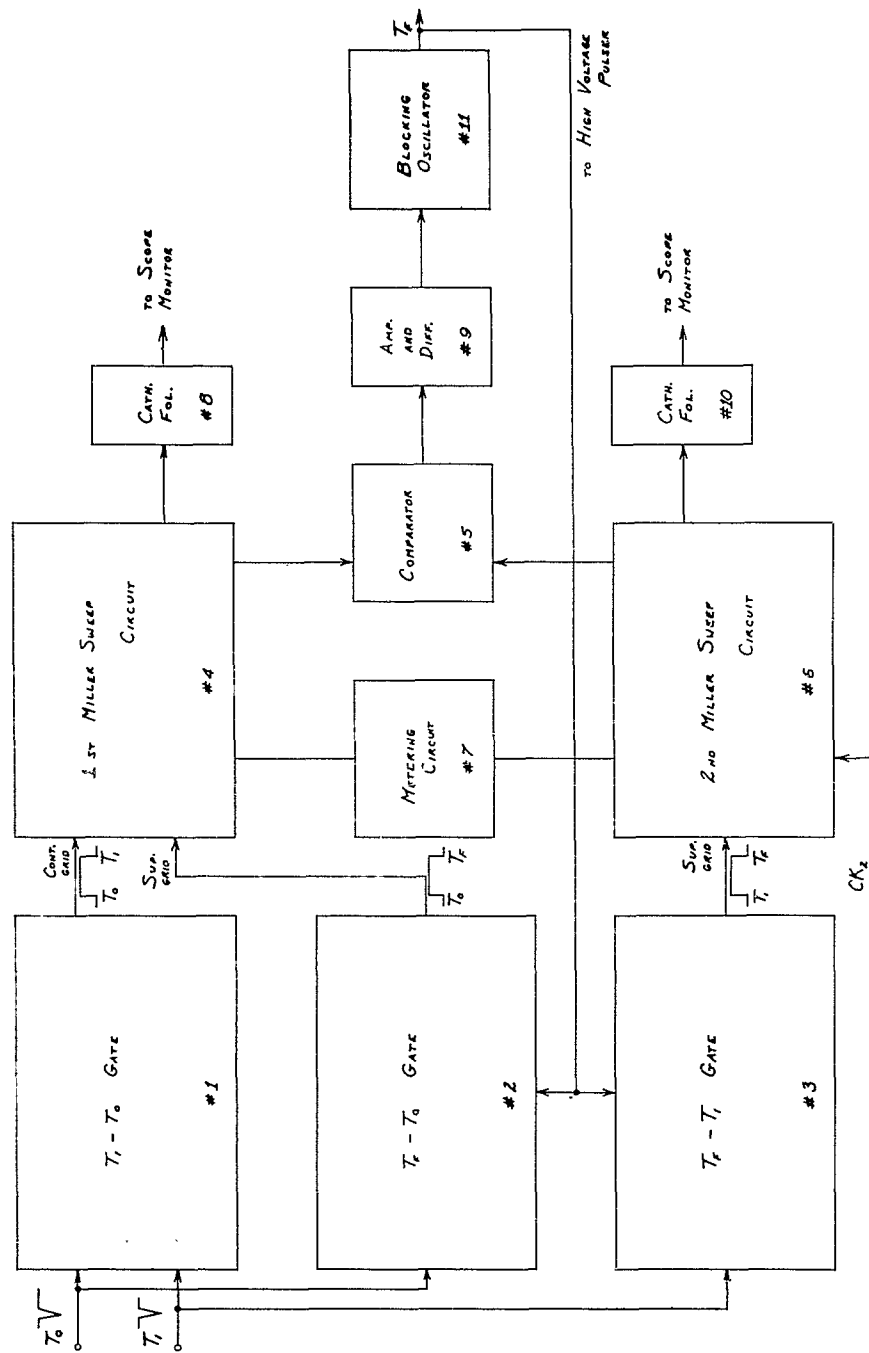


Figure 6-11. Block diagram of preliminary system

CONFIDENTIAL

**CONFIDENTIAL**

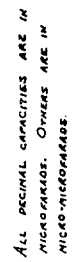


Figure 6-12. Circuit diagram of preliminary system

SECRET

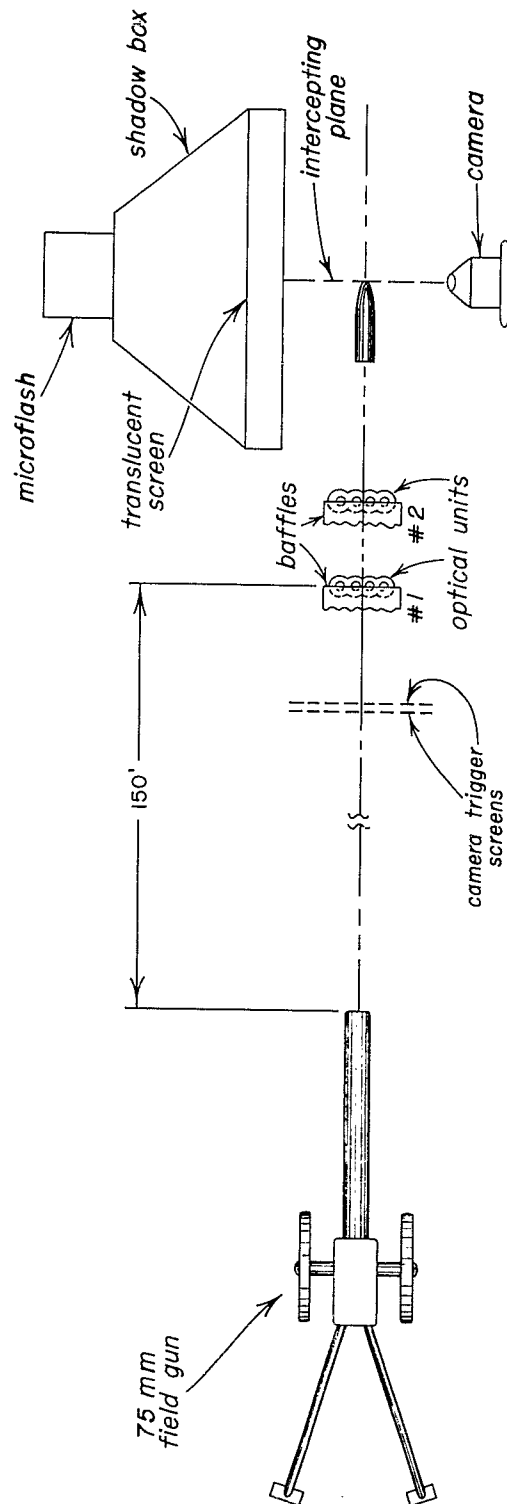


Figure 6-13. Range layout for preliminary system test

SECRET

## SECRET

(S) Figure 6-14 is the block diagram of the electronic test instrumentation. Two 1-Mc electronic timing units were used; one to monitor  $\Delta T_1$ , the time interval between the penetration of the first and second optical fence; the other to monitor  $\Delta T_F$ , the time interval between the penetration of the second optical fence and the delivery of the firing pulse from the firing-time computer. The two oscilloscopes recorded and permitted monitoring of the signals out of the PbS cells as the detection fences were traversed by the shells, the two trigger pulses derived from the cells, and the computer waveforms. It was also possible to record the firing pulse out of the computer when desired. All of the above signals could be taken on the same time base for direct comparison.

### 6.6 Test Results and Conclusions

(S) The equipment described previously made it possible for the shells to be photographed automatically. It turned out, as expected, that photographs were taken at the instant when the shells were in the fragmentation plane of the hypothetically assumed defending charges.\* It was also possible to shift the point of impact relative to the shell back and forth by predetermined distances.

(S) Figure 6-15 resulted from a typical test firing. The two oscilloscope traces in figure 6-15a are the two original signals from a 75-mm shell, coming in from the right-hand side as the shell traverses the two detection fences.

(C) Figure 6-15b shows the way the computer reacts to the signals. In the two top traces, a first Miller-sweep run-down (section 6.4) is seen to start at the time the first shell signal begins. At the beginning of the second pulse, two things are seen to happen: The first Miller-sweep run-down is stopped and held at a constant voltage, and a second run-down is started. The firing pulse in the lower trace of figure 6-15b is seen to be generated at the instant the running-down voltage of the second sweep equals the held voltage of the first one.

(S) Figure 6-15c is a photograph of the shell in front of the screen of the shadow box, taken in the light of the Microflash behind it. The darker vertical line near the center indicates the fragmentation plane of the hypothetical defending charge. As has been explained, the Microflash is triggered by the firing pulse (lower trace in figure 6-15b). The shell shadow shows the shell nose coinciding with the darker line; in other words, this particular shell has been hit on the nose.

(U) It was found that under favorable noise conditions the system would operate successfully at somewhat lower signal levels making it also possible to obtain a reliable pulse in less than 20  $\mu$ sec.

\* In order that the shell picture could be taken as the nose entered the assumed fragmentation plane, the parameter  $D_3/V_C$  in equation (1) (section 6.4) had to be set to zero, thereby simulating an infinitely high fragment velocity  $V_C$ .

SECRET

109

CONFIDENTIAL

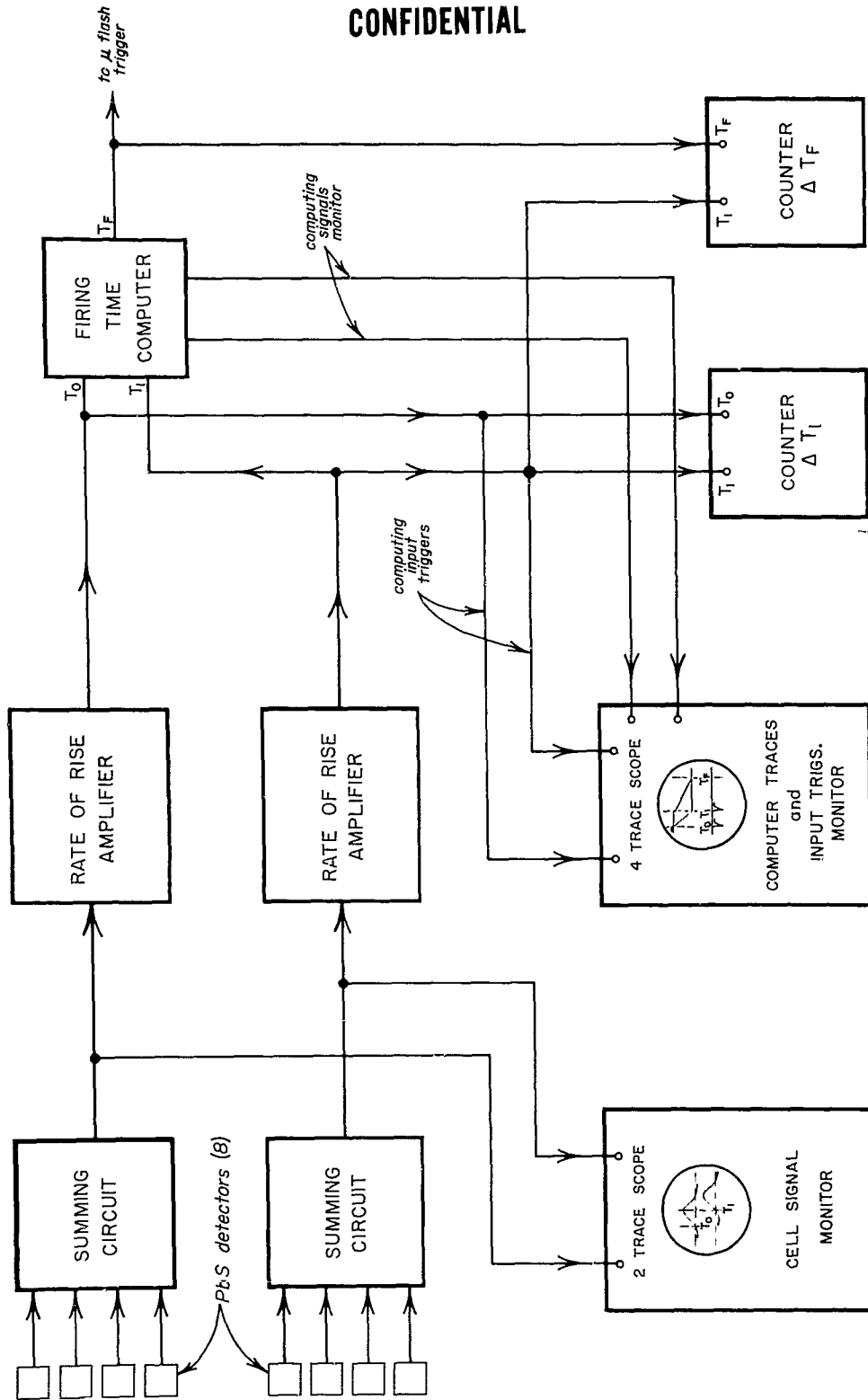
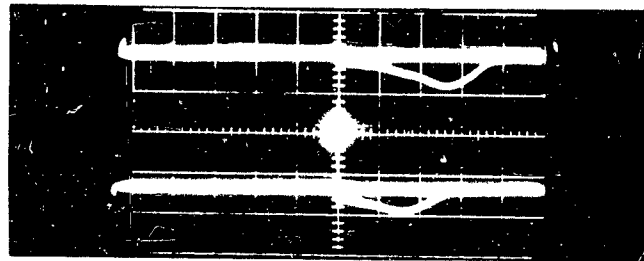


Figure 6-14. Block diagram of electronic test instrumentation of preliminary system

CONFIDENTIAL

SECRET



(a)



(b)



(c)

Figure 6-11 Recording of typical test firing

SECRET

**SECRET**

(S) As a result of the field tests it was concluded that a system of this preliminary type could be designed to perform the specified task of supplying a firing pulse to a line of charges at the proper time even while using inexpensive reflectors. It would not be possible, however, to use the simple reflectors in a system that would require the measurement of the approach angle.

(U) In addition, a valuable amount of experience was gained in the use of PbS cells in an unorthodox manner, for instance, that of generating fast pulses from them as the signal emerges out of the noise.

**SECRET**

# SECRET

## 7. EQUIPMENT SUPPLIED TO PICATINNY ARSENAL AND BALLISTICS RESEARCH LABORATORIES

A. Copeland, J. E. Miller, R. J. Paradis

(S) At the request of Picatinny Arsenal and Ballistics Research Laboratories, this installation designed, built and delivered to each of these installations a detector computer system for their use in the study of defending charges in dynamic firings. The requirements were that the system be able to detect the oncoming shell, fired at a pre-set height and in normal attack, determine its velocity, and supply a firing pulse to the defending charge when the shell reached the fragmentation plane of the charge.

(U) It appeared that the two-fence detecting units and the preliminary type "velocity-only" timing computer that was previously field tested would, with a few modifications, fulfill the requirements.

### 7.1 Improvements over Preliminary System

(U) The modifications considered to be necessary and added to the basic preliminary test system were the following:

1. A manual control for each of the constants in the velocity-only, constant-height, firing-time equation

$$\Delta T_f = K_1 \Delta T_1 - K_2 \quad (7.1)$$

2. A high-voltage firing circuit.

3. A signal simulator and sequential pulse generator.

(C) The manual controls were necessary to make the computer adaptable to tests that require that the shell be hit at various positions as measured from their noses and to allow for use of defending charges having a range of velocities. The high-voltage firing circuit was necessary in order to fire the detonators, while the simulator and sequential pulse generator provided calibrating signals for the computer.

(U) Peculiarities were encountered upon the installation of the equipment at the above named installations which required the addition of various devices in order to obtain reliable operation. At both installations, cable lines several hundred feet in length were required to feed the signal from the optical detection equipment to the computer location in the respective block houses, and the firing pulses from the block houses back to the defending charges in the firing locations. Since the signal level was comparatively low, due to weather conditions, enough

SECRET

113

## CONFIDENTIAL

noise was picked up on the lines to produce undesired firings. In addition, the energizing of the gun firing solenoid at Picatinny Arsenal caused power line transients which proved to be troublesome. Naturally, in an operational system with its short, armor-shielded connecting lines, these difficulties would not exist.

(U) The signal-to-noise ratio of the computer input was improved by amplifying the signal from the optical detection equipment by a factor of 10 at the input to the signal lines and by attenuating it by the same factor at the signal line output. An anode follower amplifier (fig 7-1) which retains the phase and maintains the required low impedance output, was connected between the output of the optical equipment and the line. The difficulty due to the power line transient caused by the energizing of the gun firing solenoid was overcome by adding a circuit that blocked the computer operation until some time after the energizing of the solenoid.

(C) The "velocity-only" firing time computer has been described in section 6.4.

### 7.2 Firing Circuit

(U) The firing circuit is shown in figure 7-2. Since physical size was of little concern in this case, a 4C35 thyratron was employed.

### 7.3 Completed Equipment

(U) Figure 7-3 is a block diagram of the equipment installed at Picatinny Arsenal. The equipment installed at Ballistics Research Laboratories was the same with the exception that no protective circuitry against firing-solenoid-caused transients was required. Figures 7-4 and 7-5 are front and back views of the computer rack as delivered to the above installations. In addition to all power supplies, it also contains some equipment for the adjustment of the computer, such as a signal simulator, that is not described in this report.

### 7.4 Results

(C) Field test results of live dynamic firings are listed in Firing Record No. Ar-21728 by Development and Proof Services, Aberdeen Proving Grounds. They show that several types of anti-tank ammunition of various velocities have been consistently defeated regardless of their velocities, employing the preliminary Dash-Dot system as a timing tool.

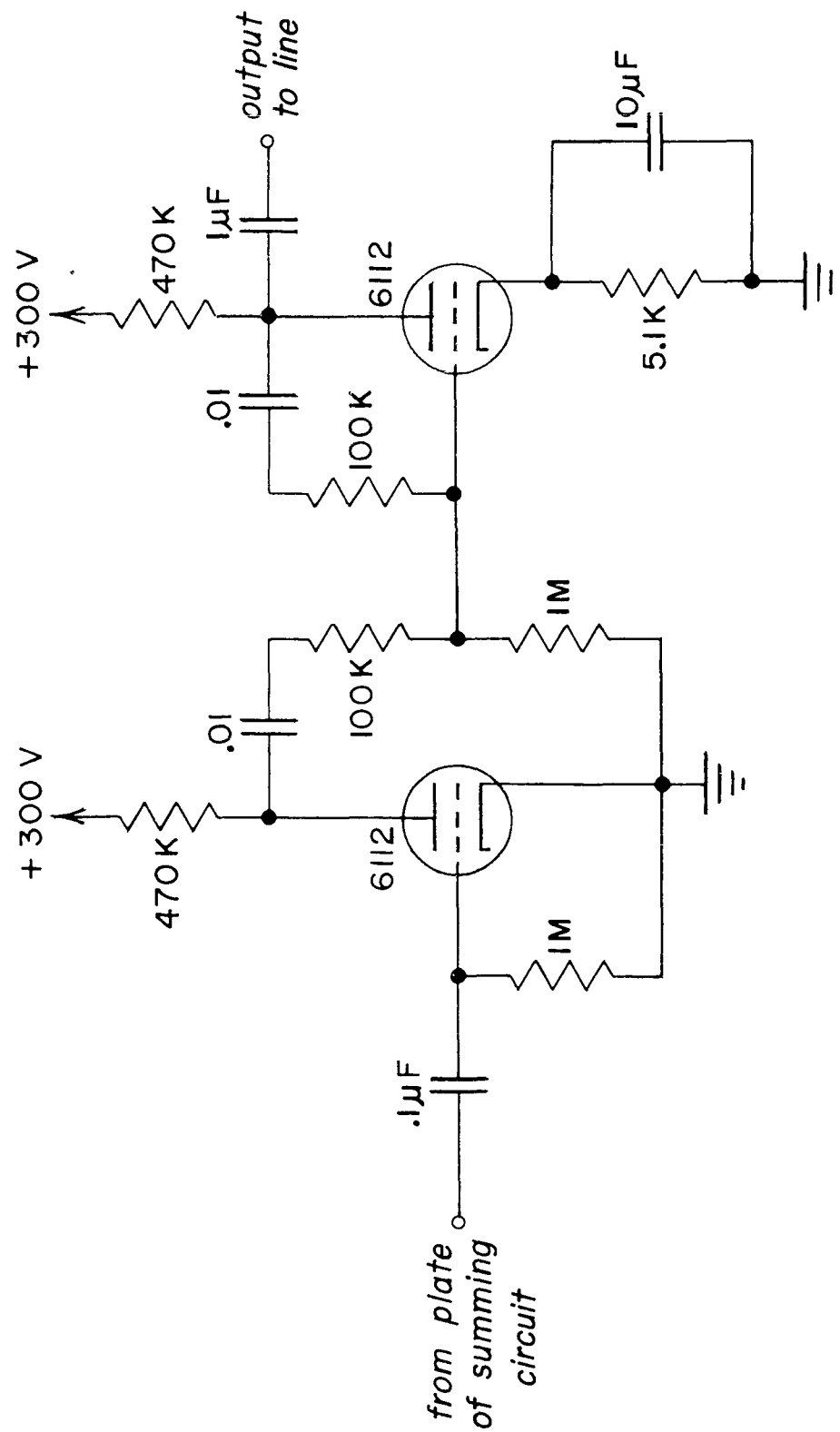
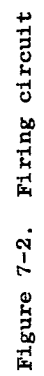
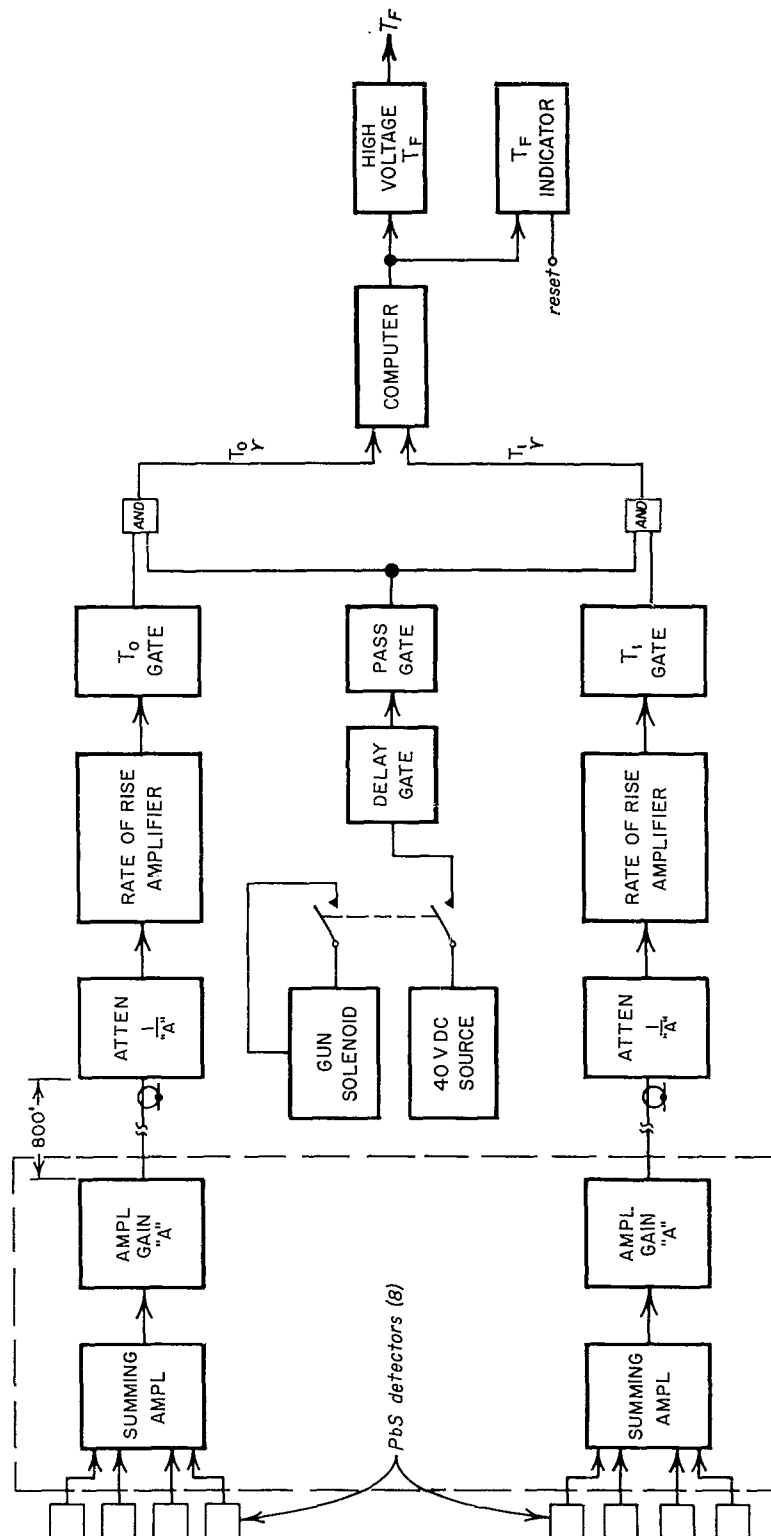


Figure 7-1. Amplifier and anode follower



CONFIDENTIAL



CONFIDENTIAL

Figure 7-3. Block diagram of equipment supplied to Picatinny and BRL.

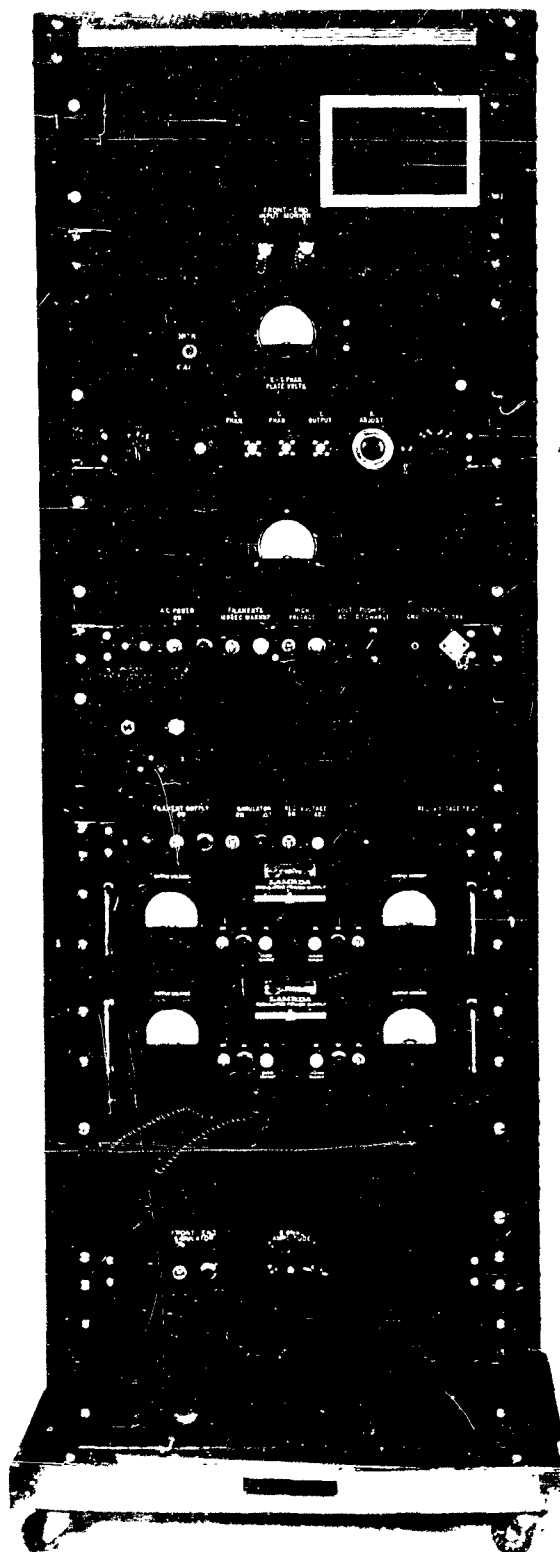


Figure 7-4. Front view of preliminary computer rack

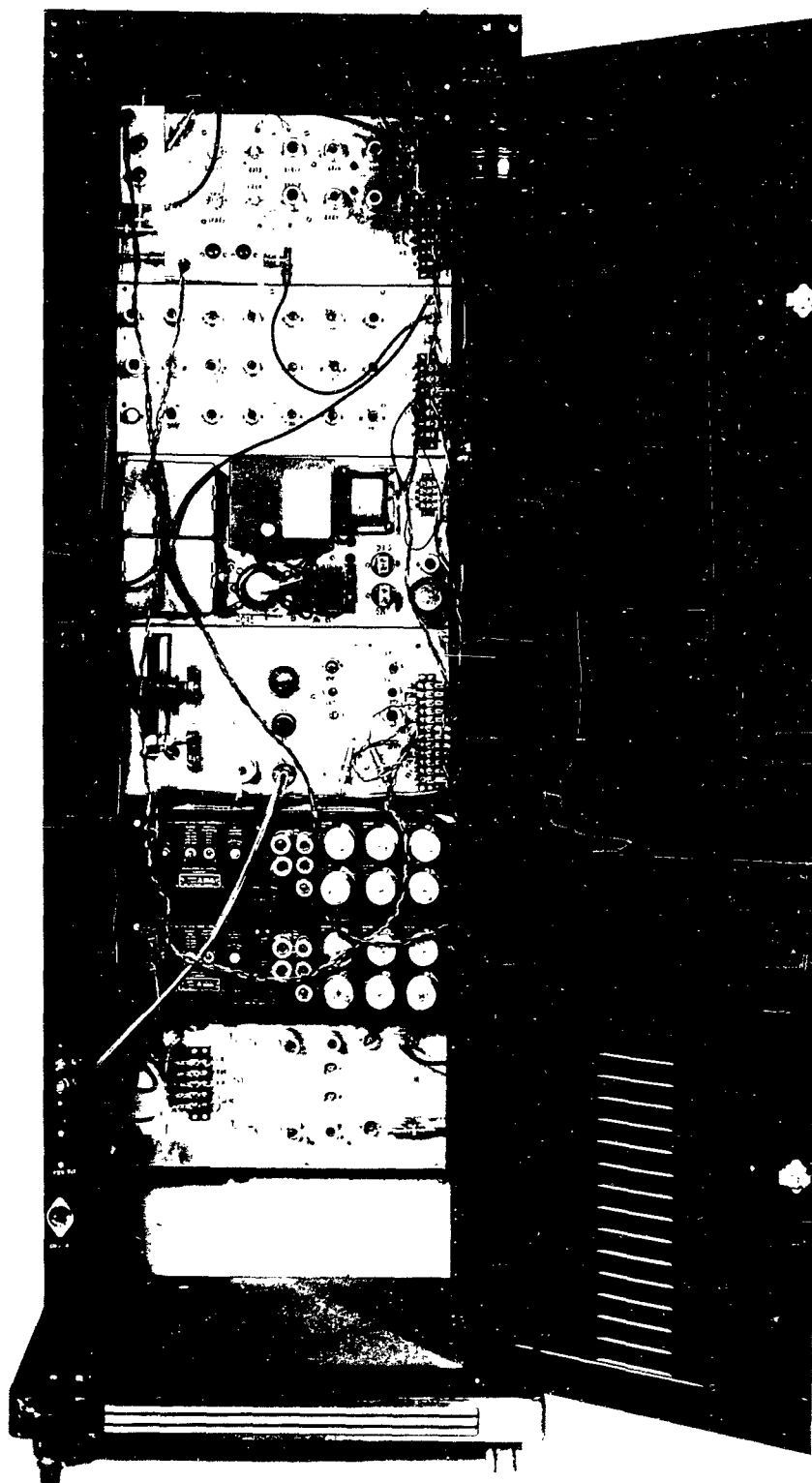


Figure 7-5. Back view of preliminary computer rack

# SECRET

## 8. FUNCTION OF OVER-ALL ELECTRONIC CIRCUITRY

W. Moore

(S) An outline of the geometry, setting forth the three-detection fence concept with multiple detection pickets, has been given in section 3. The three fences are used to provide the firing-time information, while the individual pickets are employed for the selection of the defending charge to be fired.

(S) Figure 8-1 shows in block form the interconnections of the electronic subassemblies to perform the over-all function. The three fences are designated "Optical Units" in the diagram, each block representing 84 individual detection pickets. The 84 outputs from these units in the A and B fence are fed to 84 amplifier blocking-oscillator units which contain 84 sally amplifiers (section 9.1.3) and provide easily handled timing pulses whenever a shell passes through a fence. Thus, the identity of all pickets in the first two fences is retained through this portion of the system.

(S) The outputs of the sally amplifiers associated with the A and B fences are connected to the Charge Selection Computer (section 11) and are also fed to the OR Gates (section 9.2.1). These OR gates allow any of the 84 possible sally amplifier pulses to feed a single line. The A-fence OR-gate output allows the sally amplifier pulse to be fed simultaneously to the K-factor generator (section 9.4), the 200  $\mu$ sec Delay Gate (section 9.3.2) and to the  $T_0$  input of the Sequential Blocking Gates (section 9.2.3). Similarly, the B-fence OR-circuitry feeds only one pulse to the  $T_1$  input of the sequential blocking gates, while the C or Height-Fence OR-circuit (section 9.2.2) feeds only the  $T_2$  signal to the sequential blocking gates and to an additional pass gate which was introduced as an added safety measure.

(S) The circuitry, to this point, provides the charge selection computer (section 11) with 84 individual inputs from the A fence and another 84 from the B fence. It also generates pulses at times  $T_0$ ,  $T_1$ ,  $T_2$  when the missile traverses the A, B, C fences respectively. These pulses are fed to the firing-time computer (section 10) through the Sequential Blocking Gates. These are the primary functions of the system, i.e. timing and charge selection.

(S) Another function, that of size discrimination, which causes shells of less than 50-mm diameter to be ignored, is performed by sending the A fence outputs through a subchannel designated as Peak Determining Amplifiers in the figure. Here a pulse is generated when the signal reaches its peak, that is, as pointed out in section 9.1.1, when the tail of the missile leaves the A fence. The process by which the size discrimination is accomplished is described in section 9.3.

# SECRET

121

SECRET

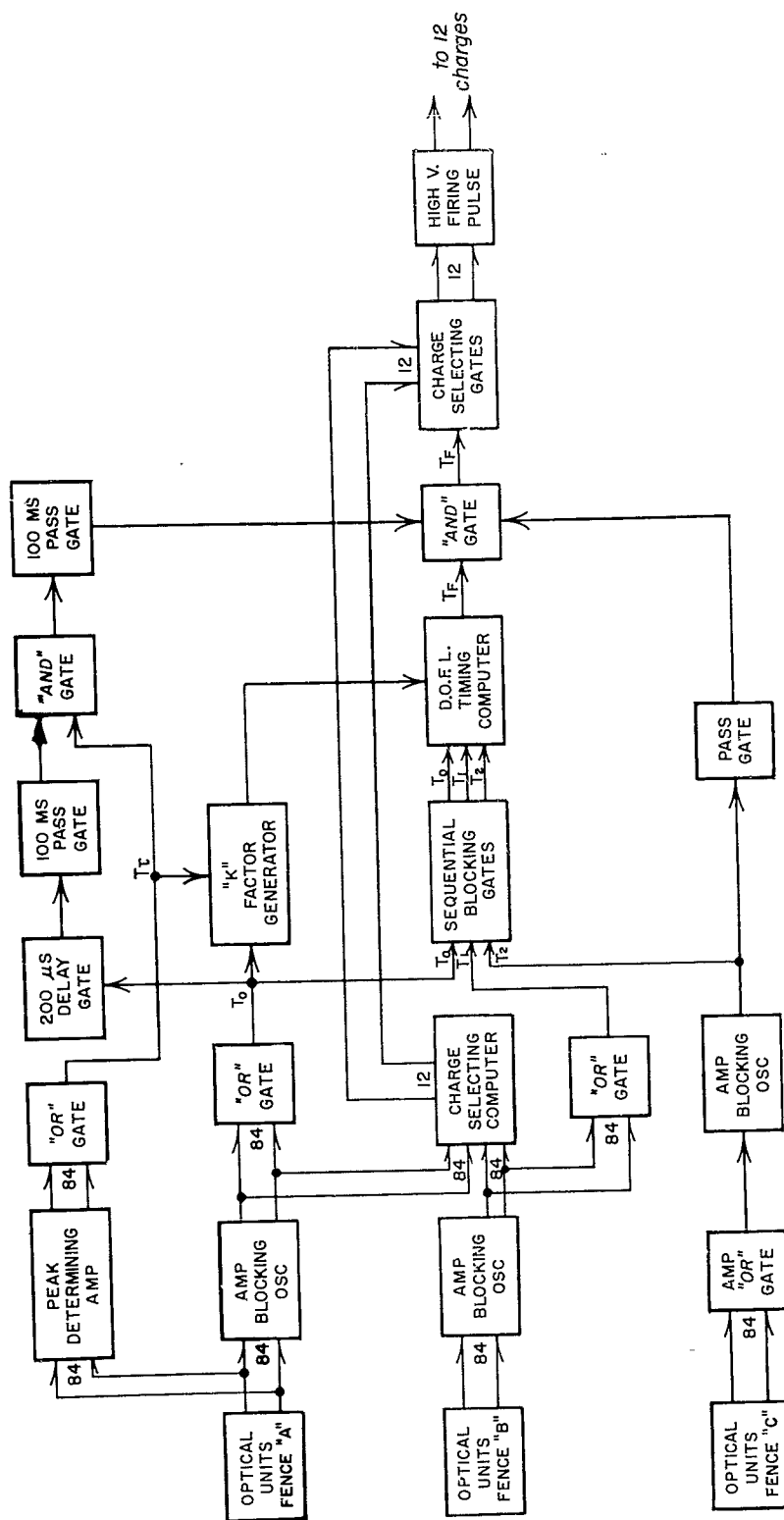


Figure 8-1. Block diagram of complete system

SECRET

**SECRET**

(S) The pulse corresponding to the missile tail leaving the A fence is also fed to the K-factor generator. This unit provides an added delay for the firing pulse so that the missile is impacted not at the nose but at a presettable fraction of its length behind the nose, regardless of its actual length. The mode of operation of this circuitry is described in section 9.4.

(S) The various gates shown in figure 8-1, such as the 200  $\mu$ sec, 100 ms, pass gate, and gates are part of the size discrimination and protective circuitry to prevent firing of the defending charges on noise or false inputs.

(S) Upon the receipt of signals from the A and B fences, the charge-selection computer opens appropriate gates which direct the low-voltage firing pulse to the high-voltage firing circuit (section 12) that is required to detonate the selected defending charge. The low-voltage firing pulse is supplied by the firing time computer which requires information from all three fences. In addition, the signal from the A fence is supplied to the size discrimination circuitry (section 9.3) which opens a pass gate for the low-voltage firing pulse only if the attacking round is larger than 50 mm in diameter. If the diameter is less than 50 mm, the gate does not open and no low-voltage pulse is transmitted to the firing circuits.

**SECRET**

123

This document contains information affecting the national defense of the United States within the meaning of the espionage laws, title, 18 U. S. C., 793 and 794. Its transmission or the revelation of its contents in any manner to an unauthorized person is prohibited by law.

# SECRET

## 9. SIGNAL PROCESSING AND SYSTEM LOGIC

A. Copeland, J. E. Miller, W. J. Moore, R. J. Paradis, F. Vratarić

### 9.1 Analysis and Shaping of Signal Pulses

#### 9.1.1 Analysis of Signal Pulses

(S) As explained in section 4.2, lead sulfide cells are used in the sensing system in preference to cells of other types. If these cells had an infinitely fast response, the signal obtained from firing a shell through one of the detection fences would ideally appear like the one shown in figure 9-1a. In this case, it would be a simple matter to correlate the position of the shell, figure 9-2, relative to the detection fence with the times  $T_0$  (nose contact),  $T_1$  (nose fully penetrated),  $T_t$  (tail emerging), and  $T_2$  (tail fully emerged). Unfortunately, however, because of the finite time constant (200  $\mu$ sec in this case), matters are not so simple. Figure 9-1b shows a typical signal from a slow shell traversing the fence and figure 9-1c a signal from a fast shell. It can be seen from figures 9-1c and 9-2 that for a fast shell, which is the usual case, the peak of the signal occurs at a time  $T_t$  when the tail of the shell is in the fence. There is an added uncertainty  $\Delta T_t$  in time (figure 9-1c) due to the combined effects of the time constant of the cells and the thickness of the detection fences. This is true even for the specially designed, well collimated detection units which were described in section 4.1.

(S) In the simplest case, the system would be so designed as to utilize the peak of the signal. As has just been shown, the consequence would be that the system would react to the tail of the shell, which is demonstrated in figure 9-3. This is not desirable. Since the distances  $d_1$  and  $d_2$  are system design parameters, the distance between the defending charge and the last detection fence would have to be greater than in the nose-reacting system. Also, the uncertainty  $\Delta T_t$  in time causes a difficulty. Since the time differential due to the first two fences is multiplied by a "leverage" factor which contains the term  $d_2/d_1$  in the firing-time equation (equation in section 9.4), any uncertainty such as  $\Delta T_t$  is multiplied by the same factor.\* Furthermore, the signatures of some shells, such as the 90 mm T300E53 HEAT round shown in figure 9-22, have bimodal structures which make it difficult for the system to sense the actual tail.

(C) Therefore, the alternative, the nose-reacting system, figure 9-4, has been chosen, which avoids the inherent difficulties of the tail-reacting type. However, it poses another problem. As can be seen from figure 9-1c, the signal from a fast shell rises relatively slowly from zero, and, in addition, is "contaminated" by noise.

\* For a more rigorous treatment of this subject see section 13.6.3.

SECRET

125

CONFIDENTIAL

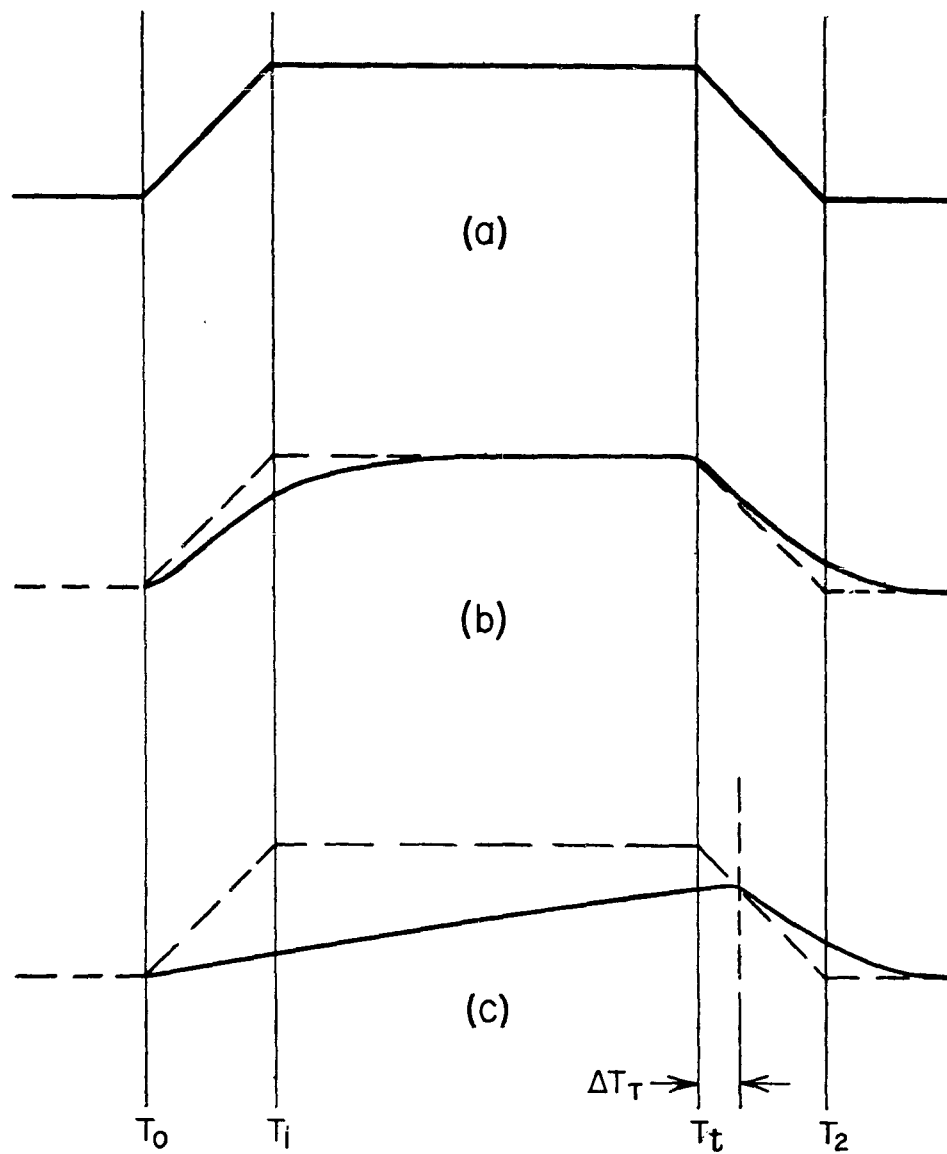
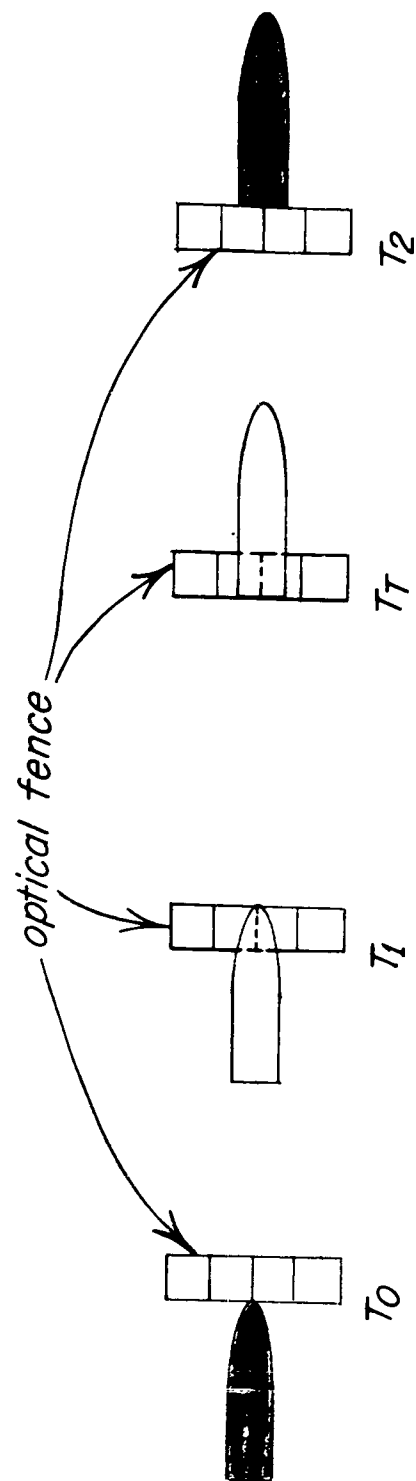


Figure 9-1. Signals from different time constant cells and different velocity shells

CONFIDENTIAL

CONFIDENTIAL



CONFIDENTIAL

Figure 9-2. Position of shell in relation to detection fence

SECRET

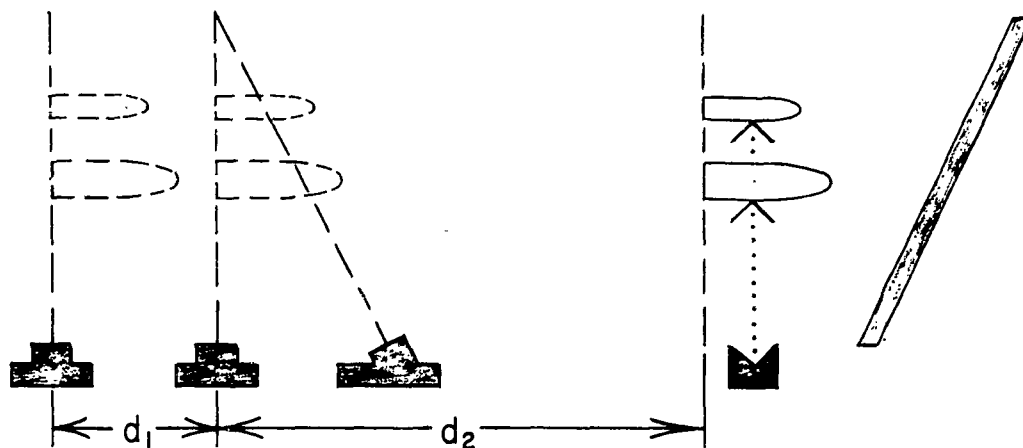


Figure 9-3. Tail reference system

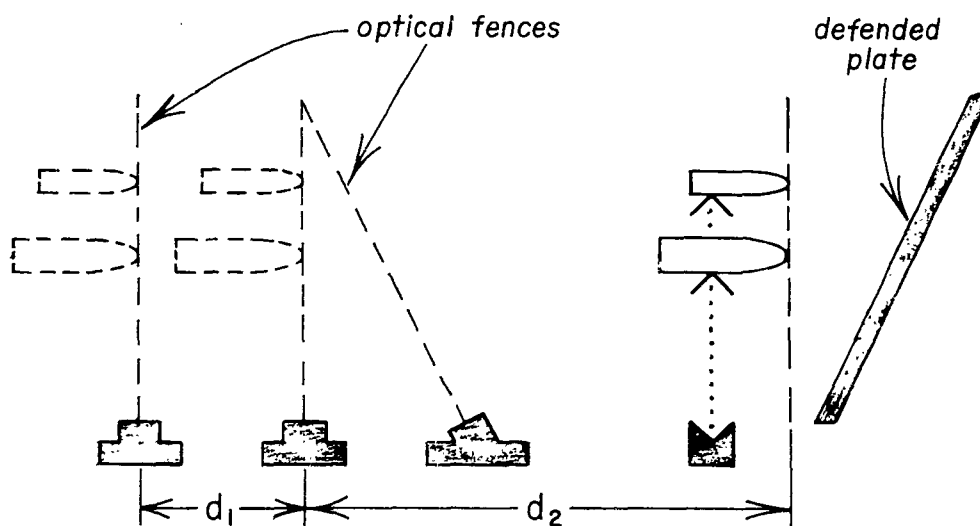


Figure 9-4. Nose reference system

SECRET

# SECRET

(U) This necessitates an analysis of the signal-to-nose ratio of the PbS photocells and the input circuit (section 9.1.2) as well as the development of a so-called sally amplifier\* which generates a sharp artificial pulse with a minimum of delay at the instant when the signal emerges from the nose (section 9.1.3).

## 9.1.2 Analysis of Signal-to-Noise Ratio

(C) The output from the detection pickets as a missile passes through them may be approximated by the ramp function  $e_o = \alpha t$ . The object of the sensing system is to determine as quickly and as simply as possible the time at which the function was initiated. Were the system ideal, that is, noiseless, the function could be detected easily by a simple rate-of-rise amplifier. However, in the real system the signal-to-noise ratio is relatively small, 2 to 3, at the time when the missile must be detected (approx. 20  $\mu$ sec after initiation of the signal). The greater the bandwidth of a shaping amplifier, the less the lag in the output signal will be, but also the greater will be the noise output. This section presents a theoretical investigation of signal-to-noise ratio in photoconductive detectors and related amplifiers as applied to the Dash-Dot project. The objective of the analysis is to provide two things: an approximation to the bandwidth required for maximum signal-to-noise ratio at a time  $T$  after initiation of the input signal, and a value for the gain required to amplify the input signal to a sufficient trigger level.

(S) The photocells generate a signal which may be approximated by

$$e_1 = \alpha t \text{ (volts)} \quad (9.1)$$

where  $\alpha$  is the rate of rise in volts per second and  $t$  is time in seconds. In the Dash-Dot system, the trigger level from the light detectors must be obtained in a maximum time of 20  $\mu$ sec after initiation of the signal. The following analysis will be based upon figure 9-5. Using the circuit shown to define the system bandwidth, the transfer function for an input signal  $e_1 = \alpha t$  is found to be:

$$e_o = \frac{\alpha T_1}{K-1} \left( K-1 - Ke^{-\gamma} + e^{-K\gamma} \right) \quad (9.2)$$

where

$$K = T_1/T_2$$
$$T_1 = R_1 C_1$$

\* Webster's Dictionary: Sally - 1. A rushing or bursting forth;  
2. A brief outbreak into activity or expression.

# SECRET

129

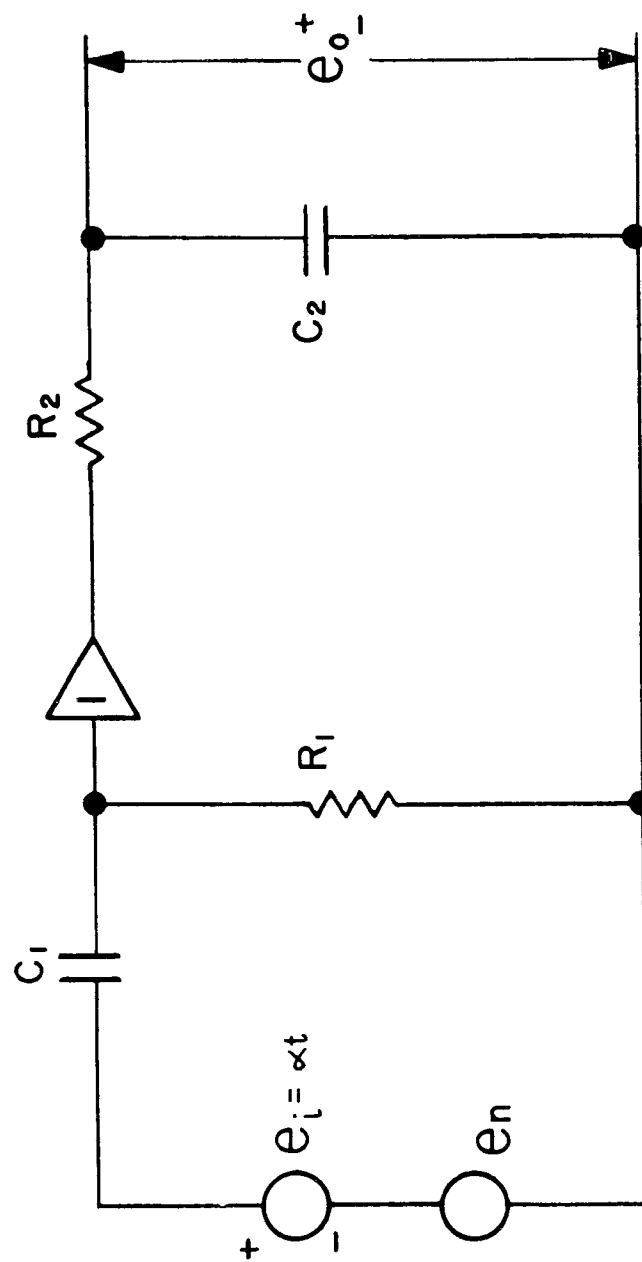


Figure 9-5. Equivalent circuit of amplifier

# SECRET

$$T_2 = R_2 C_2$$

$$\gamma = t/T_1.$$

(U) The noise in semiconductors may be placed in three major categories; semiconductor noise which is proportional to  $\frac{1}{f}$ ; thermal noise which is proportional to  $\sqrt{\omega_B}$ ; and shot noise which is also proportional to  $\sqrt{\omega_B}$ ,\* where  $f$  is the frequency and  $\omega_B$  the bandwidth expressed in radians per second. In modern transistors the  $\frac{1}{f}$  noise becomes negligible above 800 cps\*\* so that the total noise  $e_n$  may be expressed as:

$$e_n = \beta \sqrt{\omega_B} \quad (9.3)$$

where  $\beta$  is a constant. The bandwidth may be expressed as a function of the two time constants  $T_1$  and  $T_2$ :

$$e_n = \beta \sqrt{(K-1)/T_1} \quad (9.4)$$

Where it is assumed that  $T_1 = KT_2$ .

(U) By combining (9.2) and (9.4), the signal-to-noise ratio  $S/N$  is found to be

$$S/N = \frac{e_o}{e_n} = \frac{\alpha}{\beta} T_1^{3/2} \frac{1}{(K-1)^{3/2}} \left( K - 1 - Ke^{-\gamma} + e^{-K\gamma} \right) \quad (9.5)$$

Differentiating the function with respect to  $K$  and setting it equal to zero will find either a maximum or a minimum.

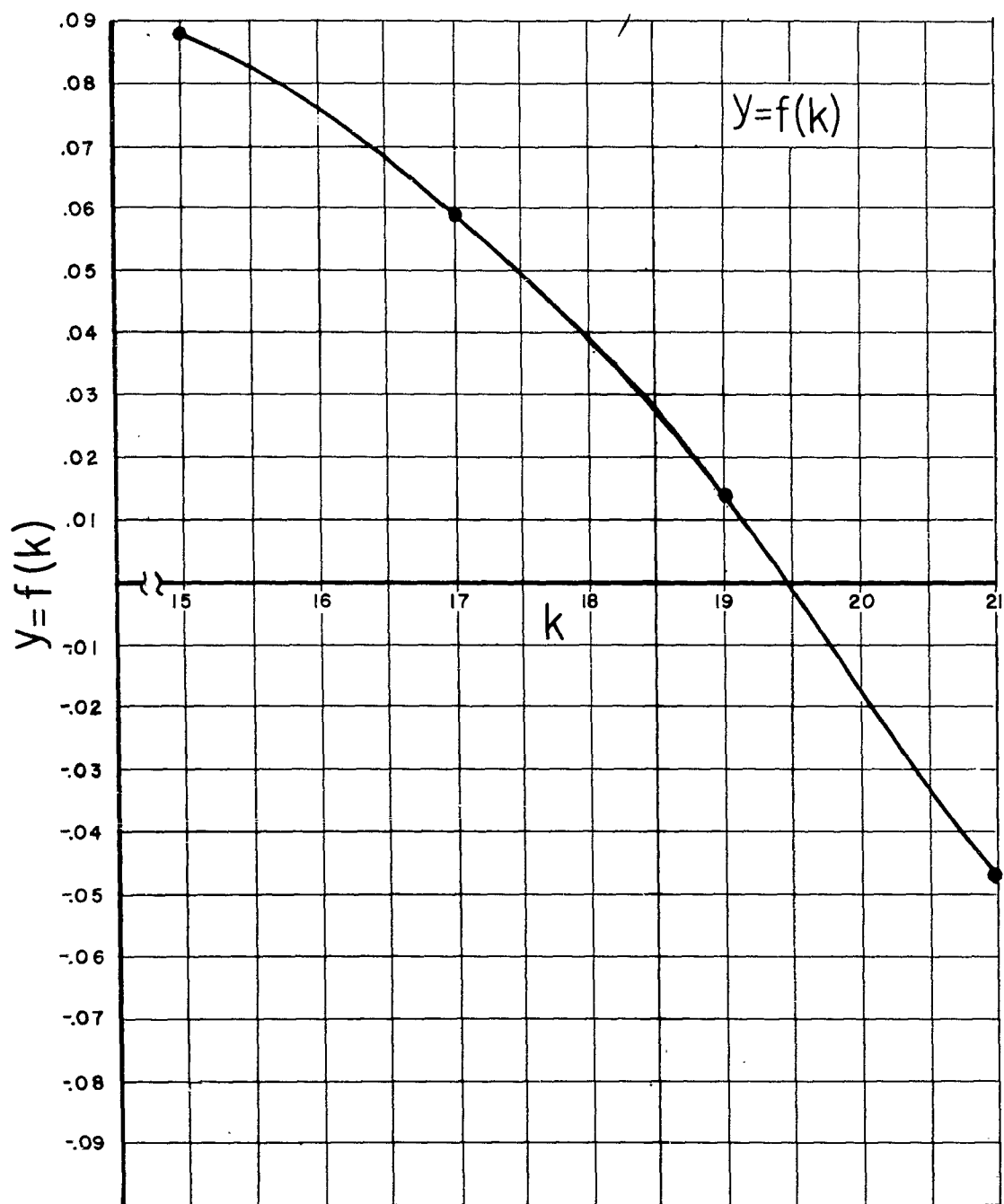
$$\frac{d S/N}{d K} = 0 = -K(1-e^{-\gamma}) - e^{-K\gamma} \left[ 3 + 2\gamma (K-1) \right] + 1 + 2e^{-\gamma} \quad (9.6)$$

Assuming that the lower frequency is 800 cps and  $t = 20 \mu\text{sec}$ , then  $\gamma$  is equal to 0.10. As  $K$  approaches 19.4 the function (9.6) goes through zero, as seen in figure 9-6. This states that the signal-to-noise ratio reaches an optimum value when  $T_2 = T_1/19.4$  or  $f_H = 15.5 \text{ kc}$ .

\*Lo, Endre, et al., Transistor Electronics, Prentice-Hall, Englewood Cliffs, N. J., 1955, pages 123-124.

\*\*L. P. Hunter, Handbook of Semiconductor Electronics, McGraw-Hill, N. Y. 1956, page 11-60.

# SECRET



132 Figure 9-6. Signal/noise function  $y$  versus bandwidth factor  $k$

## CONFIDENTIAL

(U) Figure 9-7 shows a plot of the signal-to-noise ratio normalized to the value of  $K = 19.4$ . It is clearly seen that the ratio does indeed reach a maximum and not a minimum.

(U) The required gain of the amplifier is computed on the basis that the frequency determining network precedes the amplifier and that the output of the amplifier must attain a voltage level sufficient to trigger a pulse generator.

(U) The input signal has been found experimentally to be approximated by  $e_i = 2 \times 10^{-6} t$  volts for  $0 < t < 500 \mu\text{sec}$ . The rate of rise is based upon the input signal attaining a level of 10 mv in 500  $\mu\text{sec}$ .

(U) The voltage out of the network in figure 9-5 at  $t = 20 \mu\text{sec}$  is

$$e_o = .44 e_i \Big|_{t = 20 \mu\text{sec}}$$

If the output of the amplifier must attain a level of 10 v, then the required gain is

$$A = \frac{e_o}{.44 e_i} \Big|_{t = 20 \mu\text{sec}}$$
$$A = \frac{10}{.44 \times 20 \times 10^{-6}}$$
$$A = 57 \times 10^3$$

### 9.1.3 Design of Sally Amplifier

(U) The amplifier is shown in figure 9-8. Transistor  $Q_1$  is an emitter follower which is needed to reduce crosstalk when the size discrimination unit (sect 9.3) is added. Transistors  $Q_2$  and  $Q_3$  are the bandwidth-limited amplifiers which drive  $Q_4$ . Transistor  $Q_4$  is saturated to provide a threshold level below which the signal will be blocked. This feature is added to prevent spurious noise pulses from triggering the blocking oscillator. Transistors  $Q_5$  and  $Q_6$  are the driver and blocking oscillator respectively. The pulse from the blocking oscillator is 11 v in amplitude and 10  $\mu\text{sec}$  wide.

(U) In tests using a signal simulator, the pulse from the amplifier has been attained 13  $\mu\text{sec}$  to 25  $\mu\text{sec}$  after initiation, depending upon the amplitude of the input signal (figure 9-9).

(U) The complete amplifier is mounted on a small 1-3/4 in. by 2-5/8 in. printed circuit board. Both sides of the board are shown in figure 9-10.

(C) One each of these amplifiers was to be connected to each photocell in the first two (velocity) fences and, as pointed out in section 9.2.1, to each group (subfence, sect 5.2) of 7 photocells in the third, the height fence, section 9.2.2. In the layout as originally planned for the June 1960

CONFIDENTIAL

133

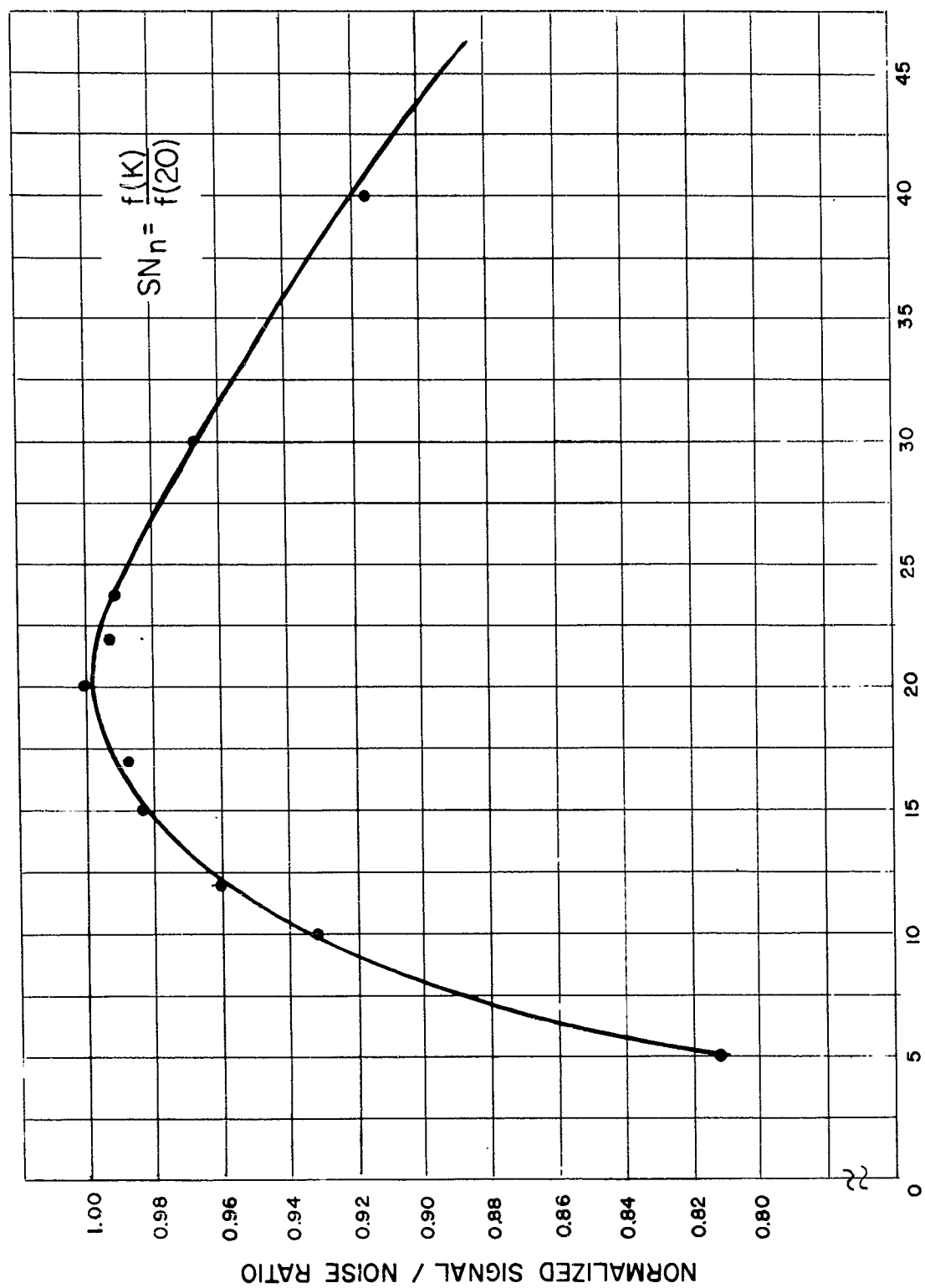
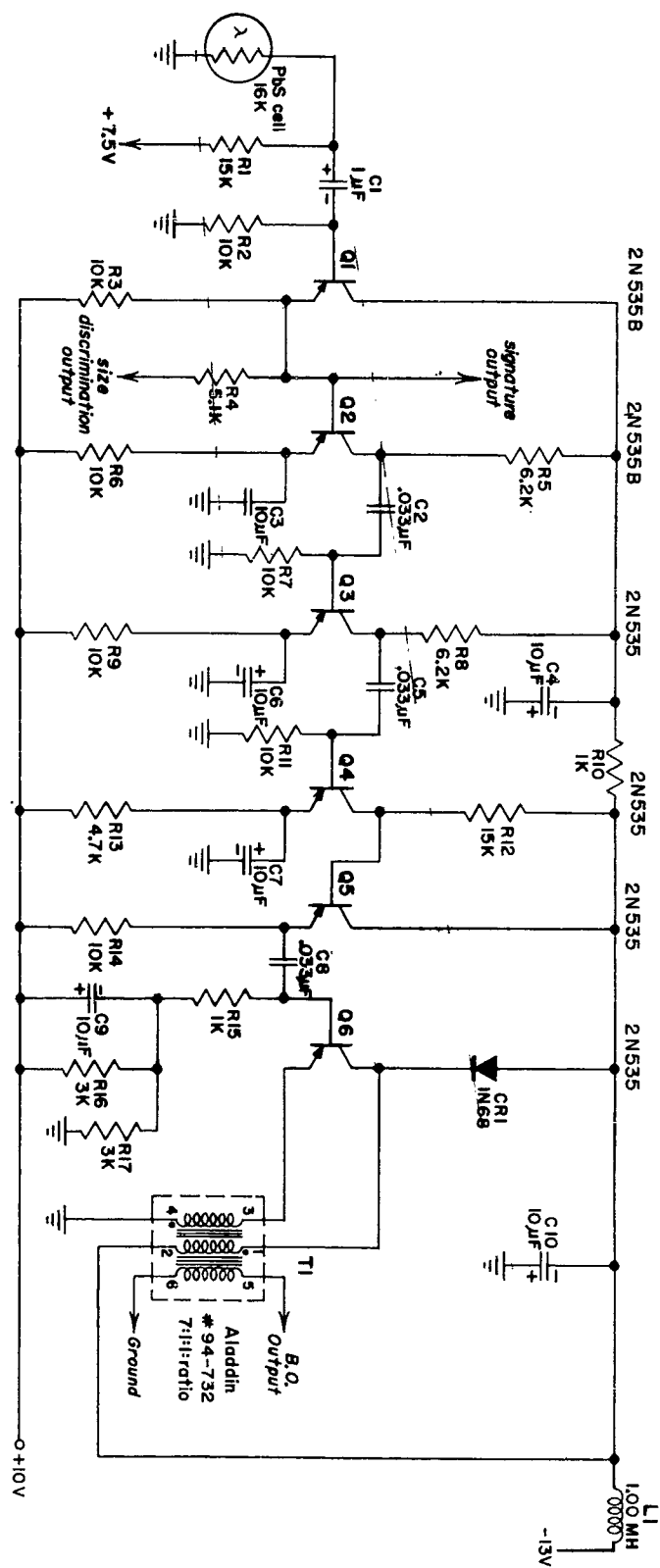


Figure 9-7. Normalized signal/noise versus bandwidth factor  $k$

Figure 9-8. Circuit diagram of sally amplifier



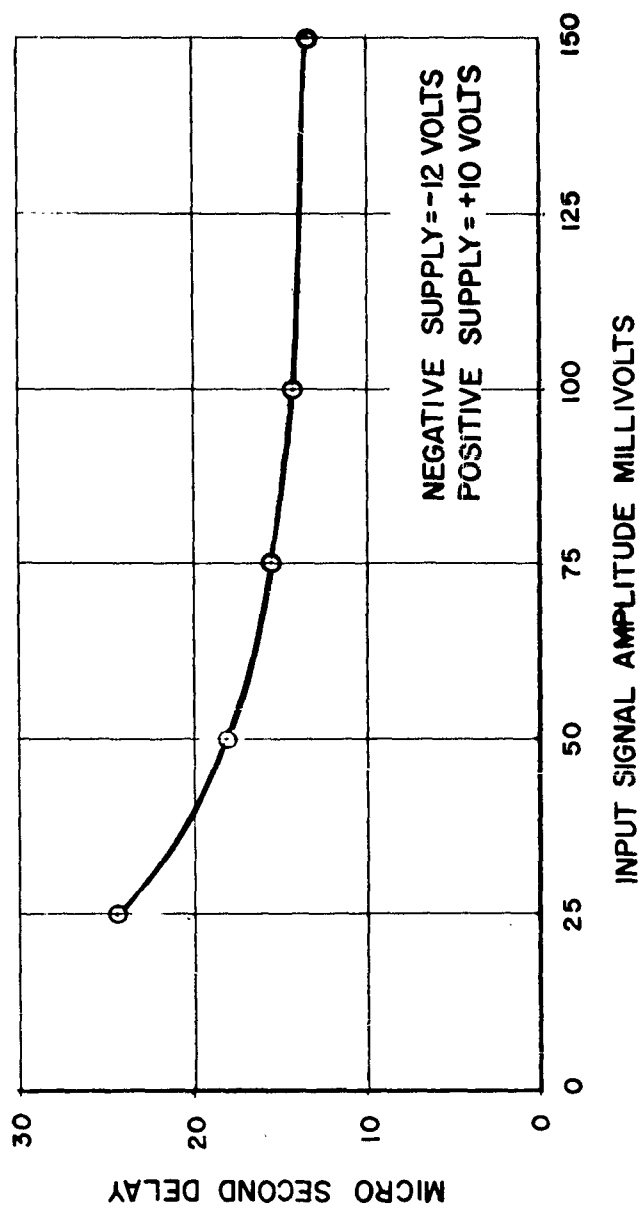


Figure 9-9. Pulse delay in sally amplifier vs signal amplitude

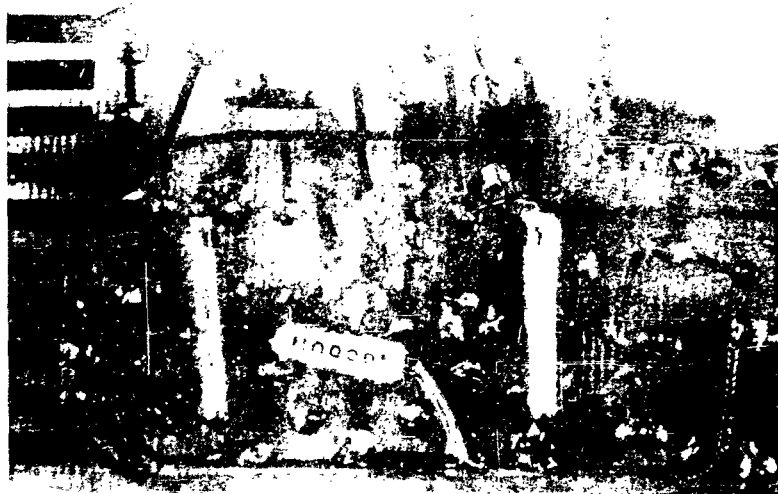
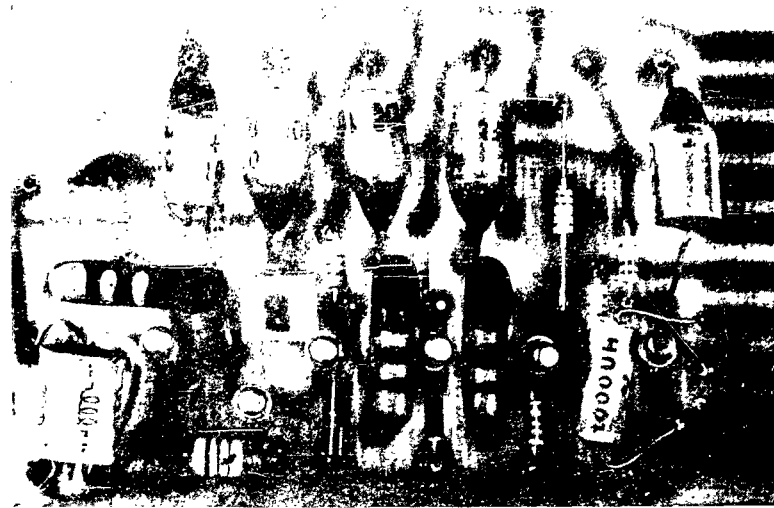


Figure 9-10. Views of sally amplifier

## SECRET

feasibility test, this would have amounted to 180 amplifiers. When, after termination of the project, DOFL went on making the final measurements, employing the Z-shaped structure mentioned in section 5.3, only 14 amplifiers for the photocells in the first two subfences were required, and one in the third subfence.

### 9.2 Logic Gates

#### 9.2.1 Diode "OR" Circuit

(C) As mentioned previously, the full system would contain 84 detection pickets in each fence. The charge-selecting computer is connected to each individual picket in the first two fences only. The diode "OR" circuit, figure 9-11, OR's seven sally amplifier outputs to a single output while maintaining the identity of the individual amplifiers. This OR circuit was used in the first two subfences (section 5.2) for field test purposes. In a final system, the entire 84 pickets must be OR'd together in each fence.

#### 9.2.2 Height Fence "OR" Circuit

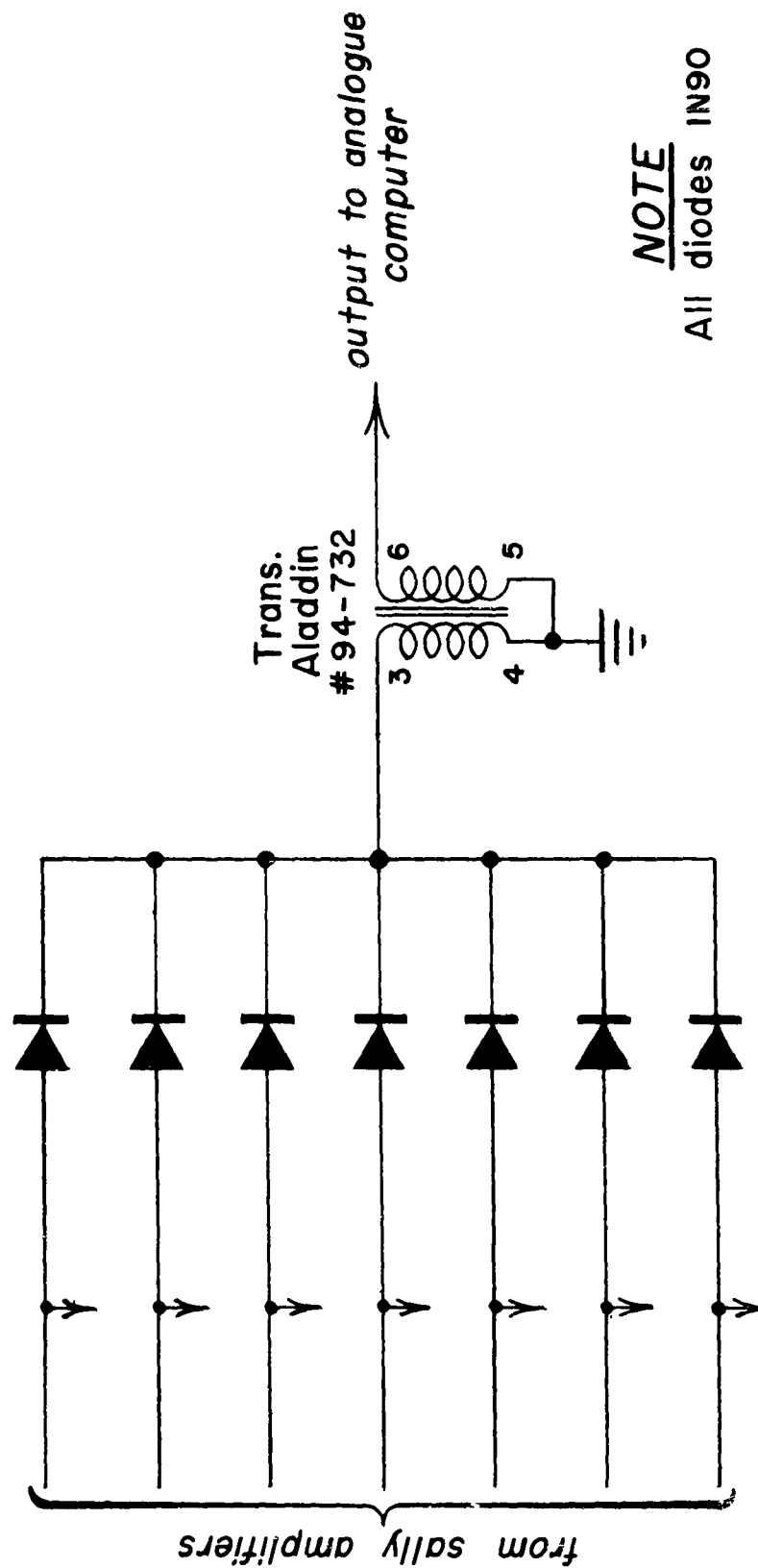
(C) The height fence contains 84 detection pickets, as do the first two fences, but there are no requirements for individual picket identity, since the output of this fence is fed to the firing-time computer (section 10). It is therefore possible to OR the individual pickets and use one sally amplifier (section 9.1.3) for a number of them. The height fence OR circuit is shown in figure 9-12. Seven PbS cell load resistors and coupling capacitors are mounted on a small circuit board, identical to those used in the sally amplifiers. The transistor, connected in a common base circuit, OR's the seven detection pickets to a single output. This output is connected to the input of a sally amplifier, the output of which is fed to the firing-time computer.

#### 9.2.3 Sequential Blocking Gates

(C) The signatures of some types of shell are bimodal and yield two output pulses from the sally amplifier, (section 9.1.3). This results in the improper operation of the Miller sweep circuits which are used in the firing-time computer. By interposing bistable multivibrators between the outputs of the sally amplifiers and the computer inputs, it is possible to allow the first pulse for each fence to reach the computer while blocking all subsequent ones. An automatic reset generator was added to this inhibiting circuitry so as to facilitate the computer calibration procedure from a repeated series of pulses.

(C) Figure 9-13 is a block diagram and figure 9-14 a schematic of the inhibiting circuitry. M-1, M-2, M-4, and M-6 are bistable multivibrators which function as trigger generators, M-3 and M-5 are bistable multivibrators functioning as pass gates, M-7 is a monostable multivibrator which

SECRET



NOTE  
All diodes IN90

Figure 9-11. Diode "OR" circuit

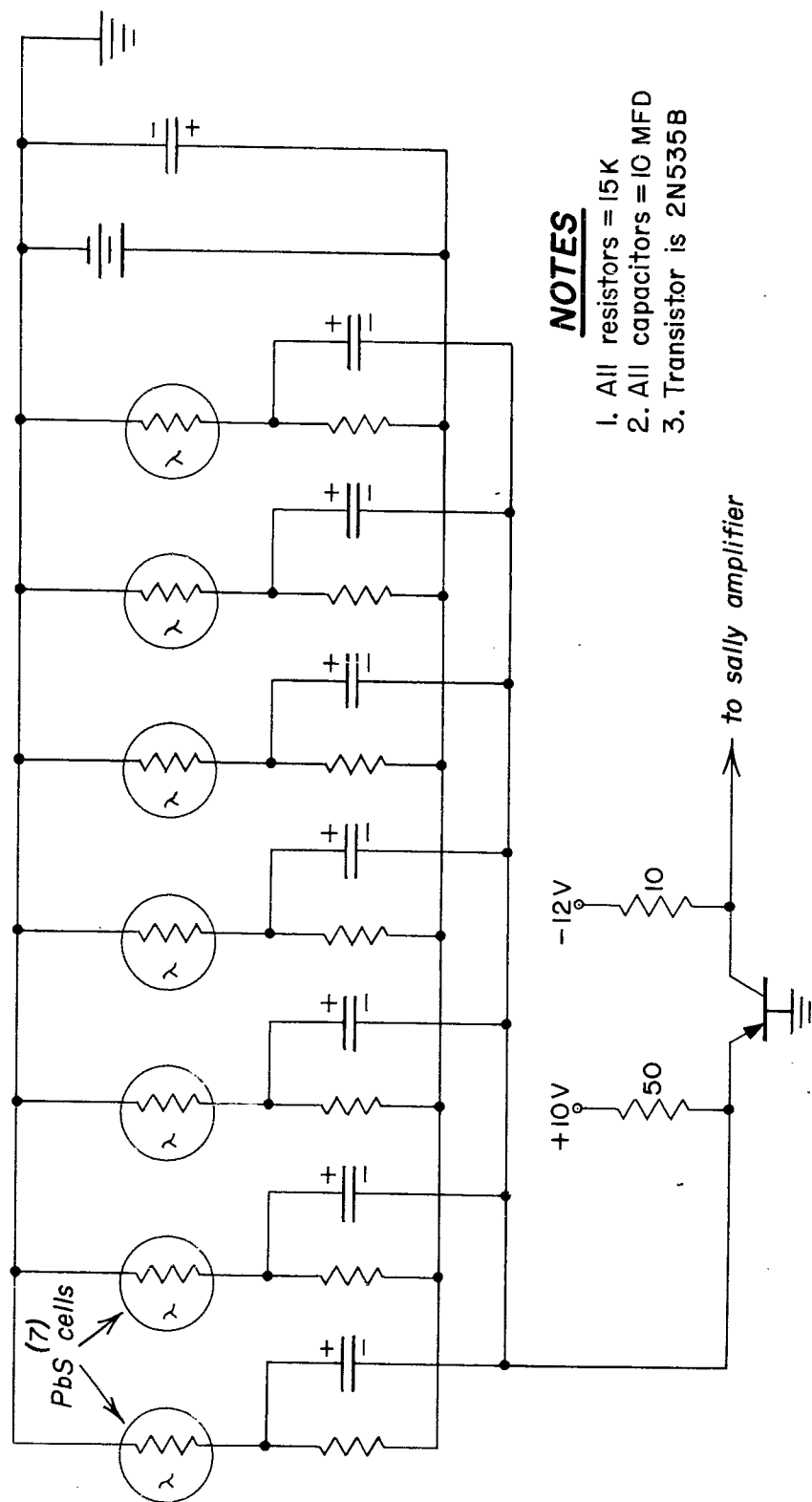


Figure 9-12. Height fence "OR" circuit

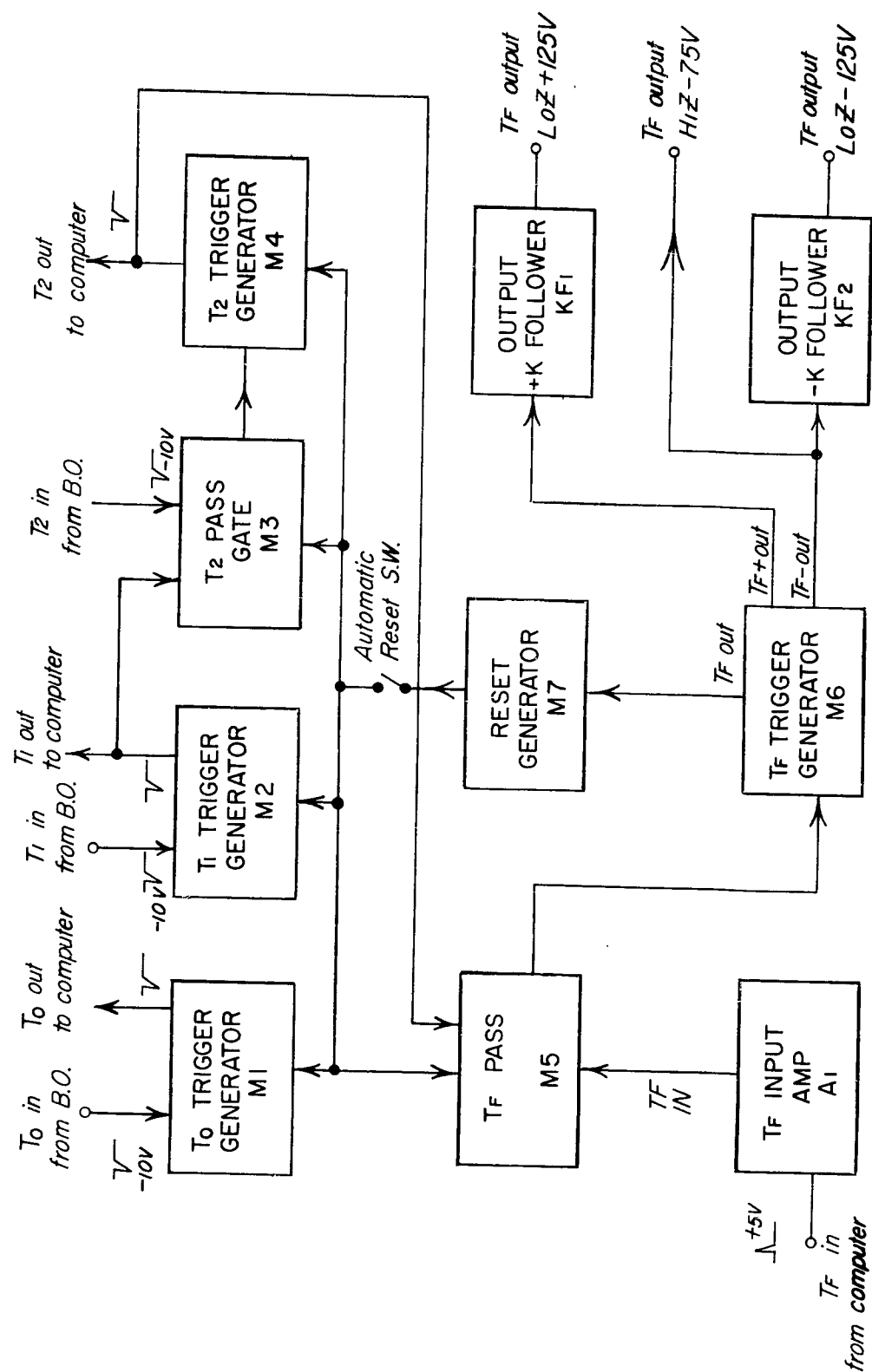


Figure 9-13. Block diagram of sequential blocking gates

## SECRET

delivers a reset pulse approximately 60 msec after the firing pulse is delivered; A is an input amplifier for the firing pulse out of the computer;  $KF_1$  and  $KF_2$  are firing pulse output cathode followers to supply positive and negative pulses to a microflash and other equipment which has been used in the field tests.

(S) The operation of the circuit may be best understood with reference to the wave shapes shown in figure 9-15. Bistable-multivibrator trigger-generators M-1, M-2, and M-4 supply trigger pulses to the firing-time computer upon receiving the  $T_0$ ,  $T_1$  and  $T_2$  pulses from the respective detecting fence. M-6 will deliver a firing pulse to the microflash and other test equipment (or the high-voltage firing circuit in the case of an actual live firing) at the proper time  $T_F$  as described earlier in this report. None of the above trigger generators will function on any but the first pulses out of their respective detecting fences until they are reset.

(C) M-3 and M-5 are also bistable multivibrators but function as pass gates. M-3 is set by the  $T_1$  pulse and is reset by the  $T_2$  pulse. M-4 being designed to trigger only on the reset of M-3. In order that M-6 deliver a firing pulse, it must first be set by M-5 which is triggered by  $T_2$ . Therefore, no firing pulse will be generated unless the proper sequence of pulses are received at  $T_1$ ,  $T_2$ , and  $T_F$  and in that order. This also acts as a protective measure.

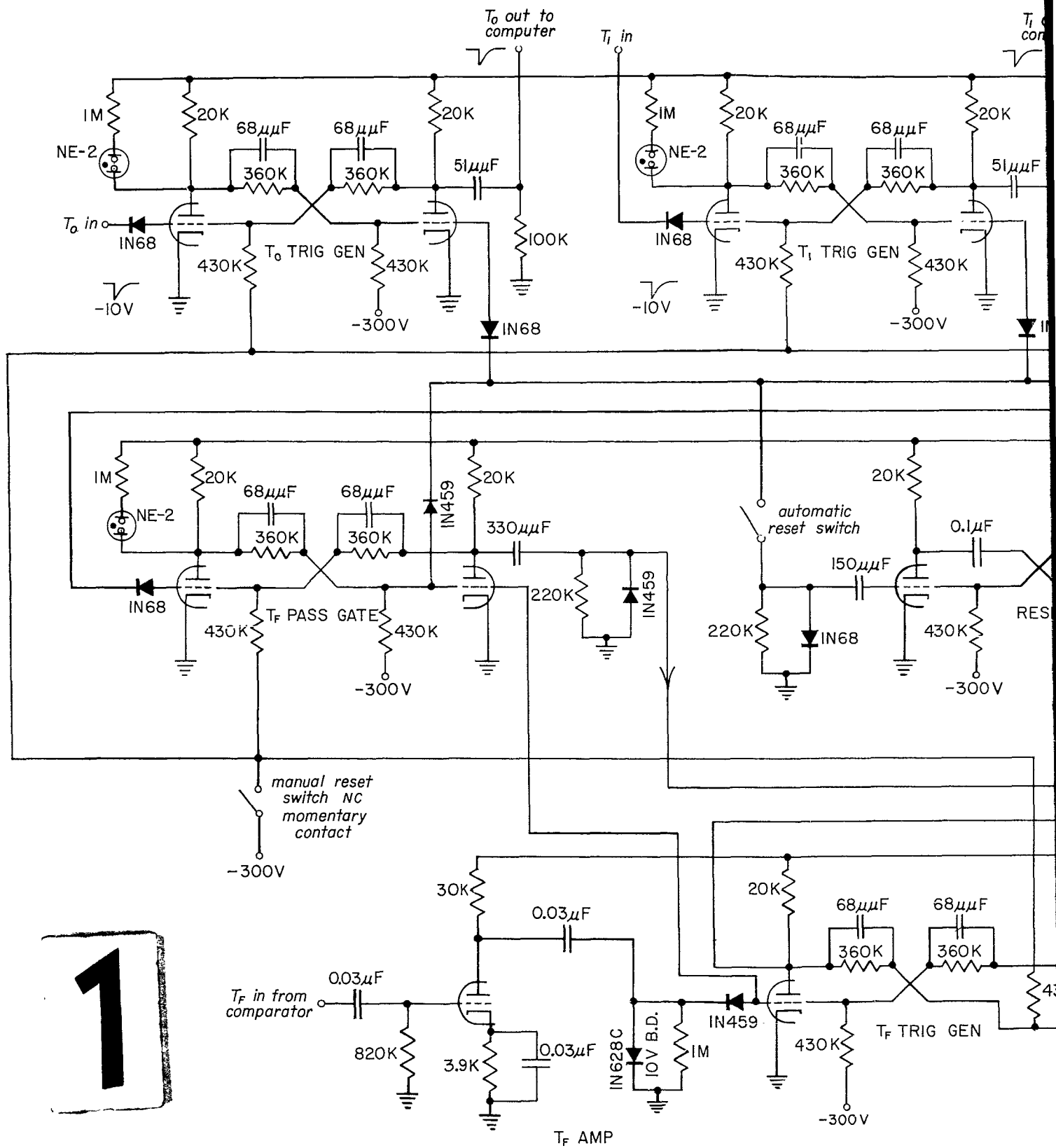
(C) It is possible to eliminate M-3 and M-5 and still obtain the sequencing effect by interconnecting M-1, M-2, M-4, and M-6 in a slightly different way. For the field test application, the added complication was worth while because it supplied positive indication of the receipt of a given pulse.

(U) Indicator lamps were added to the bistable multivibrators to indicate whether the trigger generators and blocking gates are in the required initial state for proper operation.

### 9.3 Size Discrimination

(S) The Dash-Dot System, as described thus far, reacts to the nose of a shell as it penetrates one or more of the detection pickets, without regard to diameter, shape, or length of the shell. In addition to protecting an armor plate against anti-tank rounds, the system is expected to be capable of discriminating between disabling and non-disabling rounds and of disregarding non-disabling ones, especially small-arms fire. The specifications require the system to ignore all rounds less than 50 mm in diameter.

(S) Several methods of effecting size discrimination have been considered and discarded as impracticable. The earliest attempt sought to relate the number of traversed pickets in any fence to (a) the angle of attack (b)



1

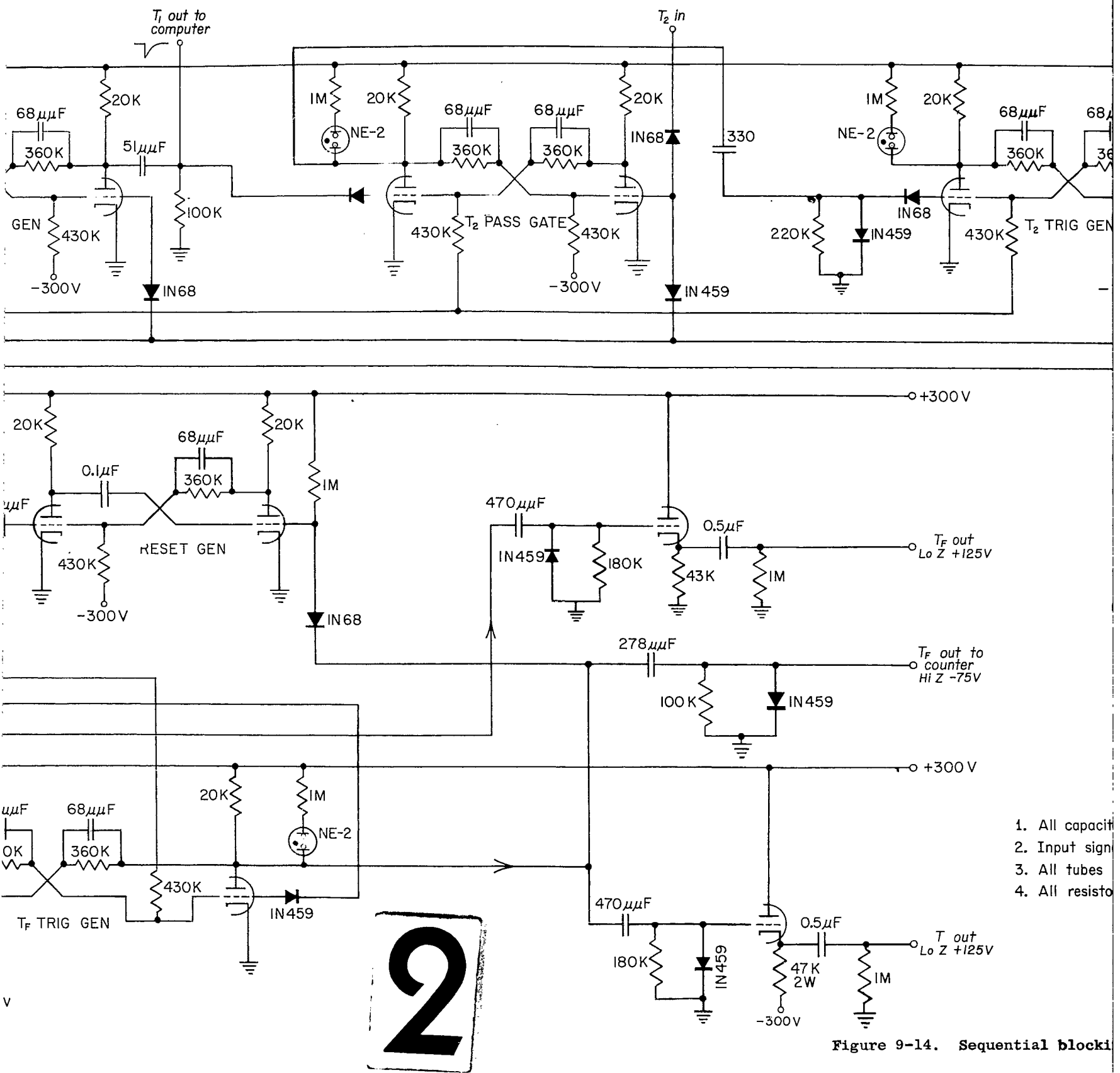


Figure 9-14. Sequential block



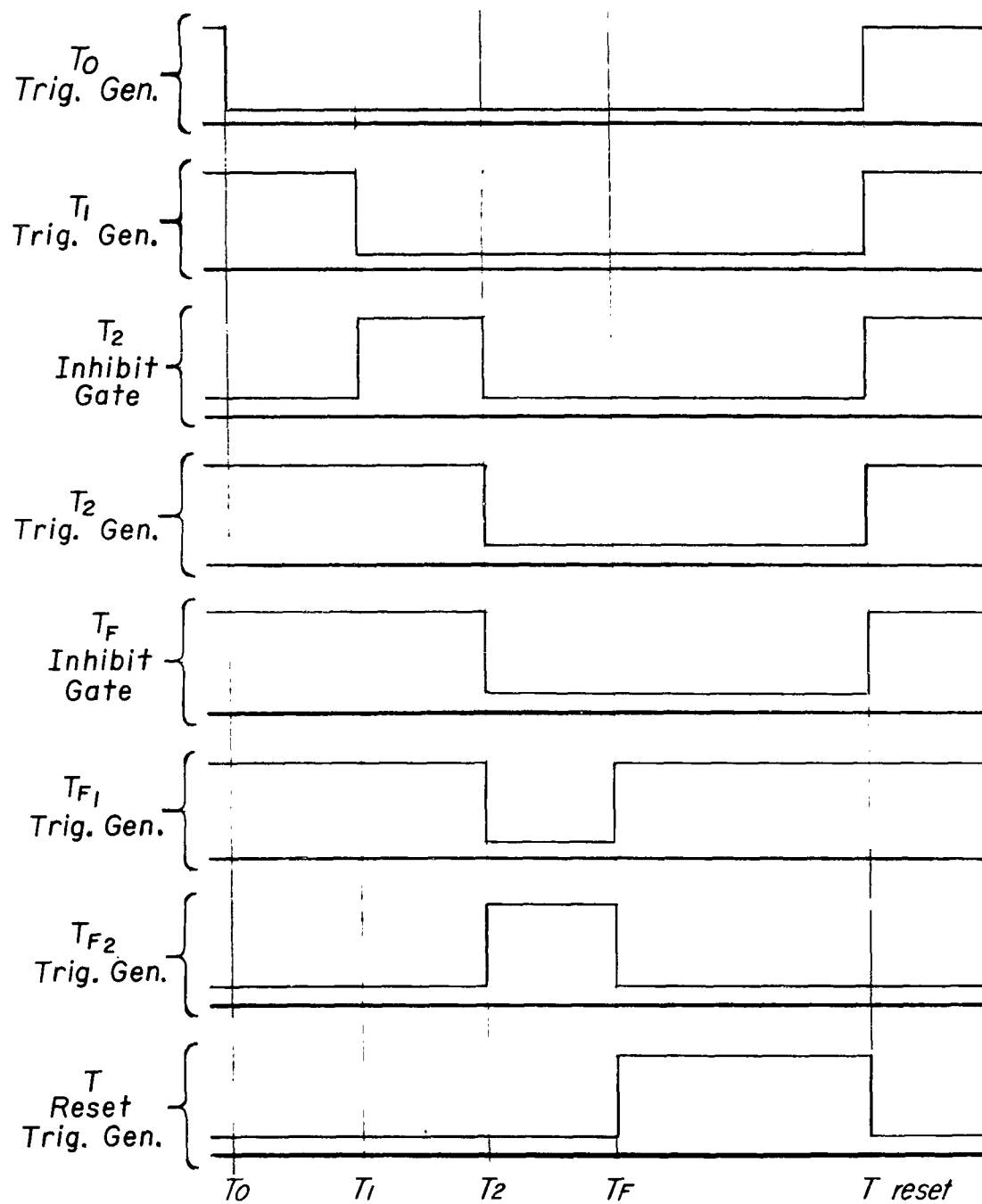


Figure 9-15. Sequential blocking gate wave shapes

## SECRET

the round calibre, and (c) the "attack attitude" (section 3.5.4). By setting up a unique correspondence between the number of pickets actually traversed and parameters a, b, and c above, a detailed analysis was made on the ability of such a scheme to unambiguously reject objects of less than 20 mm diameter while accepting all objects of greater than 57 mm diameter. This analysis produced the result that such a geometrical scheme would work only in the region from 0 to 10 deg angle of attack and again in the region from 45 to 60 deg, but would be useless in the intermediate region from 10 to 45 deg. With these results, further attempts at a purely geometrical scheme were discarded.

(S) Since shell diameters rise about proportionally to shell lengths, another contemplated method would have computed the length from the time it takes the shell to travel its own length, that is, to traverse a fence, which would have to be measured for this purpose, and from its velocity which has to be determined anyway in the firing-time computer. In this method, shells below a certain length would be ignored.

Fast-scanning methods were also considered, but the simplicity of the method actually employed and described in the next section dictated its use over the more sophisticated ones because it does not require any major system modifications.

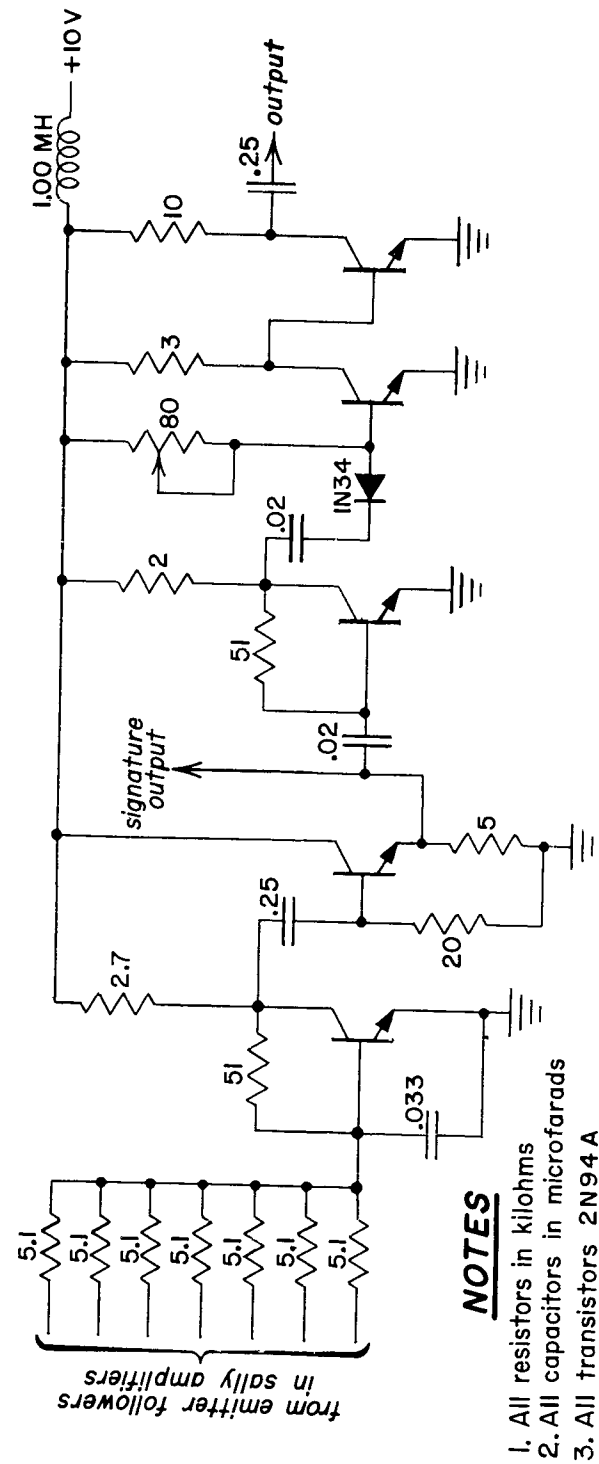
### 9.3.1 Size Discrimination Analysis

(S) The characteristics of various anti-tank rounds were analyzed and it was found that anti-tank rounds larger than 57 mm in diameter had a shell transit time greater than 200  $\mu$ sec, the transit time being defined as the time required for a shell to travel its own length, while rounds having a lesser diameter have transit times less than 200  $\mu$ sec. While it is felt that this analysis may not hold for all of the anti-tank rounds an enemy may possess, it would certainly be true for a large majority of them. The analysis of typical U.S. shell is shown in table 9-1. The size discrimination method is therefore based on accepting all rounds having a transit time greater than 200  $\mu$ sec and ignoring all rounds having a lesser transit time.

(C) The theoretical output signal that could be expected from a fast response photocell as a shell passed through a detection picket would be approximately a square wave, the rise of which would correspond to the nose entering the picket and the fall corresponding to the tail leaving the picket beam. The PbS cells that are used in this system have a relatively slow response and therefore the output waveform is distorted (see section 9.1).

(C) The shell signature information obtained from these cells is fed to the signal amplifiers, the input stage being an emitter follower used to couple the cells to the amplifiers. The size discrimination circuit, shown in figure 9-16, OR's seven emitter follower output stages

CONFIDENTIAL



### NOTES

1. All resistors in kilohms
2. All capacitors in microfarads
3. All transistors 2N94 A

Figure 9-16. Size discrimination circuitry

CONFIDENTIAL

Table 9.1. Anti-Tank Rounds and Transit Times

Diameter (mm)	Shell	Shell Use	Velocity (ft/sec)	Length (in.)	Transit time ( $\mu$ sec)
20	AP-T M95	Armor	2800	3.27	97
37	APC-T M59A	Armor, Shot	2050	4.71	191
37	AP-T M30	Armor, Shot	1825	4.24	194
37	APC-T M51	Light Armor	2900	6.36	183
40	AP-T M1A1	Armor	2870	6.17	180
57	HE-T M303	Blast and Frag.	2700	10.63	326
57	APC-T M86	Anti-Tank	2700	11.24	347
57	HEAT M307	Anti-Tank	1200	7.85	544
75	APC-T M61	Armor	2030	11.17	604
75	HEAT-T M66	Anti-Tank	1000	15.90	1327
76	HEAT-T M62	Anti-Tank	2600	13.78	422
76	HVAP-T M93	Heavy Armor	3400	11.00	269
90	APC-T M82	Heavy Armor	2800	16.19	503
90	AP-T M77	Heavy Armor	2700	10.00	308
90	HVAP-T M304	Very Heavy Armor	3350	13.20	308
105	HEAT-T M67	Anti-Tank	1250	20.05	1340

**SECRET**

THE ORIGINAL DOCUMENT WAS OF POOR  
QUALITY. BEST POSSIBLE REPRODUCTION  
FROM COPY FURNISHED ASTIA.

while maintaining their individual identities. The signals are amplified in the first three transistor stages. They are then differentiated, resulting in a positive nose pulse that is not well defined and a negative tail pulse that is well defined. The pulse is further amplified while the nose pulse is inhibited by the coupling diode in the last stages. The nose pulse is more accurately supplied from the sally amplifier (section 9.1.3).

(U) The oscilloscope traces shown in figure 9-17 are typical. The top trace is the tail pulse; the trace immediately below it is the output of the amplified signatures in the size discrimination circuit. The lower two traces are individual shell signatures.

(C) If the full experimental system is used which contains 84 detection pickets in any one fence, the size discrimination circuit would be capable of adding the signals from 14 pickets before cell noise becomes significant. Therefore, six identical circuits, whose outputs are tied to a common point, would be used to cover the first fence. In the simplified system however, in which only one 7-picket subfence (section 5.1) was used in each fence, the size discrimination circuitry was connected to the seven pickets of the first velocity subfence.

#### 9.3.2 Size Discrimination Logic Circuitry

(S) The system is required to ignore all rounds of less than 50 mm in diameter, that is, all rounds having a transit time less than 200  $\mu$ sec. Furthermore, it is desired that the firing circuit be de-energized unless an attacking round is dangerous. The block diagram and the schematic of the logic circuitry that accomplishes this are shown in figures 9-18 and 9-19.

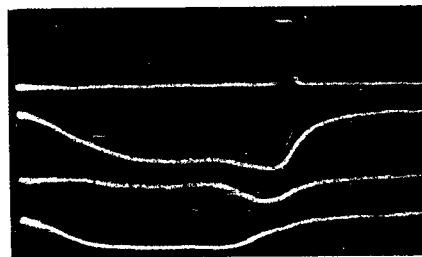
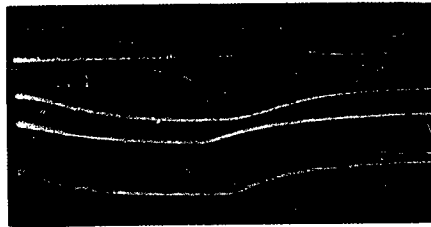
(C) A nose pulse from the sally amplifiers triggers a 200- $\mu$ sec monostable multivibrator, whose output is differentiated and clipped, resulting in a 200- $\mu$ sec delayed pulse that triggers the first 100 msec pass gate. This pass gate is also a monostable multivibrator, the output of which is applied to the first AND circuit.

(C) Subsequent to the nose pulse from the pass gate, a tail pulse is obtained from the size discrimination circuit and applied to the first AND circuit. The tail pulse will pass through the first AND circuit, if the first pass gate pulse is also present. If the tail pulse occurs less than 200  $\mu$ sec after the nose pulse, it cannot pass the first AND circuit. Therefore, only those pulses representing a shell transit time greater than 200  $\mu$ sec can trigger the second 100 msec pass gate which allows a firing pulse to pass through the second AND circuit.

(C) The firing circuit is energized only if the following conditions have been met:

**SECRET**

149



→  
Direction of travel

Figure 9-17. Tail pulses and shell signatures

CONFIDENTIAL

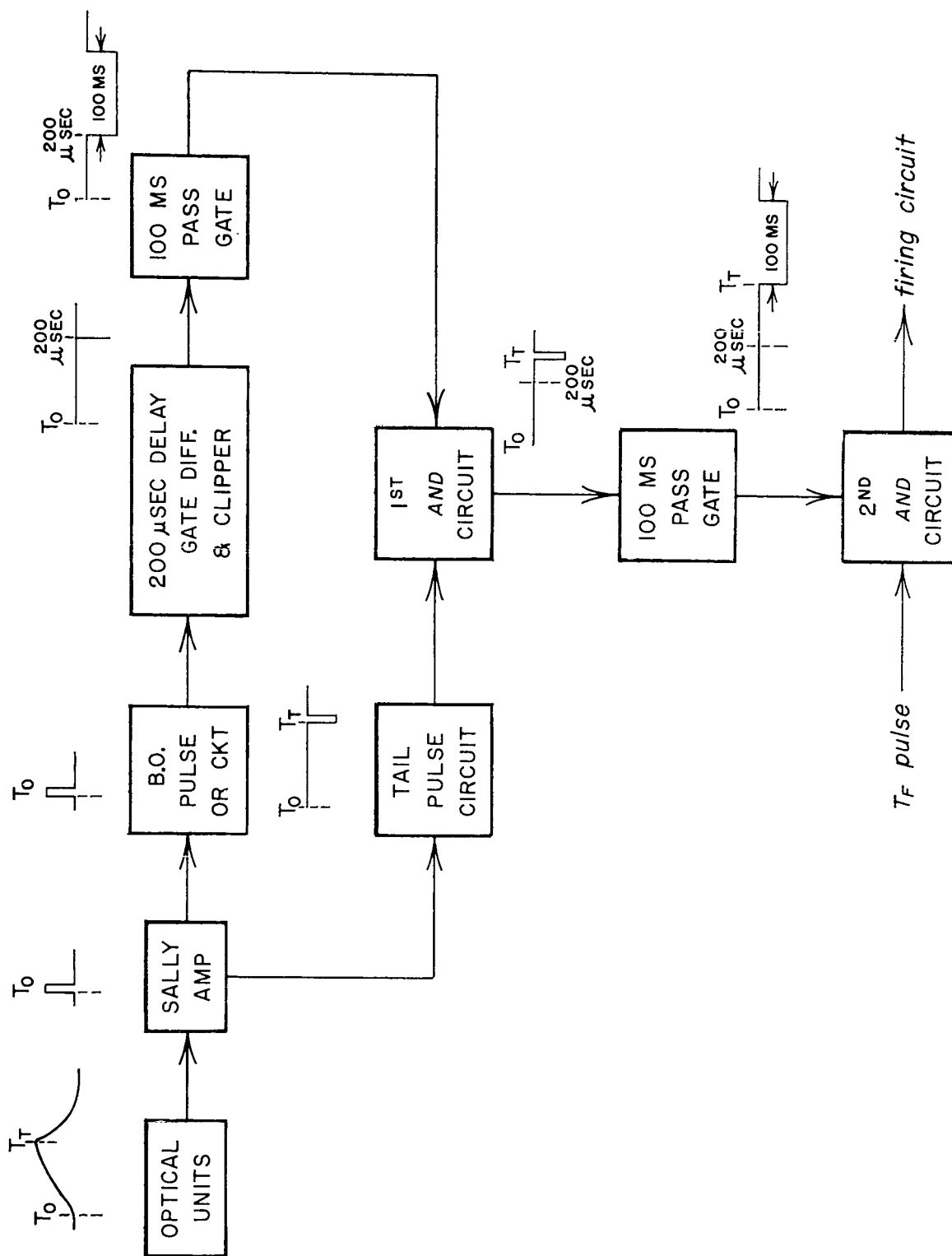
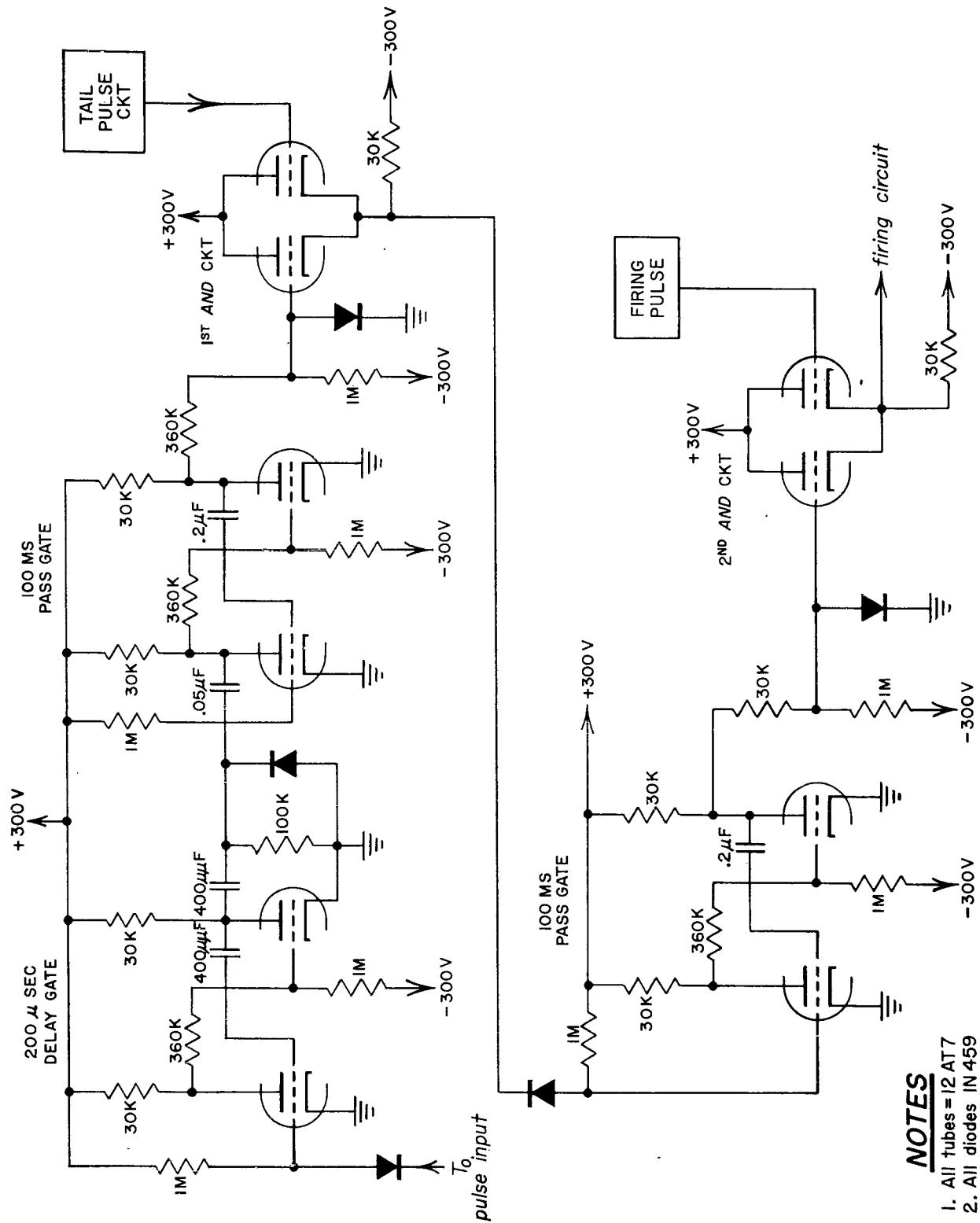


Figure 9-18. Block diagram of size discrimination logic circuitry

CONFIDENTIAL

CONFIDENTIAL



**NOTES**

1. All tubes = 12 AT 7
2. All diodes IN 459

Figure 9-19. Logic circuitry for size discrimination

CONFIDENTIAL

# SECRET

- a) A  $T_0$  pulse must be present;
- b) A tail pulse must be present more than 200  $\mu\text{sec}$  later than the  $T_0$  pulse;
- c) A firing pulse must be present after a tail pulse occurs.

## 9.4 K Factor

(S) The equation that determines the firing time of the defending charge has been shown to be (section 3)

$$\Delta T_f = \frac{d_2}{d_1} \Delta T_1 + \frac{d_1 \Delta T_2}{V_c \tan \phi \Delta T_1} - \Delta T_2 - \frac{h}{V_c}.$$

$\Delta T_f$  in this equation determines the time at which a defending charge shall be fired in order to impact an approaching round when the round has traveled a constant distance from the second detection fence normal to and beyond the line charge plane. The computer supplies a firing pulse to the line charge when the shell is at a distance

$$\frac{h}{V_c} V_m$$

along the trajectory, from the nose position, shown in figure 9-20, where  $h$  is the height of the trajectory;  $V_c$  is the effective fragment velocity of the defending charge, and  $V_m$  is the velocity of the approaching round. The position of the shell's nose is a variable, being a function of  $h$  and  $V_m$ , but when they are hit they are all in the same plane.

(S) The incompleteness of the firing-time equation becomes more apparent from figures 9-21 and 9-22. Figure 9-21 is a schematic drawing of a few projectiles the system must defeat and figure 9-22 is a schematic of representation of three shells of different lengths, having an attack angle of zero and sixty degrees. The distances  $d_1$  and  $d_2$  are constants in the firing-time equation, the latter being the distance from the second detection fence to the nose position. If it be decided that the nose position is to be 12 inches, for example, beyond the defending charge in order to impact shell A at its most vulnerable point, it can be seen that shell B and C would not be defeated in the zero-degree approach. In addition, in the sixty-degree approach none of the shells would be defeated. It is quite obvious then that the equation must be modified by a term which will include the length of the shell as well as the angle of approach. This term is subsequently referred to as the K factor.

SECRET

153

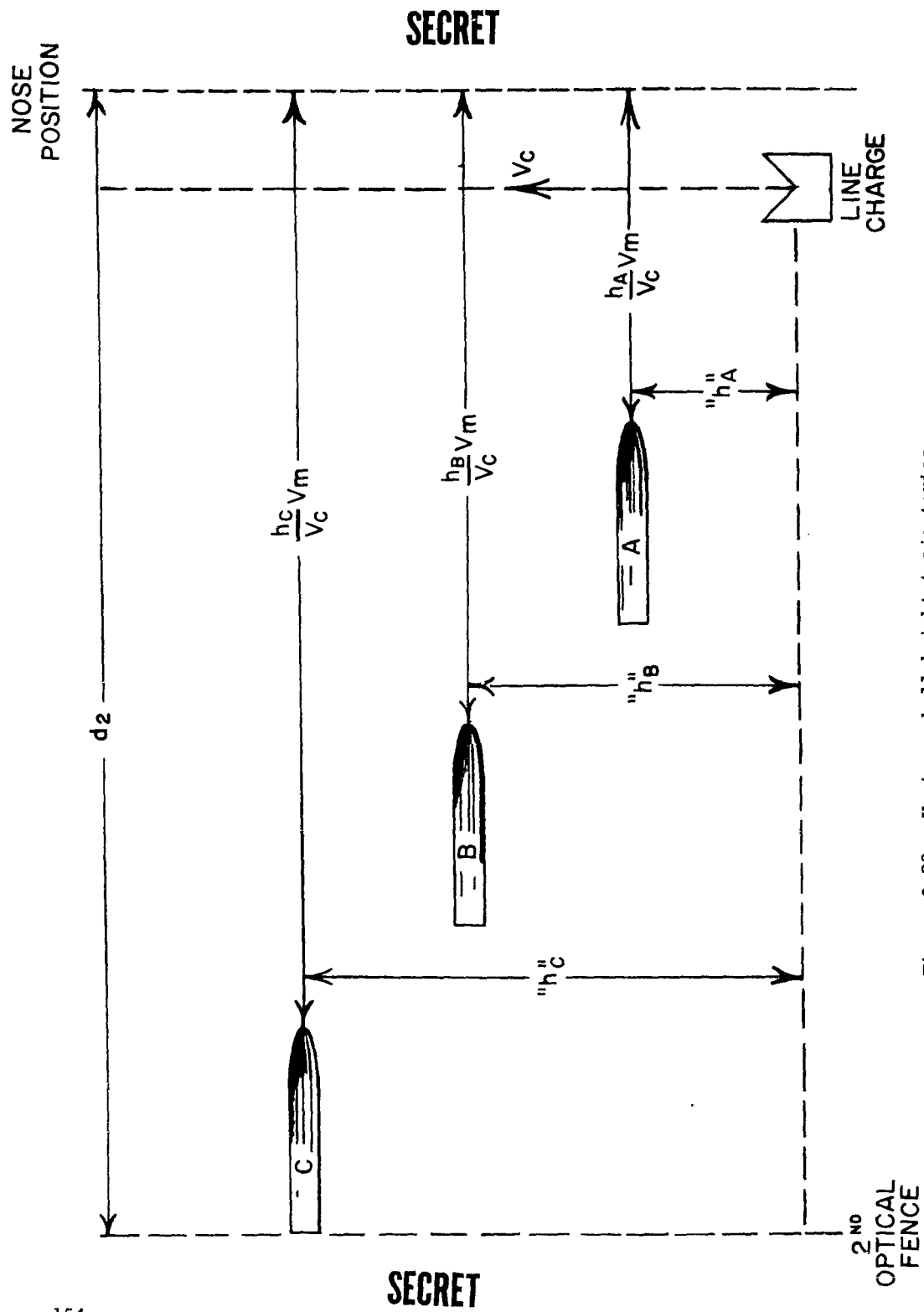


Figure 9-20. Various shell height trajectories

CONFIDENTIAL

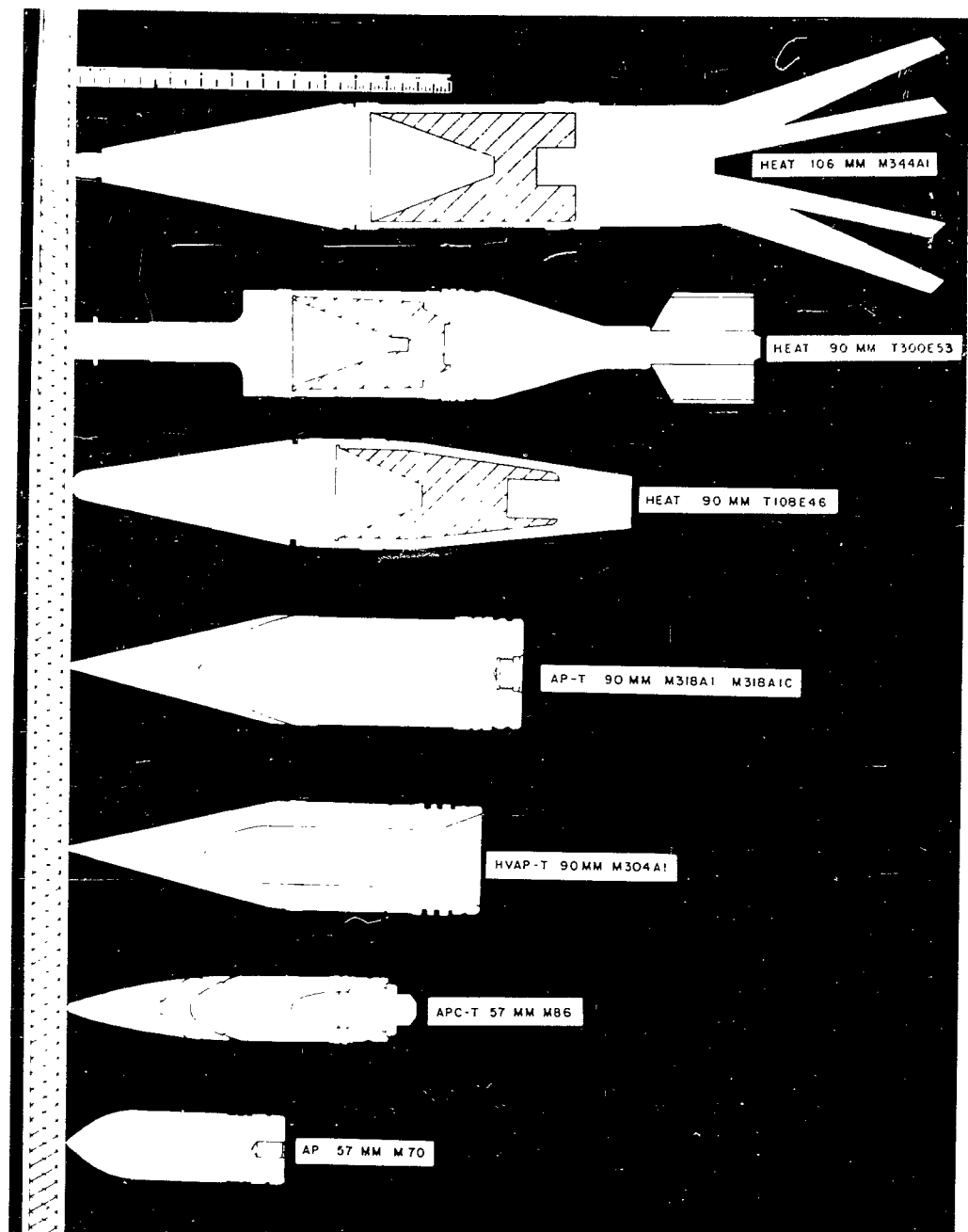


Figure 9-21. Shells specified for feasibility test

CONFIDENTIAL

SECRET

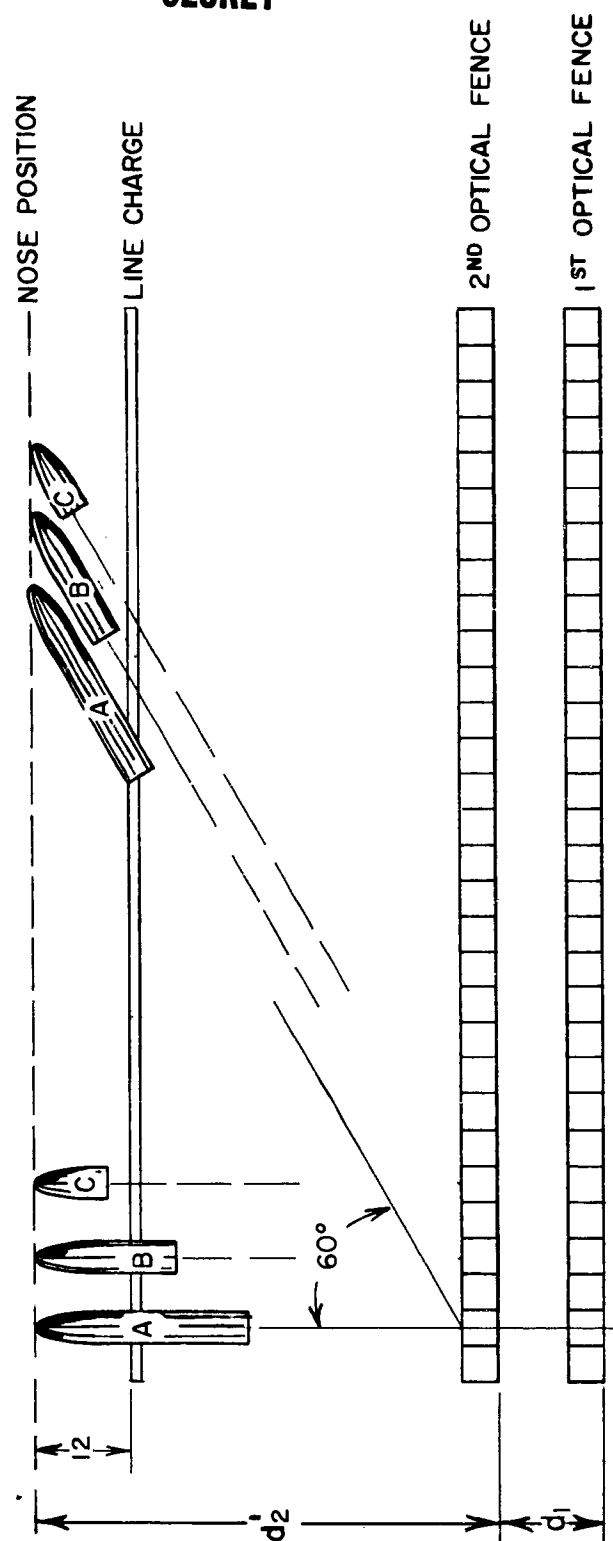


Figure 9-22. Influence of shell length and orientation without K factor

SECRET

SECRET

(S) If it is assumed that all shells must be hit near the center as shown in figure 9-23, then the distance  $d_2$  must be made a function of the length,  $L$ , of the shell and angle  $\theta$  of approach. The first term of the equation for the firing time will then be

$$\frac{d_2' + \delta d}{d_1} \Delta T_1$$

where  $\delta d = kL \cos \theta$ ,  $k$  being a fraction of the shell length  $L$  referenced to the nose, and  $d_2'$  being the distance from the second detection fence to the defending charge-line. The complete equation is now:

$$\Delta T_f = \frac{d_2' + kL \cos \theta}{d_1} \Delta T_1 + \frac{d_1}{V_c \tan \phi} \frac{\Delta T_2}{\Delta T_1} - \Delta T_2 + \frac{6}{V_c} \quad (9.7)$$

where the first term can be written as

$$\frac{d_2'}{d_1} \Delta T_1 + \frac{kL \cos \theta}{d_1} \Delta T_1$$

The term  $\frac{kL \cos \theta}{d_1} \Delta T_1$  is the K-factor. A voltage proportional to

$\frac{d_2'}{d_1} \Delta T_1$  is obtained in the same manner as  $\frac{d_2}{d_1} \Delta T_1$  is generated (section 10). It is now necessary to generate a voltage proportional to  $\frac{kL \cos \theta}{d_1} \Delta T_1$ , the K-factor, where  $L \cos \theta$  is determined by the  $T_o$  pulse from the sally amplifiers circuit and the  $T_t$  pulse obtained from the size discrimination circuit (see section 9.3.2). The time  $T_t - T_o = \Delta T_L$  is the time interval between the nose and tail pulses;

then  $V_m = \frac{V_n}{\cos \theta} = \frac{L}{\Delta T_L}$ , where  $V_m$  is the velocity of the shell and

$V_n$  is the normal component of  $V_m$  as shown in figure 9-24. Solving for  $\Delta T_L$

$$\Delta T_L = \frac{L \cos \theta}{V_n}$$

but

$$V_n = \frac{d_1}{\Delta T_1}$$

SECRET

157

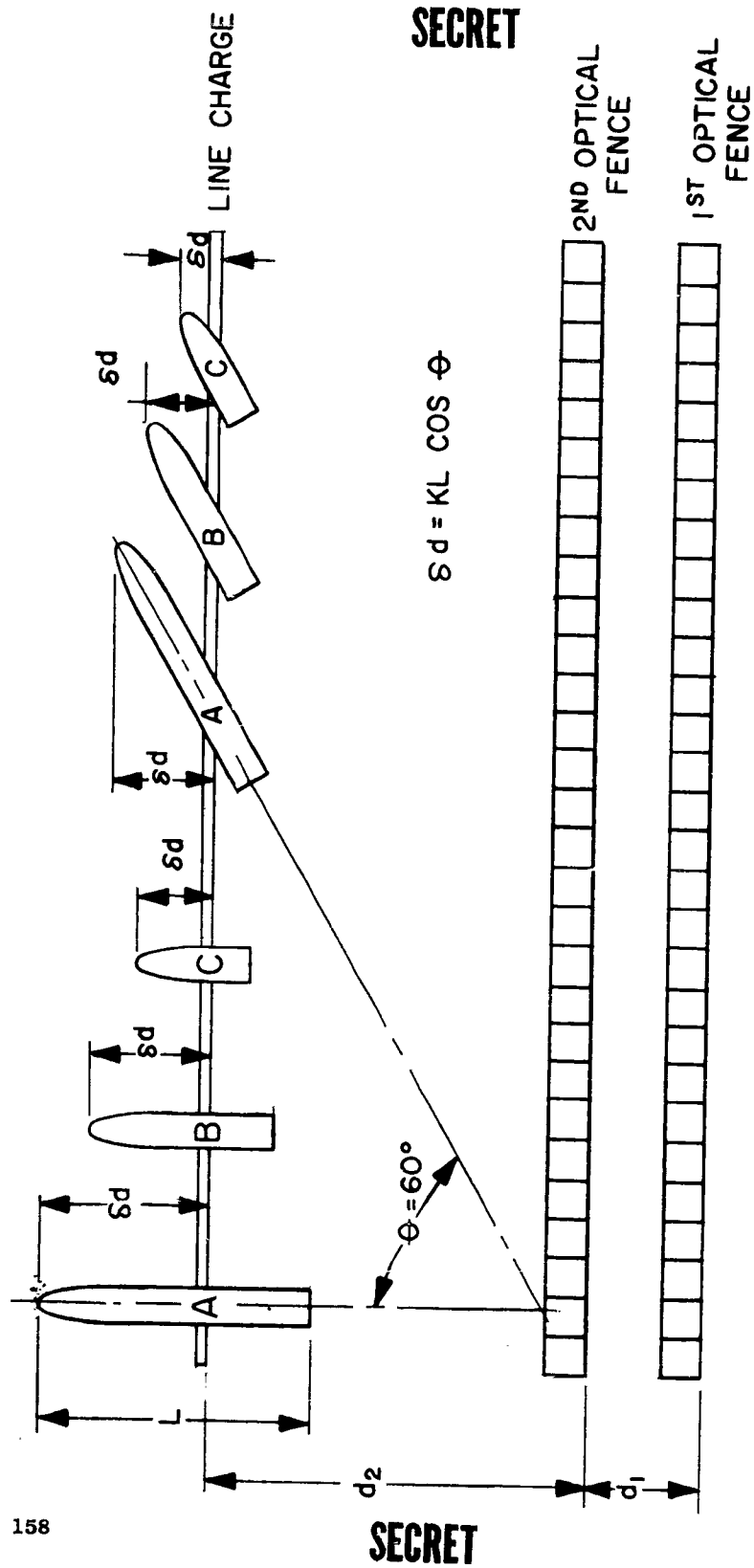


Figure 9-23. Influence of shell length and orientation with K factor

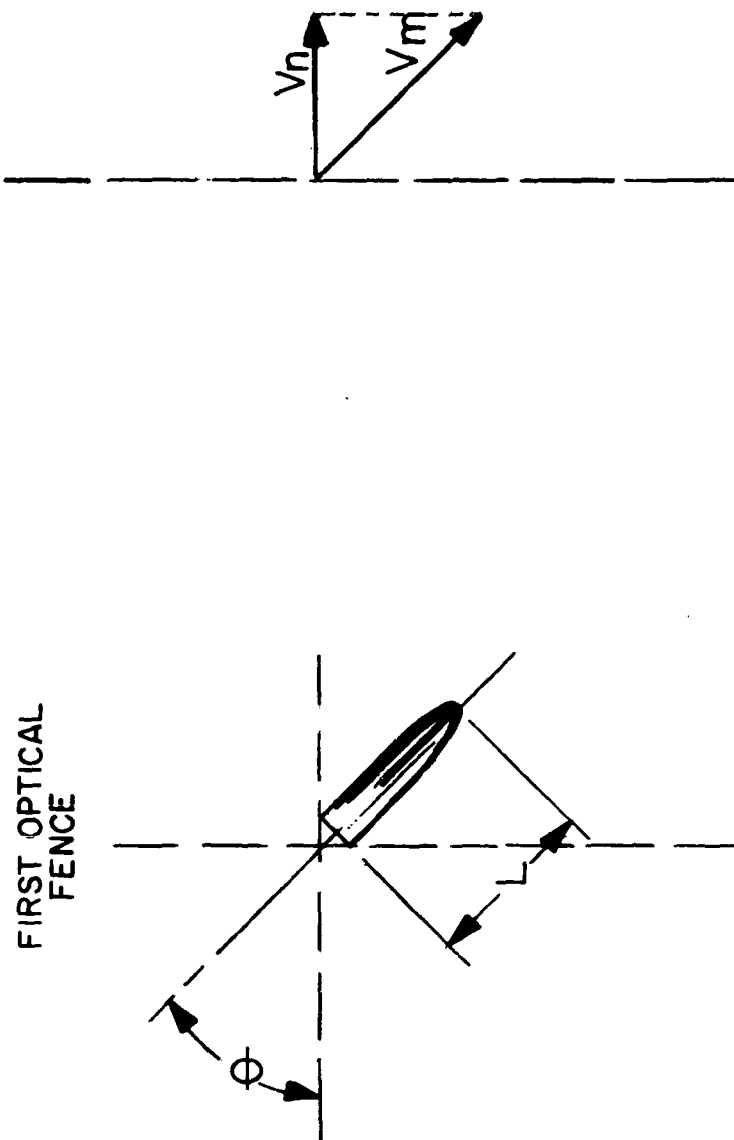


Figure 9-24. Normal component  $V_n$  of shell velocity  $V_m$

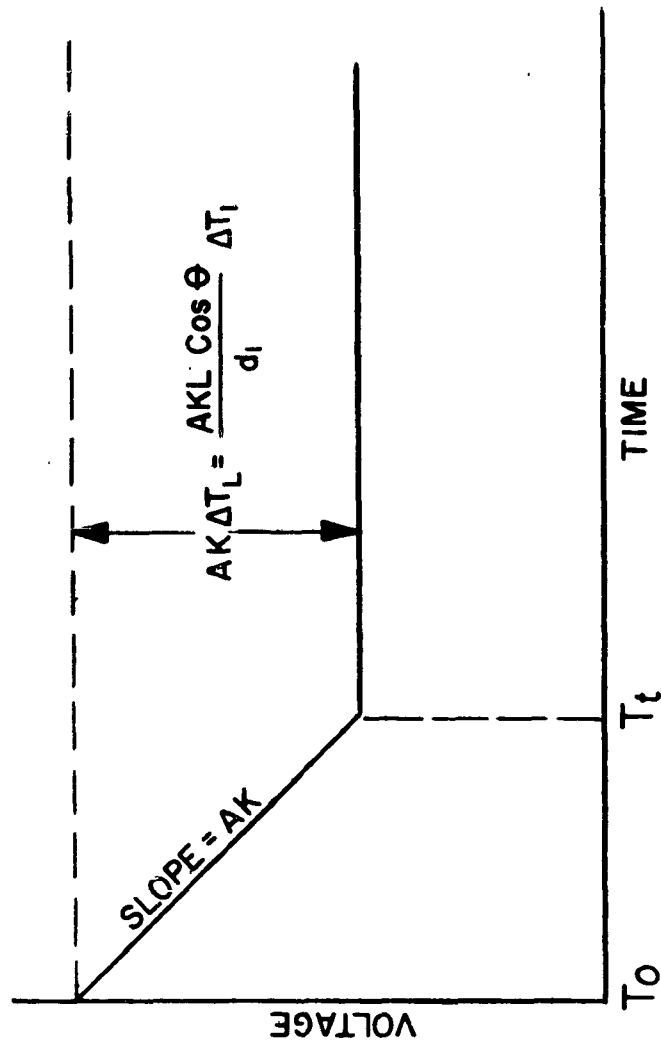


Figure 9-25. Miller sweep voltages for K-factor

Therefore,  $\Delta T_L = \frac{L \cos \theta}{d_1} \Delta T_1$ . Now then, multiplying by  $k$  and the voltage scale factor  $A$ , that is used in the  $\Delta T_F$  equation to translate from time to voltage (section 10), gives

$$Ak\Delta T_L = \frac{AkL \cos \theta}{d_1} \Delta T_1$$

If a Miller sweep is started with a slope of  $Ak$  at  $T_0$  and stopped at  $T_t$ , figure 9-25, a voltage is generated equal to

$$\frac{AkL \cos \theta}{d_1} \Delta T_1$$

This voltage is added into the computer circuit in the same manner as the

term  $K_2 \frac{\Delta T_2}{\Delta T_1}$  is added (see section 10.5).

# SECRET

## 10. FIRING-TIME COMPUTER

J. E. Miller

### 10.1 General Considerations

(S) In the Dash-Dot system it is necessary to know the velocity, height, and angle of attack of the approaching missile in order to be able to defeat it. The problem of the angle of attack is one of charge selection and is covered in section 11.

(C) In the sensing system complex, three pulses are generated at times  $T_0$ ,  $T_1$  and  $T_2$  (figure 10-1) which, due to their relative time displacements, provide information as to the velocity and height (in relation to the datum plane) of the attacking missile.

(S) The time  $T_f$ , at which the proper defending charge must be detonated to intercept the attacking missile, is related to the three pulse times by

$$\Delta T_f = 4.71 \Delta T_1 + 3.43 \times 10^{-4} \frac{\Delta T_2}{\Delta T_1} \Delta T_2 - 7.50 \times 10^{-4} \text{ [sec]} \quad (\text{section 3.3}) \quad (10.1)$$

where

$$\Delta T_1 = T_1 - T_0$$

$$\Delta T_2 = T_2 - T_1$$

$$\Delta T_f = T_f - T_2$$

### 10.2 Transformation of Firing-Time Equation to Voltages

(S) Equation (10.1) is based upon the physical parameters of the system geometry. Since the computer must operate with voltage, the equation must be multiplied by a conversion factor "A" [volts/sec] such that:

$$A \Delta T_f + A \Delta T_2 + A \times 7.50 \times 10^{-4} = A \times 4.71 \Delta T_1 + A \times 3.43 \times 10^{-4} \Delta T_2 \Delta T_1 \quad (10.2)$$

# SECRET

163

This document contains information affecting the national defense of the United States within the meaning of the espionage laws, title, 18 U. S. C., 793 and 794. Its transmission or the revelation of its contents in any manner to an unauthorized person is prohibited by law.

CONFIDENTIAL

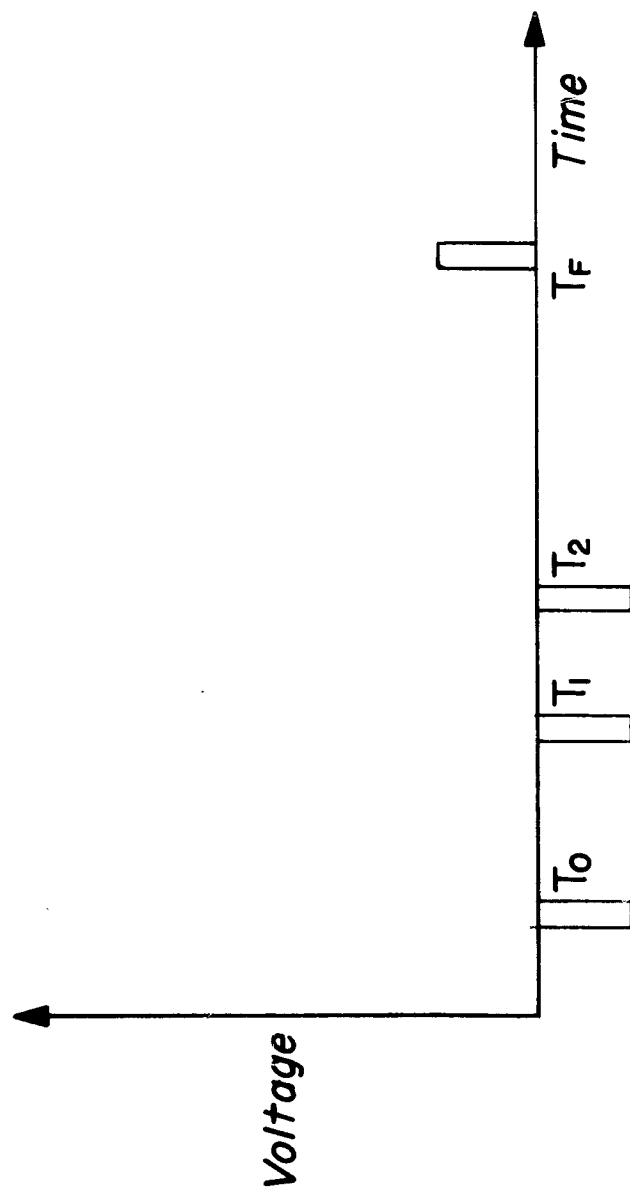


Figure 10-1. Time domain representation of pulses as used by firing-time computer

CONFIDENTIAL

# SECRET

(S) The value of A depends upon two factors; 1) the dynamic range of the computer, and 2) the accuracy which must be obtained. For example, let the maximum dynamic voltages be 230 v and  $\Delta T_1 \text{ max} = 833.3 \mu\text{sec}$  and  $\Delta T_2 \text{ max} = 1666.7 \mu\text{sec}$ , corresponding to a missile in the sensing system with a velocity of 1200 fps at a height of 17 in. Therefore,

$$230 \text{ v} = A \left( 4.71 \Delta T_1 \text{ max} + 3.43 \times 10^{-4} \frac{\Delta T_2 \text{ max}}{\Delta T_1 \text{ max}} \right) \text{ v} \quad (10.3)$$

$$A = 4.99 \times 10^4 \text{ v/sec}$$

The equation for the firing time (equation 10.3) as used in the computer is thus:

$$4.99 \times 10^4 \Delta T_f = 23.5 \times 10^4 \Delta T_1 + 17.1 \frac{\Delta T_2}{\Delta T_1} \quad (10.4)$$

$$- 4.99 \times 10^4 \Delta T_2 - 37.4 \text{ [volts]}$$

The validity of using this value of A in respect to the required accuracy is discussed in section 10.7.

(U) The terms in equation (10.4) are represented in time as shown in figure 10-2. The function  $23.5 \times 10^4 \Delta T_1$  is a straight line in the interval  $\Delta T_1$  and a constant thereafter. Also  $4.99 \times 10^4 (\Delta T_2 + \Delta T_f)$  is a straight line function in the consecutive intervals  $\Delta T_2$  and  $\Delta T_f$ . The constant 37.4 v is a displacement from the base line, which in this case is considered as the  $+E_{bb}$  bus voltage. The division is performed by an analog-digital divider which generates a number of pulses, the sum of which is proportional to the ratio  $\Delta T_2/\Delta T_1$ . The process will be more fully explained in section 10.8.

## 10.3 Computer Operation

(U) The block diagram of the computer is shown in figure 10-3, and a schematic in figure 10-4. The computer requires various gates which are activated in different intervals of time. The  $T_0$  pulse activates the  $(T_1 - T_0)$  gate which generates a positive gate in the interval. The  $T_1$  pulse terminates the  $(T_1 - T_0)$  gate, but at the same time it activates the  $(T_f - T_1)$  gate which is a positive gate in the  $(T_f - T_1)$  interval.

# SECRET

CONFIDENTIAL

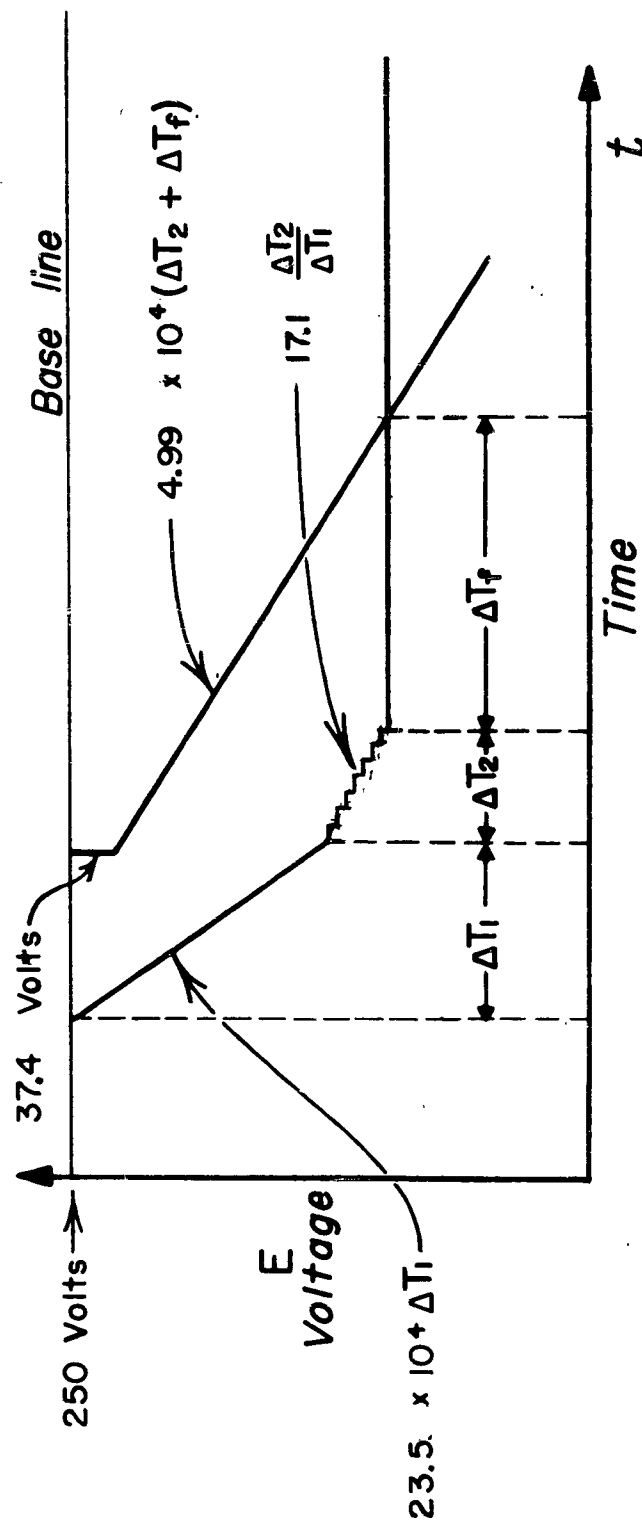
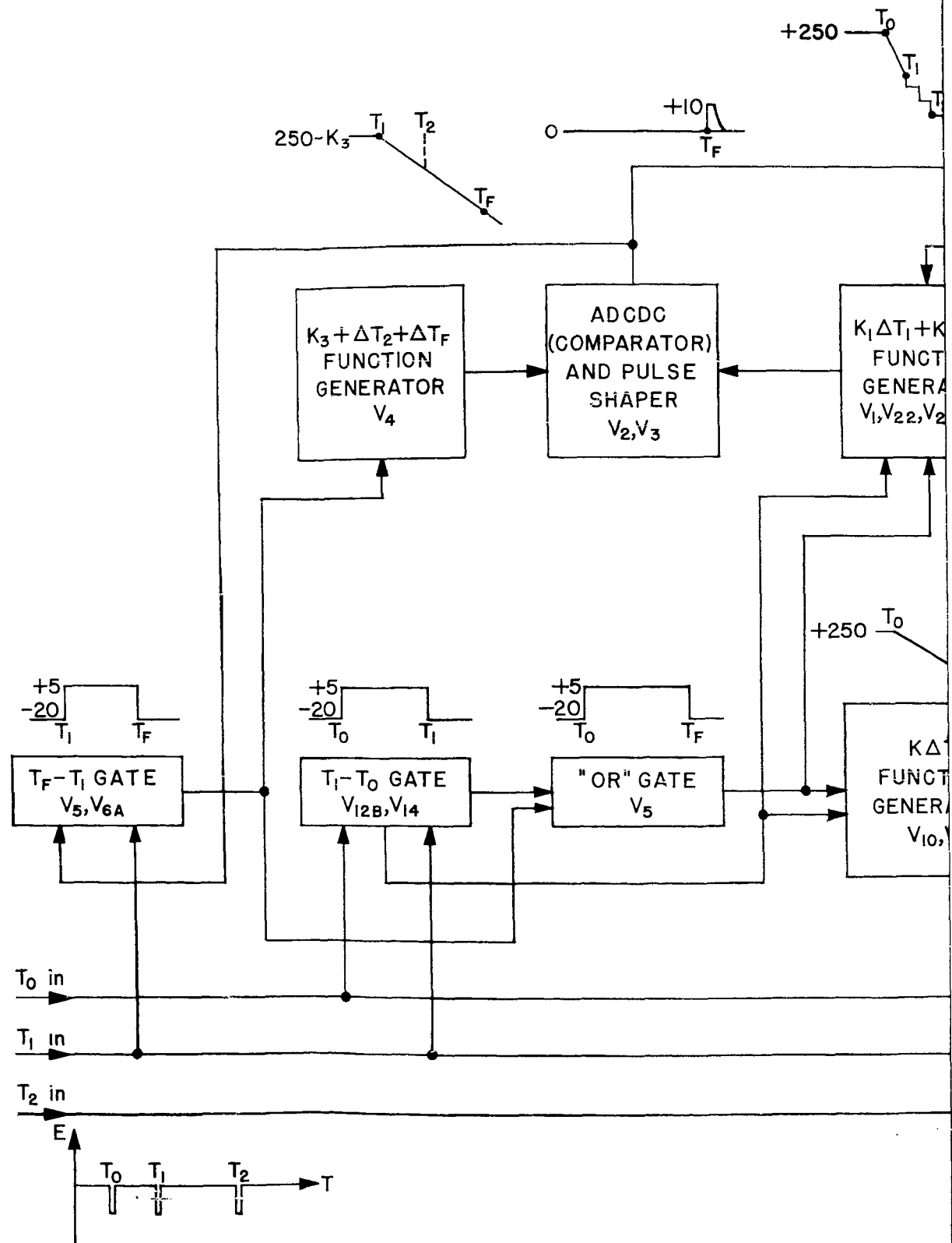


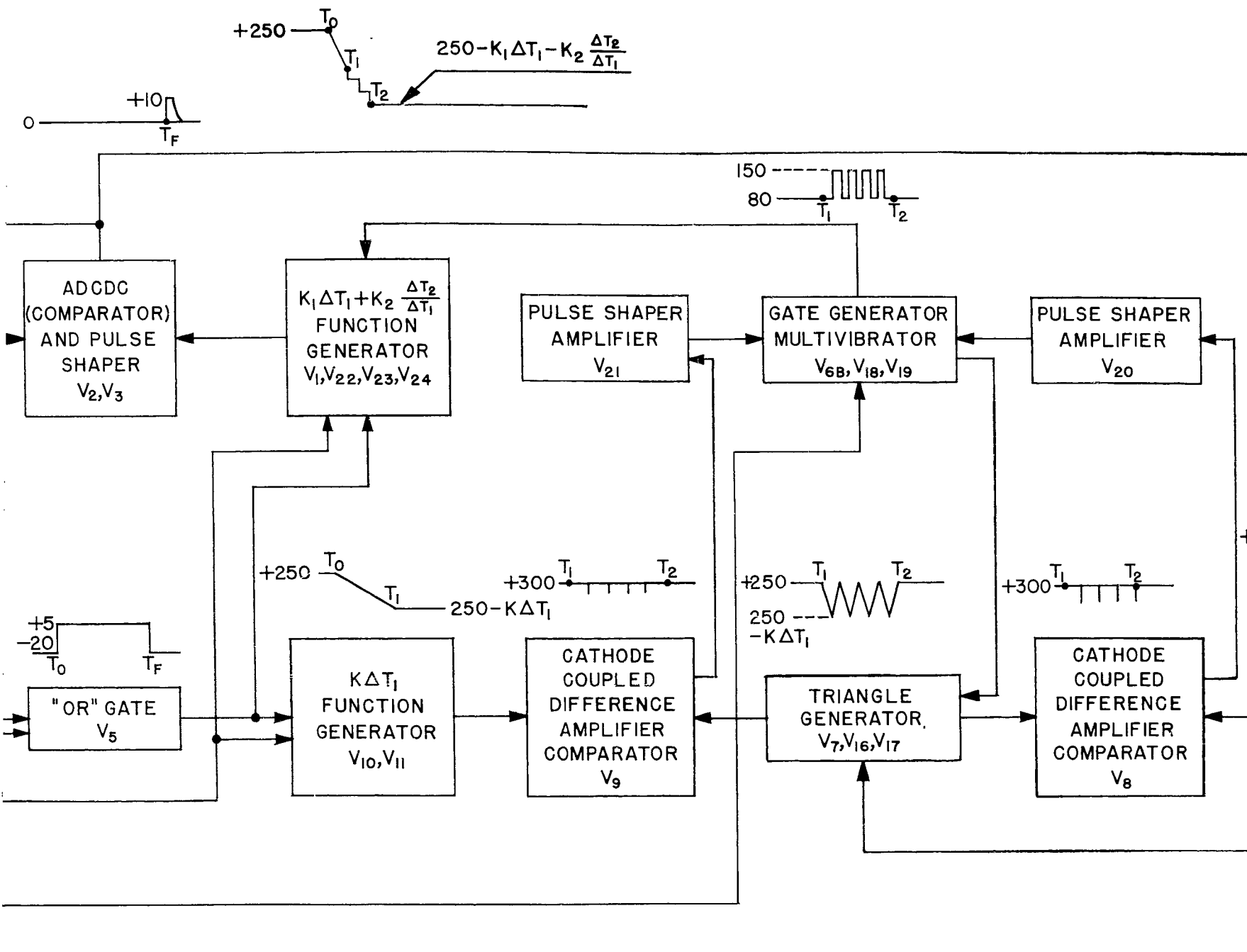
Figure 10-2. Functions generated in firing-time computer

CONFIDENTIAL

1



CONFIDENTIAL



2

Figure 10-3. Block diagram of firing-time

CONFIDENTIAL

CONFIDENTIAL

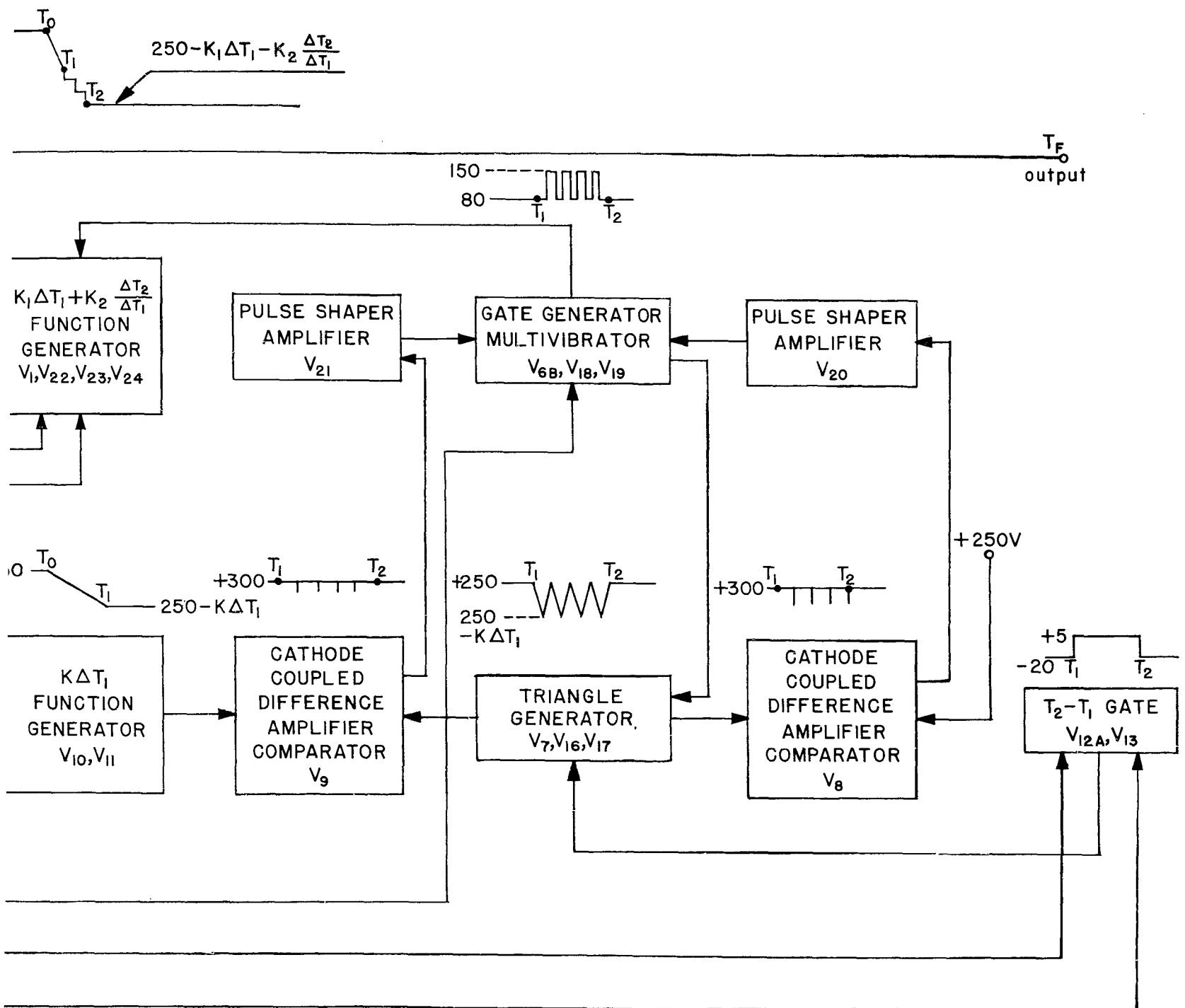
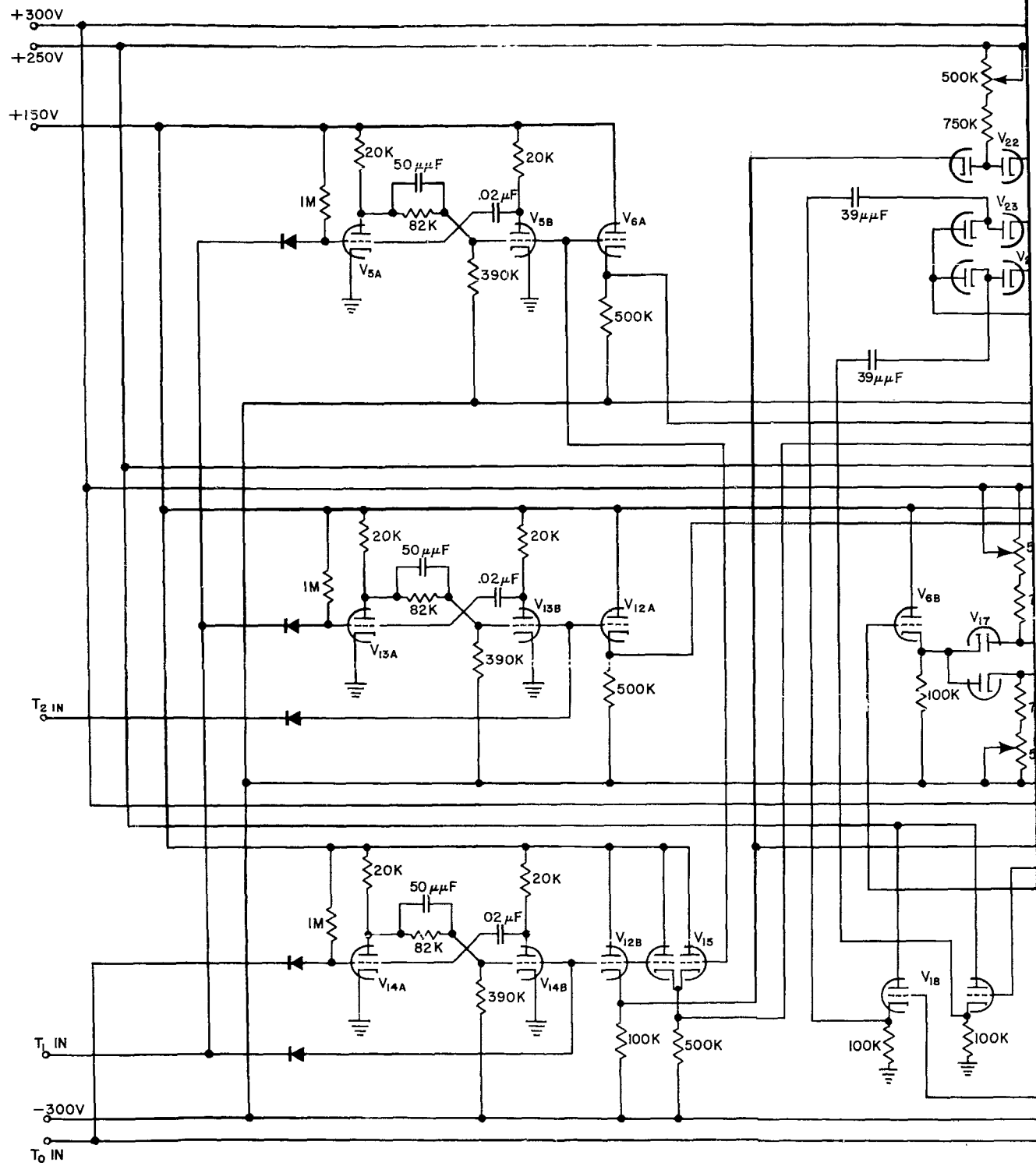


Figure 10-3. Block diagram of firing-time computer

CONFIDENTIAL

1



LEGEND

TUBES	5636	V <sub>1</sub> , V <sub>3</sub> , V <sub>4</sub> , V <sub>7</sub> , V <sub>10</sub>
	6110	V <sub>11</sub> , V <sub>16</sub> , V <sub>17</sub> , V <sub>22</sub> , V <sub>23</sub> , V <sub>24</sub>
	6111	V <sub>2</sub> , V <sub>5</sub> , V <sub>6</sub> , V <sub>8</sub> , V <sub>9</sub> , V <sub>12</sub> , V <sub>13</sub> , V <sub>14</sub> , V <sub>15</sub> , V <sub>18</sub> , V <sub>19</sub> , V <sub>20</sub> , V <sub>21</sub>

NOTES:

1. ALL RESISTORS IN OHMS AND 1/2W UNLESS OTHERWISE SPECIFIED
2. ALL DIODES IN 459 UNLESS OTHERWISE SPECIFIED.

**CONFIDENTIAL**



**Figure 10-4. Circuitry of firing-time computer**

**CONFIDENTIAL**

S AND 1/2W UNLESS OTHERWISE SPECIFIED.  
ESS OTHERWISE SPECIFIED.

The  $T_1$  pulse also activates the  $(T_2 - T_1)$  gate which is also a positive gate in the interval  $(T_2 - T_1)$ . When the  $T_2$  pulse is generated by the sensing-system complex, it is used to terminate the  $(T_2 - T_1)$  gate.

When the  $T_f$  pulse is generated by the computer it is used to terminate the  $(T_f - T_1)$  gate; however, due to the design of the gate, this feature is not required to reset the gate. The computer also requires a gate which runs from  $T_0$  to  $T_f$ , thus generating a  $(T_f - T_0)$  gate.

This is most easily generated by using an "OR" circuit to pass the  $(T_1 - T_0)$  gate or the  $(T_f - T_1)$  gate, whichever is the most positive.

#### 10.4 Divider Operation

(U) The output of the "OR" gate circuit is used to activate the  $K_0 \Delta T_1$  generator. This generator ( $K_0 \Delta T_1$ ) also requires a  $(T_1 - T_0)$  gate which allows the  $K_0 \Delta T_1$  generator to generate a voltage equal to  $K_0 \Delta T_1$ . When the  $(T_1 - T_0)$  gate terminates, the  $K_0 \Delta T_1$  generator switches functions from that of generation to storage. The value of  $K_0 \Delta T_1$  is then stored until the time  $T_f$ . The output of the  $K_0 \Delta T_1$  generator is fed to a comparator. The  $(T_2 - T_1)$  gate is used to turn on the triangle generator (see sec 10.8). The output of the triangle generator is fed to two separate comparators, one to detect the time at which the output attains the value of  $250 - K_0 \Delta T_1$  volts, and the other to detect the time it attains the value of +250 v. When the output of the triangle generator approaches the value  $250 - K_0 \Delta T_1$ , a pulse is generated by the comparator (V9) which is amplified and shaped and used to reverse the state of the gate generator multivibrator. This reversal in state is used to change the slope of the triangle generator from a negative value to a positive value. As the output of the triangle generator approaches +250 volts, the comparator V8 generates a pulse which is amplified and shaped and used to reverse the state of the gate generator multivibrator. The slope of the triangle then switches from a positive value to a negative value. This process is continued throughout the period  $T_2 - T_1$ . The ratio  $\Delta T_2 / \Delta T_1$  is obtained as the number of the pulses obtained from the gate generator multivibrator.

(U) Since the triangle generator will start to function only with a negative slope, it must be insured that the gate generator multivibrator is in the proper state. For this reason, the  $T_0$  pulse is fed into one side of the gate generator multivibrator to set the generator in the proper state.

10.5  $(K_1 \Delta T_1 + K_2 \Delta T_2 / \Delta T_1)$  Generator

(U) The output of the "OR" gate circuit activates the function generator during the interval  $T_f - T_o$ . The presence of the  $(T_1 - T_o)$  gate in the interval allows the circuit to generate the function  $K_1 \Delta T_1$ . When the  $(T_1 - T_o)$  gate terminates, the circuit switches from the generator to the storage state. In the interval  $T_2 - T_1$ , the pulses from the gate generator multivibrator are fed to the function generator which then has the form of a digital-analog converter due to the circuitry configuration (see section 8.8). In this way, the functions  $K_1 \Delta T_1 + K_2 \Delta T_2 / \Delta T_1$  are generated. The output of this function generator is fed to the Amplified Direct-Coupled Diode Comparator (ADCDC, Section 10.9).

10.6  $(K_3 + \Delta T_2 + \Delta T_f)$  Function Generator

(C) The output of the  $(T_f - T_1)$  gate is used to initiate the  $(K_3 + \Delta T_2 + \Delta T_f)$  function. The constant  $K_3$  is merely a shift in the starting point of the sweep. The output of the generator is also fed to the ADCDC, which detects the time at which the two functions,

$$K_3 + \Delta T_2 + \Delta T_f \text{ and } K_1 \Delta T_1 + K_2 \Delta T_2 / \Delta T_1,$$

are equal in magnitude. At this time, which is the desired firing time  $T_f$ , the firing pulse is generated.

10.7 Computer Design

(C) The accuracy of the system and therefore of the computer is defined as the maximum tolerable error in the position of the missile when the firing pulse is generated. With the missiles provided for the feasibility test, the accuracy of the computer was limited to  $\pm 1/2$  in. This corresponds to a maximum permissible error in time  $T_e$  of the firing time  $T_f$  and is given by:

$$T_e = \frac{\Delta D}{V_m} \text{ sec} \quad (10.5)$$

where  $\Delta D$  is the maximum displacement error of the missile in feet, and  $V_m$  is the attacking missile velocity in feet per second. For a missile with a velocity of 5000 fps, the error must be no greater than  $\pm 8.3$   $\mu$ sec (see figure 10-5).

CONFIDENTIAL

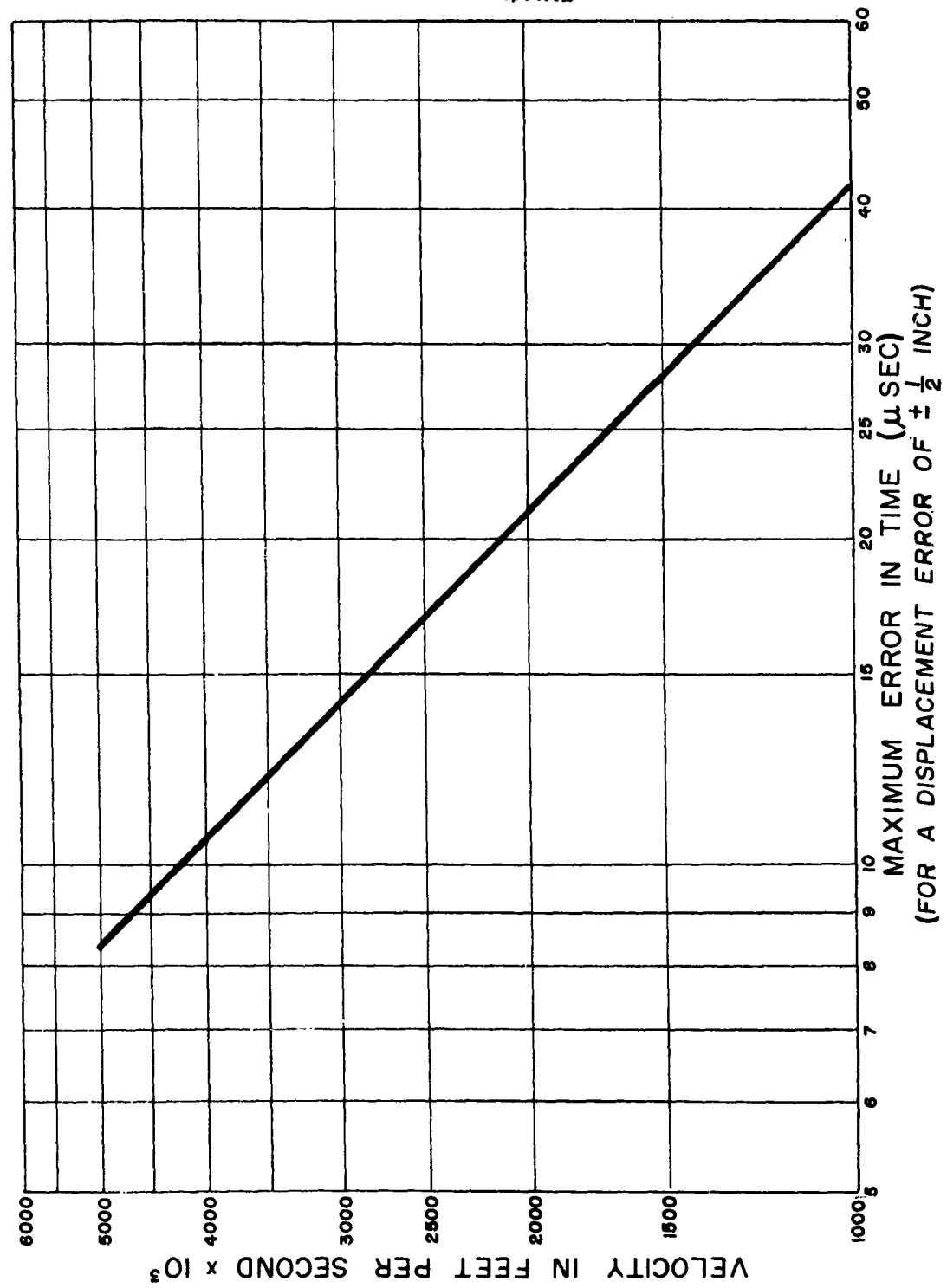


Figure 10-5. Maximum permissible error in time versus missile velocity (FOR A DISPLACEMENT ERROR OF  $\pm \frac{1}{2}$  INCH)

CONFIDENTIAL

## CONFIDENTIAL

(C) Since the maximum error is limited to  $\pm 8.3 \mu\text{sec}$  for a 5000 fps missile, the comparator must operate with an error voltage  $V_e$  of less than  $V_e = 8.3 \mu\text{sec} \cdot 4.99 \times 10^{-2} \text{V}/\mu\text{sec} = 0.414 \text{ v}$ . The silicon diodes used as the main comparators have a region of uncertainty of 0.6 v. However, since both the reference voltage  $E_r$  and the input signal  $e_i$  are amplified by the differential amplifier, the region of uncertainty of the diodes is effectively reduced by the gain of the amplifier. A nominal gain of 20 can be assumed for the amplifier. Therefore, the region of uncertainty is reduced to  $\pm 0.6/20 = \pm .03 \text{ v}$  which is well within the permissible error.

(U) The high degree linearity required for accuracy in the computer dictates the choice of Miller sweep circuits (figure 10-6) which combine high linearity and simple circuitry. The dynamic output voltage of a Miller sweep may be expressed as:

$$e_p = E_{bb} t/RC \quad (10.6)$$

The form of the equation just shown is similar to the form of the computer equation in the active intervals, so that the coefficients may be equated to determine the physical values of R and C.

### 10.8 Divider Design

(U) The division, as mentioned previously, is a quantized division where the number of pulses out of the divider is in proportion to the ratio  $\Delta T_2/\Delta T_1$ . The division is done using a circuit which generates the waveforms shown in figure 10-7. First, a voltage  $K_0 \Delta T_1$  is generated which sets a reference level, then a triangle generator is initiated whose period is a function of  $K_0 \Delta T_1$ . Defining

$$\tan \alpha = \Delta T_2/nK_0 \Delta T_1 \quad (10.7)$$

then

$$n = 1/K_0 \tan \alpha \cdot \Delta T_2/\Delta T_1 \quad (10.8)$$

which shows that the number of comparison points at  $e_p = E_{bb}$  and

$e_p = -K_0 \Delta T_1 + E_{bb}$  is a digital indication of the ratio  $\Delta T_2/\Delta T_1$ .

The gate which switches the slope of the triangle generator is also used to drive an operational step generator\* (see figure 10-8). The operational step generator is used to convert the digital representation of  $\Delta T_2/\Delta T_1$  to an analog representation.

\*J. Millman, H. Taub, Pulse and Digital Circuits, Mc-Graw-Hill Book Co., N.Y., 1956, page 467.

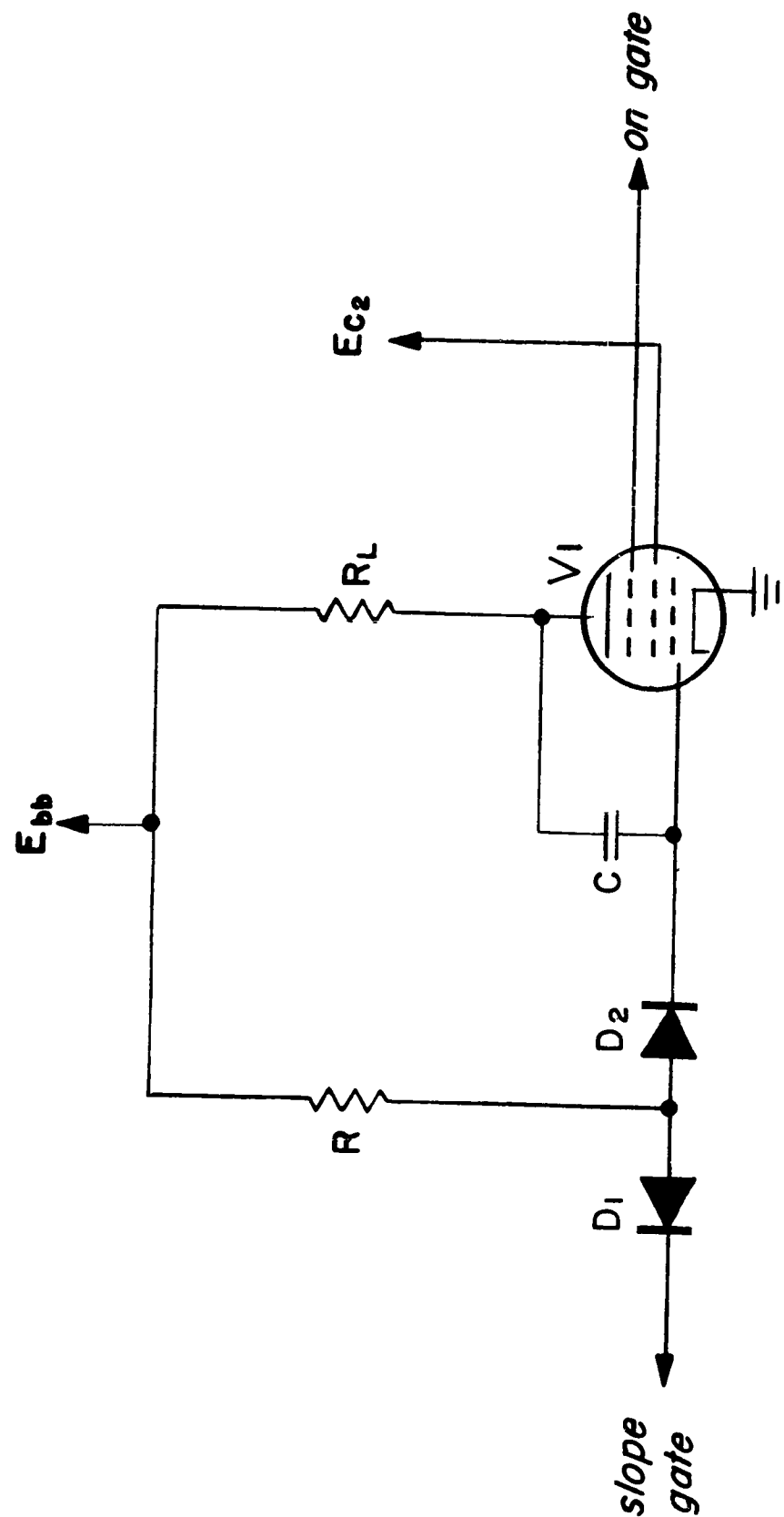


Figure 10-6. Miller sweep circuit with storage

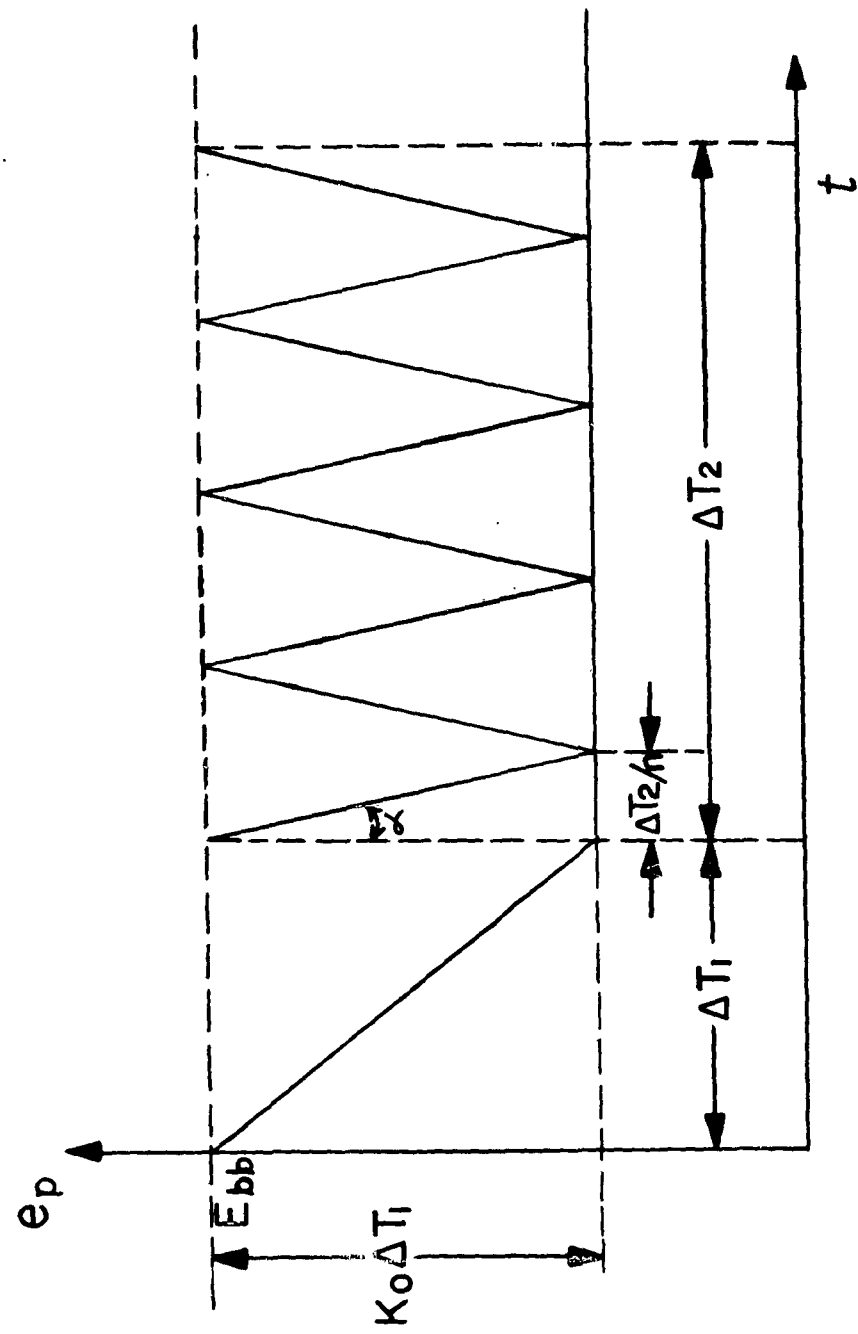


Figure 10-7. Waveform of function generated in divider

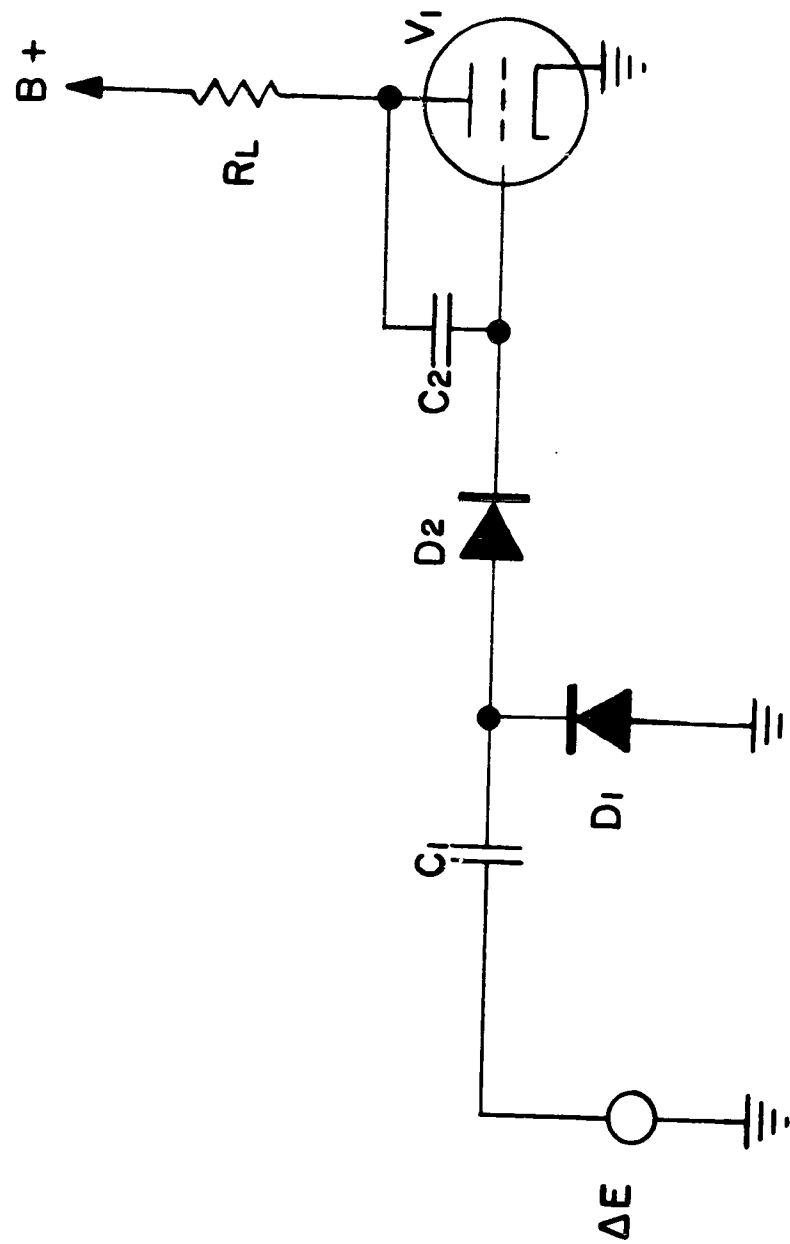


Figure 10-8. Operational step generator

(U) A unique feature of the function generator is the method by which the value of the function is stored (see figure 10-6). The circuit is a conventional suppressor-gated Miller sweep with the exception of diodes  $D_1$  and  $D_2$ . If the suppressor is at -20 v and the cathode of  $D_1$  is at +5 v, then  $D_1$  will be reverse biased,  $D_2$  forward biased, and the grid of the Miller sweep will be in clamp due to the plate current cut-off. Assume the suppressor of  $V_1$  is brought to 0 volts; the plate voltage will drop according to

$$e_p = -\frac{E_{bb} t}{(R + r_{PD_2})C} + E_{bb} \quad (10.9)$$

After a time  $T$ , a voltage of -10 v is applied to the cathode of  $D_1$ , causing  $D_1$  to become forward biased and  $D_2$  to become reverse-biased. Therefore  $r_{PD_2} \rightarrow \infty$ , causing

$$e_p = -\frac{E_{bb} T}{(R + r_{PD_2})C} + E_{bb} \quad (10.10)$$

which is a constant after the interval  $T$ .

(U) The triangle generator, figure 10-9, as used in the divider, uses the same principle as the Miller sweep with storage. Assume the suppressor grid of  $V_1$  is at -20 v and the slope gate voltage is at +5 v;  $D_1$  is reverse biased,  $D_2$  forward biased, and  $D_4$  reverse biased, and the grid of  $V_1$  is in clamp. A positive gate is then applied to the suppressor of  $V_1$  causing the plate voltage to drop as

$$e_p = -\frac{E_{bb} t}{(R_1 + r_{PD_2})C} + E_{bb} \quad (10.11)$$

A voltage of -10 v is applied at time  $T$  to the slope gate;  $D_1$  is then forward biased and  $D_2$  is reverse biased, causing  $r_{PD_2} \rightarrow \infty$ , but at the same time  $D_4$  becomes forward-biased, leading to

$$e_p = -\frac{E_{bb} T}{(R_1 + r_{PD_2})C} + \frac{E_{bb} (t - T)}{(R_2 + r_{PD_4})C} + E_{bb} \quad (10.12)$$

If this process is continued the triangular wave is generated.

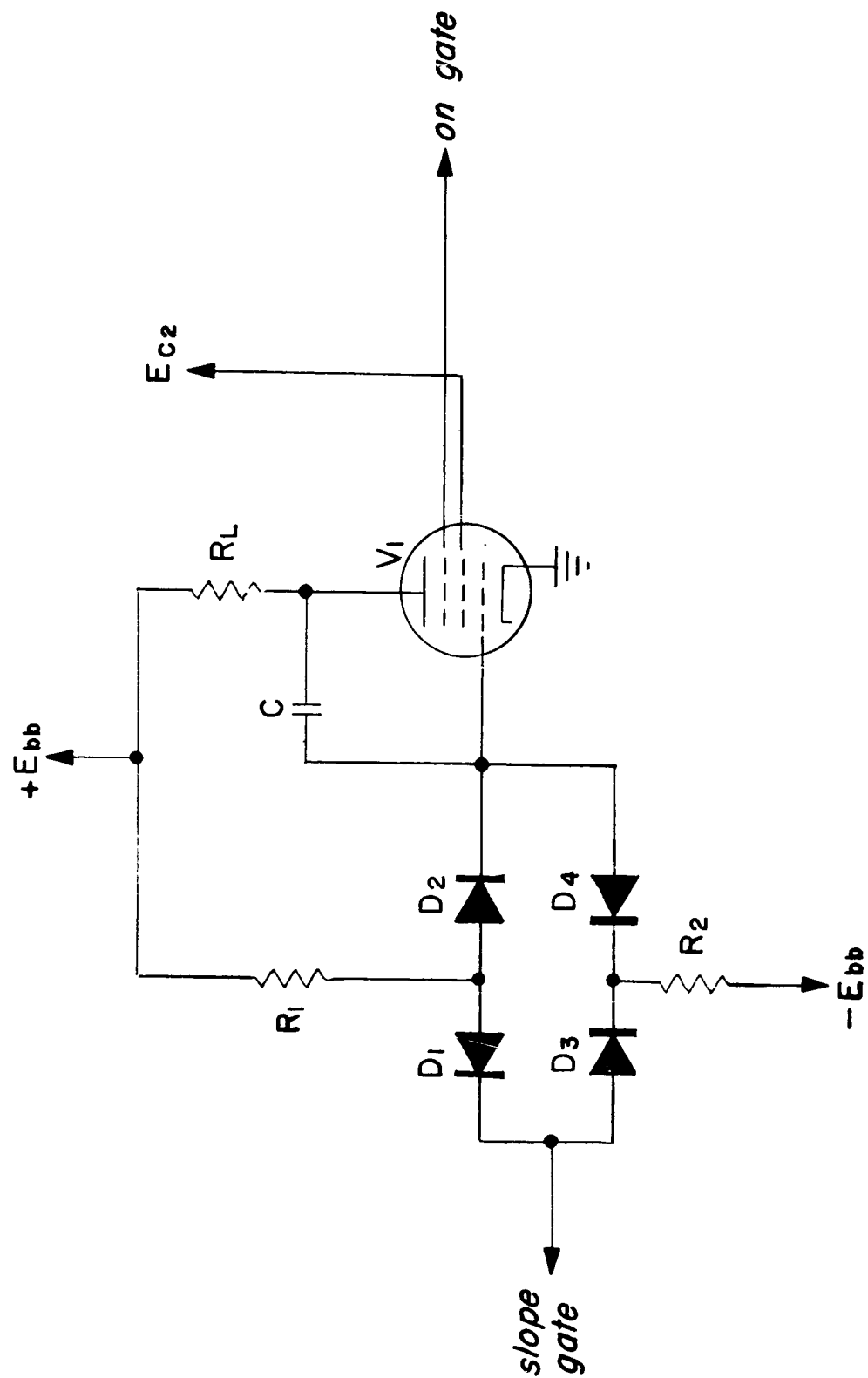


Figure 10-9. Triangular-sweep generator

## CONFIDENTIAL

### 10.9 Comparators

(C) Two types of comparators are used in the firing-time computer, depending upon the accuracy required. They are the cathode-coupled difference amplifier, figure 10-10, and an amplified direct coupled diode comparator (ADCDC), figure 10-11.

(U) In the cathode-coupled difference amplifier comparator, the plate current cutoff of one tube ( $V_1$ ) is used to indicate the time at which the input signal  $e_i$  approaches  $E_r$ . Two serious drawbacks of such a comparator are that the grid-to-cathode voltage for plate current cutoff is a function of plate-to-cathode voltage and also of filament voltage. Since there is a large fluctuation of plate-to-cathode voltage due to the large dynamic range of  $E_r$ , it is obvious that the accuracy of the comparison will be affected. A preliminary analysis of this comparator shows that for a shift of  $E_r$  from 250 v to 50 v the shift in the comparison point will be approximately 0.5 v which seriously affects the accuracy of the computer.

(U) The ADCDC is designed to reduce the errors that are due to the large dynamic range of  $E_r$  and filament voltage fluctuations. In the ADCDC, the above errors are theoretically zero because of the balanced feature of the comparator. It requires only that when the difference in grid voltages is zero, the difference in plate voltages must also be zero. The waveshapes as used in the comparator are illustrated in figure 10-12. The peak of the triangle of  $e_o$  is the point at which  $e_i = E_r$ . By differentiating the triangle the peak can be determined.

### 10.10 Gates

(U) The gates used in the computer are of the monostable multivibrator type, figure 10-13. This type is used due to the automatic reset which allows the computer to be ready to function even as shortly as 10 msec after a transient in one channel.

### 10.11 Computer Adjustment

(U) The adjustment of the computer is accomplished by inserting accurately defined time differentials  $T_1$  and  $T_2$  into the computer and by adjusting the appropriate trimmers so that the  $T_f$ 's supplied by the computer equal those calculated numerically from the firing-time equation (10.13) in section 3.6.  $\Delta T_1$  and  $\Delta T_2$  are taken from a time differential generator.

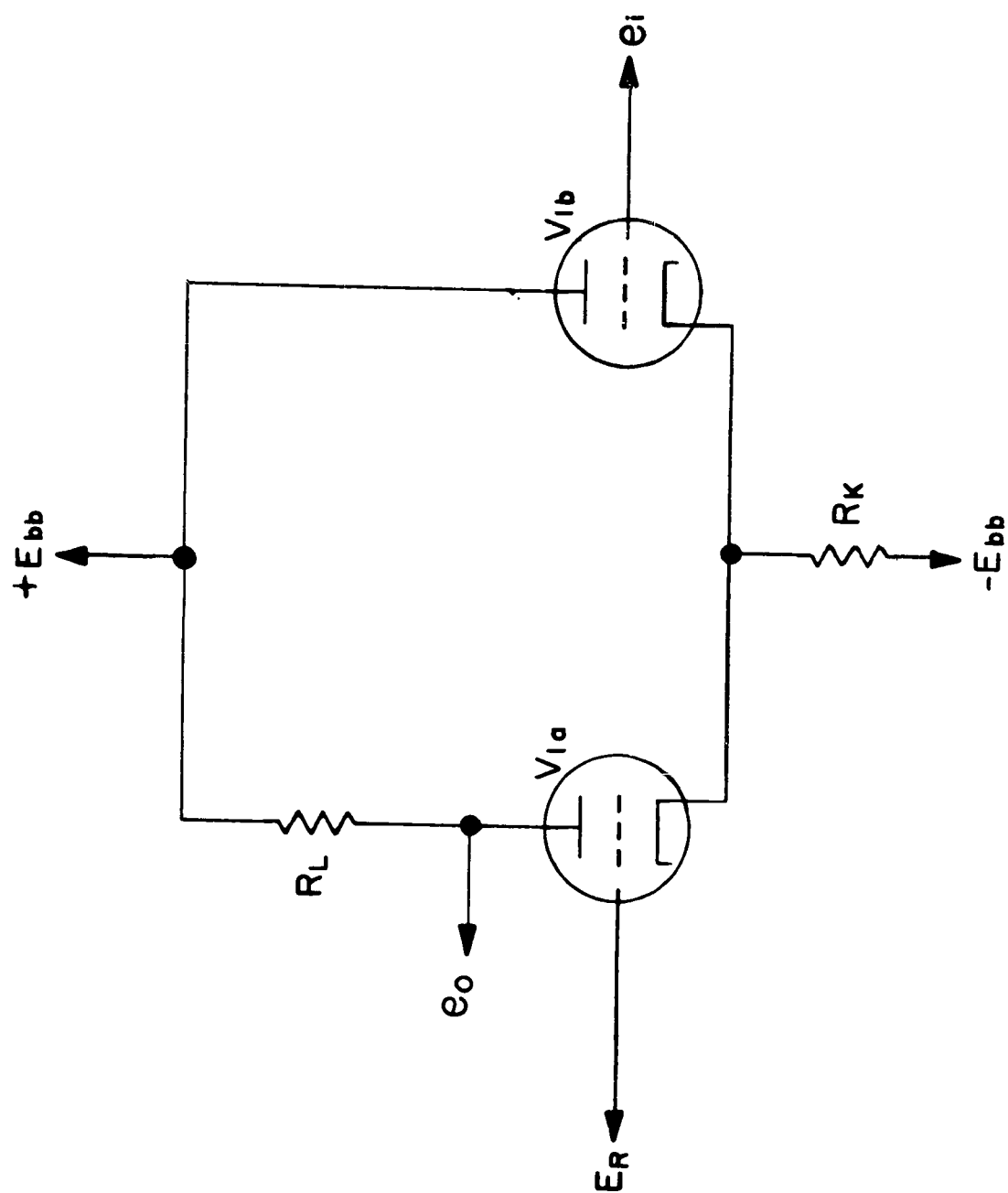


Figure 10-10. Cathode-coupled comparator

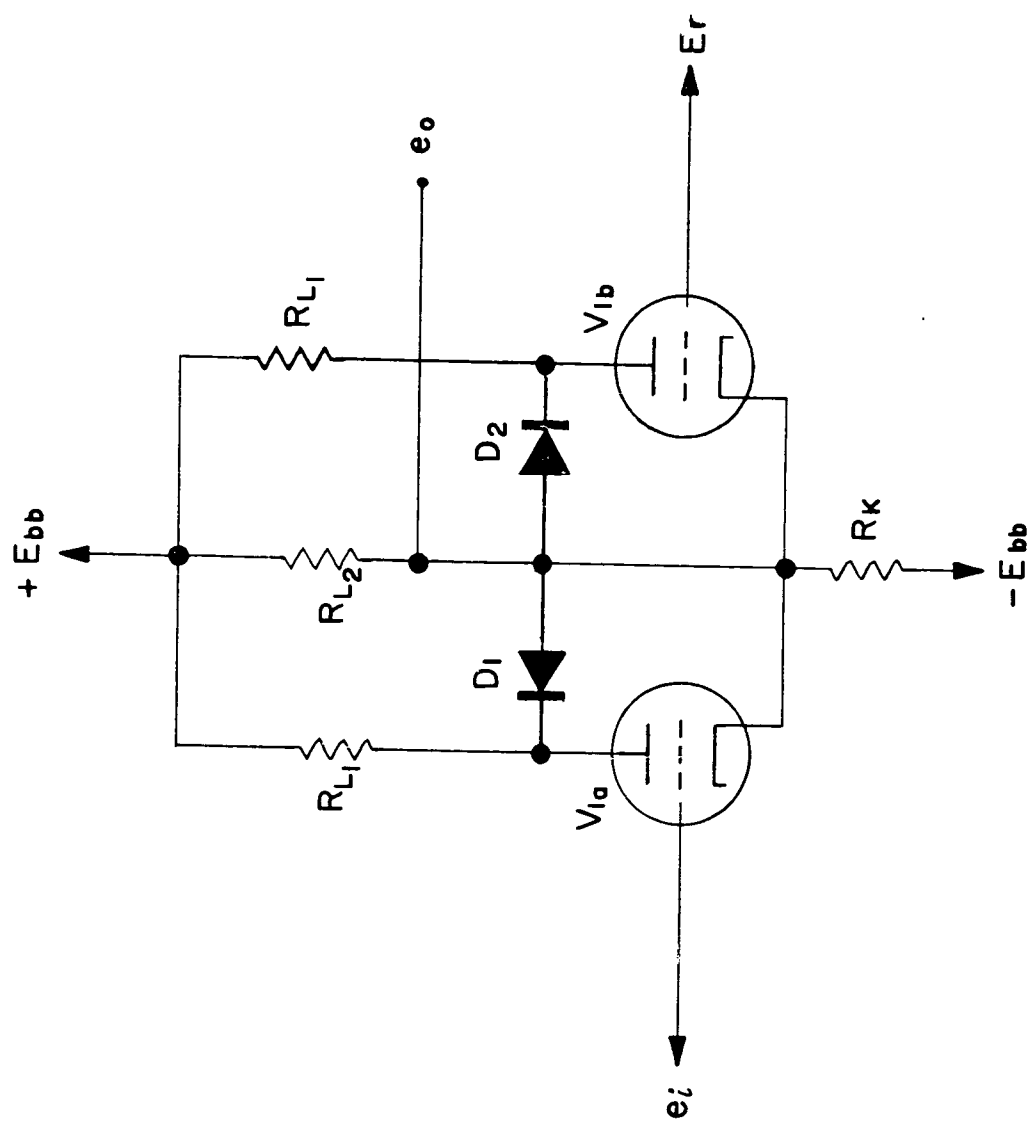


Figure 10-11. Amplified direct-coupled diode comparator (ADCDC)

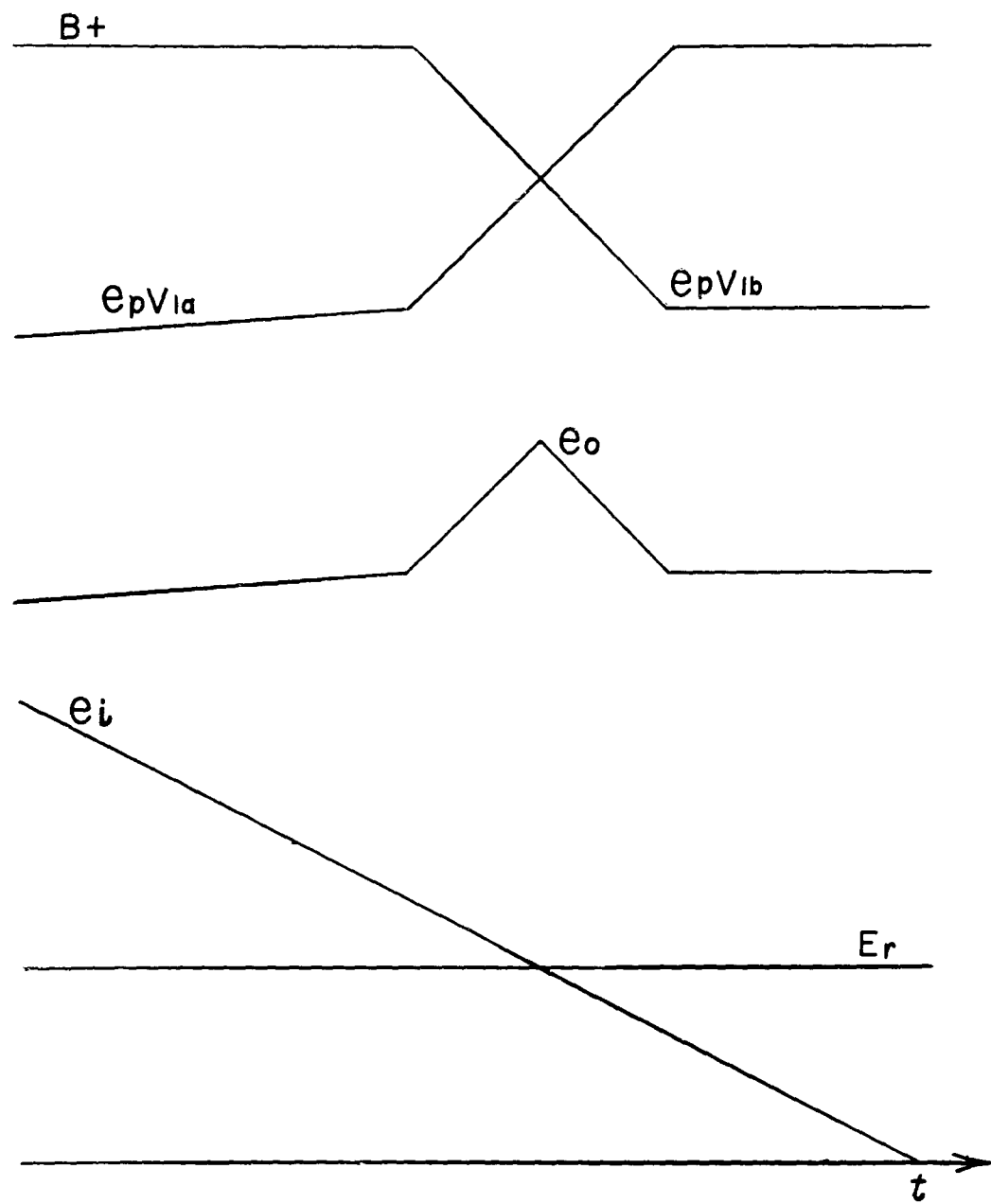


Figure 10-12. Waveforms of ADCDC of Figure 10-11

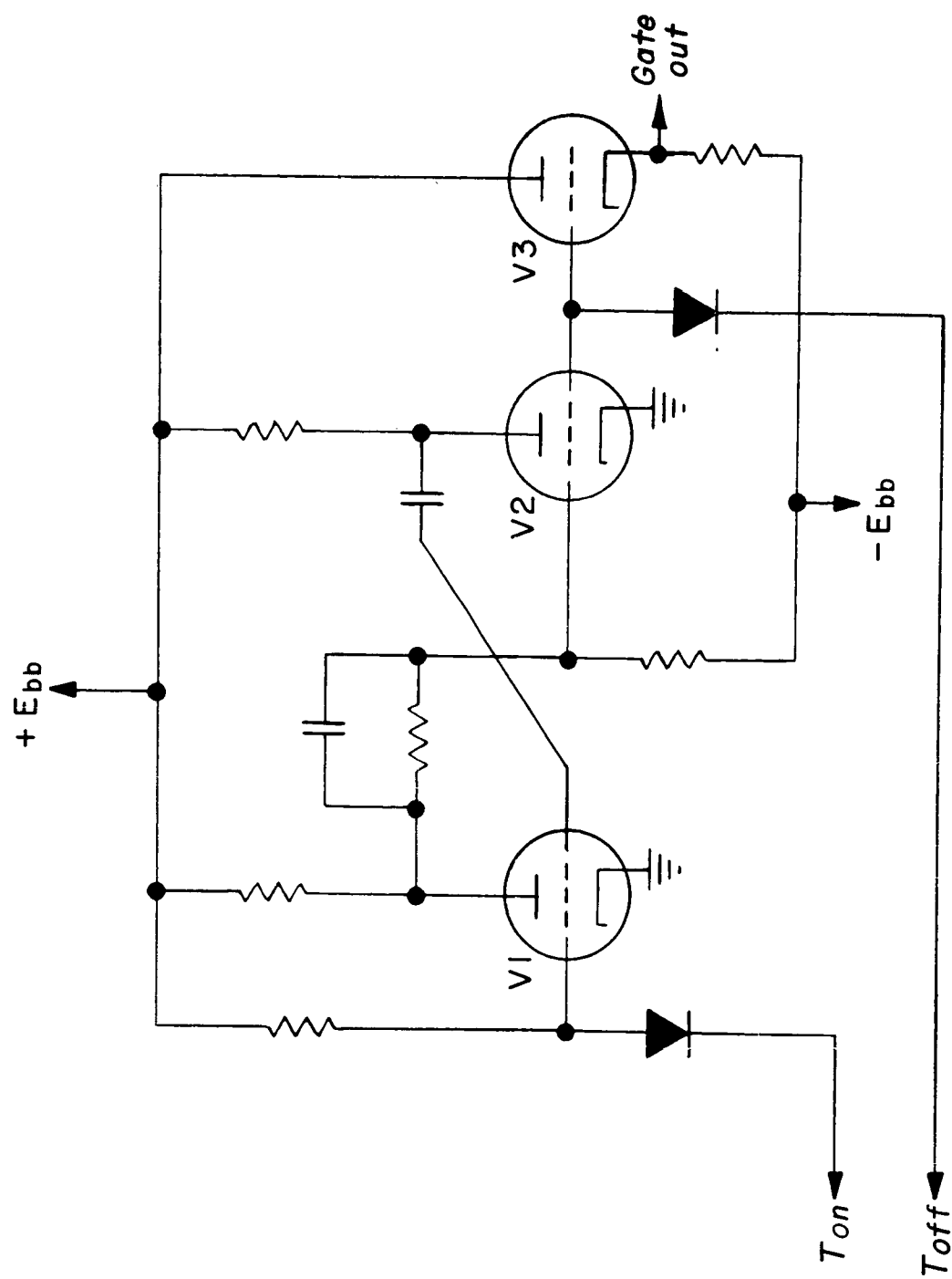


Figure 10-13. Monostable gate generator

**SECRET**

(U) The following procedure is applied to adjust the divider (section 10.8).

1.  $\Delta T_1$  is set to 800  $\mu\text{sec}$  and  $\Delta T_2$  to 400  $\mu\text{sec}$ .
2.  $K_0 \Delta T_1$  is so adjusted that the total sweep voltage of the  $K_0 \Delta T_1$  generator is 195 v.
3.  $K \Delta T_x$  and  $-K \Delta T_x$  are adjusted so that each half-period of the triangular wave is 20  $\mu\text{sec}$ .

(U) With the divider adjusted, the main functions may now be adjusted. There must be three sets of times  $\Delta T_1$ ,  $\Delta T_2$  and  $\Delta T_f$  to uniquely determine constants of the computer, since there are three independent constants in the equation. The following procedure is followed:

1.  $\Delta T_1$  is set to 200  $\mu\text{sec}$  and  $\Delta T_2$  100  $\mu\text{sec}$ .  $K_3$  is adjusted so that  $\Delta T_f$  is 264  $\mu\text{sec}$ , as required by the firing-time equation.
2.  $\Delta T_1$  and  $\Delta T_2$  are set to 200  $\mu\text{sec}$  and 400  $\mu\text{sec}$  respectively.  $K_2 \Delta T_2 / \Delta T_1$  is so adjusted that  $\Delta T_f$  is 479  $\mu\text{sec}$ .
3.  $\Delta T_1$  and  $\Delta T_2$  are both set to 800  $\mu\text{sec}$ . The  $\Delta T_2$  trimmer so adjusted that  $\Delta T_f$  is 2559  $\mu\text{sec}$ .
4. The above operation is repeated until the computer is adjusted.

#### 10.12 Field Test Results

(S) In field tests conducted at the DOFL Test Area the computer was tested with rounds whose velocity ranged from 1400 fps to 2600 fps. Over this range of velocity the computer exhibited an average error of  $-0.20$  inches  $\pm$  0.35 inches in determining the proper point at which to initiate the line charge to defeat the attacking missile.

Figures 10-14, 10-15, and 10-16 are front, top, and bottom views respectively, of the completed computer.

**SECRET**

185

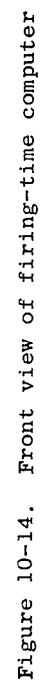




Figure 10-15. Top view of firing-time computer

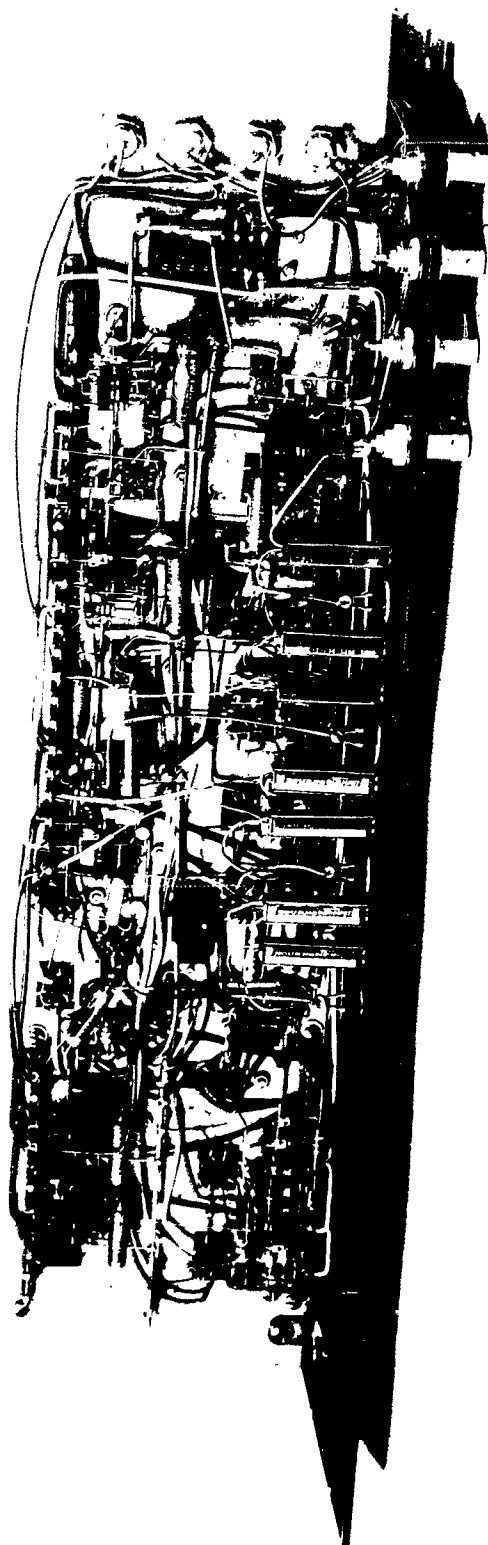


Figure 10-16. Bottom view of firing-time computer

# SECRET

## 11. CHARGE-SELECTING COMPUTER

W. Moore

- (S) The charge-selecting computer was designed and built under contract by International Business Machine Corporation, Federal Systems Division, Kingston, New York. Its purpose was to determine which defending charge in the array should be fired to intercept the trajectory of the attacking round.

### 11.1 Approach to Selection Problem

(S) For the system geometry used, the problem was reduced to a geometrical determination of the various combinations of pickets in the A fence and B fence which lie on any straight line which passes through a particular charge in the array. Figure 11-1 is an illustration of this principle. Three trajectories are shown as examples. In this case, trajectory No. 1 passes through picket A-12 and B-10 and also over charge C-2. Trajectory No. 2 passes through picket A-5 and B-5 and this combination also passes over charge C-2. Thus, there are many combinations of pickets which lie on a line which passes over each particular charge.

(S) For a given geometry of pickets and charges, these combinations may be tabulated and used to form the basis of a system for selection. The total number of combinations may be reduced by other restrictions on the system, e.g., trajectory No. 3 in the figure passes through A-10, B-7 and charge C-1, but this trajectory will not intercept the defended plate. Under such conditions this combination need not be included in the system. This reduces the total number of combinations which must be "stored" or wired into the circuitry.

(S) The selection is somewhat more complicated than this simple example may indicate, because of the finite widths of the attacking rounds, detection pickets, defending charges and spacing between such elements.

(S) It can be seen that an attacking round may, due to its diameter, pass through more than one picket in each fence. Also, the trajectory may pass between two defending charges. In such cases, the system must make a choice between a set of combinations and select one of the two charges, if it is not desirable to fire both charges simultaneously.

(U) The problem of selecting one of many pickets traversed has been attacked in this system by choosing that picket which lies closest to the center of the traversed set, or, when only two are traversed, by selecting either the right hand or left hand picket each time. Whether it will be the right or left one, depends upon the particular geometry and angle of the attacking round.

SECRET

189

SECRET

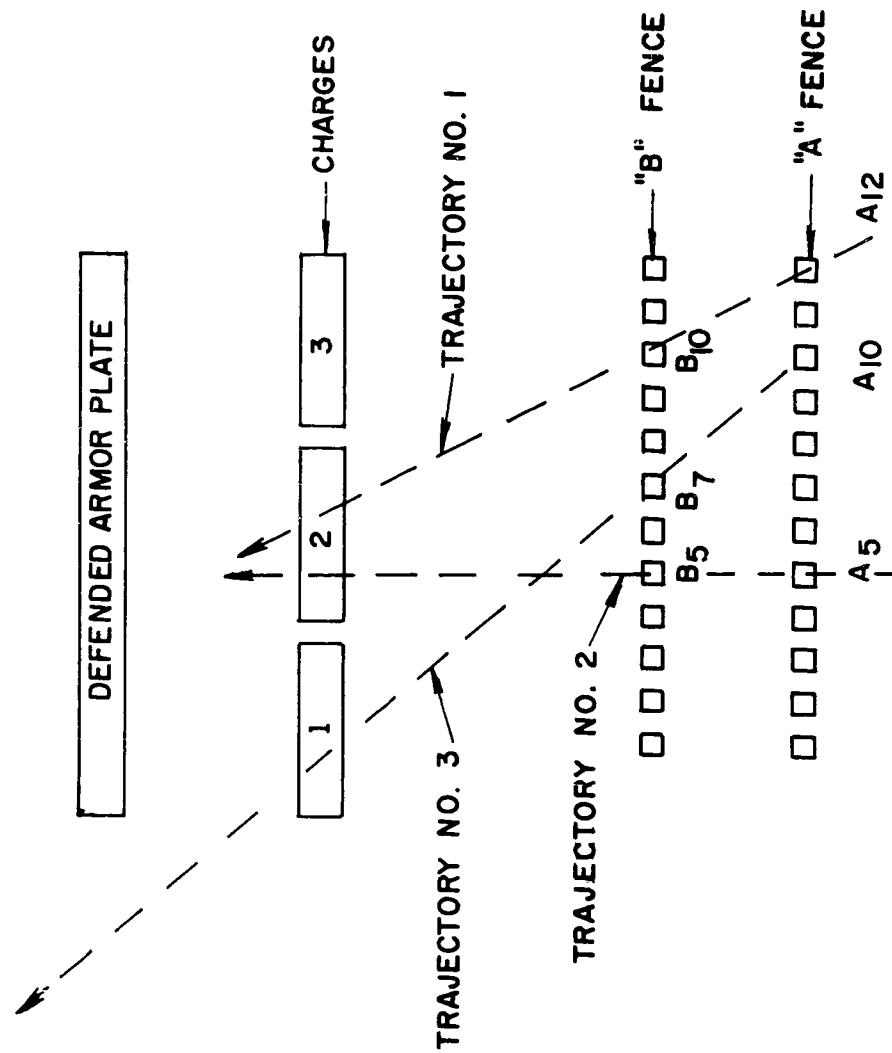


Figure 11-1. Charge selection geometry

SECRET

## SECRET

(C) When this selection has been made the choice must then be used to direct or "steer" a pulse from the firing time computer (section 10) to the proper defending charge, or to the high voltage firing circuitry associated with this defending charge.

(S) The manner in which this selection computer functions requires individual inputs from each of the optical detection units in the A fence and the B fence. For the feasibility test geometry, there are 84 optical units in each of these fences, making a total of 168 inputs to the charge selection computer. The proposed system required 12 defending charges and, therefore, directed its outputs into any one of 12 positions.

### 11.2 Input Storage

Figure 11-2 is a block diagram of the fundamental sub-units of the charge selection computer and their arrangement. As shown, it comprises two input sections, one for the A fence and one for the B fence. Each input section consists of 84 magnetic cores and associated drive circuitry for storing the information concerning which optical pickets were intercepted by the projectile.

(U) Each input section A and B has an associated unit for center resolution. The center resolution circuitry performs the functions necessary to select the approximate center of all inputs in a given fence and then clears all information stored in the input cores except that stored in the selected center input core. The center selection made in both A and B fences is then fed to the charge selection matrix.

(C) The charge selection matrix takes the A and B information and gives an output corresponding to the desired charge. This output is then fed to the output buffer register which stores the information regarding the proper charge until the firing pulse from the firing-time computer arrives. The output buffer register has conditioned the proper gate circuitry to allow the firing pulse to be passed on to the defending charge firing circuitry.

### 11.3 Center Resolution

(U) It was stated that under certain conditions the attacking round may traverse several optical pickets in a given fence and a selection has to be made to find the center picket. This is done by the selection computer in the center resolution circuitry. A block diagram of the logic associated with the center resolution problem is shown in figure 11-3. The number of pickets which could be traversed is a function of the attacking round size, and angle of attack. It was found that the maximum number of pickets traversed by existing ammunition up to 106 mm and 60° angle of attack was fifteen.

SECRET

191

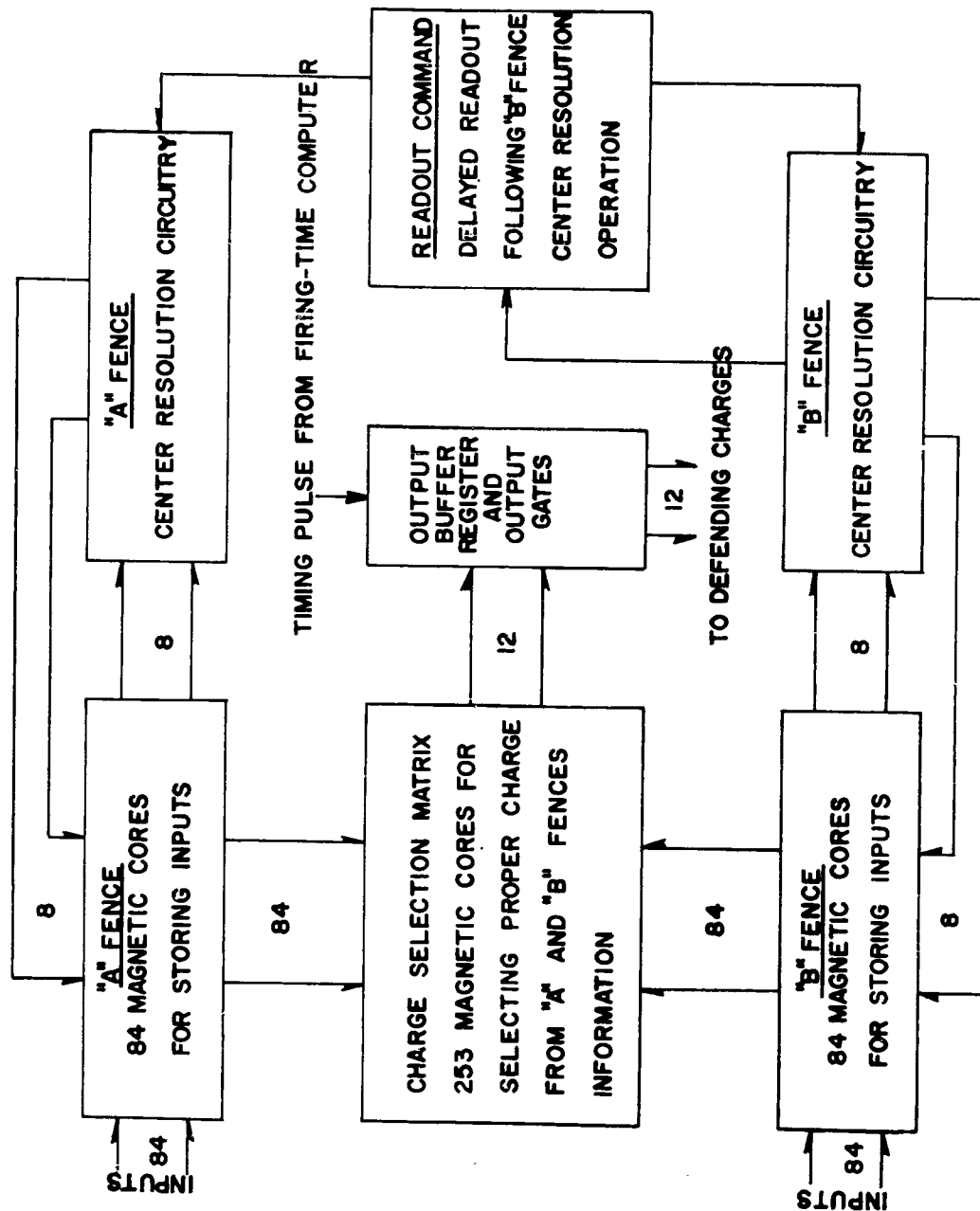


Figure 11-2. Logic diagram of charge-selection computer

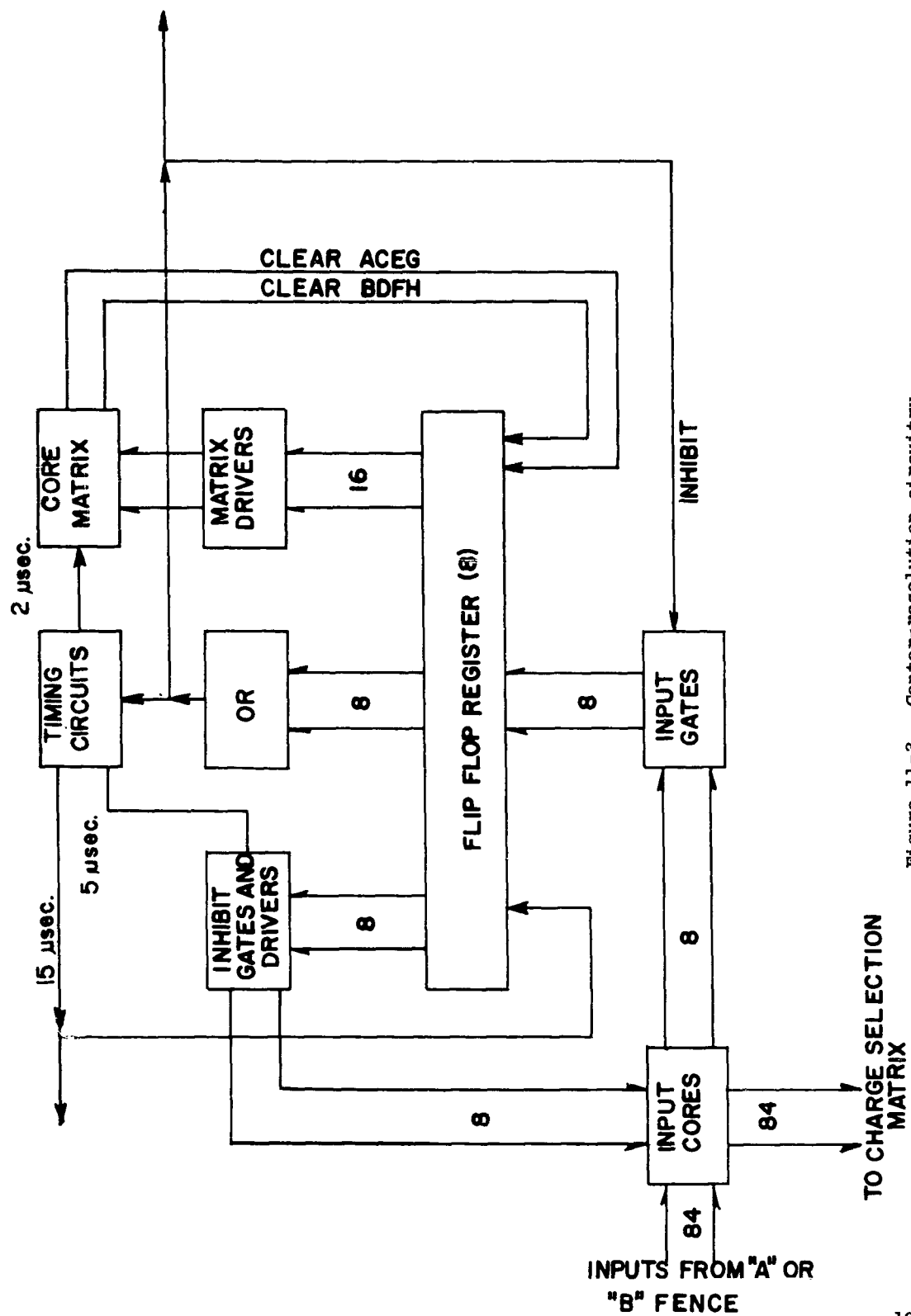


Figure 11-3. Center-resolution circuitry

(U) In each fence A or B, there are 84 pickets. The information from the individual pickets traversed in the A fence must be retained until the information is received from the B fence. This is done by having a magnetic core for each picket in the fence. When a picket is intercepted by the attacking round, the state of the core is switched and held. Since a maximum of 15 pickets can be intercepted in any fence, it is possible to switch 15 cores in the A fence and 15 cores in the B fence. Of the 15 cores set in a given fence, it is desired to select that core which corresponds to the picket which was closest to the center of the group covered.

(U) In figure 11-4 is a sample of how these cores are arranged. As shown, each of the inputs is associated with one single core, 84 for a given fence. The readout lines are linked with every ninth core in the set. If the maximum number of cores set in a fence is 15, then there are 7 readout lines each with 2 cores set and 1 readout line with one core set. It will be noticed that the readout line with one core set also corresponds to the center picket in the group covered. It can be shown that for any number of cores set, from 1 to 15, the desired core will always be on a readout line with only one set core.

(U) It is also shown that every ninth input line shares a common load resistor. Thus, there are a total of eight load resistors. When current is driven through the input line to set a core, there is a voltage drop across its load resistor. These eight load resistors establish the eight lines shown in the logic diagram (figure 11-2) which connect the input cores to the input gates and thence to eight flip-flops in the center resolution register. Each line is associated with an individual flip-flop.

(U) Since it is possible to receive or set 15 inputs, all eight flip-flops in the center resolution register can be set. However, this is not permitted to happen. From the geometry and available ammunition, it was determined that the inputs from the adjacent detection pickets traversed are not received simultaneously, but require intervals of 50  $\mu$ sec or longer. In general, the picket which corresponds to the center line will be one of the first traversed. An interval of time approximately 3 to 4  $\mu$ sec after the first input is received is usually sufficient to allow a maximum of three cores to be set. This fact is used to prohibit the setting of more than three flip-flops in the center-resolution register. When the initial flip-flop is triggered an output is taken off through the "OR" circuit shown and is used to inhibit any further inputs from reaching the flip-flop register. The time required for this action is about 3 to 4  $\mu$ sec.

(U) The three inputs which are retained in the flip-flop register come from a set of pickets which are in numerical order, such as A-3, A-4, A-5 or A-17, A-18, A-19, etc. From the geometry, the middle picket of this group is in general the one closest to the center line of the trajectory.

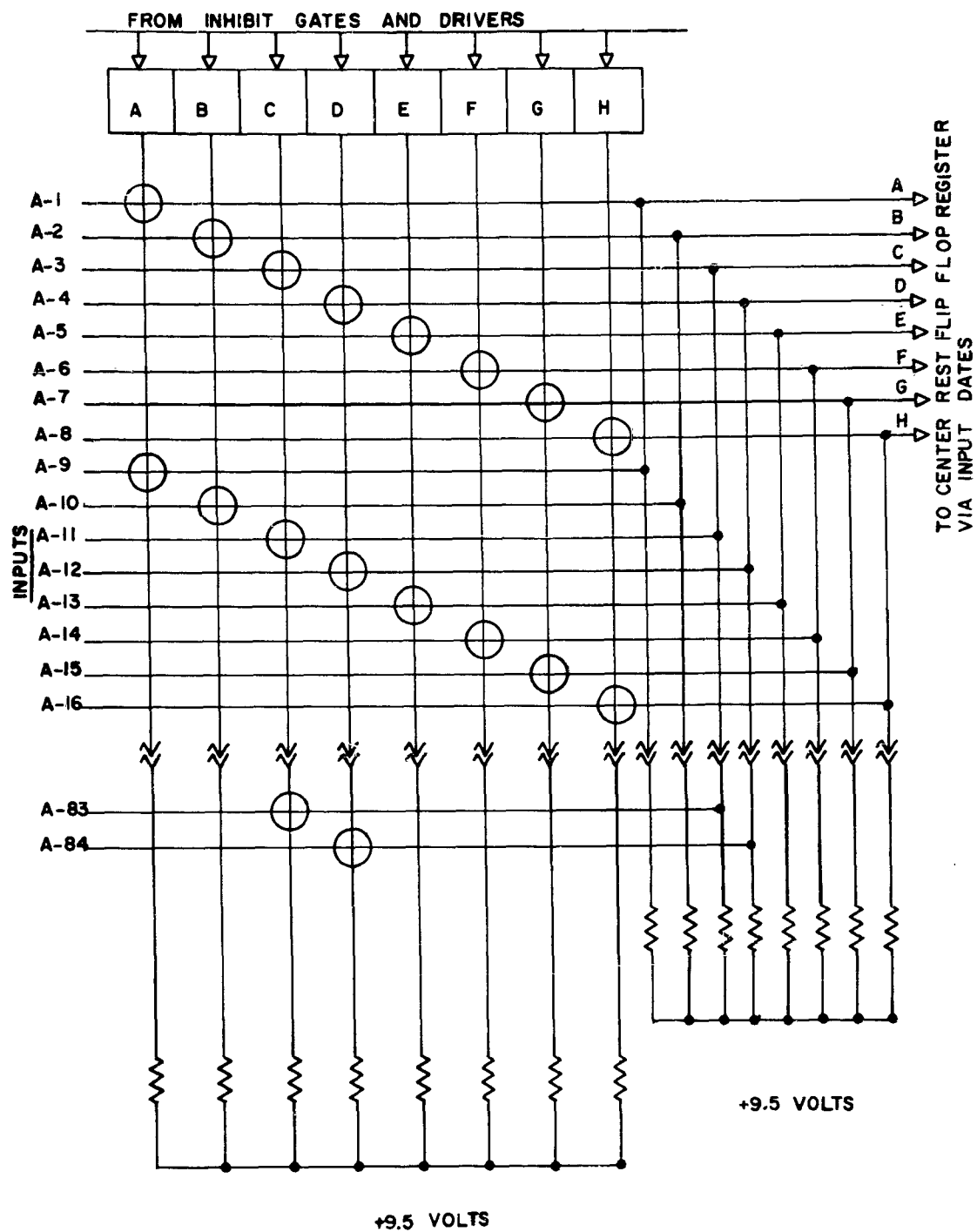


Figure 11-4. Arrangement of magnet cores in center-resolution circuitry

(U) In short, even though 15 pickets are covered and 15 input cores are set, there is a maximum of only three flip-flops set in the center-resolution register.

(U) The next step is to resolve the center one of the three in the register and clear all input cores except the one corresponding to the center picket. This is performed in the center-resolution core matrix

(U) Remembering that every ninth input shares a common load (figure 11-4), there are established groups consisting of eight inputs in a group. The individual inputs in a group are labeled A, B, C, D, E, F, G, and H, with the next group repeating the same series, i.e., A, B, etc. The flip-flops in the register are also designated in this manner, corresponding to their associated inputs.

(U) The center-resolution core matrix consists of eight cores, associated with and driven from the flip-flop register. A schematic diagram of the manner in which these cores are arranged is shown in figure 11-5.

(U) Since each flip-flop has two states, zero and one, these are used to indicate whether A, B, C, etc. was or was not intercepted. The two states of the flip-flop are designated "A" and "Not A", written hereafter "A" and " $\bar{A}$ ".

(U) The center-resolution core matrix contains windings from both sides of the flip-flop; that is, a winding for A and  $\bar{A}$ , B and  $\bar{B}$ , etc. These windings are not on the same core, but are so arranged that each core consists of a set of three windings associated with the flip-flops as tabulated below:

<u>Core No.</u>	<u>Windings</u>
1	H $\bar{A}$ $\bar{B}$
2	A $\bar{B}$ $\bar{C}$
3	B $\bar{C}$ $\bar{D}$
4	C $\bar{D}$ $\bar{E}$
5	D $\bar{E}$ $\bar{F}$
6	E $\bar{F}$ $\bar{G}$
7	F $\bar{G}$ $\bar{H}$
8	G $\bar{H}$ $\bar{A}$

(U) In addition, each core has two additional windings, one for inhibit or reset, and one to sense the state of the information in the core. The latter windings are used to clear unwanted information in the flip-flop register.

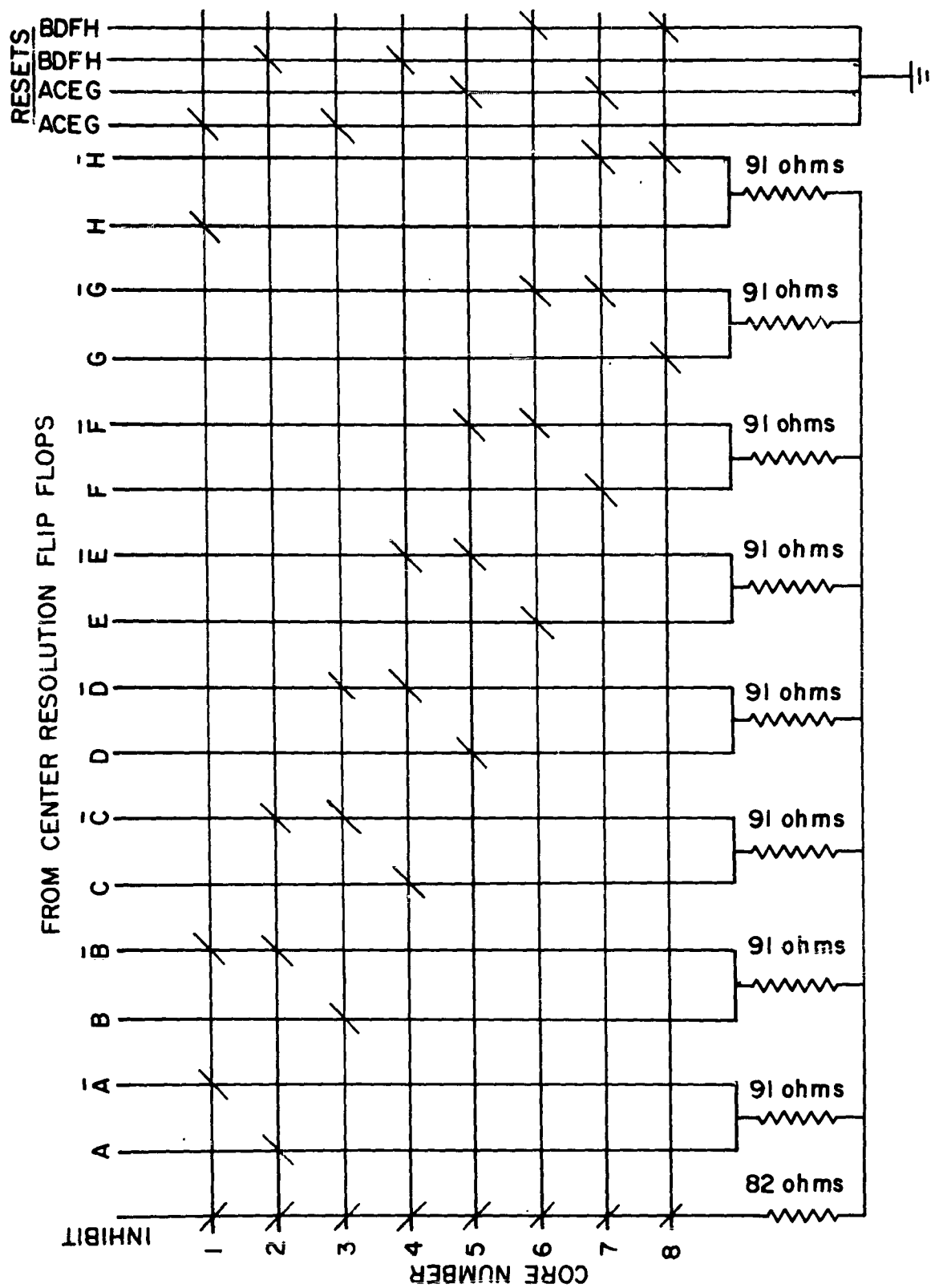


Figure 11-5. Center-resolution core matrix

(U) As stated previously, the flip-flops set will be in a sequence, such as A-3, A-4, A-5, or by the group designation CDE, EFG, or GHA. It is not necessary that there be three in the sequence, for only one or two may be set, e.g., DE, GH, AB when two are set.

(U) The center-resolution core windings tabulated are conditioned in the initial or reset state such that all "Not" windings are energized. Thus, each core has the equivalent of two units of current drive, where one unit of current is sufficient to switch the state of the core. The inhibit windings, when driven, supplies a negative unit of current, i.e., in such a direction to oppose the flux established by the flip-flop drive current.

(U) To illustrate this, assume the initial conditions of core No. 1, with a square hysteresis loop, to be those shown in figure 11-6. Both A and B windings are energized and the state of the core is at point (1). The H winding has no current in the initial state. When flip-flops A, B, C are set by the passage of a projectile, the current in windings A and B is removed. The H winding is unaffected and the state of the core is moved to point 2 in the figure. When the inhibit winding is driven, the core switches to point 3. This change of flux in the core produces a voltage in the sense winding which is used to reset flip-flops A, C, E, and G. Since flip-flops E and G are already in the reset condition, nothing happens to these two. Only A and C, which were set by the passage of the projectile, are reset. This leaves B as the only flip-flop set in the register and it is the desired one. The same situation occurs in a different core when the flip-flops set correspond to the logic established for the particular core.

(U) Obviously, if only A and B had been set, the decoding would have left B as the desired selection. When A alone is set there is no decoding done by the center-resolution core matrix and A remains the flip-flop set in the register.

#### 11.4 Resetting Input Cores and Readout to Selection Matrix

(U) Approximately 4 microseconds after the decoding has been done by the center-resolution core matrix, a command is sent by a timing circuit to reset or inhibit all of the input cores which are associated with the reset flip-flops. This takes place when current is sent through the inhibit windings of the input cores. The resetting action leaves only one input core set and one flip-flop set in the center resolution circuitry. There is only one input core set because the desired core was always in a group containing one set core, as previously described.

(U) The same action takes place in both the A fence and B fence. The function is performed in the B fence somewhat later than in the A fence because of the time required for the projectile to pass from the A fence of optical pickets to the B fence. Thus, the selection made in the A fence is retained until a choice is made in the B fence.

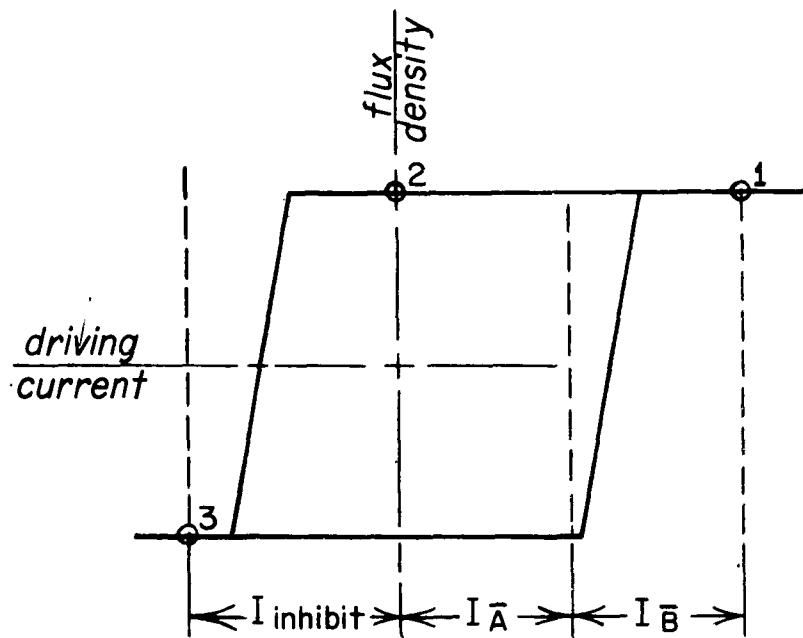


Figure 11-6. States of a center resolution core

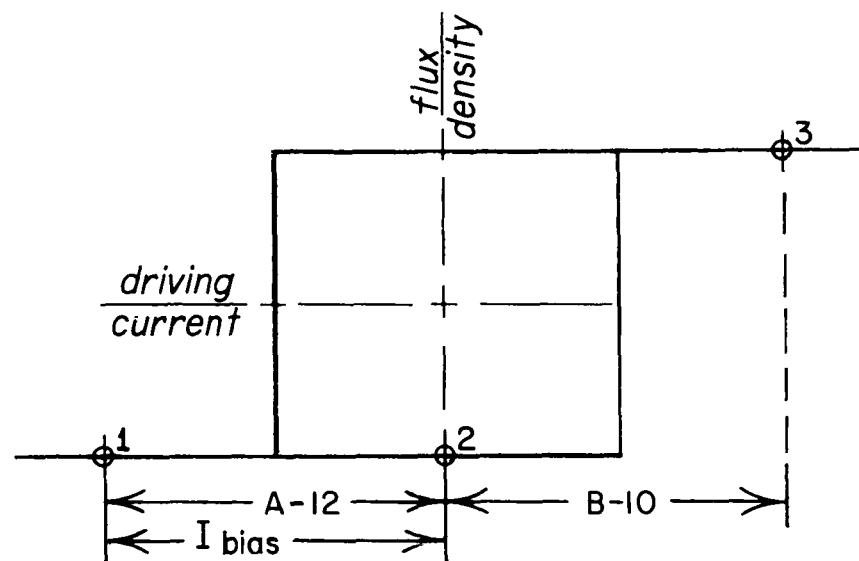


Figure 11-7. States of a selection matrix core

(U) The circuitry in A and B is identical except for an additional command readout initiated by the B center-resolution circuitry. This command is delayed approximately 15  $\mu$ sec from the initial setting of the first flip-flop in the B fence center-resolution register. The delay provides sufficient time to make the B selection. The command readout then inhibits or resets the one remaining input core in both A and B fences simultaneously; i.e., there is a coincidence readout from the A and B fences into the charge-selection matrix.

#### 11.5 Charge-Selection Matrix

(U) The charge-selection matrix consists of a number of square hysteresis loop magnetic cores, each with windings from the A and B input cores corresponding to the A and B combinations which resulted from the system geometry, such that A-12 and B-10 gives charge C-2 (figure 11-1). The selection C-2 is made in the following manner:

On some particular core in the charge selection matrix there are windings which correspond to A-12 and B-10. The selection matrix core also has a bias winding and an output sense winding corresponding to charge C-2. The A-12 and B-10 windings are driven from the coincidence readout of the A and B input cores.

(U) Figure 11-7 presents the state of the core in the selection matrix. At the beginning of the operation no current is flowing in the A-12 or B-10 windings, but current is flowing in the bias winding all the time. This puts the core at point (1) on the diagram. When current flows in the A-12 winding it is only sufficient to produce enough flux in the core to reach point (2). If the A-12 current is removed, the core will return to point (1) because of the bias current. This is also true for current flowing in the B-10 winding alone. When current flows in both A-12 and B-10 windings, the core switches to point (3) on the diagram. The corresponding change of flux in the core induces a voltage in the C-2 winding. It will be noticed that current must appear in A-12 and B-10 at the same time to produce an output. The voltage induced in the C-2 winding is fed to a flip-flop in the output buffer register.

#### 11.6 Output Buffer Register and Output Gates

(U) The output buffer register consists of 12 flip-flops, each associated with one of 12 output gates. Each output gate corresponds to one of the 12 defending charges. When drive is supplied to one of the 12 flip-flops, such as the voltage induced in the C-2 winding mentioned under charge selection matrix, the flip-flop changes its state and conditions one of the 12 output gates.

(U) The inputs of the output gates are essentially in parallel for the timing pulse from the firing-time computer. Thus, when the firing pulse arrives at the inputs to the output gates, it is passed on only by the one conditioned output gate, which is connected to the desired defending charge firing circuitry.

**SECRET**

#### 11.7 Indicator Lamps

(S) There are three sets of indicator lamps on the front panel that permit monitoring the functioning of the computer. Two vertical sets, each consisting of a row of eight numbered red lamps and a row of eight numbered yellow ones, are associated with the individual pickets in the A and B fence (figure 11-1). The red lamps, when lighted, indicate which pickets have been traversed. The yellow lamps indicate the picket selected as nearest center. The horizontal set, numbered 1 to 12, indicates which of the twelve defending charges has been selected by the computer in a firing.

#### 11.8 Completed Charge-Selection Computer

(U) The completed charge-selection computer was delivered to DOFL by International Business Machines Corporation by August 1959.

(U) The computer and its 60-cycle power supply are contained within a chassis 24 in. x 17 in. x 12 in., and weigh approximately 75 pounds. The power supply accounts for about two-thirds of the total weight. Much of this could be saved if 400-cycle ac were used. Further savings in weight and space will be possible if microminiaturization techniques are introduced.

(U) Figure 11-8 is an external view of the complete charge selection computer.

(U) Figure 11-9 shows the computer with the cover lifted to afford easy access to the logic circuits.

(U) Figure 11-10 shows the logic circuits removed from the chassis and illustrates the compact form of the units.

(U) Figure 11-11 is a picture of some of the logic cards removed from the unit and the special card extractor for removal and replacement of the cards.

**SECRET**

201

This document contains information affecting the national defense of the United States within the meaning of the espionage laws, title, 18 U. S. C., 793 and 794. Its transmission or the revelation of its contents in any manner to an unauthorized person is prohibited by law.

CONFIDENTIAL

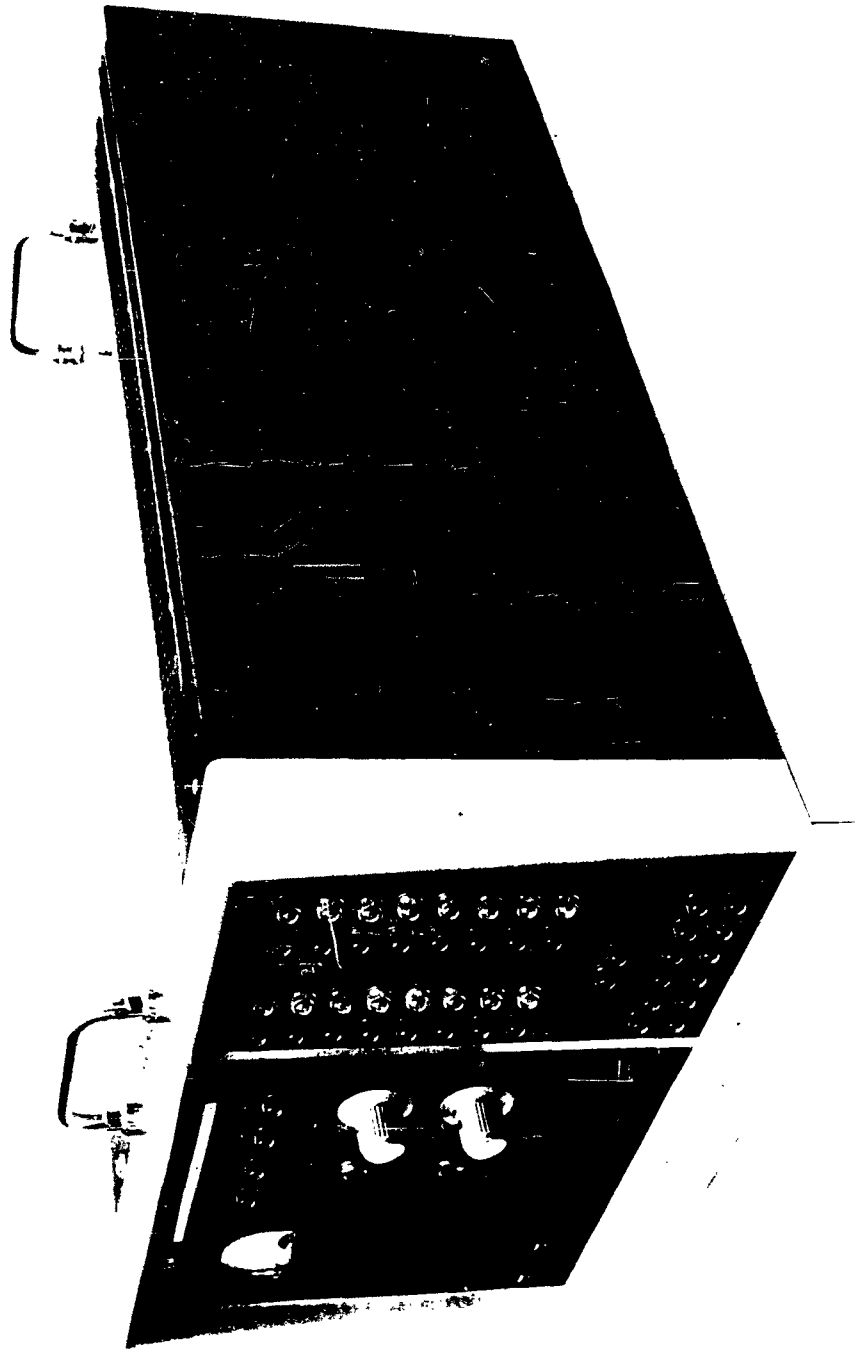


Figure 11-8. External view of charge selection computer

CONFIDENTIAL

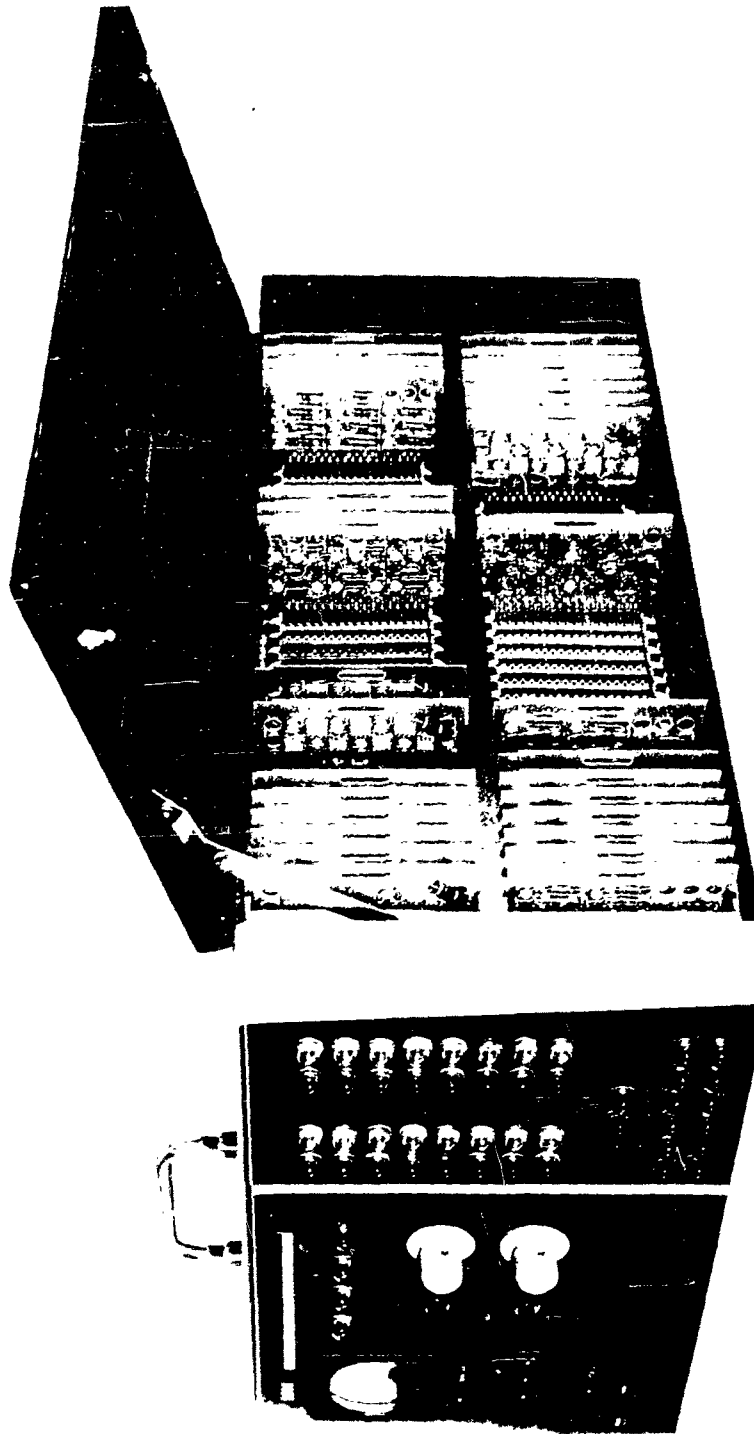


Figure 11-9. Front view of logic card side

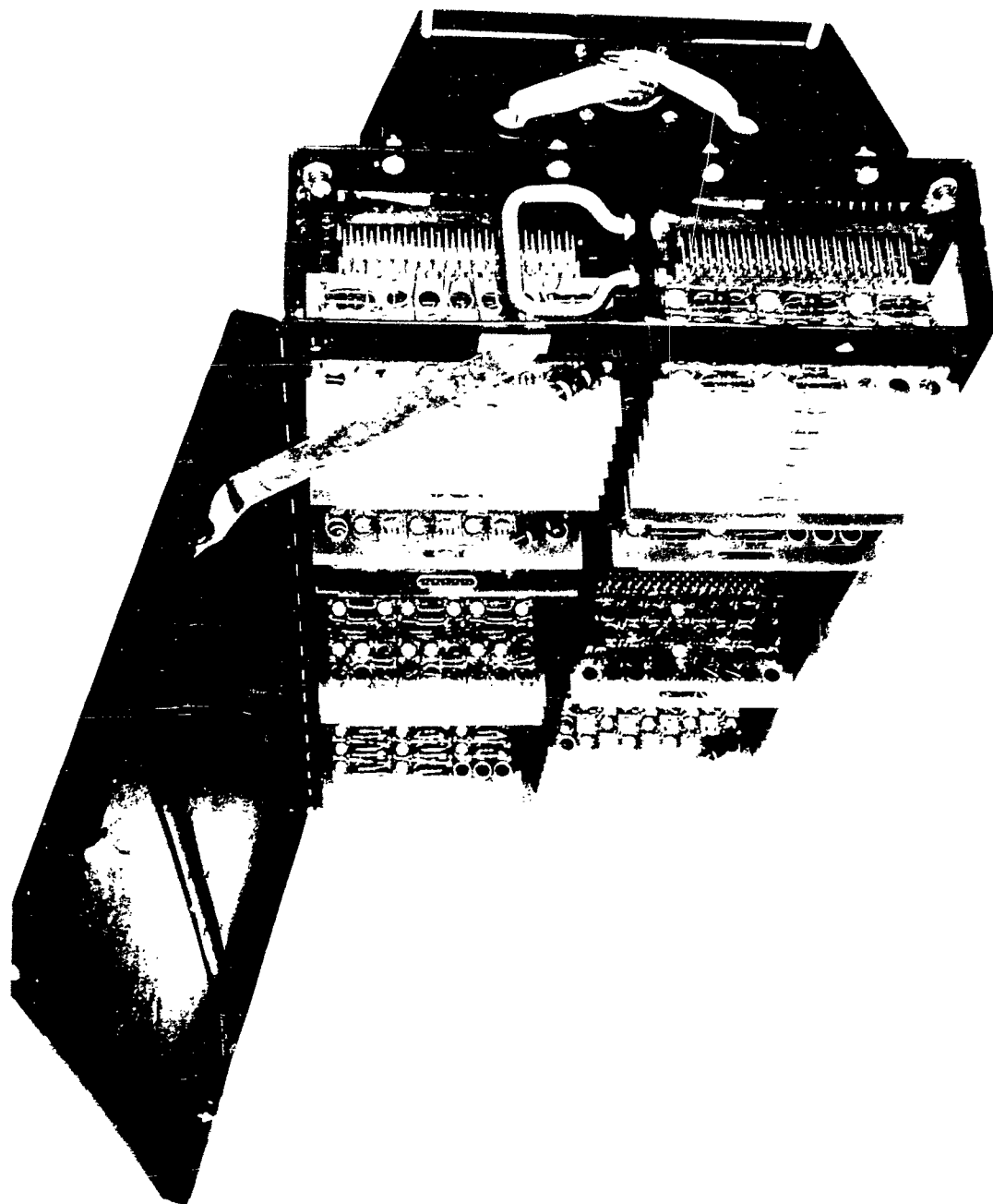


Figure 11-10. Back view of logic card side

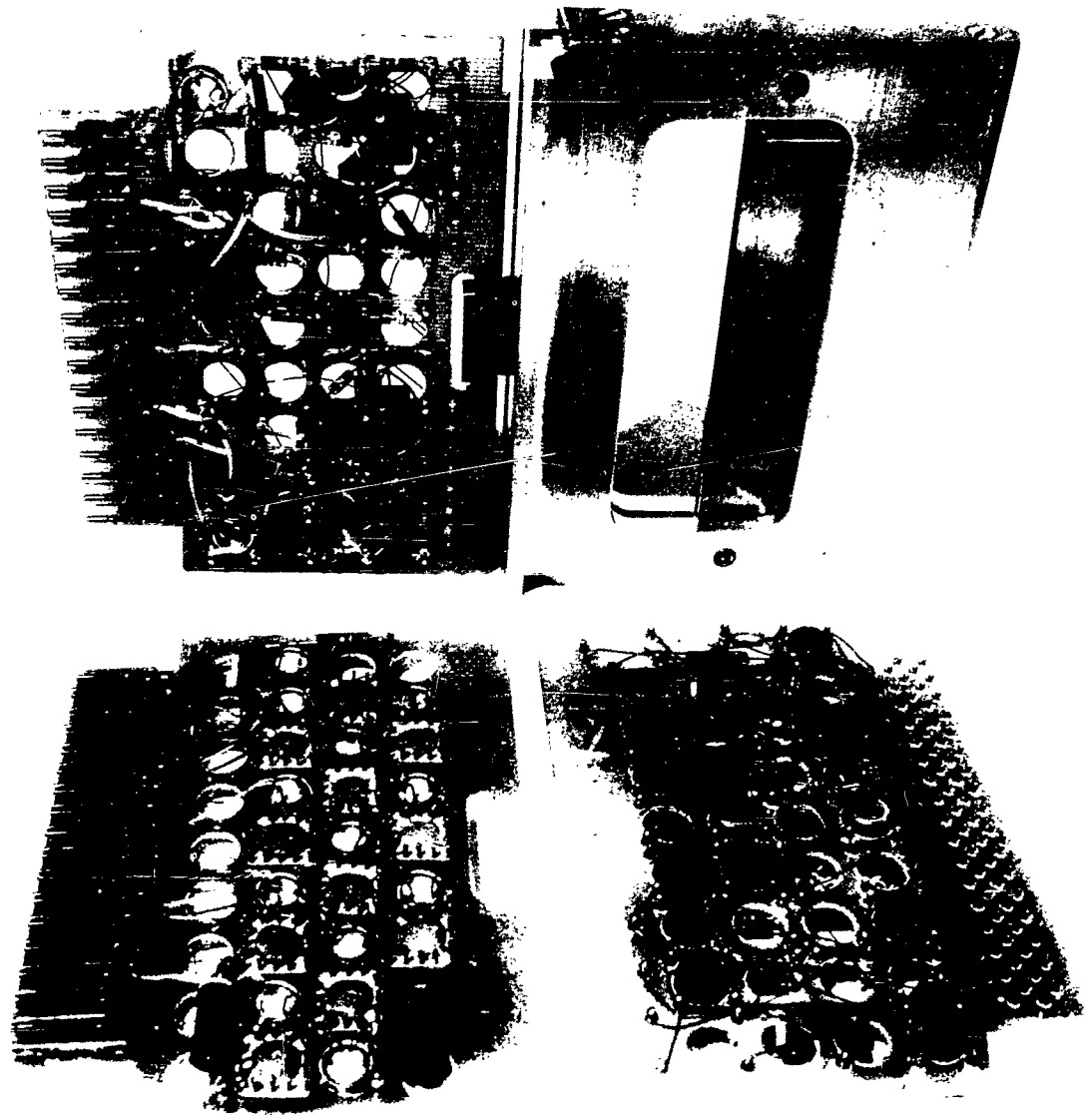


Figure 11-11. Logic cards and card extractor

## 12. FIRING CIRCUIT

R. J. Paradis

(S) The system requirements are that only the one defending charge selected by the charge-selecting computer (section 11) be detonated at any one time, but that any of the twelve be ready to be fired, if it were selected as the appropriate one.

(U) The 5-ohm M36A1 detonator, specified for the June 1960 feasibility test fires at 1-v peak pulse. At low voltages its firing delay is nonreproducible and is of the order of milliseconds, which cannot be tolerated; at 2 kilovolts, corresponding to current peaks of 1000 amperes or greater with several paralleled detonators, the delay is less than 3  $\mu$ sec. The 2-kilovolt, 1000-ampere requirement created a difficult switching problem and a special firing circuit was developed to solve it.

(C) In the feasibility test, twelve of these circuits were to be employed in connection with the twelve defending charges. Since the thyatrons normally used for such an application were too large physically, a survey of available switching devices was initiated. The 1000-ampere peak current requirement exceeded that allowed by the manufacturers' specifications for all of the switching devices that were considered. However, since the required repetition rate is very low, several devices were examined regarding their applicability for the specific purpose. A cold cathode gas switching tube, which is of the size of a miniature receiving tube, offered the best chance of success.

(U) The circuit of figure 12-1 performs the required operation. The capacitor is discharged through the tube and the resistor R which simulates an M36A1 detonator. The coil L was added as a safety measure to bypass the detonator D with 99 percent of the dc ionization current, its dc resistance being approximately 0.01 ohms as compared to the 5 ohms of the detonator.

(U) The circuit was fired several hundred times with each of three sample tubes used, without failure and with an average delay of 2.6  $\mu$ sec.

(C) Figures 12-2a and b are typical waveforms of the firing pulse produced by the circuit. In figure 12-2a the coil is not present, while in figure 12-2b it is present. It is proposed to use only one firing capacitor as shown in figure 12-3, so that its stored energy is channeled to the selected charge through the appropriate switching tube.

**SECRET**

207

This document contains information affecting the national defense of the United States within the meaning of the espionage laws, title, 18 U. S. C., 793 and 794. Its transmission or the revelation of its contents in any manner to an unauthorized person is prohibited by law.

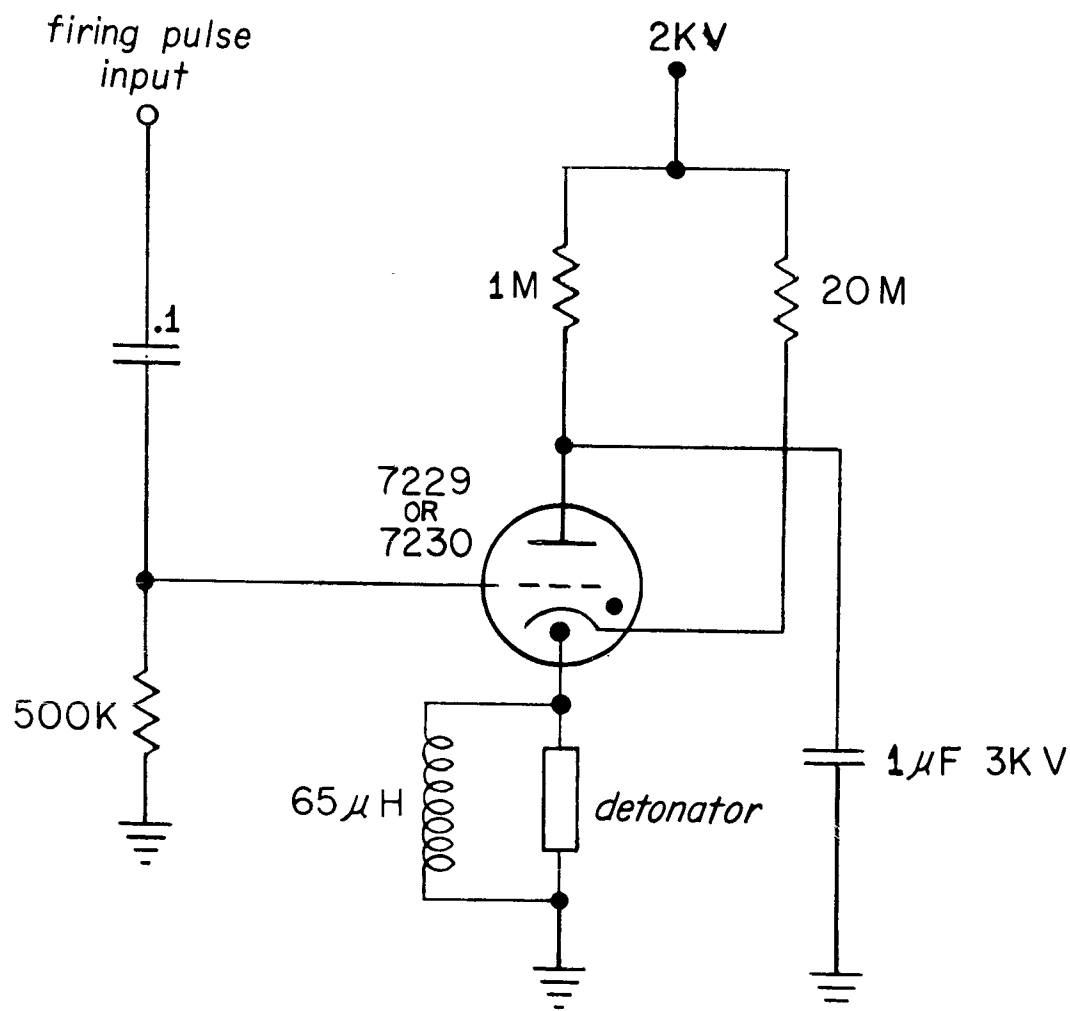
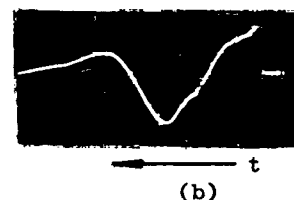
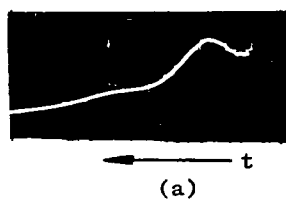


Figure 12-1. Firing circuit



Vertical Deflection 550 V/CM  
Horizontal Deflection 1 $\mu$ SEC/CM  
Without Coil

Vertical Deflection 1100 V/CM  
Horizontal Deflection 1 $\mu$ SEC/CM  
With Coil

Figure 12-2. Wave form of firing pulse

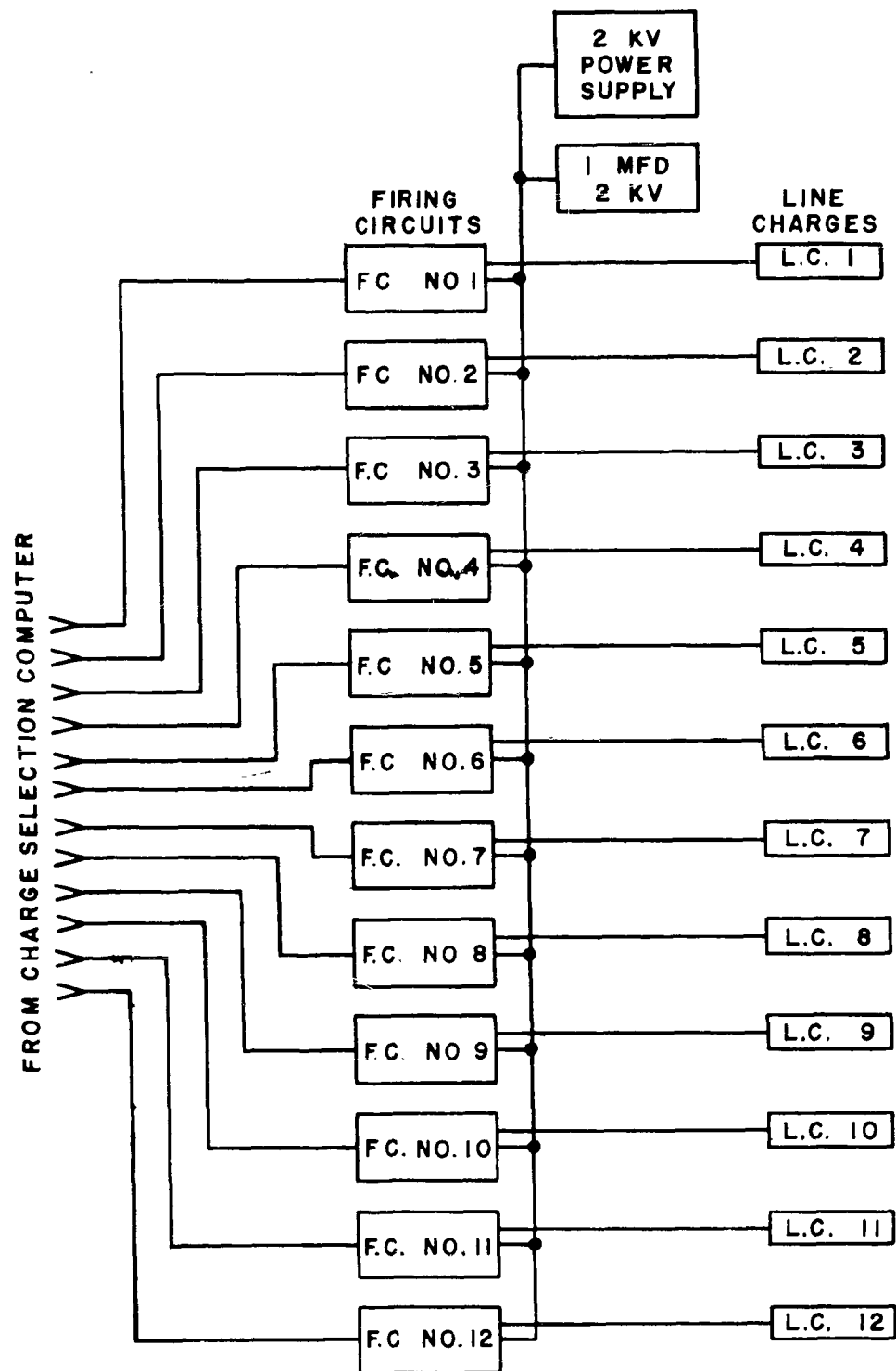


Figure 12-3. Switching array for 12 defending charges  
 FC = Firing circuit, LC = Defending charge

### 13. FIELD TESTS WITH EXPERIMENTAL PROTOTYPE SYSTEM

A. Copeland, J. E. Miller, W. Moore, R. J. Paradis, F. Vrataric

#### 13.1 Test Objectives

(U) The equipment and procedures were so designed as to permit testing the complete circuitry built for the June 1960 feasibility test without resorting to the complex optical hardware which was to be constructed while these tests were going on.

(S) The test objectives were:

1. To determine the operating parameters of the detection units.
2. To test the charge selection computer.
3. To test the size discrimination and K-factor circuitry.
4. To determine the over-all-system timing accuracy.
5. To establish the influence of the sensing-unit errors upon the over-all accuracy.

#### 13.2 Firing Range

(U) All field tests preliminary to the feasibility test were conducted at the DOFL Test Area at Blossom Point, Maryland. In order to lessen interference from other tests going on in the area, a special firing range was set up for this project. Photographs of the range layout are shown in figures 13-1 and 13-2. The guns were maintained in a fixed position and the shells were fired through the detection station into a bunker. The signal information was transmitted to the instrumentation trailer through cables in an underground conduit.

#### 13.3 Tests on Detection Unit Parameters

(S) The over-all system accuracy depends primarily upon the accuracy with which the detection units (section 4.1) can detect the nose of a shell, in other words, how far the nose has to penetrate before a signal is generated. Possible variations of shell penetration are shown diagrammatically in figure 13-3. In figure 13-3a it is shown that various nose shapes will result in different penetrations for the same signal. This is also true for a shell entering into the null region, that is, the region between two adjacent detection pickets, as shown in figure 13-3b. Figure 13-3c shows the effect of variations in the alignment of individual pickets at the maximum detection range, which are within the closely held alignment tolerances. In order to determine the random error of the system due to variations in shell penetrations, a series of penetration measurements was made. The test layout and procedures were as follows:

**SECRET**

211

SECRET



Figure 13-1. Dash-dot range at DOFL Test Area; view toward detection station

SECRET

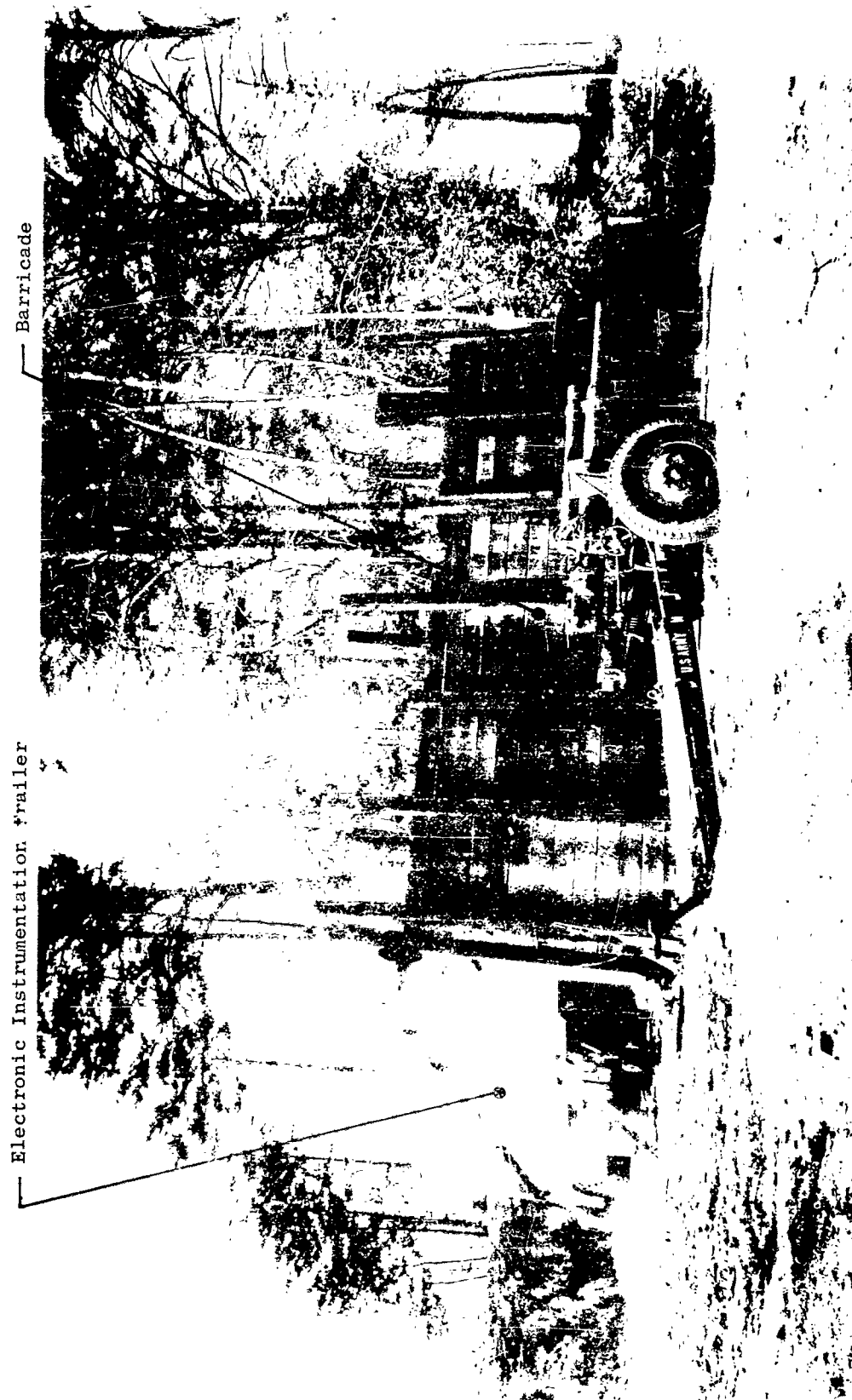


Figure 13-2. Dash-Dot range at DOFL Test Area; view toward instrumentation trailer

CONFIDENTIAL

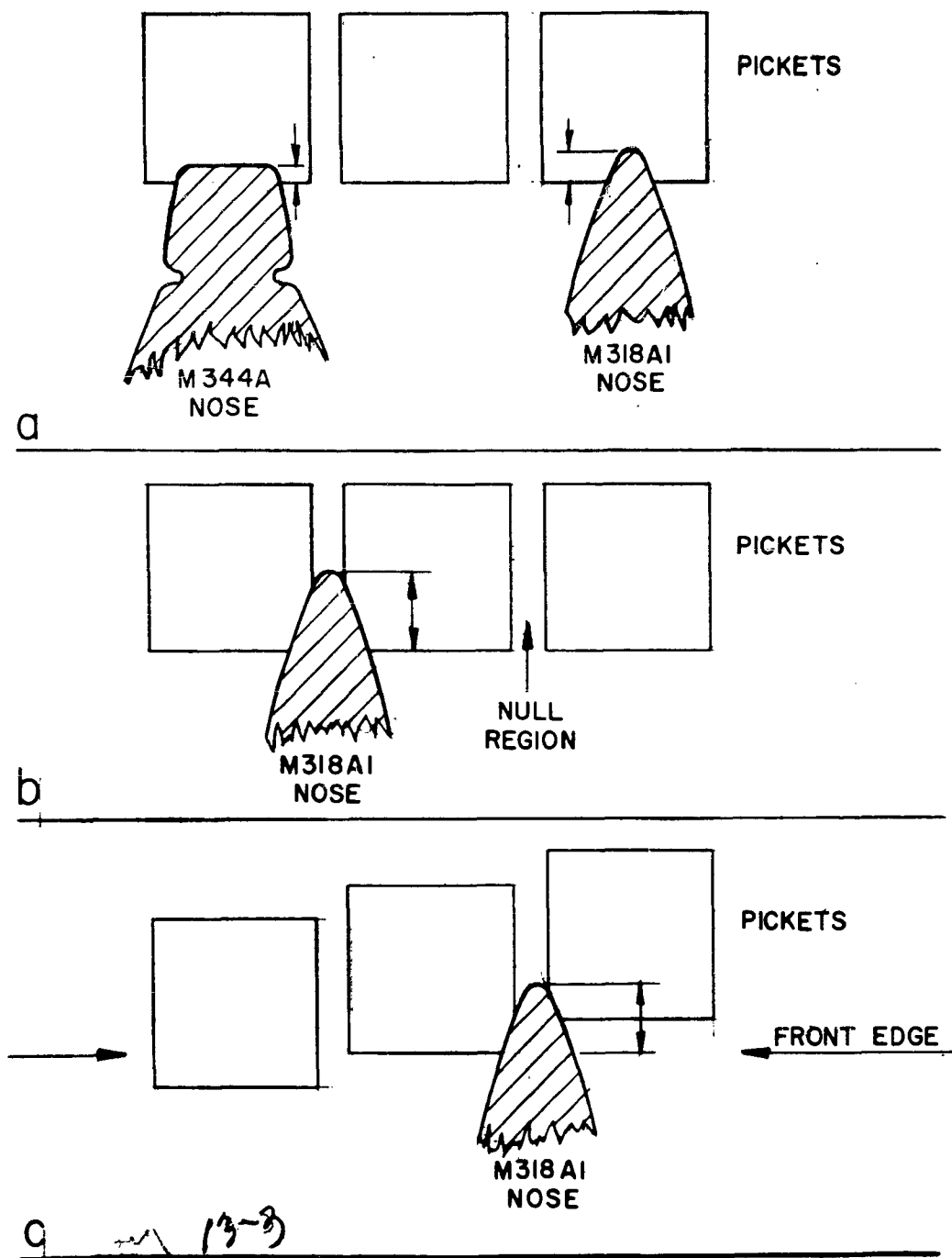


Figure 13-3. Possible variations in shell penetration

CONFIDENTIAL

**SECRET**

(S) The physical layout is shown in figure 13-4. The shell first shorts the velocity and camera trigger screen, which triggers the properly set shutters of the two cameras and starts a counter. It then enters into the optical detection fence (section 8.2), which triggers the two microflashes. In this way two pictures are taken of the shell in front of the calibrated reflecting screen at the instant the sally amplifiers (section 9.1.3) in the detection fence produces an output pulse. The shell finally shorts the second velocity screen, which stops the counters. The shell velocity is then computed from the time count and the spacing of the two screens. The circuitry used to energize the camera shutter solenoid and to start and stop the counter is shown in figure 13-11 in section 13.4.2. Figure 13-5 is a typical pair of pictures obtained in this way.

(C) For evaluating the picture, a plotting board, figure 13-6, was made in the form of a scaled model of the layout. The fixed scale in the upper portion represents the calibrated reflecting screen. The two transparent rulers with the dark tracing lines are hinged at the forward principal points of the camera lenses. In actuality the tracing lines are quite narrow; they were exaggerated to render them more conspicuous for this photograph. The projections of the seven detection units of the subfence, seen under the two rulers at their intersection, were made rotatable to permit the evaluation of oblique firings. The center board is a sliding scale with which the distance of the shell nose from the leading edge of the subfence is measured.

(C) In evaluating a shot, the tracing lines on the two hinged rulers are made to coincide with the two respective markings on the fixed scale which represent the markings read off the reflecting screen behind the shell nose in the two pictures obtained at that shot. The intersection of the two tracing lines is the position in which the shell was photographed, and its distance from the leading edge of the subfence is now measured with the sliding ruler; in this way, the penetration of the nose is determined.

(U) The delay of the Microflash, which is of the order of 10 to 40  $\mu$ sec, was measured by the method described in section 13.4.3 and evaluated numerically in terms of displacement of the shell nose on the trajectory from the known shell velocity.

(U) The results of the firings made are recorded in the tables of section 13.5.3, and an analysis of the penetration of various types of shells in various approaches to the subfence and their bearings on the over-all accuracy is given in section 13.6.

#### 13.4 Tests on Over-all System

##### 13.4.1 Test Layout

In order to avoid complications of building the full three-fence, 252-picket optical sensing system, also containing 252 sally amplifiers, and to still be able to test the full electronic instrumentation,

**SECRET**

215

This document contains information affecting the national defense of the United States within the meaning of the espionage laws, title, 18 U. S. C., 793 and 794. Its transmission or the revelation of its contents in any manner to an unauthorized person is prohibited by law.

CONFIDENTIAL

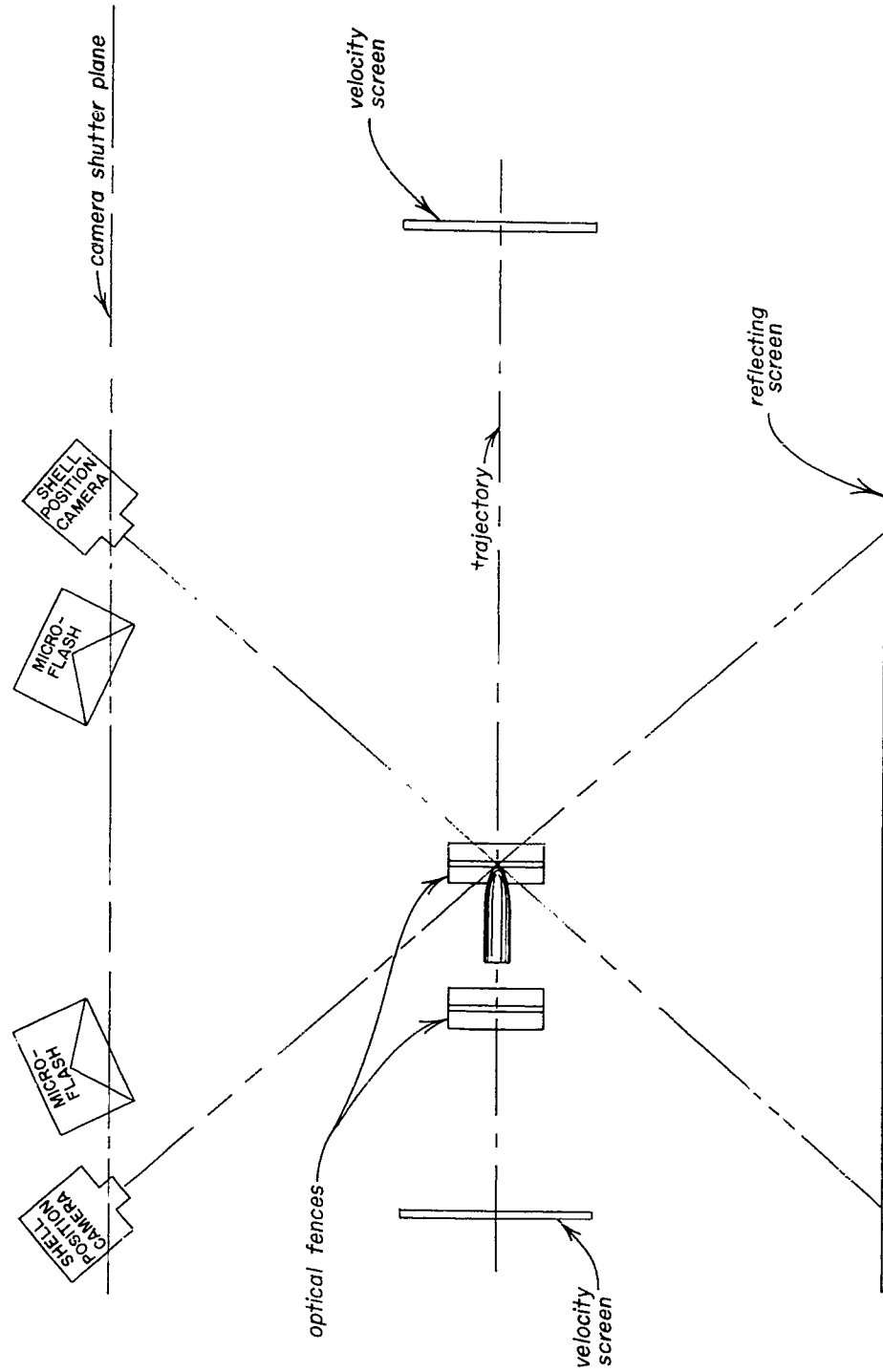
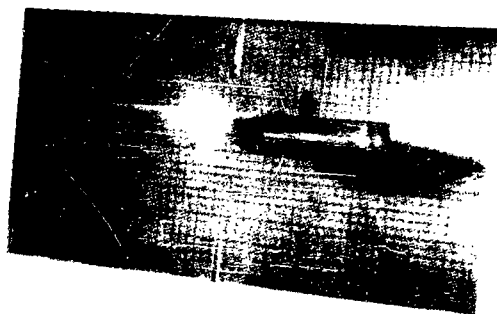


Figure 13-4. Layout for shell penetration test

CONFIDENTIAL



Picture in forward-looking camera



Picture in backward-looking camera

Figure 13-5. Typical picture pair from penetration tests;  
black dots are fiducial marks on screen



Figure 13-6 Plotting board

## SECRET

as described in sections 8 through 12, a simplified sensing system was built. Only three subfence units (section 5.2) were used. They were mounted on a Z-shaped structure (Z-frame, section 5.3), which itself was mounted on a rotatable platform, a gunmount obtained from the U.S. Navy. Figure 13-7 is a diagram of the test layout and figure 13.8 a photograph of the simplified sensing system in the detection station.

(C) The platform had to be rotatable to permit various angles of attack, since the guns were held at a fixed position. It was indexed in conformance with the angles desired for this test. The Z-frame was also indexed such that the subfence units taking the place of the A and C fences could be displaced laterally to conform to the same angles. Subfence B remained fixed at the axis of rotation for all angles.

(C) The lateral displacement of the A and C subfence was made in exact multiples of the picket spacing. In addition, the output connections of the three subfence units were arranged to allow various input connections to the charge selection computer, section 11. Each of these three units could, thus, simulate any of the 12 units of the respective fences of the complete system without actually building the latter, thus allowing the charge selection computer to be tested in its selection of a particular charge.

(C) Tests on shells of various height trajectories could also be made by merely moving subfence C along the direction of the trajectory. However, this was only possible for normal attack, that is, with the Z-frame in the zero-degree position.

(S) Referring again to figure 13-7, the shell first passed the camera trigger and velocity screen, proceeded then through the subfences A, B, and C and on through the fragmentation plane of the hypothetical defending charge, and finally through the second velocity screen. The camera was positioned with its optical axis in the fragmentation plane, to take a picture of the shell in front of the calibrated reflecting screen at the instant the Microflash was fired. The Microflash monitor phototube was used to measure the delay of the flash (section 13.4.3).

### 13.4.2 Electronic Instrumentation and Test Method

(U) An over-all view of the electronic equipment housed in one of the electronic laboratory trailers is given in figure 13-9, while figure 13-10 is a block diagram of the circuitry employed in the over-all test.

(S) The processing of the signals is as follows: As a shell passes over subfence A, an output pulse is generated in one or more of the seven sally amplifiers (section 9.1.3). Each of these amplifiers is connected to seven A fence inputs of the charge selection computer (section 11), in addition to being combined in the diode "OR" circuit (section 9.2.1). The output of this latter circuit is fed to the  $T_0$  pulse

SECRET

219

SECRET

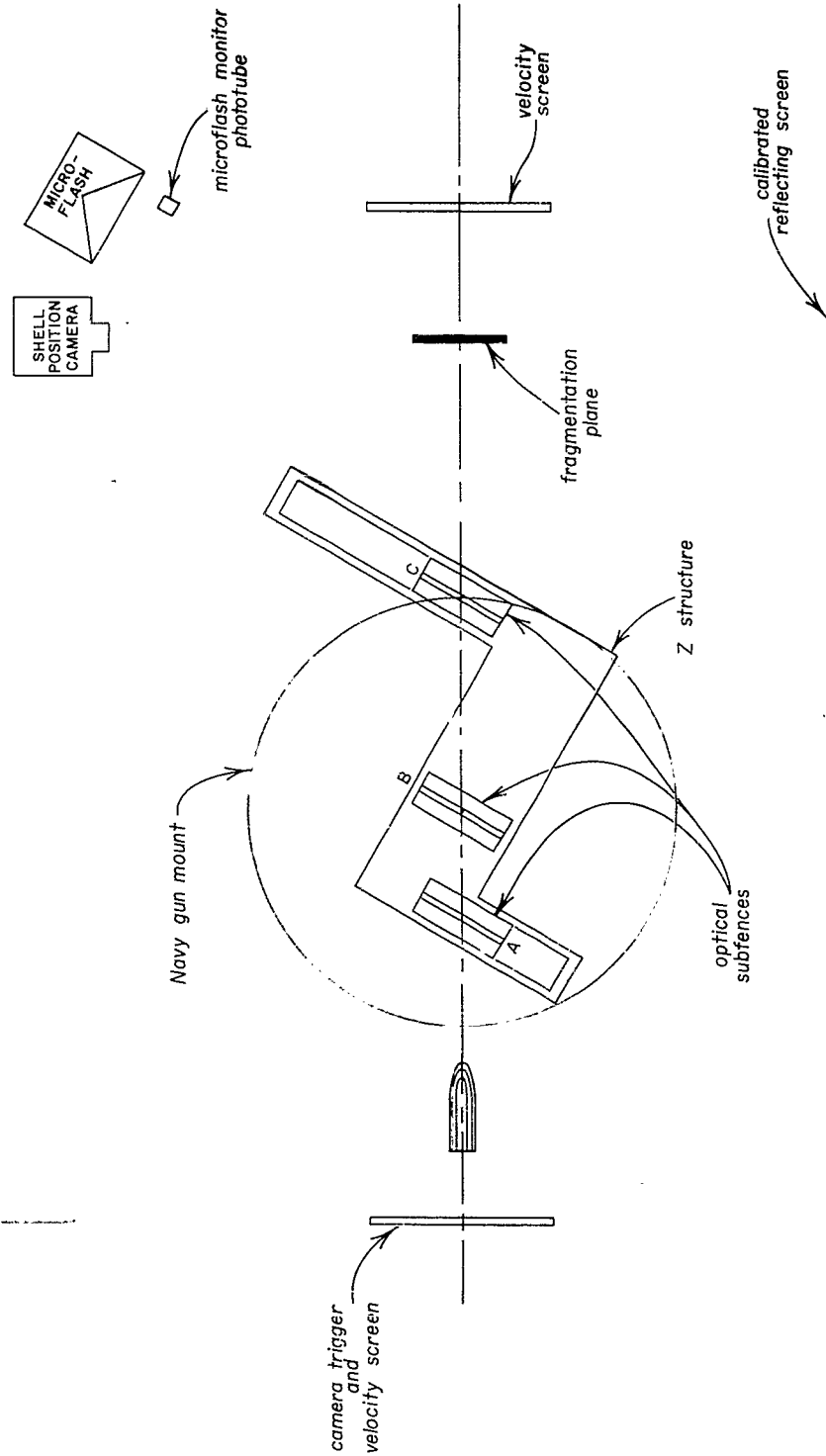


Figure 13-7. Layout for over-all system accuracy test

SECRET



Figure 13-8. Optical system in detection station



Figure 13-9. Interior of electronic laboratory trailer

# SECRET

input of the firing time computer (section 10) and also to the start-input of the  $\Delta T_1$ -counter. Subfence B also contains seven sally amplifiers which are also connected to seven B-fence inputs of the charge selection computer, and combined in the second diode "OR" circuit. When the shell passes over subfence B, the output of the second diode "OR" circuit stops the  $\Delta T_1$ -counter, thus indicating the time interval  $\Delta T_1$ , and starts the  $\Delta T_2$ -counter and is also fed to the  $T_1$ -input of the firing-time computer. The charge-selection computer has now obtained the necessary information and assigns a charge to intercept the shell. At this same time, "knowing"  $\Delta T_1$ , the firing-time computer has determined the shell velocity. When, at last, the shell passes over subfence C, its output pulse stops the  $\Delta T_2$  counter, which indicates the time interval  $\Delta T_2$ , and starts the  $\Delta T_f$ -counter and is also fed to the  $T_2$ -input of the firing-time computer. From the  $\Delta T_2/\Delta T_1$  ratio the firing-time computer determines the height of the shell trajectory and the time at which the intercepting charge is to be fired, and generates the firing pulse at that time.

(S) The firing pulse is used to do two things. It stops the  $\Delta T_f$ -counter, thus permitting reading-off the firing time for checking purposes. In the complete feasibility test system, the pulse would have been used to trigger the firing circuitry (section 11) and to detonate the defending charge selected by the charge-selection computer. In the present experimental system, however, the pulse is used to trigger the Microflash which imitates a defending-charge firing, but in reality illuminates the shell and the calibrated reflecting screen, such that a picture of the shell is taken at the position in which it would be if the defending charge were used.

(S) In imitating a shaped charge firing by the Microflash, the fact must also be taken into account that the velocity  $V_c$  of the shaped charge is finite while that of the Microflash light can be considered as infinite. Therefore the actual position of the shell at the time of impact is in advance of that at which it was photographed by a distance  $hV/V_m$ . The correction is determined numerically from the measured height  $h(\Delta T_2/\Delta T_1$  ratio), the fragment velocity  $V_c$ , which is assumed fixed at 8000 fps, and from the measured shell velocity  $V_m$ .

(U) In addition to the velocity measurement obtained from counting the time interval  $\Delta T_1$ , and independent check was made by measuring the transit time between two wire-mesh screens (figure 13-7) spaced ten feet apart on the shell trajectory, one before, the other behind the optical sensing equipment. The circuitry used for that purpose is separately shown in figure 13-11, which is self explanatory.

## 13.4.3 Determination of Microflash Delay

(U) A type 1530A General Radio Microflash unit was used in the tests. The lamp produces a high-intensity flash of light lasting two  $\mu$ sec, and there is an unavoidable, unpredictable delay, ranging from 10

# SECRET

223

# SECRET

to 40  $\mu$ sec, between the arrival of the firing pulse and the actual occurrence of the flash. Because of its unpredictability, the delay had to be measured and taken in account at every firing.

(U) The following method was employed. A monitoring phototube (figure 3-7) was placed in front of the Microflash lamp and facing it. This phototube stops the Microflash delay counter (figures 13-10 and 13-11) which has been started by the firing pulse, and the delay is read off the counter.

## 13.5 Test Results

### 13.5.1 Charge-Selection Computer

(S) Since only one hypothetical defending charge was considered, the various angles of attack being obtained by rotating the Z-frame, there was no need to connect the output of the charge selection computer to the Microflash which imitated the hypothetical defending charge. Instead of that, the computer output was left unconnected, as shown in figure 13-10, and the position of the charge that would have been selected at any particular angle was read off the lighted-up indicator lamp in the horizontal row at the right bottom of the computer panel, section 11.7. It can be stated that the position of the charge selected by the computer invariably coincided with the position of the hypothetical charge considered.

### 13.5.2 Size Discrimination and K-Factor

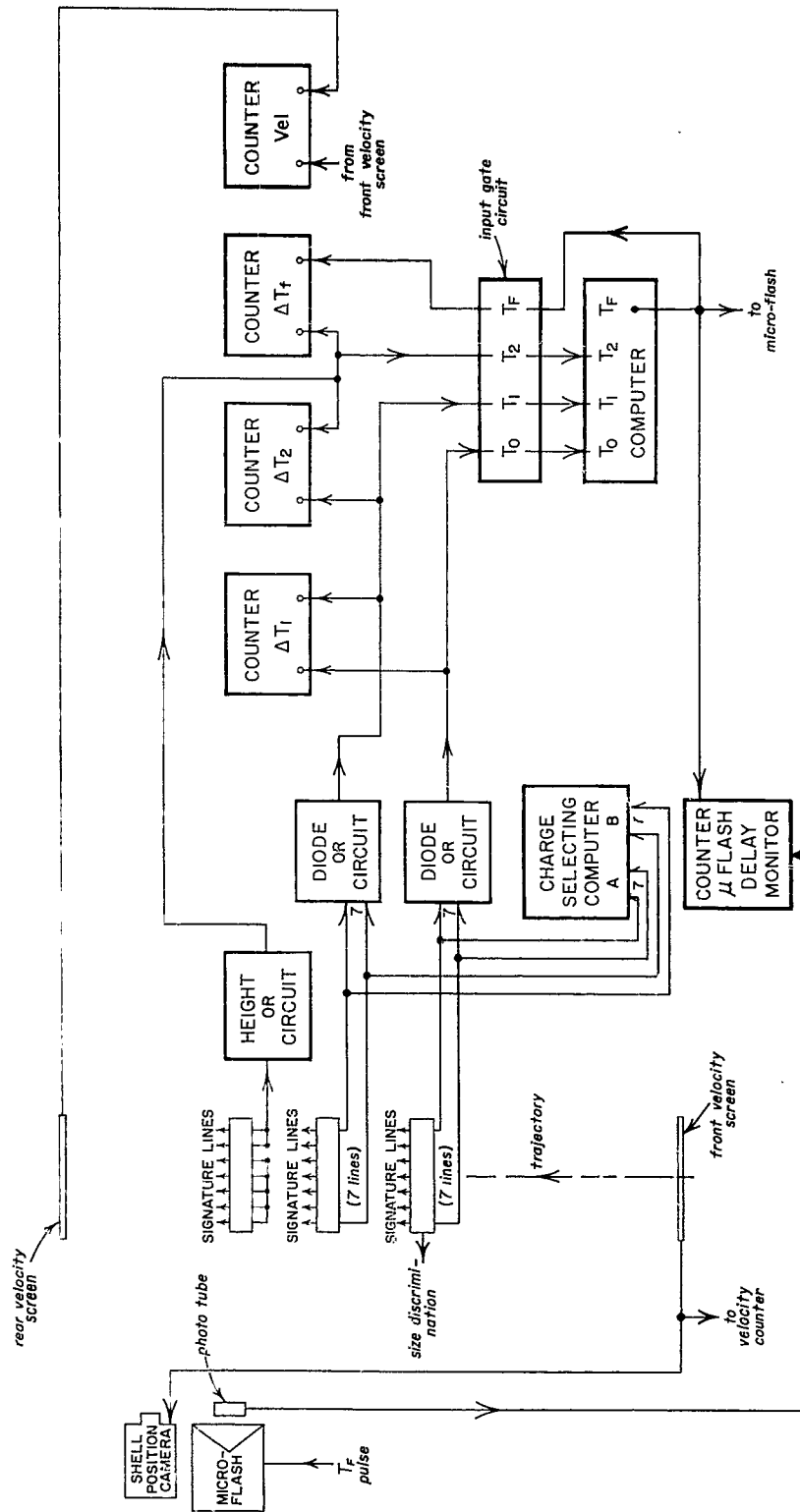
(U) Tests to evaluate the functioning the size discrimination as well as the K-factor circuitry, sections 9.3 and 9.4, were made. Although time limitations prevented accurate evaluation, the results were sufficient to indicate that the methods were indeed feasible.

### 13.5.3 Over-all Experimental System

(U) A total of 556 rounds were fired during the 1959 calendar year. The types of guns and ammunition used are listed below:

<u>Gun</u>	<u>Round</u>
12 gauge shot gun	Rifled Slug
30 Cal. M-1 Rifle	30 Cal. Ball. M-2
50 Cal. Machine Gun, M-2	50 Cal. Ball. M-2
20 mm Proof test Barrel	20 mm Ball. M56A1 & T283E1
75 mm Tank Gun, M-3	75 mm T165E11
75 mm Pack Howitzer, M-1 (81 mm bore)	81 mm mortar, T-28
90 mm Anti-Aircraft, M-2	90 mm T.P. M-71
106 mm Recoilless Rifle, M40A1	HEAT, 344 A-1

CONFIDENTIAL



CONFIDENTIAL

Figure 13-10. Block diagram of field instrumentation

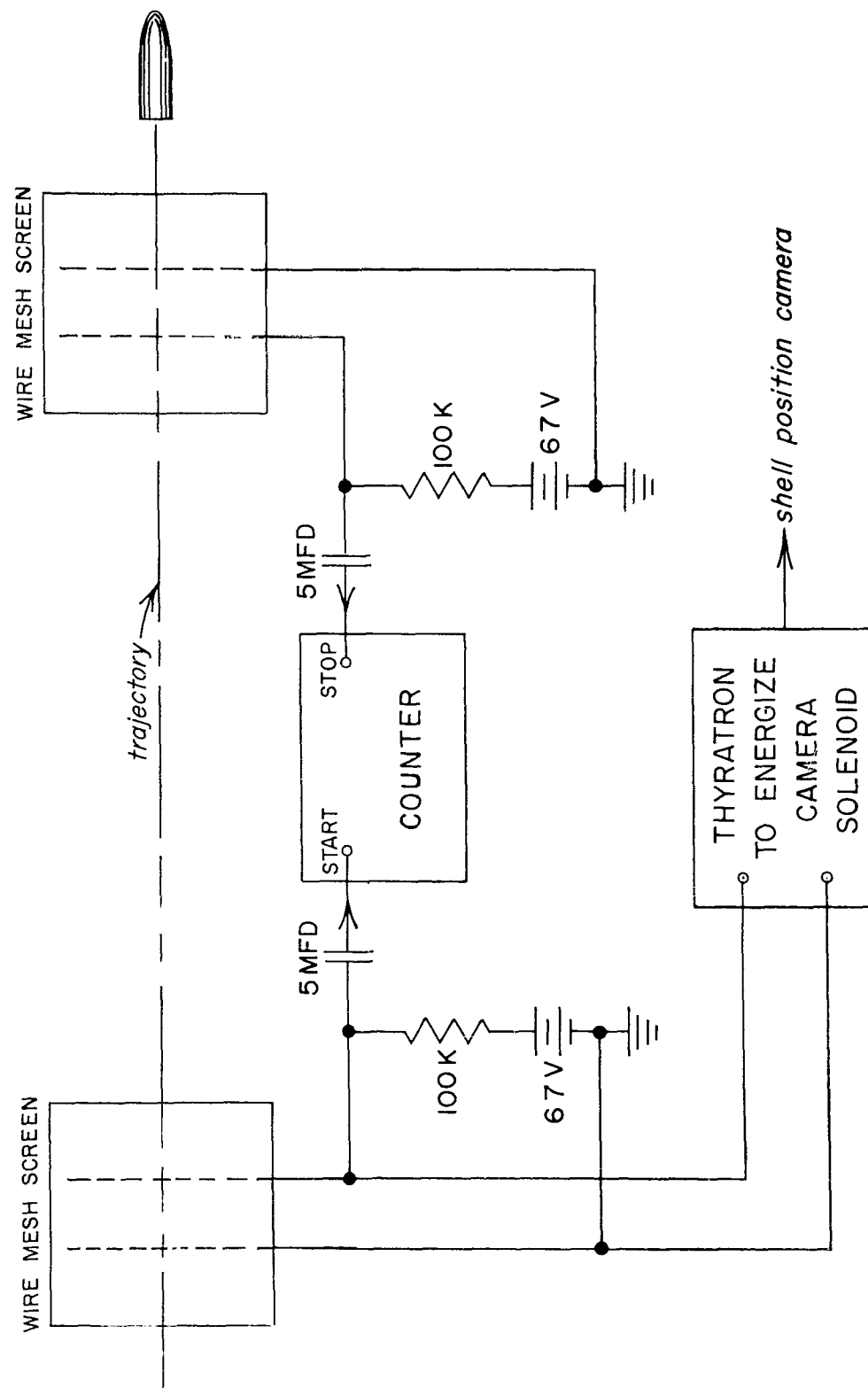


Figure 13-11. Camera-triggering and velocity-measurement circuitry

# SECRET

(U) All firings made and the results obtained from them are recorded in table 13-1.

(S) As can be seen from the table, the average error of the impact point on the shell was of the order of  $\pm 1$  in. for velocities from 1400 to 2400 ft, altitudes from 0 to 5 ft, and off-normal angles of attack from 0 to 55 deg. The analysis of the results is covered in the following section.

## 13.6 Analysis of Results

### 13.6.1 General Considerations

(C) In this analysis, the effects of errors in the input information, that is, errors in  $\Delta T_1$  and  $\Delta T_2$ , on the computation of the firing time for the defending charge are investigated. These errors are caused by the following phenomena:

1. Penetration: A shell must obscure a portion of a detection picket in order to produce a signal. The amount of penetration necessary to obtain the same signal amplitude from different type shells varies with the shape of the nose (see figure 13-3a).

2. Null Region: A shell entering the null region, that is, the space between two adjacent pickets, requires a deeper penetration to produce the same signal as one centrally entering a picket (see figure 13-3b).

3. Picket Beam Displacement: Misalignment of the pickets, resulting in a beam displacement, also influences the penetration necessary to produce a signal (see figure 13-3c).

4. Sally Amplifier Delay: The output pulse from the sally amplifiers is delayed a few microseconds due to the finite velocity of the penetrating shell. Additional error-causing delays due to variations in the time constants of the PbS cells used and the signal amplitude must also be included. The latter variable depends itself upon variations in illumination as well as in the sensitivities of the PbS cells. A graph showing the sally amplifier pulse delay versus input signal amplitude has been shown in figure 9-9.

### 13.6.2 Total Error

(C) The sum of the errors caused by the above variations was determined experimentally by photographing the shells as they passed through a single optical fence at the instant a pulse was generated by the sally amplifiers. The test procedure has been described in section 13.3.

SECRET

227

Round No.	Angle (degrees)	IBM Picket "A"	IBM Picket "B"	IBM Charge Selection	Velocity, ft/sec (from screens)	Velocity, ft/sec (from $\Delta T1$ )	Time, $\Delta T1$ , $\mu$ sec	Time, $\Delta T2$ , $\mu$ sec	Shell Position (Actual, in.) Horizontal	Shell Position (Calculated, in.) Horizontal	Position Error (in.) Horizontal	Height, Error (Actual, in.)	Height, Error (Calculated, in.)	Height, Error (in.)	Time, $\Delta Tf'$ , $\mu$ sec (Actual)	Time, $\Delta Tf''$ , $\mu$ sec (Calculated)	$d\Delta Tf$ ( $\Delta Tf' - \Delta Tf''$ ) $\mu$ sec	Displacement Error (in.)
11-30-1	0	33	33	5	1369	1392	718	672							2271	2279	-8	-131
11-30-2	0	33	33	5	1384	1392	718	671							2257	2280	-23	-382
11-30-3	0	33	33	5	1363	1388	720	752	-7.11	-7.32	+21	43.0	37.6	-5.4	2246	2247	-1	-016
11-30-4	0	33	33	5	1362	1372	729	731	-7.11	-7.32	+21	43.0	39.0	-4.0	2266	2295	-29	-475
11-30-5	0	33	33	5	1387	1387	721	746							2235	2253	-18	-30
11-30-6	0	33	33	5	1374	1392	718											
11-30-7	0	33	33	5	1370	1385	722											
11-30-8	0	33	33	5	1370*	1379	725											
12-1-1	0	33	33	5	1374	1401	714	685	-8.51	-7.38	-1.13	43.0	40.5	2.5	2231	2256	-25	-42
12-1-2	0	32	32	5	1392	1408	710	3085							969	1000	-31	-52
12-1-3	0	32	32	5	1202	1389	720	3095							979	1021	-42	-61
12-1-4	0	33	33	5	1379	1392	718	3129							950	998	-48	-795
12-1-5	0	33	33	5	1386	1404	712	3103							956	996	-40	-666
12-1-6	0	33	33	5	1378	1404	712	3210							860	940	-80	-132
12-1-7	0	33	33	5	1793	1828	547	595							1608	1604	+4	+085
12-1-8	0	33	33	5	1754	1783	561	585	-9.46	-9.32	-14	42.5	37.8	4.7	1662	1664	+2	+042
12-1-9	0	33	33	5	1758	1798	556	582	-9.74	-9.46	-28	43.0	37.6	5.4	1643	1646	-3	-062
12-1-10	0	33	33	5	1762	1798	556	599	-9.80	-9.40	-40	42.5	36.6	5.9	1620	1639	-19	-397
12-1-11	0	32	32	5	1400	1414	707	1087	-4.56	-4.46	-10	25.5	21.4	4.1	2001	2020	-19	-320
12-1-12	0	32	32	5	1383	1395	717	1144	-4.31	-4.36	+75	25.2	19.6	5.6	2003	2031	-28	-466
12-1-13	0	32	32	5	1400+	1416	706	1060	-4.31	-4.42	+11	25.2	22.6	2.6	2005	2029	-24	-40
12-1-14	0	32	32	5	1378	1385	722	1077	-4.37	-4.48	+11	25.2	22.9	2.3	2018	2059	-41	-686
12-1-15	0	32	32	5	1394	1401	714	1066	-4.59	-4.39	-20	25.0	20.9	4.6	2027	2056	-29	-486
12-1-16	0	32	32	5	1360+	1389	720	1117	-4.23	-4.34	+11	25.5	20.9	4.6	2033	2036	-3	-051
12-1-17	0	32	32	5	1396	1421	704	1070	-4.76	-4.54	-22	26.0	23.4	2.6	2033	2036	-3	-050
12-1-18	0	32	32	5	1416	1418	705	1038	-3.54	-4.59	+59	25.25	22.1	4.2	2033	2038	-5	-084
12-1-19	0	32	32	5	1398	1407	711	1081	-5.38	-5.68	+30	25.75	21.6	4.2	1540	1561	-21	-445
12-1-20	0	32	32	5	1764	1780	562	861	-5.27	-5.81	+54	25.75	22.6	3.2	1523	1526	-3	-065
12-1-21	0	32	32	5	1806	1822	549	826	-5.27	-5.89	+64	25.75	21.6	4.2	1517	1520	-3	-065
12-1-22	0	32	32	5	1830+	1859	538	823	-5.25	-5.69	+51	25.25	20.4	4.9	1513	1493	+20	+432
12-1-23	0	33	33	5	1803	1818	550	851	-5.18	-5.71	+92	25.00	20.54	4.5	1516	1511	+5	+108
12-1-24	0	32	32	5	1827+	1842	543	850	-4.79	-5.78	+1.49	25.75	20.22	5.5	1803	1821	-18	-379
12-1-25	0	32	32	5	1795	1822	549	865	-4.31	-5.78	+1.42	66.0	60.72	5.3	440	534	-96	-208
12-1-26	0	32	32	5	1758	1780	562	193							535	543	-8	-174
12-1-27	0	32	32	5	1807	1812	552	3478							523	536	-13	-282
12-1-28	0	32	32	5	1801	1808	553	3459										
12-1-29	0	32	32	5	1792	1799	556	3483										

snoutunlvaE and sgnirif test l 31 elpab

Table 13.1 Test Firings and Evaluation (Continued)

Round No.	Angle (degrees)	IBM Picket "A"	IBM Picket "B"	IBM Charge Selection	Velocity, ft/sec (from screens)	Velocity, ft/sec (from $\Delta T1$ )	Time, $\Delta T1$ , $\mu$ sec	Time, $\Delta T2$ , $\mu$ sec	Shell Position (Actual, in.)	Shell Position (Calculated, in.)	Position Error (in.)	Height, Error (Actual, in.)	Height, Error (Calculated, in.)	Height, Error (in.)	Time, $\Delta T1$ , $\mu$ sec (Actual)	Time, $\Delta T1$ , $\mu$ sec (Calculated)	$D\Delta T1 (\Delta T1' - \Delta T1'')$ , $\mu$ sec	Displacement Error (in.)
12-1-30	0	33	33	5	1792	1842	543	266	-4.46	-5.57	+1.11	61.25	55.92	5.3	1637	1708	-21	-456
12-2-1	0	32	39	5	1360	1380	725	262	10.66	10.32	-.34	60.75	60.12	-.63	2529	2525	+4	+065
12-2-2	0	32	32	5	1382	1400	715	231	11.50	10.62	-.88	61.75	61.38	-.37	2495	2496	-1	-.016
12-2-3	0	32-33	33	-	2180	2240	447	149	-	-	-	-	61.04	-	1306	1319	-13	-.340
12-2-4	0	33	33	5	2200	2260	442	323	-	-	-	-	47.96	-	1255	1259	-4	-.106
12-2-5	0	33	33	5	2178	2235	448	323	15.23	13.6	-1.63	50.00	48.29	-1.71	1273	1284	-11	-.288
12-2-6	0	33	33	5	2195	2251	444	323	-	-	-	-	48.06	-	1261	1267	-6	-.158
12-2-7	0	33	33	5	2195	2238	448	320	15.00	13.91	-1.09	50.75	48.53	-2.22	1283	1284	-1	-.027
12-2-8	0	33	33	5	2220	2240	447	326	14.24	13.71	-.53	49.5	48.04	-1.46	1277	1278	-1	-.027
12-2-9	0	33	33	5	2182	2240	447	334	14.10	13.71	-.39	49.5	47.44	-2.06	1271	1277	-6	-.158
12-2-10	0	32	32	5	2180	2215	452	324	13.72	13.67	-.05	50.25	48.46	-1.79	1304	1300	+4	+105
12-2-11	0	32	32	5	2180	2225	450	406	12.47	11.83	-.64	43.5	42.34	-1.16	1279	1273	+6	+158
12-2-12	0	32	31	4	2181	2255	444	399	11.99	11.76	-.23	43.25	42.48	-.77	1265	1250	+15	+394
12-2-13	0	33	33	5	2190	2255	444	412	12.90	11.81	-1.09	43.25	41.52	-1.73	1246	1247	-1	-.027
12-2-14	0	33	33	5	2220	2270	441	405	12.96	11.98	-.98	43.25	41.82	-1.43	1231	1236	-5	-.133
12-2-15	0	33	33	5	2180	2259	443	419	12.88	11.63	-1.25	42.75	40.39	-1.82	1235	1242	-7	-.183
12-2-16	0	33	33	5	-	2290	437	427	-	-	-	-	39.88	-	1212	1216	-4	-.106
12-2-17	0	33	33	5	2200	2265	441	653	-	-	-	-	23.34	-	1188	1182	+6	+158
12-2-18	0	33	33	5	2225	2265	441	640	7.54	7.16	-.38	25.75	24.28	-1.47	1183	1184	-1	-.026
12-2-19	0	32	32	5	2225	2275	440	632	7.35	6.53	-.82	-	24.78	-	1191	1183	+8	+214
12-2-20	0	33	33	5	2240	2295	436	626	8.38	7.35	-1.03	26.25	24.06	-2.19	1156	1170	-14	-.376
12-2-21	0	33	33	5	1421	1435	698	1026	5.14	4.56	-.58	25.75	24.00	-1.75	1998	2015	-17	-.290
12-2-22	0	32	32	5	1415	1442	693	983	5.43	4.60	-.83	27.25	25.38	-1.87	-	-	-	-
12-2-23	0	32	32	5	1389	1408	711	979	5.14	4.89	-.25	28.25	26.76	-1.49	2081	2091	-10	-.165
12-2-24	0	32	32	5	1400	1415	706	1043	-	-	-	-	23.43	-	2034	2038	-4	-.106
12-2-25	0	32	31	4	1400	1415	708	1012	4.41	3.59	-.82	25.5	25.02	-.48	2058	2062	-4	-.106
12-2-26	0	32	32	5	1800	1829	549	830	5.16	5.23	+0.06	23.25	22.32	-.93	1516	1524	-8	-.214
12-2-27	0	32	32	5	1769	1791	559	818	5.88	5.64	-.24	25.5	23.89	-1.61	1560	1566	-6	-.127
12-2-28	0	32	32	5	1768	1780	561	806	5.91	5.64	-.27	25.5	24.78	-.72	1583	-	-	-
12-3-1	40	31	31	5	1408	1513	896	1338	-6.40	-6.47	+0.07	25.5	23.01	-2.49	2637	2463	-6	-.101
12-3-2	40	32	24	-	1400	1479	913	1341	-5.28	-5.46	+0.18	25.75	24.00	-1.75	2709	2773	-64	-1.08
12-3-3	40	46	52	-	1425	1433	911	1325	-4.99	-5.10	+0.29	25.75	24.32	-1.40	2697	2713	-16	-.272
12-3-4	40	53	46	3	1400*	1430	913	1327	-4.72	-4.79	+0.07	25.5	24.32	-1.18	2704	2720	-16	-.272
12-3-5	40	53	45	3	1418	1441	906	1329	-5.28	-5.38	+0.10	25.5	24.00	-1.50	2680	2690	-10	-.17
12-3-6	40	52	45	3	1410	1460	894	1329	-	-	-	-	-	-	2614	2641	-27	-.46
12-3-7	40	53	45	3	1432	1459	895	1317	-	-	-	-	-	-	2636	2652	-16	-.272
12-4-3	40	53	46	3	1945	1835	712	1063	-	-5.65	-	25.25	22.8	-	2030	2052	-22	-.515

Table 13.1 Test Firings and Evaluation (Continued)

Round No.	Angle (degrees)	IBM Picket "A"	IBM Picket "B"	IBM Charge Selection	Velocity, ft/sec (from screens)	Velocity, ft/sec (from AT1)	Time, $\Delta T1$ , $\mu$ sec	Time, $\Delta T2$ , $\mu$ sec	Shell Position (Actual, in.)	Shell Position (Calculated, in.)	Position Error (in.) Horizontal	Height, Error (Actual, in.)	Height, Error (Calculated, in.)	Height, Error (in.)	Time, $\Delta T1$ , $\mu$ sec (Actual)	Time, $\Delta T1$ , $\mu$ sec (Calculated)	$\Delta \Delta T1 (\Delta T1' - \Delta T1'')$ $\mu$ sec	Displacement Error (in.)
12-4-4	40	53	46	3	1915	1805	724	1080	-6.33	-5.57	-.68	25.25	22.8		2069	2091	-22	-.505
12-4-5	40	53	46	3	1925	1810	722	1090	-6.15	-5.59	-.58	25.25	22.4		2074	2078	-4	-.093
12-4-6	40	53	46	3	1970	1840	708	1069	-6.24	-5.60	-.58	24.75	22.6		2036	2033	+3	+0.071
12-4-7	40	54	47	3	1910	1820	719	1098	-5.88	-5.22	-.65	23.8	21.8		2054	2061	-7	-.161
12-4-8	40	53	46	3	1935	1790	730	1091	-5.32	-5.44	-.28	24.5	22.8		2094	2109	-15	-.29
12-4-9	40	53	47	3	1950	1795	727	1064	-5.82	-5.61	-.10	25.0	23.8		2114	2112	+2	+0.047
12-4-10	40	52	47	3	1940	1880	695	1057	-5.69	-5.63	-.25	25.25	22.0		1993	1987	+6	+0.14
12-4-11	40	61	53	4	1950	1840	710	1087	-5.82	-6.31	-.21	26.25	23.2		2020	2032	-12	-.281
12-4-12	40	61	53	4	2080	2040	638	1015	-8.49	-6.31	-2.86	26.25	23.2		1947	1961	-14	-.350
12-4-13	40	61	53-54	4	1950	1830	713	1046	---	---	---	25.75	23.0		2071	2065	+6	+0.14
12-4-14	40	60	53	4	2390	2230	586	967	-6.84	-7.10	-.53	25.75	23.0		1598	1609	-9	-.258
12-4-15	40	60	53	4	2390	2280	573	853	---	---	---	27.0	25.1		1609	1606	+3	+0.086
12-4-16	40	60	53	4	2380	2240	584	835	---	---	---	27.0	25.1		1659	1655	+4	+0.114
12-4-17	40	60	53	4	2390	2260	576	821	-7.50	-7.47	-.40	26.5	25.9		1636	1630	+6	+0.172
12-4-18	40	60	52	4	2390	2240	584	820	---	-7.32	---	26.5	24.0		1650	1661	-11	-.316
12-4-19	40	60	52	4	2390	2270	575	840	-7.98	-7.32	-.51	26.5	24.0		1608	1619	-11	-.316
12-4-20	40	60	52	4	2450	2340	558	800	-8.33	-7.50	-1.01	26.5	25.0		1563	1569	-6	-.176
12-4-21	40	60	53	4	2380	2280	572	833	-7.97	-7.29	-.65	26.5	24.0		1592	1610	-18	-.515
12-4-22	40	60	53	4	2410	2270	575	823	-9.81	-7.38	-2.31	26.25	25.0		1619	1625	-6	-.174
12-4-23	60	60	53	4	2420	2280	876	1247	-8.55	-1.26	-1.26	26.25	25.0		2588	2616	-28	-.816
12-4-24	60	60	53	4	2640	2320	861	1258	-7.72	-7.46	-.44	27.00	25.65		2507	2548	-41	-1.30
12-7-3	60	65	59	---	2206+	2208	903	1271	-7.77	-7.77	---	26.00	26.30	1.35	2688	2714	-26	-.69
12-7-4	60	65	60	---	2206+	2200	910	1263	-7.65	-7.73	---	27.75	27.10	-.30	2700	2748	-48	-1.27
12-7-5	60	67	61	---	2206+	2235	895	1222	-7.91	-7.73	---	27.75	27.10	.65	2678	2711	-33	-.87
12-7-6	60	67	61	---	2206+	2245	891	1189	-8.30	-8.30	---	30.00	28.20	1.80	2675	2714	-39	-1.03
12-7-7	60	67	60	---	2185	2235	895	1219	-7.91	-7.73	---	29.00	27.10	1.90	2681	2713	-32	-.84
12-7-8	60	65	59	---	2200	2208	907	1388	-7.73	-7.73	---	27.00	27.10	---	---	---	---	---
12-7-9	60	64	59	---	2208	2110	948	4579	-7.72	-7.72	---	27.00	27.10	---	---	---	---	---
12-7-10	60	64	59	---	2200	1825	1009	4387	-7.73	-7.73	---	27.50	26.2	1.30	7785	2635	-27	-.712
12-7-11	60	68	62	---	2225	2270	877	1223	-7.80	-7.80	---	27.75	27.2	.55	2608	2695	-35	-.94
12-7-12	60	67	61	---	2215	2250	890	1213	-7.80	-7.80	---	28.00	27.1	.90	2660	2701	-40	-1.06
12-7-13	60	68	61	---	2200	2245	892	1218	-7.70	-7.70	---	27.00	27.3	-.30	2661	2780	-24	-.64
12-7-14	60	70	63	---	2215	2200	910	1211	-7.46	-7.46	---	27.00	27.3	---	3034	---	---	---
12-7-15	60	70	61	---	2208	---	3755	1515	-7.72	-7.72	---	27.00	27.3	---	2635	2680	-45	-1.2
12-7-16	60	65	59	---	2209	2203	908	1359	-7.72	-7.72	---	27.00	25.1	1.90	7458	2132	-22	-.475
12-7-17	60	65	59	---	2209	2195	912	4704	-7.72	-7.72	---	27.00	25.1	---	---	---	---	---
12-7-18	40	66	60	---	1795	1799	726	1017	-6.28	-6.28	---	27.00	25.1	---	---	---	---	---

Table 13.1 Test Firings and Evaluation (Continued)

Round No.	Angle (degrees)	IBM Picket "A"	IBM Picket "B"	IBM Charge Selection	Velocity, ft/sec (from screens)	Velocity, ft/sec (from $\Delta T1$ )	Time, $\Delta T1$ , $\mu$ sec	Time, $\Delta T2$ , $\mu$ sec	Shell Position Horizontal (Actual, in.)	Shell Position Horizontal (Calculated, in.)	Position Error Horizontal (in.)	Height, Error (Actual, in.)	Height, Error (Calculated, in.)	Height, Error (in.)	Time, $\Delta T1$ , $\mu$ sec (Actual)	Time, $\Delta T1$ , $\mu$ sec (Calculated)	$\Delta T1 (\Delta T1' - \Delta T1'')$ $\mu$ sec	Displacement Error (in.)
12-7-19	40	66	60	--	1805	1810	722	1014		-6.32		26.25	25.8	.45	2141	2161	-20	--
12-7-20	40	67	61	--	1798	1795	732	1008		-6.29		26.75	26.6	.15	2150	2168	-18	-.43
12-7-21	40	67	61	--	1788	1772	737	1033		-6.26		26.25	26.96	-.71	2123	2142	-19	-.39
12-7-22	40	67	61	--	1825	1800	725	990		-6.39		27.00	28.6	-1.6	2167	2192	-25	-.416
12-7-23	40	67	61	--	1810	1775	735	972		-6.34		27.00	28.6	-.48	2150	2172	-22	-.55
12-7-24	40	67	61	--	1806	1780	734	1004		-6.32		27.00	26.6	.4	2084	2172	-8	-.48
12-7-25	40	66	60	--	1825	1835	712	986		-6.39		27.00	26.6	-.175	2092	2092	-8	-.175
12-8-3	40	66	52	--	1820	1825	715	1009		-6.09		27.00	24.66	2.34	2072	2092	-20	-.439
12-8-4	40	67	53	--	1805	1798	726	1049		-6.28	.93	27.00	25.12	1.88	2093	2115	-22	-.478
12-8-5	40	67	52	--	1860	1846	707	1002	-5.35	-6.24	.73	27.00	25.33	2.37	2035	2064	-29	-.65
12-8-6	40	67	53	--	1850	1846	707	1028	-5.51	-6.20	.73	27.00	26.63	.62	2003	2050	-47	-1.05
12-8-7	40	67	53	--	1820	1792	728	1011		-7.56		27.25	26.63	2.22	2130	2143	-13	-.285
12-8-8	40	67	53	--	2200	2186	597	845				27.5	25.32		1695	1702	-7	-.186
12-8-9	40	67	53	--	2210	2234	584	783				27.5	25.32		1681	1676	+5	+1.33
12-8-10	40	66	51	--	2222	2212	590	776				27.5	24.00	3.5	1676	1704	-28	-.745
12-8-11	40	66	52	--	2218	2238	583	851	-7.47	-7.62	.15	27.5	24.00	3.5	1642	1645	-3	-.08
12-8-12	40	66-67	52	--	2220+	2266	576	841	-8.35	-7.72	-.63	27.25	24.00	3.25	1597	1622	-25	-.65
12-8-13	30	67	52	--	2320	2234	517	721		-7.83		27.00	26.17	.83	1431	1442	-11	-.307
12-8-14	30	67	52	--	2250	2225	519	692				27.75	27.28	.47	--	--	--	--
12-8-15	30	66	52	--	2250	2265	510	693	-8.04	-7.80	-1.24	27.75	27.28	2.47	1427	1425	+2	+0.054
12-8-16	30	67	53	--	2245	2238	516	746	-5.40	-7.51	2.11	26.75	24.33	2.42	1438	1430	+16	+4.33
12-8-17	30	67	53	--	2220+	2238	516	737		-7.48		26.75	24.98	1.77	1428	1432	-4	-.11
12-8-18	30	67-68	53	--	1845	1850	624	886	-5.66	-6.11	.45	26.5	25.32	1.18	1781	1790	-9	-.20
12-8-19	30	68	54	--	1845+	1854	623	865		-6.31		27.25	25.97	1.28	1803	1795	+8	+1.18
12-8-20	30	68	54	--	1805	1788	646	924				27.25	25.97	1.28	1861	1858	+3	+1.07
12-8-21	30	68	53-54	--	1805	1788	646	925	-3.40	-5.98	2.58	26.5	24.98	1.52	1868	1848	+20	+4.43
12-8-22	30	68	54	--	1800+	1799	642	943	-3.61	-5.91	2.30	26.25	23.73	2.52	1822	1834	-8	-.17
12-8-23	30	66-67	52	--	1782	1793	644	936	-6.09	-5.79	-.30	26.00	24.33	1.67	1836	1845	+9	+1.19
12-8-24	10	67	53	--	1795	1778	571	856	-6.89	-5.61	-1.28	25.00	22.68	2.32	1593	1597	-4	-.09
12-8-25	10	67	53	--	1800+	1784	569	801	-7.25	-6.13	-1.12	27.00	25.12	2.38	--	--	--	--
12-8-26	10	67	52	--	1800+	1800	564	820	-8.12	-6.07	-2.05	27.00	24.33	2.67	1583	1584	-1	-.03
12-8-27	10	67	52	--	1800+	1793	566	869	-7.53	-5.85	-1.68	26.0	21.36	4.64	1575	1573	+2	+0.04
12-8-28	10	67	52	--	2190	2178	466	651				28.5	27.28	1.22	1270	1273	-3	-.08
12-8-29	10	67	53	--	2230	2188	464	633	-8.32	-7.94	-.37	28.5	27.28	1.22	1263	1270	-7	-.19
12-8-30	10	66	52	--	2210	2246	452	653	-9.46	-7.87	-1.60	28.5	24.51	3.99	1223	1221	+2	-.05
12-8-31	10	66	52	--	2210	2221	457	4088				24.00	20.38	3.62	--	--	--	--
12-8-32	10	66	52	--	2220	2242	453	710	-8.36	-7.91	-.45	24.00	20.38	3.62	1206	1211	-5	-.14

Table 13.1 Test Firings and Evaluation (Continued)

Round No.	Angle (degrees)	IBM Picket "A"	IBM Picket "B"	IBM Charge Selection	Velocity, ft/sec (from screens)	Velocity, ft/sec (from $\Delta T1$ )	Time, $\Delta T1$ , $\mu$ sec	Time, $\Delta T2$ , $\mu$ sec	Shell Position Horizontal (Actual, in.)	Shell Position Horizontal (Calculated, in.)	Position Error (in.) Horizontal	Height, Error (Actual, in.)	Height, Error (Calculated, in.)	Height, Error (in.)	Time, $\Delta T1$ , $\mu$ sec (Actual)	Time, $\Delta T1$ , $\mu$ sec (Calculated)	$\Delta T1(\Delta T1' - \Delta T1'')$ $\mu$ sec	Displacement Error (in.)
12-16-3	50	66	59	5	--	1778	875	1257	-7.68	-5.64	-2.04	26.0	24.75	-.39	2673	2606	-28	-.60
12-16-4	50	67	59	4	--	1736	896	1264	-9.38	-6.72	-2.66	26.25	25.61	-.33	2689	2689	-16	-.33
12-16-5	50	65	58	5	2047	2072	751	1038	-9.77	-6.59	-3.18	26.25	26.56	-.69	2195	2223	-28	-.69
12-16-6	50	66	59	5	2089	2140	727	1040	-8.62	-6.81	-1.81	26.0	24.95	-.30	2098	2124	-26	-.65
12-16-7	50	65	58	5	2099	2099	741	1024	-7.46	-6.63	-.83	26.0	25.57	-.43	2181	2190	-9	-.23
12-16-8	50	67	59	4	2094	2146	725	1024	-7.46	-6.63	-.83	26.0	25.57	-.43	2133	2124	+9	-.28
12-16-9	50	67	59	4	2059	2105	739	1067	-6.98	-7.55	+5.7	26.5	26.89	+1.39	2143	2158	-15	-.37
12-16-10	50	67	60	5	2076	2077	749	1042	-7.53	-7.05	-.48	26.5	24.98	-.02	2200	2212	-12	-.30
12-16-11	50	67	59	4	2075	2122	733	1048	-7.23	-6.09	-1.14	26.5	22.45	+2	2136	2144	-8	-.20
12-16-12	50	65	58	5	2039	2047	760	1034	-4.78	-5.64	+8.6	26.0	26.72	+2.26	2269	2261	+8	+20
12-16-13	50	65	58	5	2367	2044	761	1044	-6.98	-7.55	+5.7	26.5	26.89	+1.39	2259	2260	-1	-.03
12-16-14	50	67	60	5	2251	2251	691	988	-7.23	-6.09	-1.14	26.5	24.98	-.02	2004	2006	-2	-.05
12-16-15	50	73	65	5	2159	2085	746	1124	-7.23	-6.09	-1.14	26.5	22.45	+2	2158	2156	+2	+0.05
12-16-16	50	73	65	5	2351	2209	591	849	-4.78	-5.64	+8.6	26.0	26.72	+2.26	1687	1676	+11	+31
12-16-17	40	73	66	6	2376	2278	573	797	-4.02	-5.62	+6.0	26.5	28.76	+2.26	1639	1629	+10	+29
12-16-18	40	74	66	6	2221	2305	588	796	-4.02	-5.62	+6.0	26.5	28.76	+2.26	1685	1687	-2	-.05
12-17-3	40	72	65	6	1754	1809	749	1023	-4.02	-5.62	+6.0	26.5	28.76	+2.26	2007	2222	-15	-.32
12-17-4	40	72	66	6	1625	1635	803	1106	-4.02	-5.62	+6.0	26.5	28.76	+2.26	2367	2398	-31	-.63
12-17-5	40	72	65	6	1635	1635	798	1095	-4.02	-5.62	+6.0	26.5	28.76	+2.26	2390	2383	+7	-.14
12-17-6	40	72	65	6	1695	1617	807	1061	-4.02	-5.62	+6.0	26.5	28.76	+2.26	2417	2440	-23	-.47
12-17-7	40	74	66	5	1828	1828	714	1127	-4.02	-5.62	+6.0	26.5	28.76	+2.26	2020	2027	-7	-.15
12-17-8	40	72	66	6	1699	1699	768	1160	-4.02	-5.62	+6.0	26.5	28.76	+2.26	2201	2225	-24	-.49
12-17-9	40	72	65	6	1711	1702	796	1070	-4.02	-5.62	+6.0	26.5	28.76	+2.26	2373	2390	-17	-.35
12-17-10	40	72	65	6	1809	1699	768	1003	-4.02	-5.62	+6.0	26.5	28.76	+2.26	2296	2311	-15	-.33
12-17-11	40	72	65	6	1710	1675	809	1048	-3.54	-5.93	+2.39	27.75	29.42	-1.67	2445	2456	-11	-.23
12-17-12	40	72	66	6	1724	1745	748	1084	-7.78	-5.82	-1.96	27.0	24.36	-2.64	2186	2186	--	--
12-17-13	40	74-73	66	6	2066	2150	607	908	-9.85	-6.84	-3.01	26.5	22.81	-3.69	1705	1714	-9	-.22
12-17-14	40	72	66	6	2081	2036	641	921	-7.04	-6.52	-.52	25.0	24.75	-.25	1805	1840	-35	-.88
12-17-15	40	72	65	6	--	--	--	--	-7.12	-7.10	-.02	27.0	27.25	+2.25	1598	--	--	--
12-17-16	30	72	66	6	2105	2044	565	769	-7.12	-7.10	-.02	27.0	27.25	+2.25	1582	1608	-26	-.66
12-17-17	30	74	66	5	2104	2104	549	804	-8.30	-6.58	-1.72	25.5	22.98	-2.52	1528	1565	-37	-.92
12-17-18	30	73	66	6	2063	2115	546	814	-8.30	-6.58	-1.72	25.5	22.98	-2.52	1494	1519	-25	-.62
12-17-19	30	74	67	6	2070	2070	558	811	-8.02	-6.82	-1.20	26.5	24.13	-2.37	1558	1565	-7	-.17
12-17-20	30	74	67	6	2066	2037	567	789	-8.07	-7.01	-1.06	27.5	24.62	-2.63	1610	1608	+2	+0.05
12-17-21	30	73	66	6	2055	2096	551	802	-8.07	-7.01	-1.06	27.5	24.62	-2.63	1537	1532	-5	-.12
12-17-22	30	73	66	6	2058	2112	547	788	-8.07	-7.01	-1.06	27.5	24.62	-2.63	1535	1532	+3	+0.07

\*Corrected for the one inch - 12-21-59.

# SECRET

(C) The analysis of 21 pairs of pictures shows that the average penetration was 4.7 mm with a standard deviation  $\sigma$  of  $\pm 7.02$  mm. This distance is measured from the leading edge of the fence to the position of the shell nose at the instant a pulse was obtained from the sally amplifier. The average penetration of 4.7 mm can easily be included by adding the proper constant to the firing-time equation.

## 13.6.3 Firing-Time Error

(S) The equation for the firing time, including the K-factor (section 9.4) is

$$\Delta T_f = \frac{d_2' + kL \cos \theta}{d_1} \Delta T_1 + \frac{d_1}{v_c \tan \phi} \cdot \frac{\Delta T_2}{\Delta T_1} - \Delta T_2 - \frac{h}{v_c} \quad (13.1)$$

For the matter of convenience,  $\Delta T_f$ ,  $\Delta T_1$ , and  $\Delta T_2$  will be labeled  $T_f$ ,  $T_1$ ,  $T_2$  respectively. These new notations, however, should not be confused with those used in the previous sections. Differentiating equation (1) partially with respect to  $T_1$  and  $T_2$  gives

$$dT_f = \left\{ \frac{d_2' + kL \cos \theta}{d_1} - \frac{1}{v_c \tan \phi} \frac{T_2}{T_1} \frac{d_1}{T_1} \right\} dT_1 + \left\{ \frac{1}{v_c \tan \phi} \frac{d_1}{T_1} - 1 \right\} dT_2$$

Writing the terms in the first and second brackets as  $K_1$  and  $K_2$ , respectively, one gets

$$dT_f = K_1 dT_1 + K_2 dT_2 \quad (13.2)$$

(U) Equation (13.2) will be used in either one of two ways, depending on whether or not the penetration is a function of velocity. Figure 13-3 illustrates the two cases. For case a in figure 13-12, the product  $V$  times  $dT$

$$VdT = V_1 dT_1' = V_2 dT_1'' = V_3 dT_1''' = \text{etc},$$

is a constant distance independent of the velocities  $V_1$ ,  $V_2$ ,  $V_3$ , and the variation about this constant value has to be considered as an uncertainty error. Equation (13.2) is multiplied through by the shell velocity  $V$ , giving

$$V dT_f = K_1 V dT_1 + K_2 V dT_2 \quad (13.3)$$

# SECRET

CONFIDENTIAL

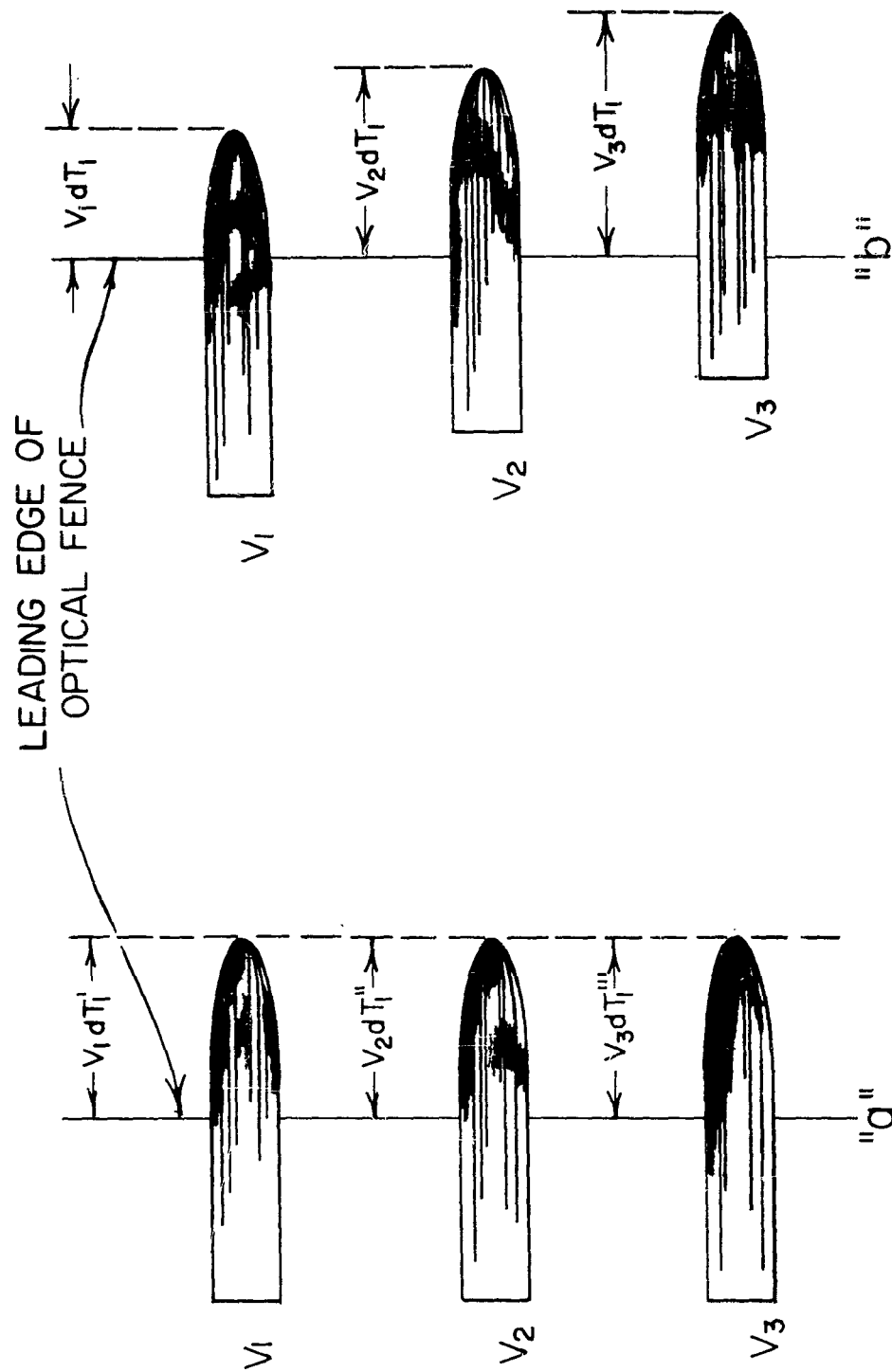


Figure 13-12. Penetration error

CONFIDENTIAL

The error equation for the area of the rms uncertainty of hitting a projectile is

$$E_{p_t} = \sqrt{K_1^2 E_{p_1}^2 + K_2^2 E_{p_2}^2} \quad (13.4)$$

where  $E_{p_t}$  = total rms positional error,

$E_{p_1}$  = rms error associated with the product  $V dT_1$ , and

$E_{p_2}$  = rms error associated with  $V dT_2$ .

(U) For case b in figure 13-12, where the penetration is a function of the velocity, the time  $dT_1$  is constant and variations about the value of  $dT_1$  would now have to be considered as an uncertainty error. The error for the firing time would be

$$E_{T_t} = \sqrt{K_1^2 E_{T_1}^2 + K_2^2 E_{T_2}^2} \quad (13.5)$$

where

$E_{T_t}$  = total error in the firing time,

$E_{T_1}$  = rms time error associated with  $dT_1$ , and

$E_{T_2}$  = rms time error associated with  $dT_2$ .

The positional error  $E_p$ , then, is

$$E_p = V E_{T_t} = V \sqrt{K_1^2 E_{T_1}^2 + K_2^2 E_{T_2}^2} \quad (13.6)$$

(U) From the scatter diagram, figure 13-13, for which the 21 firings mentioned in section 13.6.2 were used, it can be seen that there is no correlation between the penetration, as measured, and the velocity. Therefore, case a in figure 13-13 and equation (13.4) are the correct ones, and not case b or equation (13.6). \*

\* It may be that, to a slight degree, the penetration still is a function of the velocity. However, other effects predominate, so that no correlation can be found experimentally.

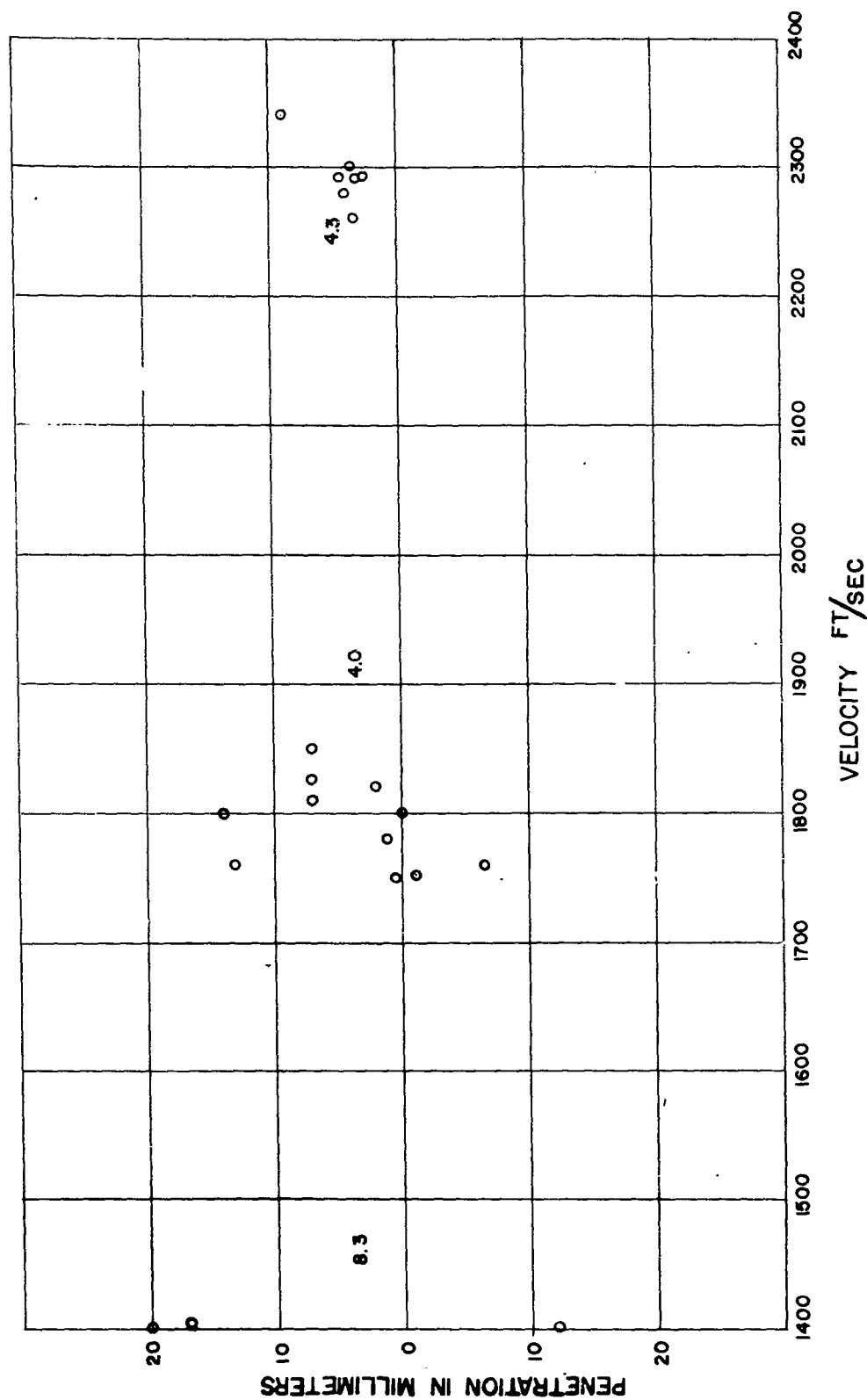


Figure 13-13. Scatter diagram of penetration vs velocity

SECRET

(U) Since the time interval  $T_1$  is the result of the projectile passing through two fences, the total rms error associated with it is  $\sqrt{2}$  times the error of one or  $\pm 1.41 \times 7.02 \text{ mm} = \pm 9.8 \text{ mm} = 0.39 \text{ in.}$ , where 7.02 mm is the standard deviation of the penetration as arrived at in section 13.6.2. Similarly, the rms error associated with  $T_2$  is assumed to be also  $\pm 0.39 \text{ in.}$

(U) For the numerical computation, the terms  $K_1$  and  $K_2$  from equation (13.2) are introduced in equation (13.4) which gives

$$E_{P_t} = \sqrt{\left\{ \frac{d_2^2 + kL \cos \theta}{d_1} - \frac{1}{V_c \tan \phi} \frac{T_2}{T_1} \frac{d_1}{T_1} \right\}^2 E_{P_1}^2 + \left\{ \frac{1}{V_c \tan \phi} \frac{d_1}{T_1} - 1 \right\}^2 E_{P_2}^2} \quad (13.7)$$

$K_1$  and  $K_2$  contain the velocity term  $d_1/T_1$ ;  $k_1$  has also a height term  $T_2/T_1$ . The term  $(d_2^2 + kL \cos \theta)/d_1$  has a maximum value of 4.7, and  $1/V_c \tan \phi = 3.44 \times 10^{-4} \text{ sec/ft.}$  for the geometry used. When these values and terms are introduced in equation (13.7), and with  $E_{P_1} = E_{P_2}$ , the total positional error becomes

$$E_{P_t} = \sqrt{(4.7 - 3.44 \times 10^{-4} \frac{T_2}{T_1} V)^2 + (3.44 \times 10^{-4} V - 1)^2} \quad (13.8)$$

With this error equation, the total positional error has been plotted in figure 13-15 as a function of the shell velocity  $V$  for three values of  $T_2/T_1$ , namely, 2, 1, 0.5, which result from the lowest, middle and greatest height, respectively, of the shell trajectories over the optical sensing units.

(C) Analysis of shell pictures taken with the firing pulse from the firing-time computer results in a standard deviation  $\sigma$  of  $\pm 0.51 \text{ in.}$  for shell velocities around 1400 fps of  $\pm 1.23 \text{ in.}$  for 1800 fps, and  $\pm 1.05 \text{ in.}$  for 2000 fps.

(C) As figure 13-14 shows, these experimentally found errors are smaller than the calculated ones. Actually, they can be expected to be smaller, since the instrumentation made it necessary to have the shell trajectories as closely over the centers of the optical fences as possible, thereby eliminating the variations of the different positions along the fences as sources of error.

(S) For the matter of clarity, it should be borne in mind, what the standard deviation of about 1 in. means: It means that 68.3 percent of the shells having velocities between 1400 and 2000 fps could have been hit at a predetermined point on their axes with an accuracy of about  $\pm 1 \text{ in.}$

SECRET

237

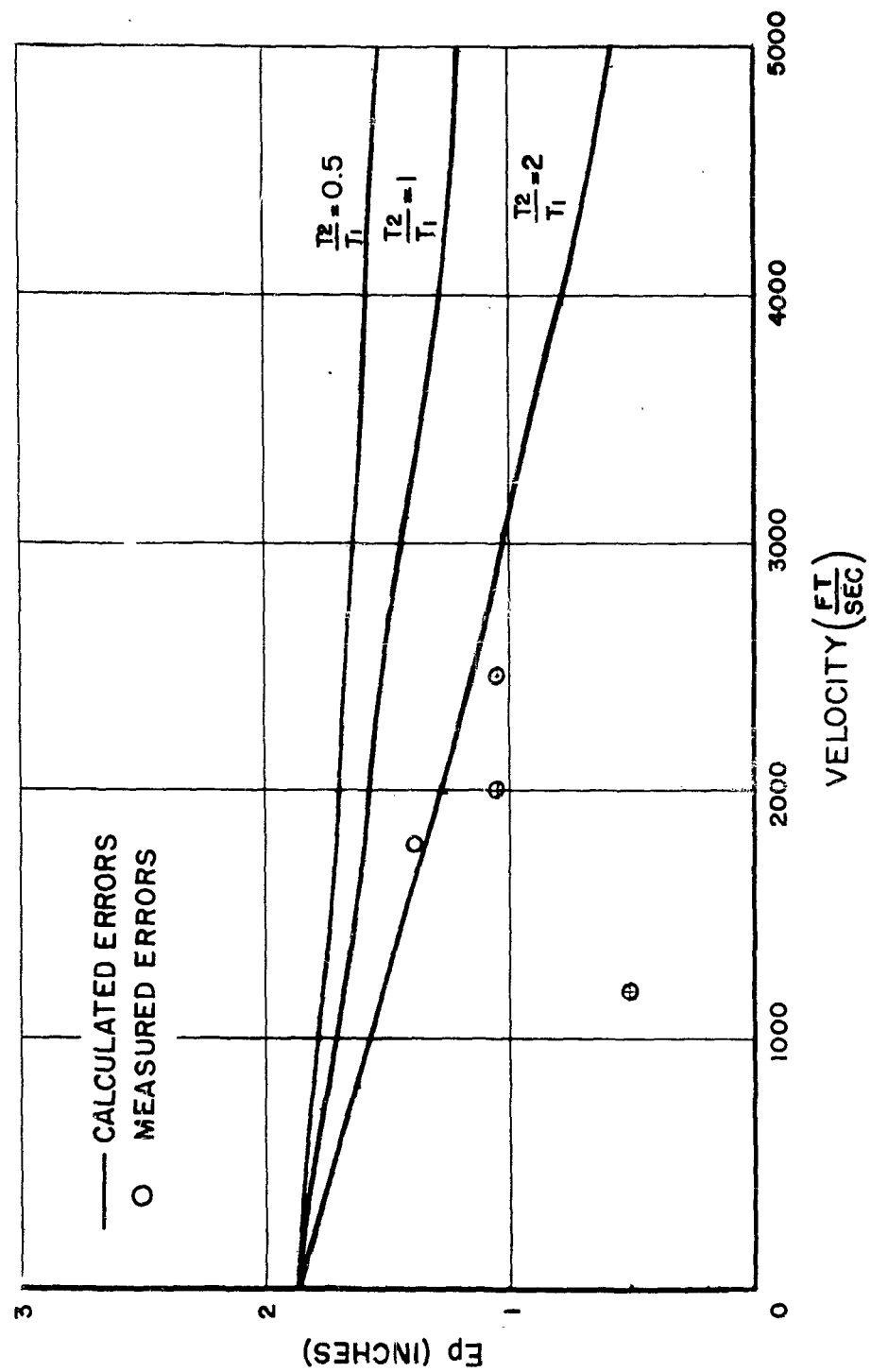


Figure 13-14. Positional error vs shear velocity

# SECRET

## 14. MICROWAVE APPROACH

W. Moore

(U) The microwave approach to the Dash-Dot problem was carried on under contracts DAI-19-020-501-(P)-49 and DA-49-186-502-ORD-586 by the United Shoe Machinery Corporation, Beverly, Massachusetts. A brief summary of the basic approach considered by the contractor will be outlined here.

(U) Because misunderstandings have arisen in the past regarding the microwave approach to the problem, it is well to emphasize at this point that "radar techniques," in the generally accepted sense, were not employed.

(C) The greater portion of these investigations was based upon a cw system and high-resolution antennas, operating in the near-field to establish detection planes through which the shell passes sequentially. Thus, the problem essentially reduces to the same form as that encountered with the optical approach, with the exception of the velocity measurement, and the necessary hardware.

### 14.1 Velocity Measurement

(U) The velocity measurement is made with the well known Doppler method. A cw magnetron operating at X-band and capable of about one watt output was used to feed a horn antenna of relatively low gain. This may be used both for transmitting and receiving, or a separate receiving horn may be used. The receiver for the velocity measurement is essentially a zero I-F type. The Doppler frequency signal of the reflected return signal is limited and counted to give an output which is proportional to the approach velocity.

(S) System requirements call for operation against shell speeds from approximately 200 to 5000 fps. The velocity measuring equipment therefore, has to be capable of covering a 25:1 frequency range.

(C) The output from the velocity measurement unit usually will have to be stored for a short period of time until information is obtained from other parts of the system regarding the position of the attacking round.

### 14.2 Methods for Height Determination

(C) Two methods were investigated for determining the height of the attacking round trajectory. These methods were termed the Multiple Bi-static System and the Three Horn System. Both approaches relied upon high-resolution antennas, operating in the near field, to establish sharp detection areas.

SECRET

239

#### 14.2.1 Multiple Bistatic System

(C) This system employs quantized height determination. It utilizes two sets of horn antennas. One set is for transmitting; the second set is for receiving (figure 14-1). The transmitting antennas are arranged one above the other and face the receiving horns which are similarly "stacked". The particular transmitting and receiving antennas which are directly opposed form a "bistatic pair", e.g., antenna 1-T and 1-R; 2-T and 2-R, etc. When a projectile passes between a pair, it produces a change in the received signal and this change is used to trigger height compensation circuitry.

(C) It is obvious that the height information so obtained is quantized in height, since the projectile may be anywhere in the region between the horns of a pair and still activate the circuitry connected to it. This system, therefore, only gives height information to an accuracy of  $\pm kH/2$ , where  $1/k$  equals the number of bistatic pairs in the total height  $H$ , if the detection regions are all of the same width vertically and contiguous to one another.

(S) An error in height of this magnitude will manifest itself in a positional error for intercepting the attacking round of  $\pm kHV_m/2V_c$  from a chosen position. For instance, for a system where  $kH = 12$  in.  $V_c = 8000$  fps, and the maximum attacking round velocity  $V_{max} = 4000$  fps, the error is  $\pm 3$  in.

#### 14.2.2 Three-Horn System for Height Determination

(C) The "Three Horn System" of height determination is based upon the same principle as that used in the optical approach. Figure 14-2 shows the main features of this method. It consists of one transmitting and two receiving antennas arranged to form two detection planes making an angle with respect to each other. As the projectile passes through the planes, two pulses are generated by the receivers  $R_1$  and  $R_2$ . The time interval  $t_2 - t_1$  between these pulses is directly proportional to the height  $h$  and inversely proportional to the shell velocity. As velocity information has already been obtained from the Doppler signal, it is possible to use this information to extract  $h$  from  $(t_2 - t_1)$ .

(S) From figure 14-2, the equation for the firing time  $T_f$ , that is, the time the defending charge has to be fired after the shell has passed through the second beam, may be obtained. For the dimensions given in the figure, the equation is

$$T_f = 5 (t_2 - t_1) - 10 (t_2 - t_1) \frac{V_m}{V_c},$$

where

$V_m$  = velocity of the attacking projectile,

$V_c$  = fragment speed of the defending charge.

SECRET

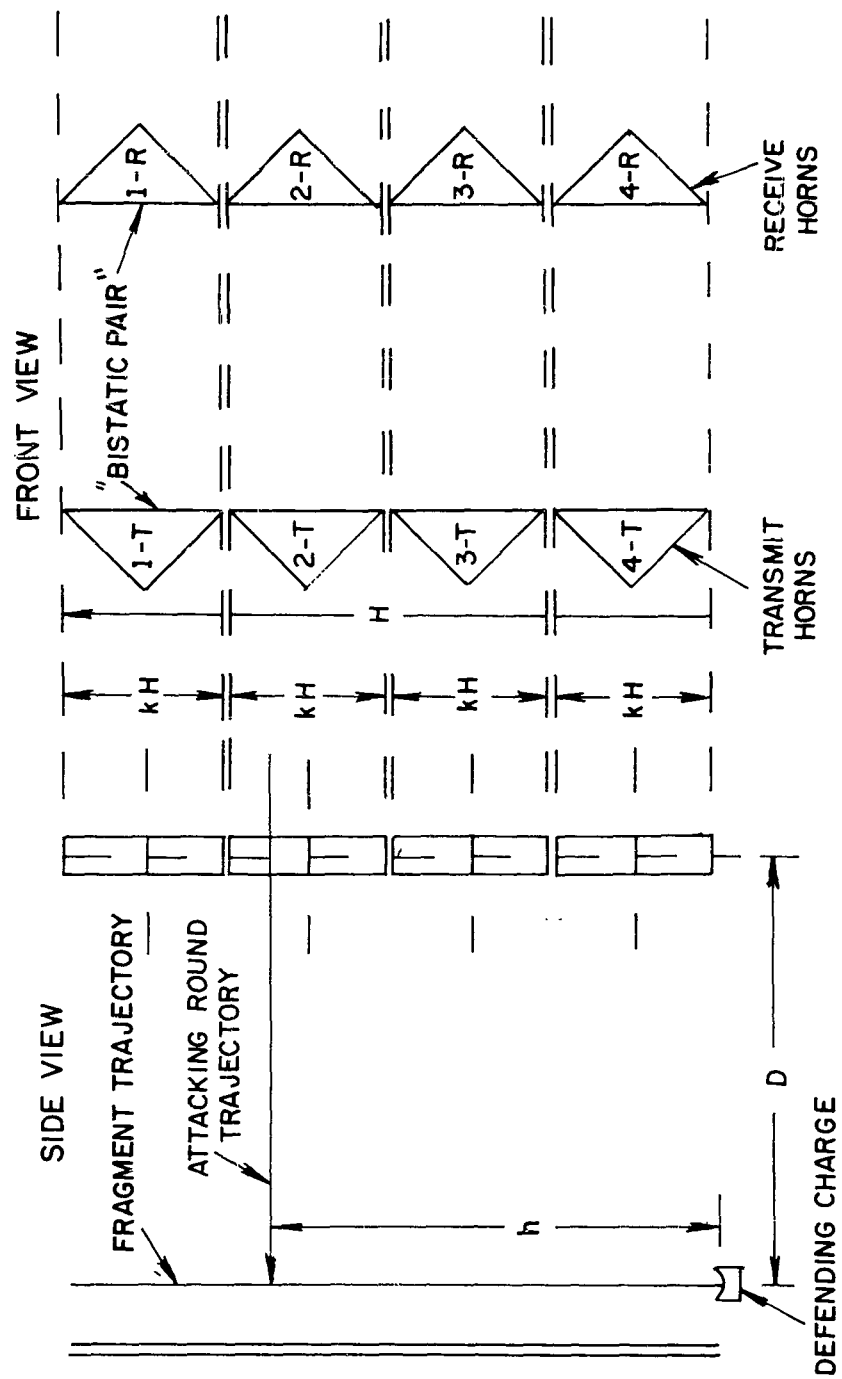


Figure 14-1. Multiple bistatic system

SECRET

SECRET

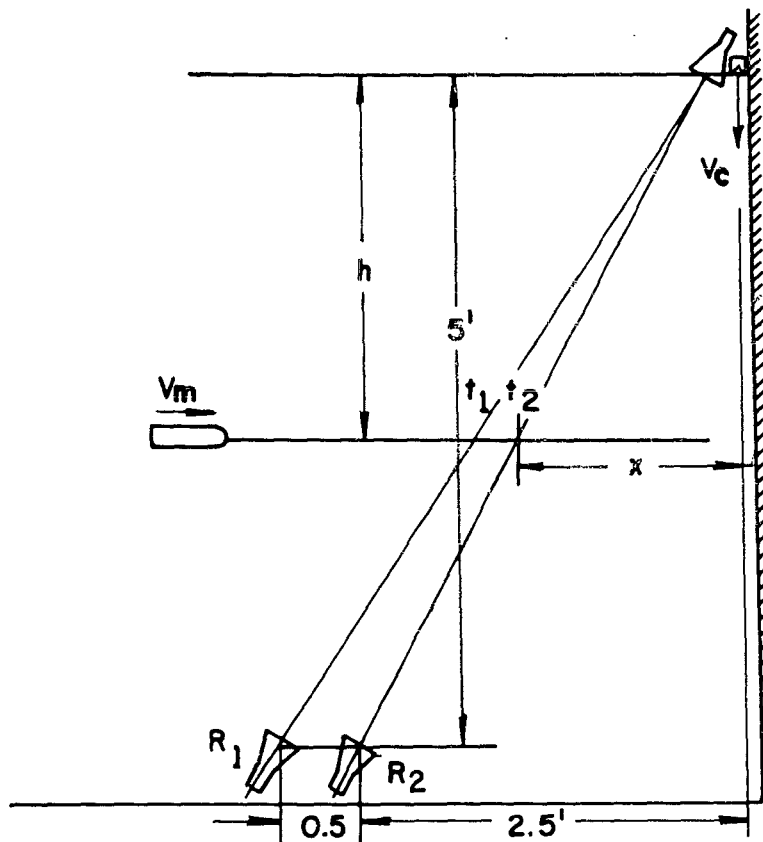


Figure 14-2. Practical three-horn system  
(Reproduced from contractor report No. 29)

SECRET

**CONFIDENTIAL**

(C) The equation is similar to that obtained for the inclined-beam optical approach, and therefore, the firing-time computer may also be essentially the same.

#### 14.3 FM Ranging Techniques

(U) In addition to the method outlined in section 14.2.1 and section 14.2.2, a study was made of frequency-modulation ranging techniques. These are outlined in the contractor's Quarterly Report for the period 1 Oct - 31 Dec 1956, Contract DAI-19-020-501-ORD-(P)-49, Dash-Dot.

(U) As stated in the above report, the following methods were investigated:

1. Ismail's method whereby both range and speed information are simultaneously provided.
2. Single-range plus speed measurement where the time when a projectile is at a preset range and its speed at this time are independently determined.
3. Two-range system where the speed is determined by the time required for the projectile to move from the first to the second preset range.
4. Fixed-frequency-constant-delay system where a "zero" beat between the difference frequency,  $f$ , and a reference frequency serves to initiate a fixed delay before triggering.

#### 14.4 Bibliography of Contractor's Reports

(U) In order to avoid encumbering this report with information that can be obtained elsewhere, the above description of the microwave approach has been held to a minimum.

(U) For complete information, reference is made to the reports by United Shoe Machinery Corporation, Beverly, Massachusetts, copies of which are available through ASIIA. A bibliography follows:

\* Ismail, M. A. W., "A precise New System of FM Radar," Proc. IRE, Vol. 44, September 1956

**CONFIDENTIAL**

243

Bibliography of Reports by United Shoe Machinery Corporation  
Beverly, Massachusetts, on Microwave Version  
of Project Dash-Dot

Contract No. DAI-19-020-501-ORD-(P)-49

<u>Period</u>		
6/10 - 7/9, 1954	Monthly Progress Report	1
7/1954	Monthly Progress Report	2
8/1954	Monthly Progress Report	3
9/1954	Monthly Progress Report	4
10/1954	Monthly Progress Report	5
11/1954	Monthly Progress Report	6
12/1954	Monthly Progress Report	7
1/1955	Monthly Progress Report	8
2/1955	Monthly Progress Report	9
8/54 - 9/55	Interim Report	11
6/1955	Monthly Progress Report	13
5/1 - 5/31, 1956	Monthly Status Report	16
6/1 - 6/30, 1956	Monthly Status Report	17
7/1 - 7/31, 1956	Monthly Status Report	18
8/1 - 8/31, 1956	Monthly Status Report	19
5/1 - 9/30, 1956	Quarterly Progress Report	20
10/1 - 10/31, 1956	Monthly Status Report	21
10/1 - 10/31, 1956	Quarterly Progress Report	21
1/1 - 1/31, 1957	Monthly Status Report	24
2/1 - 2/28, 1957	Monthly Status Report	25
1/1 - 3/31, 1957	Quarterly Progress Report	26
4/1 - 4/30, 1957	Monthly Status Report	27
5/1 - 5/21, 1957	Monthly Status Report	28

Contract No. DA-49-186-502-ORD-586

8/1 - 8/31, 1957	Monthly Status Report	1
9/1 - 9/30, 1957	Monthly Status Report	2
10/1 - 10/31, 1957	Monthly Status Report	3
12/1 - 1/31, 1958	Status Report	5
11/1957 - 7/1958	Interim Progress Report	6
8/1/1958 - 1/31/1959	Interim Progress Report	7
2/1959 - 3/1959	Interim Progress Report	8
4/1959 - 7/1959	Final Progress Report	
11/13/1959	Final Report on Dot-Dash	
8/1/1959 - 7/31/1960	Continuation Proposal	

# SECRET

## 15. CONCLUSION

H. W. Straub

(S) In June 1959, it became apparent that, contrary to previous assumptions, the Dash-Dot system was expected to be capable of being mounted on a present-day tank. The maximum front overhang tolerable was specified by OTAC\* as six inches beyond the fenders and/or one foot below the turret race. This requirement cannot be fulfilled, at the present state of the art, by the system described in this report.

(S) For instance, the 106 mm M344A1 HEAT round must be hit 14 inches behind the nose. This necessitates the innermost detection fence to be at least 14 inches outside the defending charge line if the charges fire vertically, which is already a multiple of what OTAC can concede, and this does not take in account the minimum safe distance between the defending charge line and the tank wall.

(U) Under these circumstances, DOFL made the following recommendations to OTAC\*\*

"(S) 1. If the words "vehicular application" . . . are to be interpreted as meaning application on a presently available vehicle, or

"(S) 2. If OTAC insists on the requirement that only 6 inches of front overhang and/or one foot below the turret race can be tolerated, and

"(S) 3. If a fragment velocity of the defending charge very much higher than 8200 feet per second cannot be expected in the near future,

"(S) then DOFL has to recommend that work on the sensing system of Dash-Dot be terminated after field tests of Phase III (firing time depending on velocity plus altitude), Phase IV (line charge selection), and Phase V (size discrimination) have been completed."

(U) The project was placed on the deferred list in September 1959 before the above-indicated phases were completed. It was then decided at DOFL, as has been pointed out in the introduction, that the last phases would be completed and a report written even if need be, on DOFL S-R funds. Otherwise much of the funds spent would have been spent with no results, and much technical knowledge would be irretrievably lost.

\* Oral communication

\*\* Letter Report "Status of Project Dash-Dot (U)" (Secret Report), dated 27 August 1959, from DOFL to OTAC.

# SECRET

245

This document contains information affecting the national defense of the United States within the meaning of the espionage laws, title, 18 U. S. C., 793 and 794. Its transmission or the revelation of its contents in any manner to an unauthorized person is prohibited by law.

(S) This report shows that the basic problems, namely, those of determining the trajectories of attacking shells at short ranges of a few feet only, of selecting the one out of a multitude of defending charges that is in the right position, and of generating a firing pulse at the correctly computed time for the selected charge to defeat the attacking shell, have been solved in the optical approach.

(S) The main shortcoming of the optical sensing system, which is lack of compactness, can be remedied as defending charges of fragment velocities higher than 8000 fps become available. It was shown in the discussion on the front overhang, sections 2.2.1 and 2.2.3, that the velocity  $V_c$  of the defending charge fragments appears in the denominator of the equations, meaning that the front overhang can be reduced with increasing fragment velocity.

(C) It should be noted that improvements in the photocells regarding higher sensitivity or shorter time constant would have no influence on the size of the sensing system. If, ideally, low-cost, small-size, zero time constant, infrared sensitive photocells became available, they would permit considerably simpler electronic devices to be built, but the compactness of the optical sensing system proper would not be affected.

(C) Although the approach described does not appear to lend itself to tank defense, it is felt that, when properly modified, it is well suited to solve other defense problems.

## 16. ACKNOWLEDGMENTS

Many persons other than the authors have contributed to this work. Notable among them are E. E. Chapin, Jr., for the laboratory construction of most of the electronic devices and other/variable assistance, and E. Katzen for constructing, assembling, aligning, and testing the optical equipment and special measuring devices.

# DISTRIBUTION

Copy No.

Office of the Director of Defense Research & Engineering  
The Pentagon, Washington 25, D. C.

Attn: Director of Weapons Systems Evaluation Group (rm 2E812) 1

Department of the Army  
Office of the Chief of Ordnance  
The Pentagon, Washington 25, D. C.

Attn: ORDTW, W. J. Morawski (10 copies) 2 - 11

Commanding General  
Aberdeen Proving Ground, Maryland

Attn: BRL, S. Kronman 12

Attn: BRL, R. J. Eichlberger 13

Commanding Officer  
Picatinny Arsenal  
Dover, New Jersey

Attn: Feltman Research & Engineering Laboratories 14

Attn: ORDBB-TE9, P. B. Tweed 15

Commanding General  
Ordnance Tank Automotive Command

Detroit Arsenal

Centerline, Michigan 16

Attn: M. Michaelson

Commander  
Air Proving Ground Center  
Eglin Air Force Base, Florida

Attn: Deputy Commander for Development & Test (PGTRIL) 17

Commander  
Armed Services Technical Information Agency  
Arlington Hall Station  
Arlington 12, Virginia

Attn: TIPDR (10 copies) 18 - 27

Infrared Information & Analysis Center  
Willow Run Research Center  
University of Michigan  
Ann Arbor, Michigan

Attn: William L. Wolfe (2 copies) 28 - 29

# DISTRIBUTION (Continued)

Internal	Copy No.
Hinman, W. S., Jr./McEvoy, R. W.	30
Apstein, M./Gerwin, H. L./Guarino, P. A./Kalmus, H. P.	31
Fong, L. B. C./Sures, A. H.	32
Hardin, C. D., Lab 100	33
Horton, B. M., Lab 200	34
Rotkin, I., Lab 300	35
Landis, P. E., Lab 400	36
Hatcher, R. D., Lab 500	37
Campagna, J. H., Lab 600	38
White, H. L./Apolenis, C. J., Div 700	39
DeMasi, R., Div 800	40
Seaton, J. W., 260	41
Griffin, P. W., 240	42
Sommer, H., 250	43
Straub, H. W., 240	44
Arthaber, J., 240	45
Copeland, A., 240	46
Melamed, L., 240	47
Miller, J. E., 240	48
Moore, W. J., 240	49
Paradis, R. J., 240	50
Ulrich, R., 240	51
Vrataric, F., 240	52
Technical Reports Unit, 800	53
Editorial & Duplicating, 841	54
DOFL Library (5 copies)	55 - 57

(Two pages of abstract cards follow.)